Identification and evaluation of monoclonal antibodies against Surface-Layer Proteins of Clostridioides difficile

Lise Hunault

Sorbonne Université

Ecole doctorale 394 : Physiologie, Physiopathologie et Thérapeutique

Centre d'Immunologie et des Maladies Infectieuses

Institut Pasteur Paris / Anticorps en Thérapie et Pathologie

Identification and evaluation of monoclonal antibodies against Surface-Layer Proteins of *Clostridioides difficile*

Par **Lise Hunault**

Thèse de doctorat d'Immunologie

Dirigée par le Pr. Guy Gorochov, le Dr. Pierre Bruhns et la Dr. Delphine Sterlin

Présentée et soutenue publiquement le 18 Septembre 2023

Devant un jury composé de :

Dr. Ludovic Tailleux	Rapporteur
Pr. Emma Slack	Rapportrice
Pr. Alban Le-Monnier	Examinateur & Président
Dr. Catherine Eckert	Examinatrice
Pr. Yves Germani	Examinateur

To my family,

my friends,

and my colleagues.

Acknowledgements

« Sans la curiosité de l'esprit, que serions-nous ?
Telle est la beauté et la noblesse de la science : un désir sans fin de repousser les frontières du savoir, de traquer les secrets de la matière et de la vie sans idée préconçue des conséquences éventuelles. »

« Dans la vie, rien n'est à craindre, tout est à comprendre. »

Marie Curie

I would first like to thank the jury members who accepted to review my work: Pr Emma Slack and Dr Ludovic Tailleux, as well as Pr Alban le Monnier, Dr Catherine Eckert and Pr Yves Germani. Thank you for the time allowed to review and evaluate this work.
Un merci très spécial au Dr Ludovic Tailleux qui a accepté de prendre le rôle de rapporteur au pied levé à la suite du désistement d'une de mes rapportrices. Je lui suis réellement reconnaissante de m'avoir sortie de cette impasse et permis de soutenir à la date prévue.

Merci au trio que forme mes encadrants de thèse, Delphine, Guy et Pierre, pour la formation de qualité qu'ils m'ont prodiguée pendant ces 4 années de master et thèse.

Merci à toi Delphine, de m'avoir prise sous ton aile en stage de master, de m'avoir introduite au projet et formée aussi bien techniquement qu'intellectuellement pendant ces 4 années. Merci de m'avoir laissé l'espace pour proposer mes raisonnements, formuler mes propres hypothèses et désigner les expériences en conséquence. Tu m'as laissé la liberté de prendre les rênes de mon projet tout en me permettant, grâce à tes suggestions judicieuses, de garder le cap. Merci pour toutes les discussions scientifiques et personnelles et ton enthousiasme omniprésent. Cela a été un véritable soutien pendant les périodes plus compliquées de ce travail de recherche. J'ai pu grâce à toi prendre la mesure de la figure de scientifique et chercheur, dans toute la complexité que ce métier implique. Merci également de m'avoir permis d'avoir une petite expérience d'encadrement en me laissant co-encadrer des stagiaires. Merci enfin pour toute ton aide sur la dernière partie de rédaction de la thèse. Cela aura été un véritable plaisir d'effectuer ce travail de synthèse, et de progresser dans ce travail de rédaction, ce qui a pu être possible grâce à tes retours constructifs et bienveillants. Au-delà de l'apprentissage conséquent, ce fut un réel plaisir d'effectuer ma thèse sous ton encadrement.

Un merci empli de gratitude pour toi Guy, de m'avoir prise sous ton encadrement, de m'avoir fait confiance pour mener à bien ce travail de thèse, ainsi qu'à Delphine pour m'y accompagner. Cela est à mon sens une belle démonstration de l'esprit d'équipe et de ce que

l'on peut accomplir dans un climat de confiance. Merci également pour les discussions scientifiques et ton aide sur le travail de rédaction, j'ai beaucoup appris grâce à tes retours.

Pierre, je me souviens du premier e-mail que je t'ai envoyé en réponse à ton offre de thèse pour un profil PPU, à la suite duquel tu m'as présenté tous les projets de ton labo, examinant lequel pourrait correspondre le plus à ce que j'avais envie de faire, et puis la présentation à Delphine. Merci pour l'incroyable liberté que tu m'as laissée au sein de ton laboratoire et de l'environnement Pasteur. J'ai plusieurs fois eu le ressenti que la seule limite à mes recherches était mon imagination, que je pouvais trouver, que ce soit sur le campus ou dans des collaborations, tout ce qui était nécessaire à ce travail de recherche. Si cela constitue à mon sens le cœur du travail d'un chercheur, je suis également consciente des limites parfois matérielles auxquelles celui-ci doit faire face, et cela me permet d'apprécier d'autant plus la chance que j'ai eu à cet égard. Merci pour tout le temps que tu as consacré à mon encadrement, pour ton exigence scientifique aussi bien sur la démarche que sur les résultats. L'apprentissage que j'ai pu gagner en raisonnement, synthèse et rigueur est considérable. Merci enfin pour ton aide sur le travail de rédaction, j'ai énormément appris grâce à tes conseils.

Un grand merci aux nombreuses personnes de mes deux laboratoires de la Pitié-Salpêtrière et de l'Institut Pasteur. Travailler dans ces deux environnements et avec ces deux équipes a été une souche d'enrichissement considérable. Coté CIMI, merci à Karim et Christophe de m'avoir accueillie dans le labo, répondu à mes nombreuses questions aussi bien scientifiques que techniques. Merci entre autres, à toi Christophe pour tes précieuses connaissances de cytométrie en flux, Karim pour l'aide sur les PCR et les peptides, merci à Omaira également à ce propos, Lejla pour le travail autour du microbiote, Alicia pour les discussions scientifiques. Merci aux stagiaires Eliana, Ines et Léo pour votre travail sur mon projet et votre enthousiasme, et de m'avoir permis d'avoir ces premières expériences d'encadrements. Coté ATP, merci à Odile et Ophélie de m'avoir accueillie à la paillasse, répondu à toutes mes questions techniques et intellectuelles, et merci d'être les piliers de ce labo. Ophélie, merci pour toute l'aide avec les souris, j'appréhendais réellement ce travail et tu l'as rendu beaucoup moins pénible que ce que j'avais pu imaginer. Merci à Bruno pour toutes les purifications d'anticorps, tu n'as jamais sourcillé quand je venais avec mes trentaines de rollers, et cela m'a permis de pousser mon travail encore plus loin. Alice, Vanessa, Lorenzo et Matteo, mes co-thésards, ce fut un réel plaisir de partager ces années de thèse et cet esprit d'équipe à vos côtés. Vanessa et Alice, merci pour l'amitié qui en a découlé, vous avez été un réel soutien scientifique et personnel pendant ces trois années. François, merci pour toute l'aide

sur les tris, Freddie, merci pour l'organisation des journal club, l'aide sur le séquençage. Chaque personne de ces deux équipes participe à l'environnement stimulant et bienveillant que j'ai pu trouver au sein de ces deux laboratoires, et vous avez chacun participé au fait que je prenne plaisir chaque matin à venir au laboratoire.

Un merci bien spécial à Émile et Bruno, et de manière plus générale à tous les membres du LPBA. J'ai sollicité des explications ou de l'aide à chacun d'entre vous et vous m'avez toujours apporté cela avec bienveillance et détails, me faisant sentir comme l'un des membres de votre équipe. Émile, un merci infini de m'avoir pris sous ton aile pour les biofilms, de m'avoir formée, accompagnée sur toute l'interprétation des résultats et permis de relancer cette partie du projet. Jazmin, merci pour toute l'aide sur les essais de transwell, j'ai également beaucoup apprécié échanger avec toi sur les organ-on-chip et sur nombreux autres sujets scientifiques et personnels. Léo et Cyril, merci pour l'aide sur les toxines et les spores.

Enfin Bruno, je te suis extrêmement reconnaissante de m'avoir pris sous ton aile, formée et aidée sur la microbiologie de *C. difficile*. Ton aide a été précieuse pour me diriger vers chacun de tes membres de ton labo qui possédait les expertises dont j'avais besoin, et je n'aurais pas pu approfondir autant mes hypothèses de recherche et mes explications des phénomènes sans ton savoir. Je suis ravie que mon projet m'ait autant amené à travailler avec toi, et je garde en mémoire toutes nos discussions aussi bien scientifiques que sur des aspects plus humains. Enfin, une reconnaissance éternelle de m'avoir sortie de l'ultime impasse de ma thèse lorsque ma rapportrice a dû se désister au dernier moment.

J'aimerais aussi chaleureusement remercier l'équipe BaPS de Saclay et tout particulièrement Cécile, Séverine, Sandra et Jeanne avec qui j'ai travaillé sur les essais d'adhésion et les essais animaux, ainsi que Thomas et P-A pour les discussions autour de *C. difficile*. Vous avez été ma première collaboration et l'accueil chaleureux que vous m'avez réservé m'a très vite fait comprendre l'importance en recherche du travail entre différentes équipes aux expertises distinctes. Malgré l'absence de résultats positifs de nos expériences, j'ai énormément appris sur la démarche scientifique, la façon de formuler, tester et valider ou réfuter les hypothèses de travail, et cet apprentissage a à mon sens une valeur considérable, et m'a permis d'avoir une formation que je n'aurais sans doute pas eu si tout avait marché comme nous l'avions initialement pensé.

J'aimerais ensuite adresser de chaleureux remerciements à tous nos autres collaborateurs : Julien et Romain pour les expériences de microscopie autour de biofilms, Thierry et Camille

pour le test de ribotypage rapide, Samy pour les expériences d'intestine-on-chip, Patrick pour la formation et les discussions autour des affinités, Ahmed pour les essais de cristallographie, Frédéric et Catherine pour les selles, Alban et Assaf pour le projet SERODIFF, Suzanne pour la collaboration avec les anti-FliC.

Un merci plus personnel à mes amis, mes copains de l'ESPCI -cela aide tout de même énormément d'avoir de bons amis embarqués dans la même aventure que nous- ; un merci spécial à Anick, Irène et Gab pour le partage d'expériences et les conseils tout au long de ces trois années, merci à mes amies d'enfance Mathilde[2] et Mallaurie, ainsi qu'à Laura. Votre intérêt pour mon projet et vos questions m'ont apporté un éclairage nouveau, forcés à réfléchir d'une manière différente, et confortée dans l'idée que malgré les périodes plus compliquées, j'étais exactement à ma place dans ce projet professionnel.

Marc, ta confiance en mes capacités, ta logique et ton pragmatisme m'ont permis de réaliser (presque) sereinement l'écriture du manuscrit et des papiers. Nos nombreuses discussions m'ont permis de prendre conscience d'un nombre conséquent de principes et d'idées, et m'ont fait réaliser que le chemin professionnel que j'ai emprunté me permet d'être pleinement épanouie.

Enfin, un merci empli d'une profonde gratitude envers ma famille et tout particulièrement mes parents. Merci de vous être intéressés à mes travaux, à mon environnement de travail, et merci pour votre soutien le long de mes études. Vous avez toujours été là dans les moments compliqués ou incertains, m'aiguillant au mieux. Vous m'avez donné la possibilité, aussi bien entre terme de liberté de choix que de support financier de poursuivre le projet professionnel que je souhaitais. Cette liberté m'a permis de me poser les bonnes questions pour décider quel sens je voulais lui y donner, et c'est à mon sens l'une des plus belles choses que l'on peut offrir à ses enfants. Je ne peux qu'aspirer à reproduire ce modèle pour mes propres enfants, et vous en suis infiniment reconnaissante.

Table of contents

Figures

Tables

Acronyms

C. difficile: clostridioides difficile

CDI: *C. difficile* Infection

ESCMID: European Society of Clinical Microbiology and Infectious Diseases

SHEA/IDSA: Society for Healthcare Epidemiology of America/the Infectious Diseases Society of America

ASID: Australasian Society of Infectious Diseases

WBC: White Blood Cells

TCA: taurocholate

CA: cholate

DCA: deoxycholate

MCA: muricholate

LCA: lithocholate

UDCA: ursodeoxycholate

HDCA: hyodeoxycholic acid

TcdA: toxin A of *C. difficile*

TcdB: toxin B of *C. difficile*

CDT: *C. difficile* transferase

SLP: S-layer proteins

HMW: High Molecular Weight

LMW: Low Molecular Weight

LID: LMW interaction domain

CWB: cell wall binding

IBD: inflammatory bowel disease

PPI: Protons Pumps Inhibitors

rCDI: recurrent CDI

PAMPs: Pathogen-Associated Molecular Patterns

PRRs: Pattern Recognition Receptors

TLRs: Toll-Like Receptors

ILCs: Innate Lymphoid Cells

DCs: Dendritic Cells

Ig: Immunoglobulin

Ab: antibody

VL: light chain variable domain

CL: light chain constant domain

VH: heavy chain variable domain

CL: heavy chain constant domain

CDRs: complementarity-determining regions

FcR: Fc receptors

GALT: Gut-Associated-Lymphoid-Tissue

pIgR: polymeric Immunoglobulin receptor

sIgA: secretory IgA

V: variable segments

D: diversity segments

J: joining segments

RAG: recombination-activating gene

TdT: terminal deoxynucleotidyl transferase

SHM: somatic hypermutation

AID: Activation-induced (cytidine) deaminase

mAb: monoclonal antibody

HAIs: healthcare-associated infections

CA-CDI: community associated

HA-CDI: Healthcare-associated CDI

rRNA: ribosomal RNA

CRP: C-Reactive Protein

CCNA: Cell culture cytotoxicity neutralization assay

TC: Toxigenic culture

GDH: Glutamate dehydrogenase

EIA: Enzyme immunoassays

NAAT: Nucleic acid amplification test

tcdB: toxin B gene

tcdA: toxin A gene

tcdC: CDT gene

rAb: recombinant antibodies

Fab: fragment antigen-binding

scFv: single-chain fragment variable

FMT: fecal microbiota transplantation

FDA: Food and Drug Administration

sdAb: single-domain antibody

scFv: single-chain variable fragments

SlpA: Surface-Layer Protein A

LuLiSA: luciferase-based ELISA

BLI: Bio Layer Interferometry

K_D: equilibrium dissociation constant

ADC: Antibody-Drug Conjugates

MOI: Multiplicity Of Infection

RCDF: Rassemblement *Clostridioides Difficile* France

L. helveticus: Lactobacillus helveticus

Introduction

I. *Clostridioides difficile* infection (CDI) in the 21st century

1. Generalities of *C. difficile* infection

Clostridioides difficile (formerly *Clostridium difficile*) is a spore-forming Gram-positive bacterium, which was first described in 1935 by Hall and O'Toole[1].

Gram-positive bacteria possess a thick layer of peptidoglycan but lack an outer membrane. On the contrary, Gram-negative bacteria possess a thin peptidoglycan cell wall which is then surrounded by an outer membrane containing lipopolysaccharide[2] (Fig. 1).

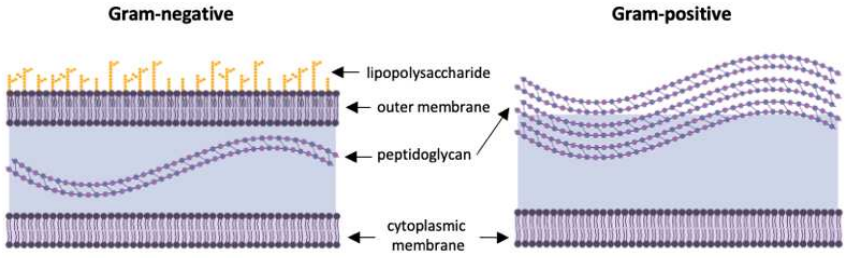

Figure 1. Differences between Gram-negative and Gram-positive membranes

C. difficile name comes from the difficulties to isolate this bacterium and its slow growth in culture medium. This bacterium is strictly anaerobic. Nonpathogenic and pathogenic species exist. Pathogenicity is due to the pathogenicity locus (Paloc) that encodes for the two glucosylating toxins produced by this bacterium: TcdA and TcdB. A third toxin, unrelated to the glucosylating toxins has also been demonstrated to be produced by ~20% of *C. difficile* strains[3]. This last toxin is encoded by a binary toxin encoding locus and is called the binary toxin CDT.

C. difficile infection (CDI) is a public health problem and was identified by the CDC in 2019 as an urgent threat[4]. Indeed, it is the first cause of antibiotic-associated diarrhea and is responsible for more than 95% of pseudomembranous colitis[5]. CDI possesses different degrees of severity, that goes from non-severe, severe, and severe-complicated also named "fulminant"[6]. Guidelines from the European Society of Clinical Microbiology and Infectious Diseases (ESCMID), the Society for Healthcare Epidemiology of America/the Infectious

Diseases Society of America (SHEA/IDSA), and the Australasian Society of Infectious Diseases (ASID) to classify CDI severity are summarized in Table 1. Complications such as pseudomembranous colitis and toxic megacolon carry mortality of ~5% and can reach up to 30% for the most virulent strains[7]. The incidence of this infection has increased of 70% since 2008 and it is a disease with a high percentage of relapses (around 20% after the primary infection)[8].

	IDSA/SHEA 2021	ESCMID 2021	ASID 2016
Non-severe	WBC count of ≤15 000 cells/mL and a serum creatinine level <1.5 mg/dL.	WBC count of ≤15 000 cells/mL and a serum creatinine level ≤50% above baseline, and core body temperature at presentation ≤38.5°C. No imaging features of severity.	Absence of all features consistent with severe CDI.
Severe	One of the following factors at presentation: WBC count of >15 000 cells/mL or a serum creatinine level ≥1.5 mg/dL.	One of the following factors at presentation: WBC count of >15 000 cells/mL or a rise in serum creatinine level >50% above baseline or core body temperature >38.5°C. Additional supporting factors, when available, are distension of the large intestine, pericolonic fat stranding or colonic wall thickening (including low-attenuation mural thickening) at imaging.	Any of the following features if no other explanation can be provided: WBC count of >15 000 cells/mL or a rise in serum creatinine level >50% above baseline or core body temperature >38.5°C. Rigors, haemodynamic instability, peritonitis or evidence of bowel perforation, ileus or toxic megacolon, elevated lactate level, albumin level <25 mg/L, large intestine distension, colonic wall thickening, fat stranding, unexplained ascites (imaging) or pseudomembranous colitis on colonoscopy.
Severe-complicated 'fulminant'	Presence of hypotension or shock, ileus or megacolon.	Presence of one of the following factors that needs to be attributed to CDI: Hypotension, septic shock, elevated serum lactate, ileus, toxic megacolon, bowel perforation or any fulminant course of disease (i.e. rapid deterioration of the patient).	An episode of CDI complicated by: Toxic megacolon, admission to intensive care for severe sepsis, requirement for surgery or death due to CDI.

Table 1. Severity classification of CDI in the three guidelines[6]. WBC: White Blood Cells.

2. Physiopathology of CDI

C. difficile colonizes large intestine of humans, domestic and wild animals. Both toxigenic and nontoxigenic strains exist, but only toxigenic forms lead to disease in humans. Symptoms of this infection range from asymptomatic intestinal colonization to diarrhea, colitis, pseudomembranous colitis, and death. *C. difficile* spores are transmitted via the fecal/oral pathway. These spores can be found on inanimate objects, and one main problem is that they are resistant to commonly used decontaminants. They can persist for a long period of time as spores without losing any viability[9]. For instance, spores of hypervirulent *C. difficile* strains such as the BI/NAP/027 can stay for up to six months in the dormant state[10].

Once spores have been ingested and to cause successful infection, *C. difficile* spores must germinate, grow within the intestinal lumen, and produce toxins that mediate tissue damage and inflammation[11]. Specific chemical signals are needed for each of these steps. Bacterial spore germination requires the presence of small molecules called germinants that will be sensed by the bacterium. *C. difficile* germination mechanisms are complex, but studies converge in pointing the role of specific primary bile acids such as cholate and its derivatives (taurocholate (TCA), glycocholate, cholate (CA) and deoxycholate (DCA)), with L-glycine acting as a co-germinant (Fig. 2)[12]. Primary bile acids assist in digesting fat and to do so, they are produced in the liver, released into the small intestine, and reabsorbed from the small intestine. A small amount of these is not reabsorbed and passed into the colon. In the colon, these primary bile acids are metabolized into secondary bile acids by certain members of the normal gut microbiota. These secondary bile acids inhibit growth of *C. difficile* vegetative cells[13]. Some bile acids have an ambivalent role: for instance, DCA helps in the germination of the spores but inhibits vegetative growth[14].

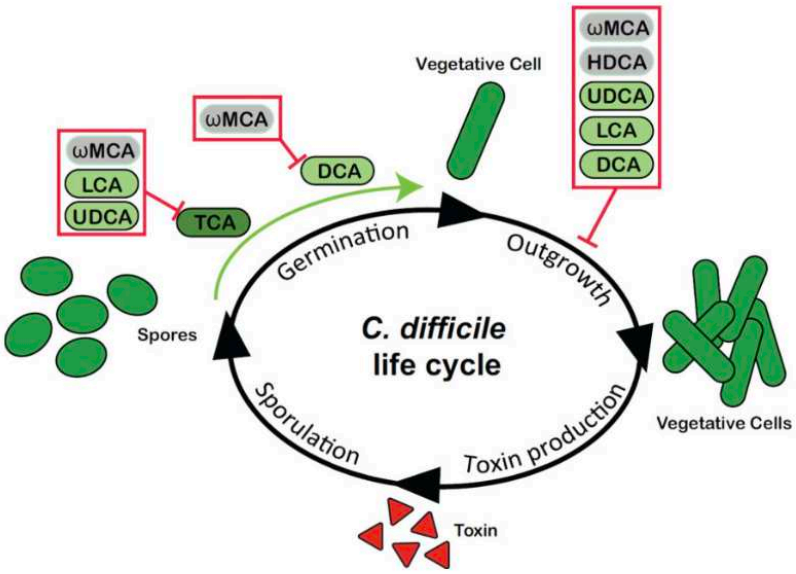

Figure 2. Impact of bile salts on *C. difficile* life cycle[15]. MCA: muricholate, LCA: lithocholate, UDCA: ursodeoxycholate, TCA: taurocholate, DCA: deoxycholate, HDCA: hyodeoxycholic acid.

Once spores have germinated, vegetative cells arrive in the duodenum where they will encounter host gut microbiota. The human gut contains around 10^{14} bacterial cells with a diversity of thousands bacterial species[16]. Four major phyla of bacteria reside in our lower

intestine: *Firmicutes*, *Bacteroidetes*, *Actinobacteria* and *Proteobacteria*. Along with protozoans, fungi and bacteriophages, these bacteria play an important role in maintaining the balance that prevent pathogens from colonizing and invading the human body and provoking diseases[17]. The normal gut microbiota normally prevents the overgrowth of *C. difficile* ingested spores, through production of secondary bile acids, competition for essential nutrients and attachment sites to the gut wall[18]. However, antibiotic treatments, by disrupting the gut microbiota, provide a niche for colonization by intestinal pathogens (Fig. 3). Two phyla: *Bacteroides* and *Firmicutes* appear to play a major role in the pathophysiology of *C. difficile*[19]. Indeed, these members have been described to be involved in the transformation of primary bile acids to secondary one[20]. Loss of secondary bile acids and an increase in primary bile acids create a favorable environment for spore germination and vegetative cells growth of *C. difficile*.

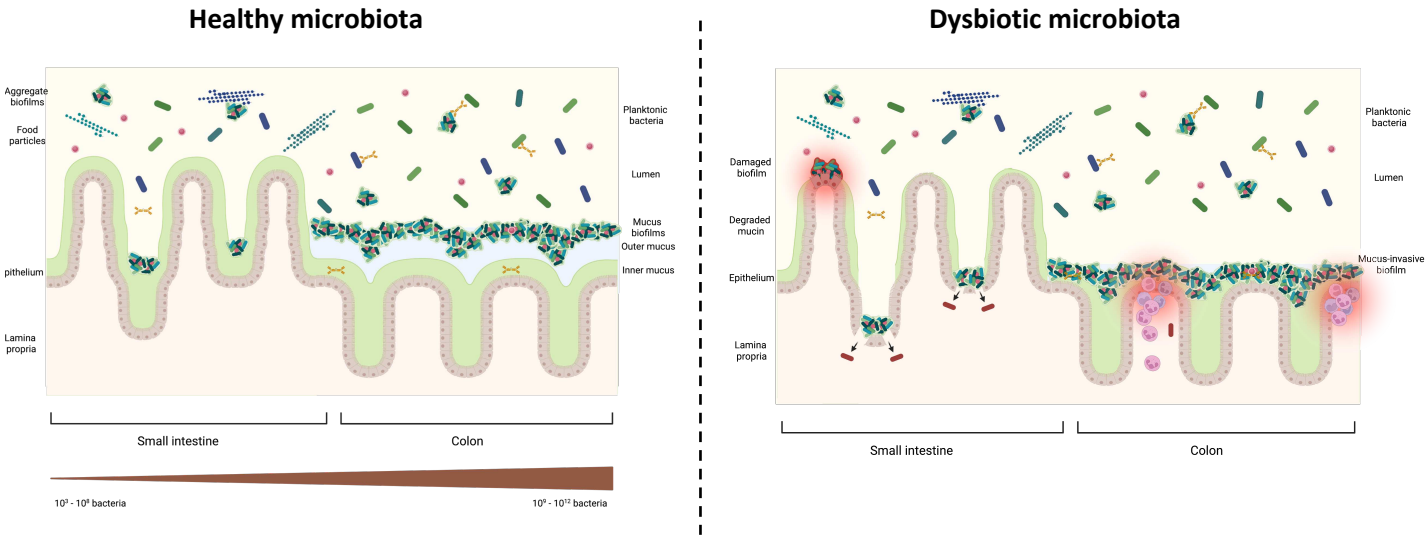

Figure 3. Healthy *versus* dysbiotic microbiota, adapted from Meza-Torres *et al.*[21] Healthy microbiota is characterized by the presence of a thick mucus layer and bacteria that are embedded in biofilms. Mucus is degraded in the case of dysbiotic microbiota and bacteria can invade and breach the epithelium. Immune cells are therefore recruited and can start to secrete pro-inflammatory signals. Created with Biorender.com.

Colonization by *C. difficile* is accompanied by secretion of toxins for the pathogenic strains. Both pathogenic and non-pathogenic strains of *C. difficile* exist, with only the pathogenic strains possessing the PaLoc locus. This locus is responsible for the production of toxins and can be transferred on to non-pathogenic strains via horizontal gene transfer[22]. *C. difficile* pathogenicity is mainly due to the release of two major toxins: toxin A (TcdA), toxin B (TcdB) and in 25%

of clinical strains, of the *C. difficile* transferase (CDT) or binary toxin. Both TcdA and TcdB share a common molecular mechanism of action that consists of inactivating the Rho GTPases through enzymatic glycosylation of a conserved threonine residue. This leads to actin disorganization, opening of tight junctions and finally cell death. They also contribute to inflammatory response that exacerbates tissue damage, diarrhea, and pseudomembranous colitis (Fig. 4.a)[23]. The mechanism of the binary toxin resembles the one of iota-toxin from *Clostridium perfringens*: both toxins cause disruption of the actin cytoskeleton that induces the formation of microtubule-based cell protrusions. These protrusions increase the adherence of *C. difficile* to the gut epithelium and therefore its colonization (Fig. 4.b)[24]. Both enhanced bacterial toxins and diminished host response contribute to symptomatic disease.

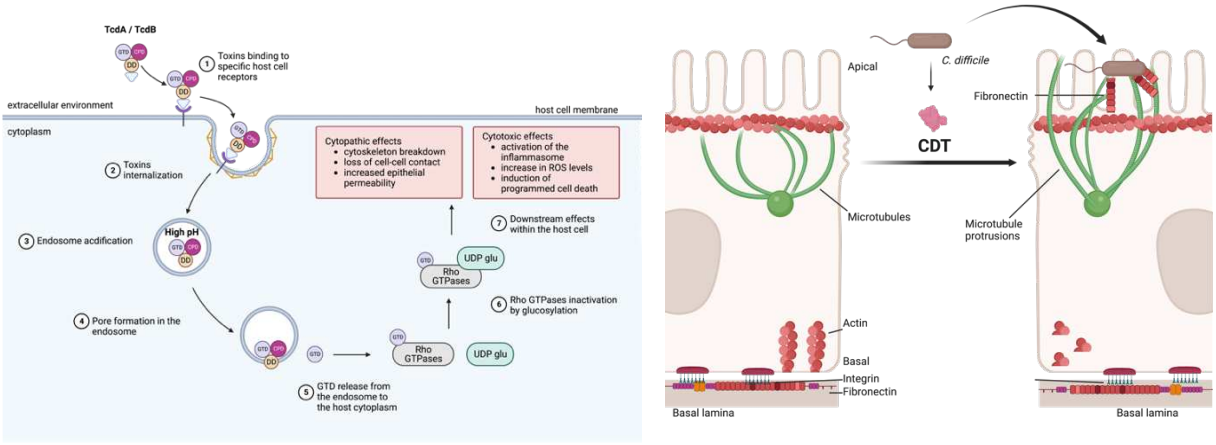

Figure 4. *C. difficile* toxins mechanisms. **a)** Mechanisms of action of TcdA and TcdB toxins, adapted from Bella *et al.*[25]. **b)** Mechanisms of action of the binary toxin CDT, adapted from Aktories *et al.*[26]. Created with Biorender.com.

After gut microbiota disruption by antibiotics, pathogenesis of *C. difficile* infection can be summarized as a three-step process that starts with (1) contamination and germination of spores, followed by (2) multiplication of vegetative cells in the colonic niche using colonization factors and (3) production of toxins TcdA, TcdB and for some strains CDT[27]. Among the colonization factors, the S-layer of *C. difficile* plays a major role[28].

3. S-layer

3.1. Bacterial S-layer

Cell-surface layers or S-layers are structures of the bacterial cell envelope with a lattice-like appearance that are formed by a self-assembly process[29]. Composed of two-dimensional crystalline arrays formed of individual subunits, they have first been described in prokaryotic organisms in 1952[30]. S-layers subunits self-assemble into regular and highly porous arrays with oblique (p1, p2), square (p4) or hexagonal (p3, p6) symmetry that fully cover the microorganism during all stages of growth (Fig. 5)[31].

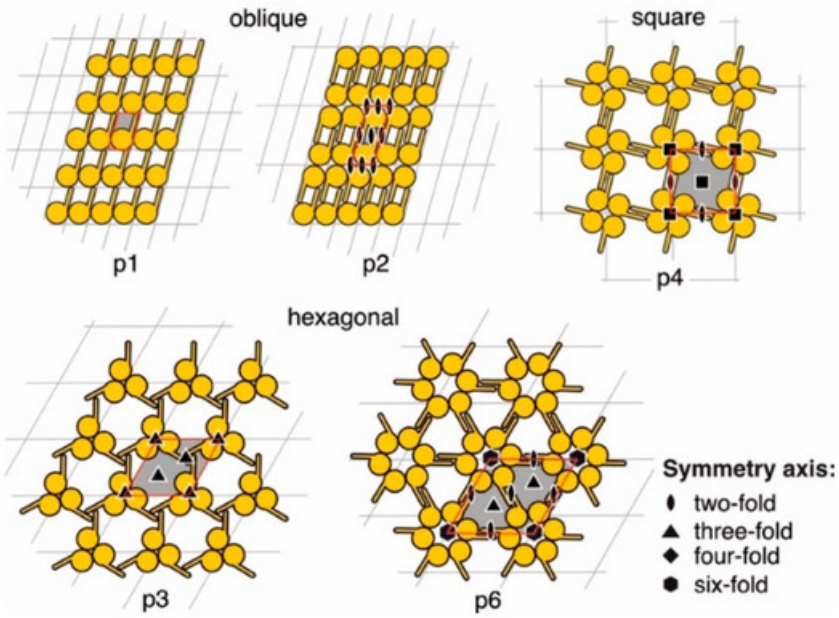

Figure 5. Schematic drawing of different S-layer lattice types with their symmetry axes[32].

S-layer genes are highly expressed by microorganisms, but there is a low overall sequence similarity between them and no universal signature sequence. Therefore, S-layer detection on a microorganism relies on electron microscopy. S-layer proteins (SLP) are modified with covalently linked glycan chains that are facing the extracellular environment. Contrary to the glycans of the flagella and pili that are relatively short (1-20 residues), long-chain glycans (~150 glycoses) are attached to S-layer glycoproteins[33]. SLP are water-insoluble proteins regardless of the glycosylation.

As the outermost layer, SLP are in direct contact with bacterial environment and are thus involved in adherence to various substrates, mucins or eukaryotic cells, aggregation with other microorganisms, biofilm formation and are responsible for bacterial protection against detrimental environmental conditions. Therefore, these proteins play an important role in surface recognition or as carriers of virulence factors[21].

3.2. *C. difficile* S-layer

C. difficile S-layer was discovered in 1984 by *Kawata et al.,* showing two main proteins of 42 - 48 and 32 - 38 kDa whose size varies in different strains of *C. difficile*. This cell wall, arranged in a square array, is composed of a two-layered structure, an inner one of 20 nm and an outer one of 10 nm[34]. Of note, the expression of two SLPs is unusual as most bacteria express only one. The structural gene slpA that codes for the SLPs in *C. difficile* has been identified by *Calabi et al*. in 2001. After the removal of a signal peptide and cleavage, a common precursor releases two mature proteins termed High Molecular Weight (HMW) and Low Molecular Weight (LMW) SLP, which vary in conservation among strains and glycosylation. The HMW is highly conserved among strains and is glycosylated whereas the LMW shows considerable sequence diversity and is not glycosylated[35]. Both the HMW and LMW are exposed at the cell surface[36]. These two subunits are associated through the N-terminus of the HMW protein and the C-terminus of the LMW protein[37], forming two layers in which the LMW layer is the most external one. Different domains of the LMW have been recently characterized. One is involved in the interaction with the HMW and is called LMW interaction domain (LID). The LMW then protrudes from the interacting domains with D1 domain that is the closest to the HMW and D2 domain that extends outwards at an angle of 120°[38].

Secretion of SlpA to the membrane involves SecA2 protein and the secretory channel SecYEG. SlpA is produced as a pre-protein that is then secreted and processed by the cell surface cysteine protease Cwp84 into LMW and HMW SLP subunits[39]. This heterodimeric complex is anchored to cell wall polysaccharide PS-II via three cell wall binding (CWB) motifs within the HMW region[37] (Fig. 6).

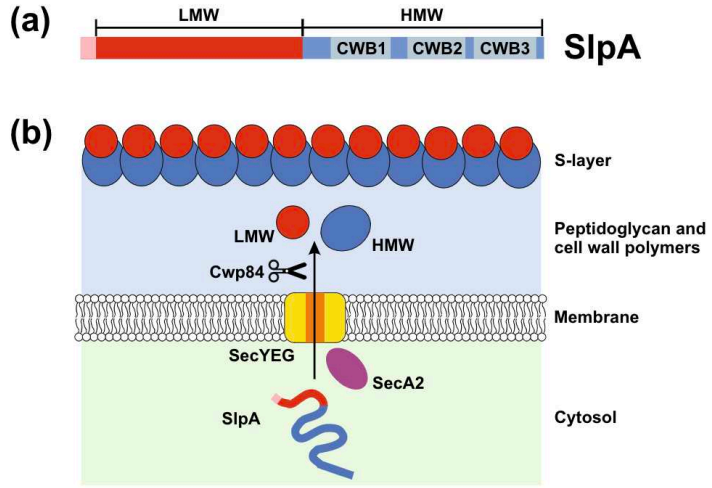

Figure 6. Schematic representation of the S-layer and mechanisms that form it. **a)** SlpA precursor protein with signal sequence in pink, LMW in red and HMW in blue with the three CWB domains in grey. **b)** Schematic diagram of SlpA secretion and processing at the membrane[40].

SlpA is secreted all over the cytoplasmic membrane and constitute a pool within the cell wall which is available to fill the gaps that form during cell growth or disruption (Figure 7). Of note, SlpA is present in the spores' proteome, but its exact place on the spore is not known[41].

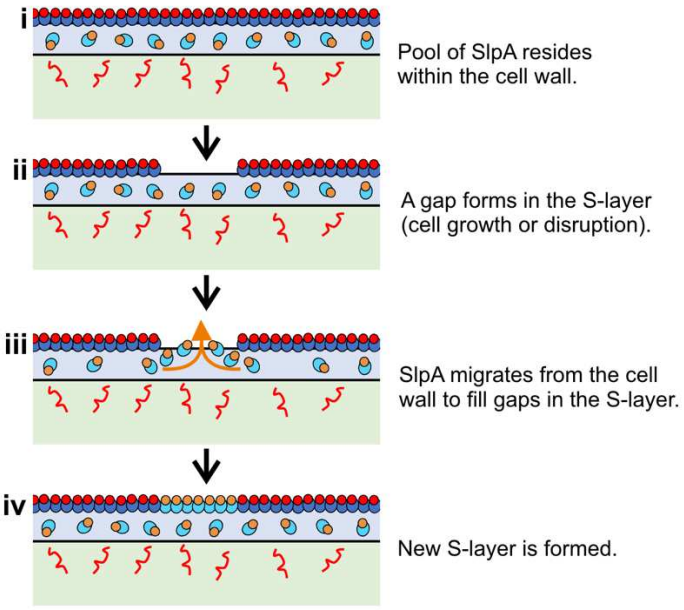

Figure 7. Model proposed by Fagan *et al.* for the formation of new S-layer[40]. LMW is in red while HMW is in blue. SlpA is produced and forms mature S-layer composed of LMW and HMW subunits that are in the cell wall (i). When a gap forms in the S-layer because of cell growth or disruption (ii), SlpA migrates from the cell wall to the surface to fill the gaps (iii), therefore creating new S-layer that maintains the integrity of the bacterial surface (iv).

In a study conducted by Pantosti *et al.*, sera from CDI patients were able to recognize the LMW SLP, suggesting for the first time that other *C. difficile* antigens than toxins were able to elicit an immunological response[42]. Other studies confirmed LMW SLP immunogenicity in CDI patients and vaccination in animal models (mice and hamsters) showed production of specific IgG and IgA antibodies against SlpA[43,44].

SlpA is involved in adherence to host cells[28,45], and vaccination in mice and hamsters allowed decreased colonization and a slight prolonged survival in hamsters [43,44], confirming the key role of the S-layer in CDI. Of note, SlpA is not a typical adhesin since it covers the whole bacterium and is continuously produced as the bacteria grow. Several other adhesins of *C. difficile* have been characterized: the flagellin FliC, the flagellar cap protein FliD[46], fibronectin-binding proteins[47], a heat-shock protein GroEL[48], the surface associated protein Cwp66[49].

3.3. Roles of *C. difficile* S-layer

Only two mutants lacking the S-layer were obtained by groups working on *C. difficile*. These two mutants appeared at a frequency of $< 1 \times 10^{-9}$, confirming the crucial role of the S-layer in the viability of the bacteria. Derived from the ribotype 027, these mutants did not have a growth that was significantly different from *C. difficile* with an S-layer, even if one mutant had an earlier entry into stationary phase. Despite having a normal growth, these mutants were abnormally sensitive to lysozyme and LL-37, an antimicrobial peptide found at mucosal surfaces[50]. Salagado *et al.* showed that the S-layer harbors pores of only 10Å compared to 30-100Å described in other bacterial surface, confirming the role of the S-layer in providing integrity to the bacteria and resistance to large biomolecules[38].

SlpA is also involved in the sporulation process, as it was shown that the mutants lacking an S-layer had severe sporulation defects. Spores were less resistant to heat, and this could be linked with minor defects in their morphology, which could not be observed with transmission electron microscopy[50].

The role of SlpA in toxin secretion has not been studied yet. There is one study with S-layer null mutants that showed a decreased production of TcdB *in vitro.* These mutants were also avirulent in hamsters *in vivo* despite a colonization comparable to the reference strain[50] but

evidence that this is linked to the S-layer are lacking. Indeed, bacterial fitness in this mutant is so affected that the bacterium might favors its survival over its virulence. How the toxins go through the S-layer remains to be elucidated.

Finally, it has been demonstrated that SlpA is a common receptor used by many siphophages and myophages[51]. This is of crucial importance since therapeutic bacteriophages could soon be part of the alternatives to treat antibiotic-resistant bacteria, and therefore CDI. Using the mutants lacking the S-layer, Royer *et al.* showed that they were resistant to infection with various phages. More precisely, deletion of the D2 domain within the LMW SlpA was found to abolish infection by some phages[51]. Variability of the LMW SlpA is nonetheless a limitation for phage recognition.

The roles of the S-layer in various physiology processes of *C. difficile* are summarized in Figure 8.

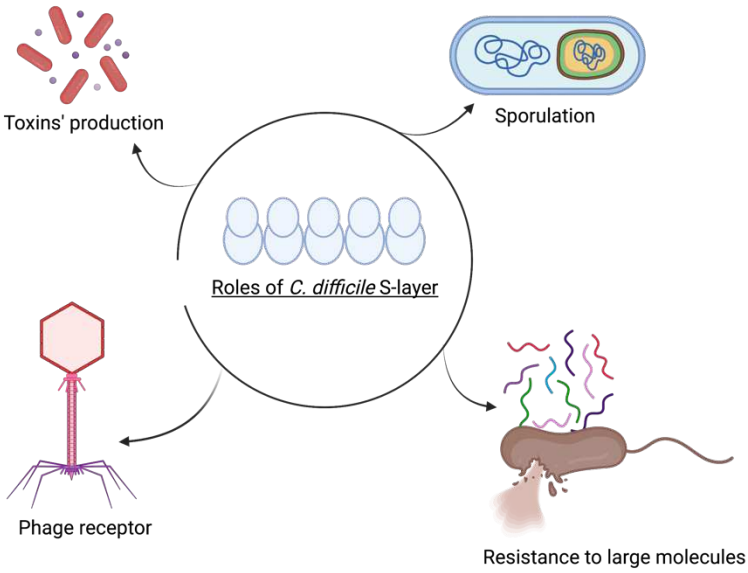

Figure 8. Recapitulative scheme of the involvement of *C. difficile* S-layer in various processes. Created with Biorender.com.

4. Risk factors and recurrent CDI (rCDI)

4.1. Risk factors

The use of broad-spectrum antibiotic, hospitalization, advanced age, and comorbidities increase the risk of developing CDI[52]. Indeed, patients at highest risk for CDI are hospitalized >65 years old persons, with recent antibiotic exposure[53]. On the contrary, clinical illness is rarely reported in infants that are aged of less than 12 - 24 months[54].

Broad-spectrum antibiotics disrupt gut microbiota of patients, leaving room for *C. difficile* colonization. The main culprits are clindamycin, cephalosporins, carbapenems, fluoroquinolones and trimethoprim/sulphonamides[55].

Comorbidities notably include inflammatory bowel disease (IBD), diabetes, leukemia or lymphoma, renal failure, and solid cancer[56].

Other risks factors have been discussed in the literature, such as the use of Protons Pumps Inhibitors (PPI). These are used to treat acid-related upper-gastrointestinal disorders such as peptic ulcer disease and gastro-esophageal reflux. PPIs have been linked with CDI and recurrent CDI (rCDI) in several studies[57–59]. However, results mainly come from observational studies, and it is not clear what is the predominance of polypharmacy and co-morbidities compared to usage of PPIs. As of now, causality between PPIs and CDI is not clearly established.

Immunosuppressive treatments are also a risk factor for CDI. One study found that immunosuppressed patients were more colonized with *C. difficile* and that relapses were happening more frequently whereas other found that it increased the risk of CDI recurrence by 3.88 times[60,61]. Indeed, immunosuppression leads to higher consumption of antibiotics, therefore creating dysbiosis in the microbiota that favor the development of CDI.

4.2. Recurrent CDI (rCDI)

A first episode of CDI is followed by a symptomatic recurrence in 15 - 35% of patients affected, and in the patients who had a first recurrence, the risk of having another one is around 45%[62,63]. rCDI can either be due to a relapse which is caused by the same strain of *C. difficile* or reinfection that is caused by another new strain. 33% to 75% of rCDI are due to reinfection.

Relapse with the same strain typically happens during the 14.5 days after the first episode, whereas reinfection happens during the next 42.5 days[64,65].

Persistence of *C. difficile* in the gut has been associated with the presence of spores that will survive antibiotic treatment and germinate once the antibiotic treatment is ceased. Evidence is based on studies which showed that spores can enter epithelial cell[66] and that non-sporulating mutants are unable to cause relapse[67]. However, this evidence seems to explain the recurrence only partially, and biofilms have been hypothesized to play a role in recurrent CDI.

Biofilms are bacterial communities embedded into a matrix composed of proteins and extracellular DNA. *C. difficile* is able to form mono and mixed biofilm *in vitro*, as shown with *C. scindens*[68], and can be hosted by multi-species biofilms which could then be a reservoir for recurring infections[69]. In hamsters or mice, biofilm-like structures have been observed[70,71]. Altogether, these findings provide good evidence that *C. difficile* can form biofilm communities in the gut and a rational for a mechanism for recurrent infections. Based on these findings, Jazmin *et al.* proposed a model for short-term and long-term relapses (Fig 9). Short-term relapses are mainly due to spores that are internalized by enterocytes, which, when the epithelium renew will release the spores into the intestine. Spores will then germinate under favorable conditions leading to colonization by vegetative cells. On the contrary, long-term relapses are linked with biofilms formed with *C. difficile*. In these biofilms, vegetative cells are less sensitive to antibiotics and will not be destroyed during the first treatment. Spores are also packed into biofilms. Then, both spores and vegetative cells can detach from biofilm and start a new episode of CDI.

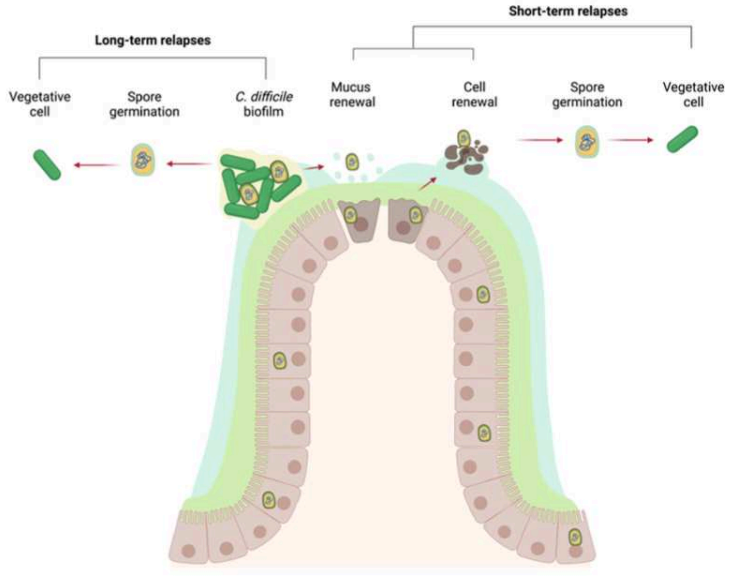

Figure 9. Model for persistence of *C. difficile* in the gut and cause of recurrence[72]. In this model, short-term relapses are due to spores that are endocytosed by enterocytes that are then released when the cell renew. Spores then germinate into vegetative cell. Long-term relapses are due to *C. difficile* biofilm that contain spores that can then detach from the biofilm and germinate into vegetative cell which will start a new cycle of colonization.

- *C. difficile* is a Gram-positive, anaerobic bacterium giving CDI.
- Toxins are responsible for the symptoms of this infection.
- The S-layer plays important roles in the colonization and development of the infection.
- Relapses are one of the main issues of this infection.

II. Immunity against *C. difficile*

After infection with *C. difficile* spores, the host immunity reacts with two lines of defense: the innate immune system and the adaptive immune system.

1. Innate immune response in CDI

The first line of defense is made of the epithelial barrier, composed of enterocytes and mucus. In addition to its functions in digestion, nutrient transport, water and electrolyte exchange, as well as endocrine and paracrine hormone production[73], the intestinal epithelium defines the barrier between the host and external environment. This barrier protects the body against invasion and systemic dissemination of both pathogenic and commensal microorganisms. The intestinal barrier provides a combination of sensing and defense mechanisms that lead to permanent protection against intrusion by commensal microorganisms. This leads to a state of physiological inflammation. Moreover, a thick layer of mucus enables protection. Indeed, interactions between mucins and bacterial cell-surface polysaccharides and proteins, as well as the release of mucin granules when atypical signals are sensed provide defense to the host. Entero-invasive bacterial pathogens however stimulate these innate mechanisms of mucosal protection that can result in rupture and inflammatory destruction of the epithelium.

In the case of CDI, *C. difficile* toxins breach this epithelial barrier, by causing disruption of the tight junctions, inflammation, cell death and therefore allowing the infection to spread. The second line of defense, the innate immune response, then activates[73]. Recognition of a pathogen by the innate immune system goes through Pathogen-Associated Molecular Patterns (PAMPs) that are molecular motifs characteristic of micro-organisms. These motifs are recognized by host receptors that are called Pattern Recognition Receptors (PRRs). These non-specific interactions between PRRs and PAMPs provide a very quick defense against bacteria but are not specific of *C. difficile*[74].

C. difficile interacts with Toll-Like Receptors (TLRs) with its surface components. Then, TLRs activate the transcription factor NF-kß which lead to the production of inflammatory cytokines and chemokines. Indeed, SLPs, flagella, and heat-shock proteins were demonstrated to trigger

the production of pro-inflammatory cytokines (TNF-α, IL-1β, IL-6, IL-8 and IL-12p70) by macrophages[75]. S-layer proteins interact with TLR4 and both the HMW and the LMW proteins were demonstrated to be needed for this interaction. In this line, it was also shown that flagellin interact with TLR5. Flagellin monomers can be secreted during the assembly of the flagella or sheared by bacteria. It is not completely understood how TLR5 distinguishes between pathogenic and commensal bacteria. Part of this explanation might reside in the fact that most TLR5 are distributed on the basolateral side of colonic epithelial cells so that detection of flagellin relies on bacteria that are able to deliver flagellin to the basolateral surface, implying breaches and invasion of the epithelium[76]. Extracted flagellin from *C. difficile* has been demonstrated to induce activation of NF-kB and promoting the production of IL-8 and CCL20 in intestinal epithelial cells via TLR5[77]. These results were also confirmed with recombinant *C. difficile* flagellin and *C. difficile* strains by another team[78]. Moreover, the authors observed the up-regulation of genes mainly involved in NF-kB signaling pathway by *C. difficile* FliC.

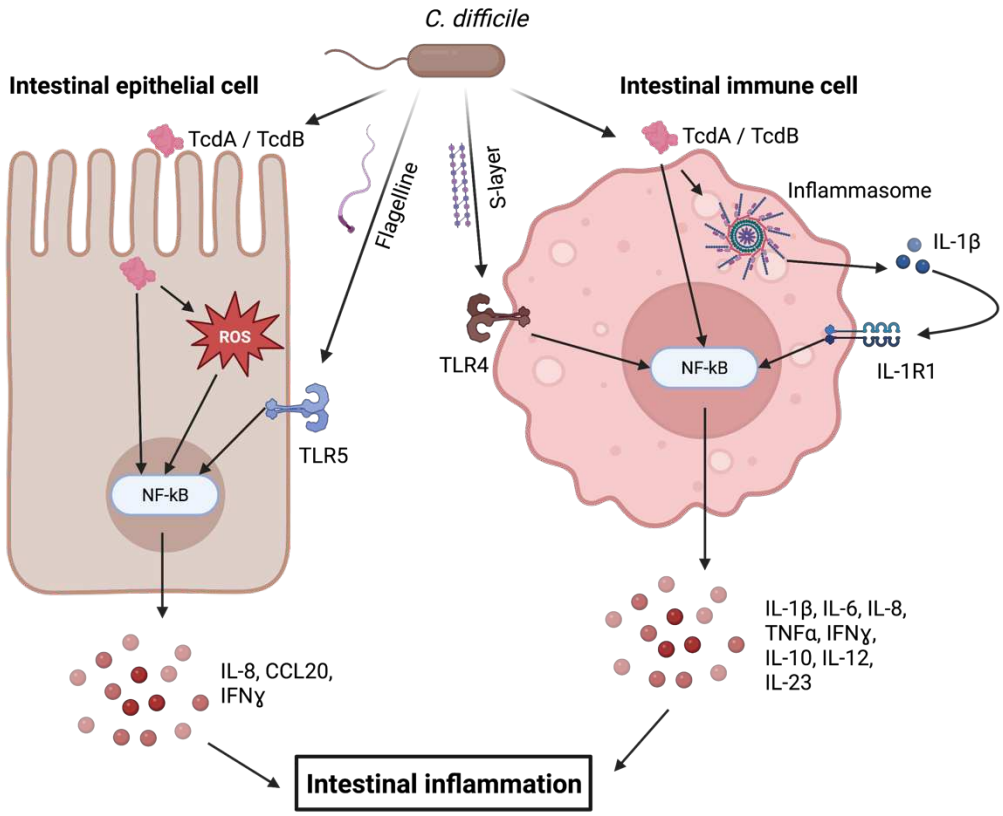

Figure 10. Innate signaling pathways activated by *C. difficile* in intestinal epithelial and immune cells, adapted from Péchiné *et al.*,[74]. Created with Biorender.com.

C. difficile toxins, by disrupting the epithelium, induce a pro-inflammatory response with the secretion of inflammatory chemokines (IL-8, CCL20, CXCL13, CXCL10) and cytokines (Interleukin-1ß (IL-1ß), IL-6, IL-8, IL-17A, IL-16, TNF-α, IFN-γ), which triggers neutrophil recruitment and defensin production (Fig. 10)[79–83]. Neutrophil influx in the mucosa is a characteristic of CDI and a first step that is then leading to the formation of pseudomembranes in severe cases. *C. difficile* toxin A was shown to elicit intestinal fluid secretion and neutrophil infiltration in mice, both by mast cell-dependent and independent pathways[84]. Intestinal inflammation is central in CDI, and magnitude of the inflammatory response correlates with a poor outcome[85].

Innate Lymphoid Cells (ILCs) have also been demonstrated to play a critical role in defense against *C. difficile*. Indeed, mice with a developmental defect in ILC maturation were more susceptible to CDI[86]. More recently, RAG-deficient mice that were lacking T and B cells but not ILCs showed an upregulation of ILC1 and ILC3 following *C. difficile* infection and in a model lacking ILCs as well as T and B cells, mice rapidly succumbed to infection[87].

At the border between innate and adaptative immunity, Dendritic Cells (DCs) play a major role in the regulation of intestinal mucosa inflammation. SLPs induce maturation of DCs and therefore the generation of a T-helper cell response that push cytokines production of the host towards an inflammatory state (IL-12p70), which contributes to the intestinal epithelium damage[88,89]. In cases of spontaneous resolution of CDI, antigen processing by DCs generates a non-inflammatory Th2 response suggesting that this regulatory mechanism evolved to maintain gut immune homeostasis in response to the inflammation triggered by the bacteria.

2. Adaptative immune response in CDI

2.1. Generalities on effectors

2.1.1. At the beginning: T and B cells

Induction of an adaptive immune response begins with the activation of specialized antigen-presenting cells such as DCs. Then lymphocytes proliferate in response to antigen in peripheral lymphoid organs, therefore generating effector cells and immunological memory. Two types of

cells form this immune component: T cells and B cells[90,91]. On one hand of this immune response, T cells are divided in two major subtypes which are the CD8+ cytotoxic cells and the CD4+ helper cells[92–94]. On the other hand, B cells produce immunoglobulin molecules called antibodies which are either secreted or inserted into the plasma membrane where they form what is called B-cell receptors[95,96]. The following paragraphs will focus on this branch of adaptive immunity.

2.1.2. The center of the humoral response: antibody

Immunoglobulin (Ig), also called antibody (Ab) is a Y-shaped protein whose role is to identify and neutralize molecules that are unknown from the organism[97,98]. To do so, it recognizes a unique epitope at the surface of a molecule called an antigen. This particular epitope on the antigen can be recognized by the two paratopes of the antibody, that are located at the tip of the Y-shape (Fig. 11).

.

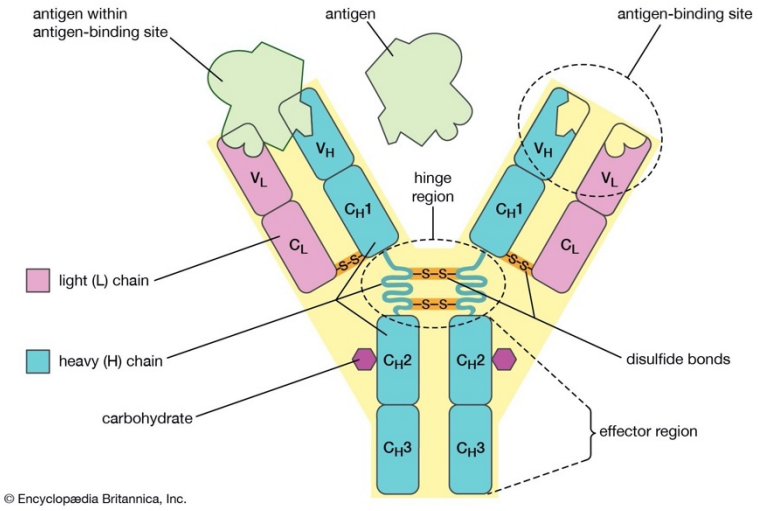

Figure 11. Structure of antibody and binding to its antigen[99]. Antigen-binding site involves V_H and V_L while effector functions rely on constant parts C_H2 and C_H3 corresponding to the Fc of an antibody. Variable parts with the constant part C_L or C_H1 are called Fab region. Hinge region links the Fab region to the Fc.

These 150 kDa proteins are composed of four polypeptides chains which include two identical heavy chains and two identical light chains, connected by disulfide bonds[100,101]. Light chains are composed of one variable domain (VL) and one constant domain (CL), while heavy chains

are composed one variable domain (VH) and three to four constant domains, (CH1, CH2, CH3, CH4), depending on their classes[102]. Indeed, an antibody is composed of two antigen-binding fragments that are called Fab and which contain one V_L, V_H, C_L and CH1 domain each, and the crystallizable fragment Fc that forms the base of the Y shape[103,104]. On the variable domains of the antibody can be found complementarity-determining regions (CDRs). A set of three CDRs constitutes a paratope and there are therefore six CDRs in one antibody. The Fc region, formed by the constant domains from the heavy chain, plays a major role in modulating immune cell activity. It is where effector molecules bind, and it triggers various effects once the Fab region on the antibody has bound to an antigen[105,106]. Effector cells such as macrophages, neutrophils, natural killer cells have Fc receptors (FcR) that bind to this Fc region. Complement system is also activated by binding of IgG and IgM to the C1q protein complex. Of note, IgA cannot bind to C1q and therefore does not activate the classical complement pathway[107].

There are 5 classes or isotypes of antibodies in humans, depending on the Fc portion: IgA, IgD, IgE, IgG and IgM (Fig. 12)[108–110]. Ig classes operate in distinct compartments (Fig. 13) and have distinct effector functions.

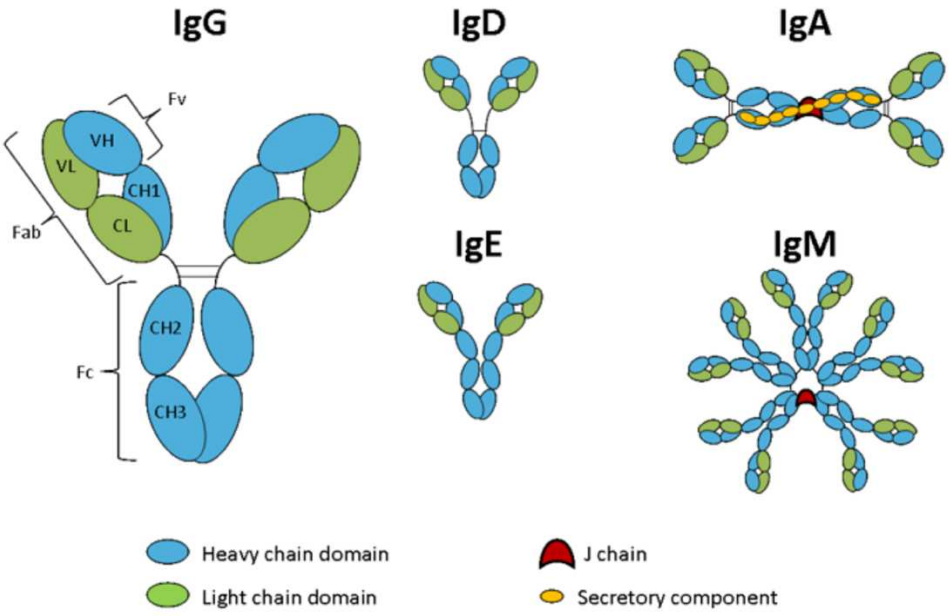

Figure 12. Schematic representation of the five immunoglobulin classes or isotypes in humans[111]. Heavy chains are represented in blue while light chains are in green.

IgM are the first to be produced in a humoral response and form pentamers. They are mainly found in the blood and in the lymph[106]. IgG and IgE are monomeric whereas IgA can form dimers. IgG is the principal isotype in the blood and extracellular fluids whereas IgA predominates in secretions, the most important being those of the epithelium lining the intestinal and respiratory tracts[112]. This isotype therefore plays a critical role in mucosal bacterial infections.

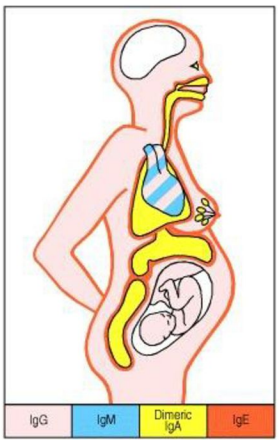

Figure 13. Distribution of immunoglobulin isotypes in the body[106].

2.1.3. Focus on IgA

There are two types of IgA in humans: IgA1 and IgA2. These two types are not always found in mammals, especially not in mice. Interestingly, IgA1 possesses a longer hinge region than other IgA2 composed of 13 amino acids, covered by O-glycans (Fig. 14). This particularity appeared late in evolution and is not present in murine IgA[113,114]. Consequently, IgA1 has more a “T” shape than a “Y” shape and is susceptible to bacterial proteolysis whereas no protease has been described for IgA2 as of now[107,115].

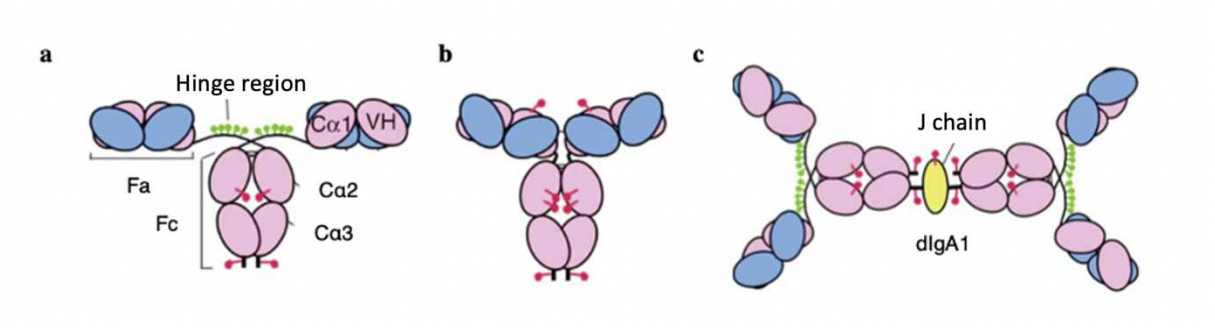

Figure 14. IgA structure. **a)** Schematic representation of IgA1. **b)** Schematic representation of IgA2. **c)** Schematic representation of dimeric IgA1. Heavy chains are in pink, light chains in blue and J chain in yellow. N- and O- glycosylation sites are represented in red and green respectively[107].

Daily production of IgA exceeds every other immunoglobulin class, with a total of 66 mg/kg/j [116]. However, repartition of IgA subclasses varies in the body: IgA1 is mainly found in serum (90-95% of total IgA, corresponding to a mean of 1,7g/L)[117] whereas IgA2 is mostly found at the mucosa. However, IgA1 still represents 80% of nasal IgA and 60% in the saliva and ileon[118,119]. In maternal milk which contains a lot of IgA, isotypes can be found in equal proportions[120].

IgA is mainly found as monomer in serum but predominates as dimers at the mucosa -and to a lesser extend trimers and tetramers-[107,112]. Both IgA1 and IgA2 subclasses can form dimers and polymers, where IgA monomers assemble with a covalent liaison between Fc fragment and J chain. This J chain is synthesized by plasma cells and is a highly conserved peptide composed of 8 cysteines forming disulfide bonds with terminal residues of Fc fragments[121,122].

IgA is secreted by plasma cells in the lamina propria. These long-lived B cells are specialized in Ig secretion and reside in Gut-Associated-Lymphoid-Tissue (GALT)[118,123,124]. Once synthesized, IgA is actively transported in the intestinal lumen across epithelial cells with the polymeric Immunoglobulin receptor (pIgR). This receptor is constitutively expressed at the basal pole of enterocytes. Dimeric IgA fixes to the pIgR and once internalized, the complex goes across epithelial cell and is excreted in the intestinal lumen. This process is called transcytosis. Extracellular part of pIgR is cleaved during transcytosis and becomes the secretory component of IgA that protects dimeric IgA from proteolysis[125,126]. Intramembranous part of pIgR is re-internalized (Fig. 15). This dimeric IgA – secretory component complex is frequently described as secretory IgA (sIgA)[127].

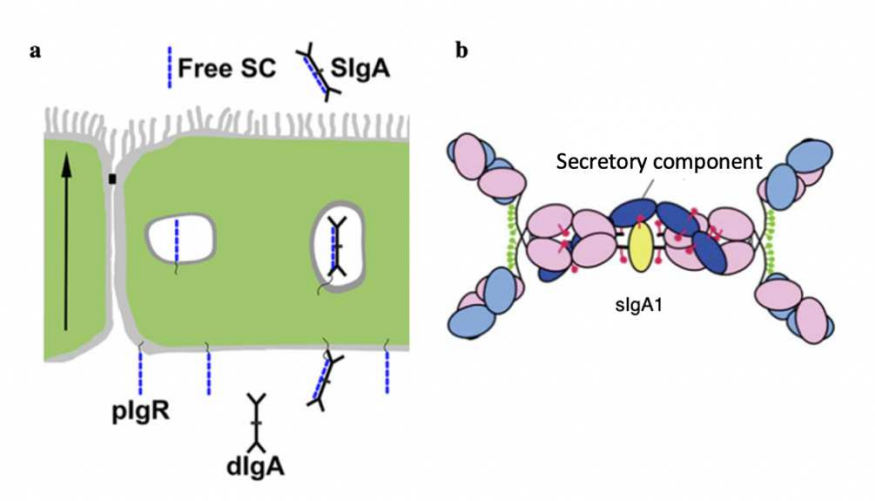

Figure 15. Transcytosis of IgA through enterocytes. **a)** Dimeric IgA bound to pIgR (blue) through the J chain at the basal pole of enterocytes. This complex is endocytosed and crosses cytoplasm of epithelial cell. pIgR is cleaved at the apical pole and free sIgA is released in the intestinal lumen. **b)** Schematic representation of secretory IgA1 with its glycosylation sites. pIgR domains are represented in blue. N-glycosylation sites are indicated in red[107,128].

This transcytosis mechanism is used for IgM and IgA independently of their sub-classes or the type of mucosa[129,130]. On the contrary, monomeric IgA and IgG synthesized in the lamina propria are not transported by pIgR. IgG is only found in the lamina propria under pathologic conditions[131–133].

2.1.4. The diversity of immunoglobulins: how to generate billions of antibodies?

Humans can generate billions of different antibodies, capable of binding to distinct epitopes[134]. This diversity relies on complex genetic mechanisms allowing B cells to generate a diverse pool of antibodies from a relatively small number of antibody genes[135]. The variable regions of each immunoglobulin heavy or light chain are encoded in several gene segments. These segments are called variable (V), diversity (D) and joining (J) segments[136]. V, D and J gene segments are found in Ig heavy chains but only V and J segments are present in Ig light chains. As there are multiples copies of each type of gene segment and that different combinations of gene segments can be used to generate each immunoglobulin variable domain, this process can generate a maximum 10^6 antibodies with different paratopes and therefore different antigen specificities (Fig. 16)[137]. Moreover, the involvement of several enzymes such as recombination-activating gene (RAG) and terminal deoxynucleotidyl transferase (TdT) proteins is crucial in V(D)J

recombination and generating antibody diversity. RAG enzymes are involved in recombination and participate in combinatorial diversity while TdT randomly add nucleotides during recombination, creating junctional diversity. Junctional diversity is far more important than combinatorial diversity[138].

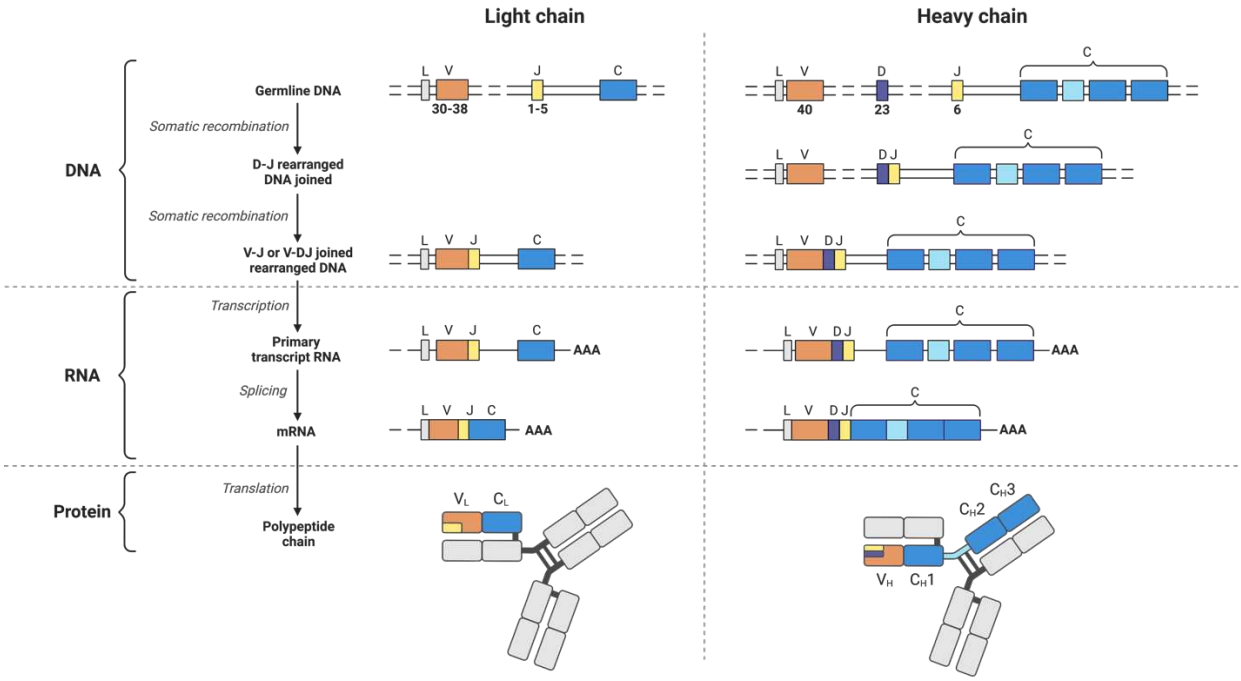

Figure 16. Schematic representation of V(D)J recombination of immunoglobulin chain and transcription and translation into an antibody. Created with Biorender.com.

Antibodies newly generated then undergo affinity maturation and class switching. Affinity maturation is the process by which Follicular Helper T cells activate B cells to produce antibodies with increased affinity for their antigen. This takes place in the germinal centers of the secondary lymphoid organs and is composed of two processes which are somatic hypermutation (SHM) and clonal selection. Activation-induced (cytidine) deaminase (AID) is the principal enzyme involved in SHM. This enzyme incorporates mutations mainly in CDRs of the immunoglobulin genes. Of note, CDR1 and CDR2 are found in the V region while CDR3 includes some of V, and all of D and J regions. CDR3 is the most variable. Clonal selection involves the fact that once B cells have undergone SHM they must compete for limiting growth resources, one among them being the availability of antigen. Indeed, as antigen becomes limited overtime in the host, clones with higher affinity that will therefore bind better to the antigen will have a selective advantage[139,140].

Finally, class switching is a mechanism that changes isotype of an immunoglobulin to another, such as from the isotype IgM to IgG. In this process, the constant region of the antibody heavy chain is changed but the variable region of the heavy chain stays the same, therefore antigenic specificity remains unchanged. Naïve mature B cells produce both IgM and IgD which are the first two heavy chain segments in the immunoglobulin locus. After activation by antigen, antigen-specific B cells will proliferate and for the ones that encounter signaling molecules via CD40 and cytokine receptors, they will undergo antibody class switching to produce IgG, IgA or IgE antibody[140,141].

2.2. What happens with the adaptive component in CDI?

The third line of host defense against *C. difficile* infection is therefore adaptative immunity. Humoral immune response is mounted against the toxins of *C. difficile* as it has been confirmed by the presence IgG and IgA antibodies against TcdA and TcdB in serum from patients[142,143]. These antibodies are also found in healthy children and adults that remain colonize asymptomatically. Indeed, despite high carriage rates, children rarely develop the disease, probably due to antibodies in breast milk that inhibit the binding of toxin A to its intestinal receptor, and absence in the newborn gut of the intestinal receptor that binds TcdA[144–146]. Moreover, presence in serum of anti-toxin antibody is associated with a favorable clinical outcome and absence of recurrence. Indeed, Kyne *et al.*, who followed antibody responses to *C. difficile* toxins in hospitalized patients, found significantly lower levels of toxin A-specific IgG in relapsing patients compared to patients who did not have any relapse[147]. In another study, anti-TcdB antibody levels were higher in sera of convalescent CDI patients than in sera of healthy donors[142]. Antibodies against the binary toxin CDT could be elicited in a hamster model of vaccination but no study has looked for the presence of these antibodies in patients[148].

Secretory IgA are a major component of mucosal immunity and could be expected to provide a protective role against *C. difficile* antigens in the intestinal lumen. IgA in patients' stools have been demonstrated to neutralize toxins[143]. Similarly, low levels of fecal IgA and reduction in colonic IgA-producing cells have been shown to be associated with prolonged CDI and recurrences[149].

While adequate toxin-specific antibody responses have been associated with asymptomatic carriage, insufficient humoral responses correlate with rCDI. This adequate response mainly relies on generation of sufficient titers of neutralizing antibodies[150,151]. Polyclonal sera

displayed greater activity than monoclonal antibodies (mAbs) suggesting that targeting multiple toxin domains is more efficient than targeting a single one[152].

Other proteins than toxins can induce humoral immune response. Pantosti *et al.* were the first in 1989 to bring evidence of an IgG response against *C. difficile* surface proteins that correlates with acute and convalescent phases of CDI. The LMW SLP is immunogenic, as demonstrated by the presence of antibodies against this protein in sera of patients infected by *C. difficile*[153]. Likewise, patients with recurrences did not show an efficient IgM immune response to SLPs compared to patients with a single episode of CDI[154]. However, these studies are limited by the variability of the SlpA and a reference strain was generally used to screen all the patients without considering the strain they were infected with. Moreover, little is known about the mechanisms which confer protection by these antibodies.

Other surface-expressed antigens such as FliC, FliD, Cwp84 and Cwp66 trigger antibody responses. Indeed, in a study of 33 patients, anti-Flic, FliD, Cwp66 were detected in sera by ELISA. The immune response toward FliC was notably low and authors hypothesized that this might be attributed to the high variability of the surface-exposed antigenic part of the flagella. High level of antibodies was detected against FliD, in line with the presence of specific conserved domains[155]. The extent to which this response is protective remains to be elucidated.

Humoral immunity against *C. difficile* toxins has been largely studied and mechanisms that confer protection deciphered. Moreover, several studies underlined the importance of humoral immunity against surface proteins but the precise mechanisms behind this protection remain to be uncovered.

- The epithelial barrier is the first line of defense against CDI.
- Innate responses involving neutrophils and pro-inflammatory cytokines and chemokines characterize CDI.
- Humoral response involves the generation of anti-toxin antibodies as well as anti-surface layer proteins antibodies. To what extend these last ones confer protection remains to be elucidated.

III. Epidemiology of CDI

1. In the world

The infection caused by *C. difficile* has been described for more than 30 years and was once considered as an annoying byproduct of antibiotic use. Over the years, this disease has become more frequent, with patients exhibiting relapses and few efficient treatments available to treat it[156]. With its worldwide prevalence, this bacterium is currently the leading cause of antibiotic-associated nosocomial diarrhea and colitis in the industrialized world[157]. *C. difficile* is responsible for all cases of pseudomembranous colitis and is implicated in 10 - 25% of antibiotic-associated diarrhea[158]. A study in 2011 in the United States (US) identified 453, 000 cases and 29,000 deaths associated with CDI[159]. Of note, a quarter of those infections were community-acquired. Nosocomial CDI increases annual expenditures by $6.3 billion, quadrupling the cost of hospitalizations in the US[160]. CDI is among the top five most expensive healthcare-associated infections (HAIs) in the US, while accounting for 15.4% of all HAIs[161]. In Europe, the direct cost associated with CDI was estimated to be €3 billion even if these costs vary widely from a country to another[162]. In France, CDI attributable cost is estimated to be €9575 per case[163] while it is €7147-7654 in Germany[164,165], €4396 in Spain[166] and £4000 in UK[167]. CDI, once thought to be an easy-to-treat bacterial infection, has evolved into an epidemic that is associated with a high rate of mortality, causing disease in patients thought to be low risk.

CDI epidemiology reflects *C. difficile* phylogenetic diversity with at least 86 distinct ribotypes reported around the world, including hypervirulent lineages associated with increased transmission and mortality[56,59,168–170]. Latest epidemiology data worldwide revealed that 5 ribotypes (R001, R002, R014, R027, R078) account for more than 60 % of the infections (Fig. 17)[170].

One hypervirulent ribotype of *C. difficile*, the BI/NAPI/027 strain, which has been discovered in 2002 led to the latest epidemy in the US. This strain produces the binary toxin CDT, as well as toxins A and B, and has been associated with increased mortality and severity[171]. In the first decade of the 21st century, it was responsible for most of the cases in North America, as well as in Eastern Europe[172]. Surprisingly, in UK where this strain was responsible for most of the infections, its prevalence decreased since 2007 and has led to the emergence of a diversity of

strains[173]. Similar binary-toxin-producing strains have also been discovered in Australia, even if there are no findings about the BI/NAPI/027 strain, which might reflect the relative pressure of antimicrobial selection. For instance, this ribotype 027 is resistant to fluoroquinolone which is not an antibiotic frequently prescribed in Australia[174,175]. In Asia, non-binary toxin strains such as ribotypes 017, 018 and 014 remain dominant[176]. CDI epidemiology nonetheless lacks some understanding, due to the poor surveillance of this infection in certain countries, especially ones that are still in development.

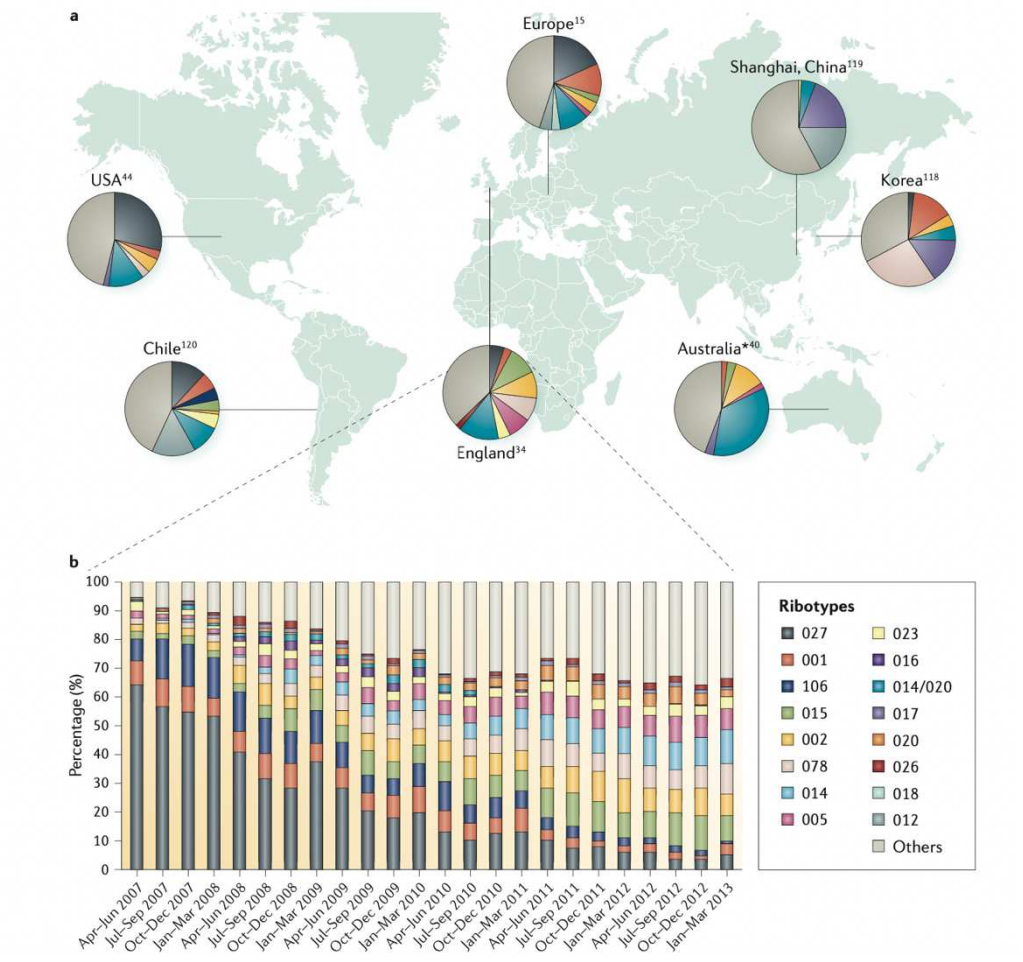

Figure 17. Global epidemiology of common *C. difficile* ribotypes[177]. These are the latest data on CDI epidemiology worldwide.

2. Healthcare-associated *vs* Community-associated CDI

In European hospitals, seven CDI cases occur for every 10,000 overnight patient stays[178]. This incidence is the same in the USA. However, the proportion of CDI occurring in patients outside health-care facilities has increased, suggesting that this infection is also affecting the wider community. CDI cases are categorized as community associated (CA-CDI) if patients had diarrhea onset in the community and had not been discharged from a healthcare facility in the prior 12 weeks[178].

CA-CDI incidence in the US increased from 52.88 per 100,000 people in 2012 to 65.93 per 100,000 people in 2017[179]. The overall number went from 170,000 in 2011 to 226,400 cases in 2017. It is interesting to compare this number to the total number of CDI cases that slightly decreased from 476,400 in 2011 to 462,100 in 2017, showing a shift in the epidemiology dynamic of CDI, with a decrease in Healthcare-associated CDI (HA-CDI) from 60.7 per 100,000 people in 2011 to 47.9 per 100,000 people in 2017[180].

Unlike the regular patients with microbiota disturbed with antibiotics, with a certain age, persons who are infecting by *C. difficile* outside health-care facilities are younger and healthier patients, and a significant proportion of these patients (36%) with no prior antibiotic exposure during the 12 weeks before diagnosis[159,181].

3. Reservoirs of *C. difficile*

C. difficile bacteria are transmitted from human to human via the faecal-oral pathway, but other sources of *C. difficile* can also be found in the environment.

C. difficile can be found in farm animals such as pig and cattle, with a prevalence that goes up to 96% in the first and 22% in the lattest[182–184]. A more worrying fact is that 90% to 100% toxigenic strains circulate in these animal farms. Less studied animals include poultry that are natural host since they remained asymptomatic when colonized (prevalence of 33.1%), goat and sheep with a prevalence of 8.6% and 5.8%[185–187]. The prevalence of *C. difficile* in these farm animals in Europe is recapitulated in Figure 18.

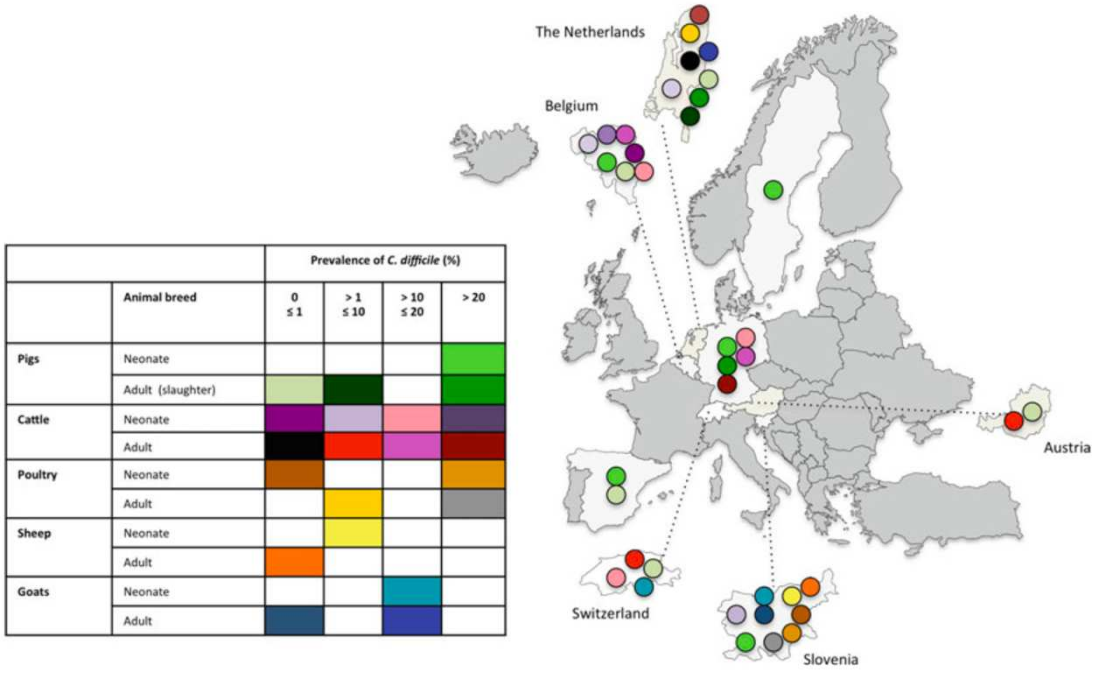

Figure 18. Prevalence of *C. difficile* in farm animals in Europe[188].

C. difficile is also found in domestic animals such as cats and dogs, and prevalence can go up to 30%. The bacteria do not cause disease in them and for now it is not clear whether shedding is the result of a long lasting colonisation or associated with a short transient passage[189–191]. In contrast, horses are domestic animals that are reported to develop CDI[192].

In wild animals, few studies have been performed regarding the presence of *C. difficile* outside their direct or indirect relationship with livestock. There is one study in Slovenia which found that *C. difficile* was carried by barn swallows and which therefore concluded on a possible role for national and international dissemination of the bacterium[193]. However, another study in the same country from the same team which look at migrating passerine birds did not find any positive results for the presence of the bacterium[194]. Some studies have also been carried in zoo animal species and *C. difficile* was found with an infection prevalence of 3.5%[195,196]. Interistingly, a study conducted in zooplankton populations demonstrated the presence of *C. difficile*, suggesting for the first time that this bacterium could be transmitted through the ingestion of raw or undercooked seafood[197].

Various ribotypes are present in these animal reservoirs, with some animals carrying always the same one, whereas other carry a variety. A summary table done by Rodriguez et al., in 2018 recapitulate the most prevalent ribotypes carried by animals (Table 2).

Species	References	Reported prevalence and the most prevalent ribotypes
Pigs	Pirs et al. (2008), Avbersek et al. (2009), Alvarez-Perez et al. (2009), Indra et al. (2009), Hoffer et al. (2010), Hopman et al. (2011), Keessen et al. (2011b), Koene et al. (2012), Rodriguez et al. (2012, 2013), Alvarez-Perez et al. (2013), Schneeberg et al. (2013a), Noren et al. (2014)	22.6–96% (neonates);
		0–36% (adults)
		002, 005, 014, 013, 015, 023, 046, 066, 078,126
Cattle	Pirs et al. (2008), Avbersek et al. (2009), Hoffer et al. (2010), Koene et al. (2012), Rodriguez et al. (2012), (2013), Romano et al. (2012a), Zidaric et al. (2012), Schneeberg et al. (2013a), Schmid et al. (2013)	1.8–22.2% (neonates);
		0–9.9% (adults);
		002, 003, 012, 014, 015, 029, 033, 038, 045, 066, 070, 077, 078, 081, 126, 137
Goat and ship	Koene et al. (2012), Romano et al. (2012a), Avbersek et al. (2014), Rieu-Lesme and Fonty (1999)	Goats 0–10.1%
		001, 010, 014, 020, 045, 066
		Sheep 0–18.2%
		015, 056, 061, 097
Poultry	Zidaric et al. (2008), Indra et al. (2009), Koene et al. (2012)	0–100%
		001, 010, 014, 023, 446
Horses	Avbersek et al. (2009), Ossiprandi et al. (2010), Koene et al. (2012), Rodriguez et al. (2014a, b, 2015)	3.7–33.3%
		005, 006, 010, 012, 014, 023, 033, 035, 039, 042, 045, 051, 078, 126
Cats	Koene et al. (2012) and Schneeberg et al. (2012)	3.7–15.7%
		009, 010, 039, 014/020, 045
Dogs	Schneeberg et al. (2012), Koene et al. (2012), Wetterwik et al. (2013), Pirs et al. (2013), Álvarez-Pérez et al. (2015, 2017), Orden et al. (2017a), Spigaglia et al. (2015)	0–100% (neonates);
		4.8–25% (adults);
		009, 010, 012, 014/020, 021, 027, 031, 039, 045, 056, 078, 106, 107, 154, 213, 430
Rabbits (farm)	Drigo et al. (2015)	3%
		002, 014, 020, 078, 012, 205
Wild animals	Burt et al. (2012), Bandelj et al. (2016), Andres-Lasheras et al. (2017)	0–100%
		078, 033, 045, 126

Table 2. Overview of recent European studies on *C. difficile* prevalence and ribotypes in animals[188].

Severals factors such as animal species, age, microbiota, breeding effect and seasonality have been associated with *C. difficile* colonisation in farm animals[198–200]. *C. difficile* is moreover probably better adapted to some animal hosts than to others, this in linked with factors that remain for now unknown.

Animals serve as source of environmental contamination as their intestinal tracts are colonized by *C. difficile* and they excrete bacterial spores in the faeces. Contaminations happen in the manure and farm waste recycling, in soils or waters. One study reported a prevalence between

4% and 100% in vermin of pig farms, with the PCR-ribotype 078 always identified[201]. Another study in spain also found the PCR-ribotype 078 and 126 in pest species including rodent and pigeons in pig farms and the associated environment[202]. This study confirmed the cross-transmission of the bacterium between wild animals and farm animals.

C. difficile transmission by contaminated food has not been extensively inverstigated. It has been reported for the first time in 1983 by Borriello *et al.*, but the importance of *C. difficile* as a zoonotic disease remains largely unkown[203]. Contamination could occur with spores remaining in the meat. Vegetables could be contaminated with spores from manure spread or irrigation with contaminated water, and root vegetables by spores directly present in soil.

Meats contaminated with *C. difficile* have been found in Europe. The main PCR ribotypes identified were 078, 014, 045, 012 and 053 (Table 3). Some other studies did not find the presence of *C. difficile* in meat samples[204]. There is a lower variety of PCR ribotypes in meat samples than in farm animals, which could be explainded by susceptibilities to external agents present in the meat supply chain. As described previously, *C. difficile* has been found in seafood by one study[197], and the prelavence in vegetable has been described by Eckert et al[205]. Interestingly, the PCR ribotypes detected in these types of samples correlate with the ones that have been associated with CDI in humans[206].

Food	References	Reported prevalence and detected ribotypes
Meats	Indra et al. (2009), Von Abercon et al. (2009), Bouttier et al. (2010), De Boer et al. (2009), Hoffer et al. (2010), Jobstl et al. (2010), Rodriguez et al. (2014b)	0–6.3%
		001, 003, 012, 014, 045, 053, 071, 078, 087
Seafood	Pasquale et al. (2011, 2012)	49–75%
		001, 002, 003, 005, 010, 012, 014, 020, 045, 066, 078, 106
Vegetables	Eckert et al. (2013)	2.9–4.5%
		001, 014, 015, 020, 077

Table 3. Overview of recent European studies on *C. difficile* prevalence and ribotypes in food[188].

Likewise, a 3-year study showed that 11 of 90 PCR ribotypes were shared between human CDI and food, animal and environmental reservoirs[207]. A question nonetheless arises regarding the

risk for food consumers. To date, no study has reported a direct infection from food, animal or environmental source. If the gut microbiota is normal, intestinal colonization by *C. difficile* may indeed be transient and no pathology should be developped. Precautionary measures need to be taken in case of an altered gut microbiota to avoid spore ingestion. While *C. difficile* spores are heat-resistant until 70°C which corresponds to gentle cooking of foods, they are destroyed at 85°C for 10 min. Thermal treatment may therefore be the best strategy to avoir the risk of foodborne transmission and special attention should be given to raw foods such as raw meat and fish, fruits or vegetables. Reservoirs of *C. difficile* are summarized in Figure 19.

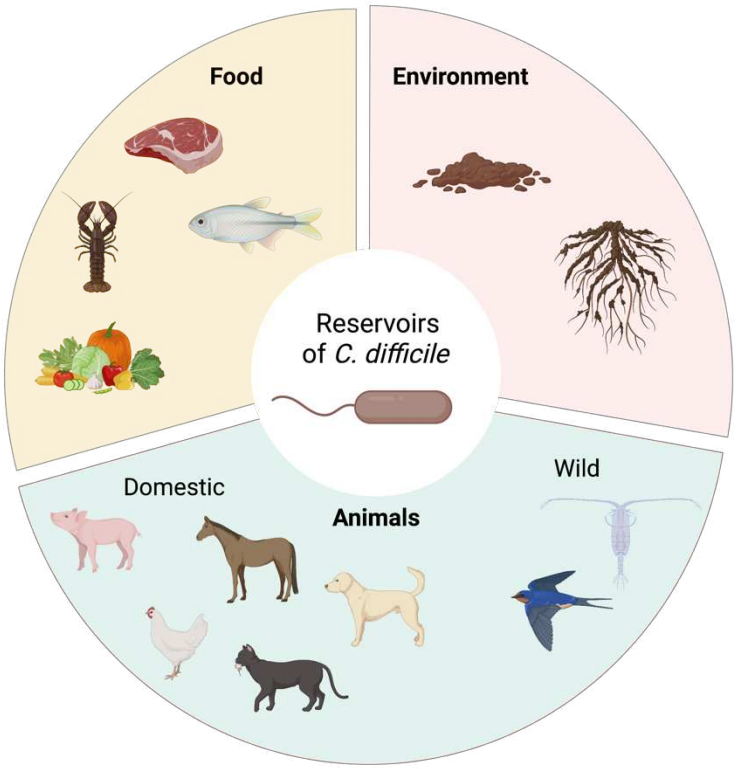

Figure 19. Reservoirs of *C. difficile*. Created with Biorender.com.

4. CDI in children

Children under 1 year of age are colonized by *C. difficile* but the reasons for why they do not develop the disease are still poorly understood. The dynamics shift between the ages of 1 and 3, transitioning from asymptomatic colonization to classical CDI[208].

The epidemiology in infants differs from adults in terms of ribotypes. Moreover, cases are predominantly community-associated[209–211]. Complications and mortality rates are also lower than in adults[212].

5. PCR ribotyping to follow CDI epidemiology

Incidence and severity of CDI increased since 2000s, and this can be related to the worldwide spread of the hypervirulent PCR ribotype 027. Since then, European countries successfully controlled the dissemination of the 027 clone, but several other virulent or unusual strains have emerged.

To follow epidemiology of *C. difficile*, the most common method is PCR ribotyping based on amplification of the ribosomal RNA (rRNA) operon in *C. difficile* genome. The region between 16S and 23S rRNA genes results in ribotype-specific patterns after amplification and migration[213]. Ribotype profiles are available in an online database[214] (WEBRIBO, https///webribo.ages.at). PCR ribotyping is now done using capillary gel-based electrophoresis which allows better standardization and easier comparison between laboratories than agarose gel electrophoresis[215]. Differences still lie in the choice of primers as primers that can do PCR ribotyping directly from stools have been developed. Consequently, a universal protocol is still lacking, as well as the uniformization of the nomenclature to be able to reliably detect the emergence of new and unreferenced ribotypes precisely and in a time-dependent manner. As of now, 86 ribotypes have been reported around the world[168].

Another way to classify *C. difficile* strains is toxinotyping which is a PCR-restriction based method[216]. Toxinotypes are defined based on their differences in the PaLoc compared to the reference strain VPI 10463 which is the nonvariant toxinotype 0. Toxinotyping and PCR

ribotyping are well correlated since changes in each ribotype correspond to change in the PaLoc and thus belong to a single toxinotype.

6. Link between ribotype and severity

Although data on this question is still scarce and subject to debate, it has been demonstrated that colonization with certain toxigenic strains increases the severity of CDI[169]. Spreading of the hypervirulent strain 027 increased CDI incidence in the 2000s and was associated with more severe outcomes[217,218]. Several teams have demonstrated an increased mortality rate associated with PCR RT078, although contradictory results have been published[219,220]. A recent study in Slovakia showed that two fluoroquinolone-resistant ribotype RT176 and RT001 were giving most of the infection, but they did not find strong evidence that these two ribotypes were worsening the course of infection or infection outcome compared to other strains[221]. In a Swedish hospital, RT046 was associated with higher mortality compared to other strains (20.2% to 7.8%). This higher mortality could not be explained by concomitant diseases, differences in age, exposure to antimicrobials that are high-risk for CDI or choice of treatment for the primary infection. Patients infected with RT046 had a higher mean blood leukocyte and median C-Reactive Protein (CRP) count, indicating that RT046 caused a more severe illness in link with higher mortality[222]. Finally, a team demonstrated recently that RT220 was giving more severe disease and longer persistence[168].

Rapid expansion of certain strains has been observed in link with the ribotype, even if spreading factors are not always understood. For instance, RT106 which showed 100% lethality in hamsters became the second-most prevalent ribotype in Arizona from 2015 to 2018. Contrary to RT027 and RT078 that can grow on low levels of trehalose, RT106 lacks the genetic elements necessary for such growth[223]. Multidrug resistance also seems to influence the spreading of certain ribotypes. In South Korea, RT017 prevalence reached 50% between 2004 and 2008 before being supplanted by RT018 since 2009[224–226]. Interestingly, this strain has been found in Japan but also in Italy and this change was associated with high levels of resistance to ampicillin, cefotetan, imipenem and moxifloxacin[227–229].

The link between *C. difficile* strains and mortality mainly relies on the presence of inflammatory biomarkers, therefore stressing the importance of the inflammatory pathways on the poor

outcome of CDI[230]. Due to the multiple parameters and the limited availability of patients and samples, the precise link between some ribotypes and a significant modification of the infection course remains to be precisely deciphered. Identifying hypervirulent ribotypes is also of clinical relevance with the development of phage-therapy in link with antibiotic resistance. As phages are not specific for all the strains of *C. difficile*, identification of the ones active on severe ribotypes will be essential to develop successful therapies[231].

7. Limitations to follow CDI epidemiology

Epidemiology of CDI continues to challenge. Significant reductions in CDI have been reported in countries across Europe and the need to improve surveillance is increasingly recognized. However, incidence rates still vary widely between countries and capacity for surveillance and diagnosis remain highly variable from a country to another[220,232,233]. Therefore, there is a need to strengthen the capacity for surveillance of CDI within Europe[234].

As of now, there is no standardized approach to surveillance, diagnosis and typing, which would allow the estimation of the total burden of CDI in each country. Moreover, continuously monitoring the incidence, severity, outcome, and risk factors for developing CDI could allow an improved understanding and therefore management and control of CDI. Indeed, in countries where the incidence of CDI significantly dropped, a comprehensive national surveillance program has been implemented, with the standardization of diagnosis, sampling, and reporting. Coordinated approaches on how to treat and prevent CDI have been put in place, according to the evolving epidemiology of CDI[235].

Clusters and cross-transmission routes can be identified with the help of local laboratories that in the end report to a national reference center[236,237]. These national centers, in an international collaboration, can then identify the spread of new virulent lineages of *C. difficile* and anticipate new epidemic[238].

- Epidemiology of *C. difficile* is rapidly evolving and involves more than 86 ribotypes around the world.
- Community-associated CDI cases are increasing.
- Children are not susceptible to CDI.
- PCR ribotyping is the main method to identify different strains of *C. difficile*.
- Reservoirs of *C. difficile* are found in the soils and manure, as well as in the intestine of domestic and wild animals.
- Food can be contaminated with *C. difficile*.

IV. From diagnosis to treatment of CDI

1. Diagnostic methods for CDI

There is currently no optimal laboratory assay as well as no standardized test to diagnose CDI, which has an impact on the incidence rate found in countries. The various diagnostic methods are described below.

Diagnosis of CDI is based either on the detection of the toxins secreted by *C. difficile* and/or the presence of a *C. difficile* strain that is known to produce the toxins[239].

1.1. Cell culture cytotoxicity neutralization assay (CCNA)

Detection of toxins in stools is done by a reference test called cell cytotoxicity neutralisation assay. Cell lines such as Vero cells, HeLa cells or Hep-2 cells are incubated *in vitro* with stool filtrates from patients. Readout is based on the cytopathic effect that is due to toxin B and confirmed by the addition of anti-toxin B[240,241].

This test nonetheless lacks standardization and suffers from suboptimal storage or collection conditions of stool, leading to false-negative results.

1.2. Toxigenic culture (TC)

This assay is performed with stool samples that are inoculated onto selective media. After 48h of incubation, toxigenic potential of *C. difficile* colonies is evaluated with CCNA or other tests -described below-[240].

However, there are some cases where toxigenic strains are carried asymptomatically, therefore leading to overdiagnosis of CDI.

Both tests described above require trained personnel and are expensive in terms of time and money. Therefore, some easy-to perform and rapid assays -giving the results in a few hours[242]- have been developed to complement these two reference tests.

1.3. Glutamate dehydrogenase (GDH) detection

These tests detect glutamate dehydrogenase, which is an enzyme produced by both toxigenic and non-toxigenic strains of *C. difficile*. They are therefore detecting the presence of *C. difficile*. These tests possess a high sensitivity and the main advantage of being easy to perform and low cost. However, since they cannot distinguish between a toxigenic or a non-toxigenic strain, they cannot conclude about a CDI if they are used solely and are therefore generally used in association with other diagnostic tests[243].

1.4. Enzyme immunoassays (EIA) for Toxins A and B

These tests directly detect toxins from the stools. Their main advantage is that they are low cost, have a specificity as high as 99% compared to CCNA and TC and they don't require trained personnel. However, they have a suboptimal sensitivity compared to CCNA and TC[243].

1.5. Nucleic acid amplification test (NAAT)

Most of these tests target conserved regions within the gene for toxin B (tcdB) but some also target a highly conserved sequence in toxin A gene (tcdA). Some of these tests combined RT027/NAPI detection by targeting CDT gene and a deletion at position 117 of the regulatory gene tcdC[244].

The sensitivity of these tests is high (96%[243]) and they are more specific than GDH EIA since they only detect toxigenic *C. difficile*. However, the presence of toxins' genes is not always associated with symptomatic *C. difficile* therefore these tests can lead to overdiagnosis.

These various tests are summarized in Table 4.

Test	Substance detected	Sensitivity %	Specificity %	Time required	Limitations	Reference
TC	*C. difficile*	95	80–90	3–5 days	Long turnaround time, trained personnel	Davies et al. (2009), Moon et al. (2016)
CCNA	Toxin	95	90–95	1–3 days	Long turnaround time, trained personnel, technical demands	Huang et al. (2009), Reller et al. (2010)
GDH	*C. difficile*	95–100	88–92	Hours	Low specificity, false-negative results	Eastwood et al. (2009), Cheng et al. (2015), Ramos et al. (2020)
EIA toxin	Toxin	51–80	98–99	Hours	Low sensitivity	Davies et al. (2009), Eastwood et al. (2009)
NAATs	*C. difficile*	92–97	83–100	Hours	Low specificity, costly and technical demands	Davies et al. (2009), Eastwood et al. (2009), Paitan et al. (2017)
GDH and EIA toxin	Toxigenic *C. difficile*	83–100	97–100	Hours	Dependent on toxin results, some variation in reported sensitivity	Kim et al. (2014), Cheng et al. (2015)
NAATs and EIA toxin	Toxigenic *C. difficile*	77–100	91–100	Hours	Some variation in reported sensitivity, technical demands	Huang et al. (2009), Humphries et al. (2013)

TC, toxigenic culture; CCNA, cell-culture cytotoxicity neutralization assay; EIA, enzyme immunoassay; GDH, glutamate dehydrogenase; NAATs, nucleic acid amplification tests.

Table 4. Diagnostic tests for CDI[242].

1.6. Limitations and future perspectives

Despite the multiplicity of tests that have been developed to diagnose CDI, there is currently no test that can be used alone. GDH EIA and NAAT tests do not directly correlate with clinical symptoms and therefore can lead to overdiagnosis of CDI whereas Tox A/B EIAs are not specific enough to be used alone[243]. Therefore, multi-step diagnostic algorithms have been recommended by ESCMID and SHEA/IDSA, leading to an accuracy of more than 98% (Fig. 20)[5].

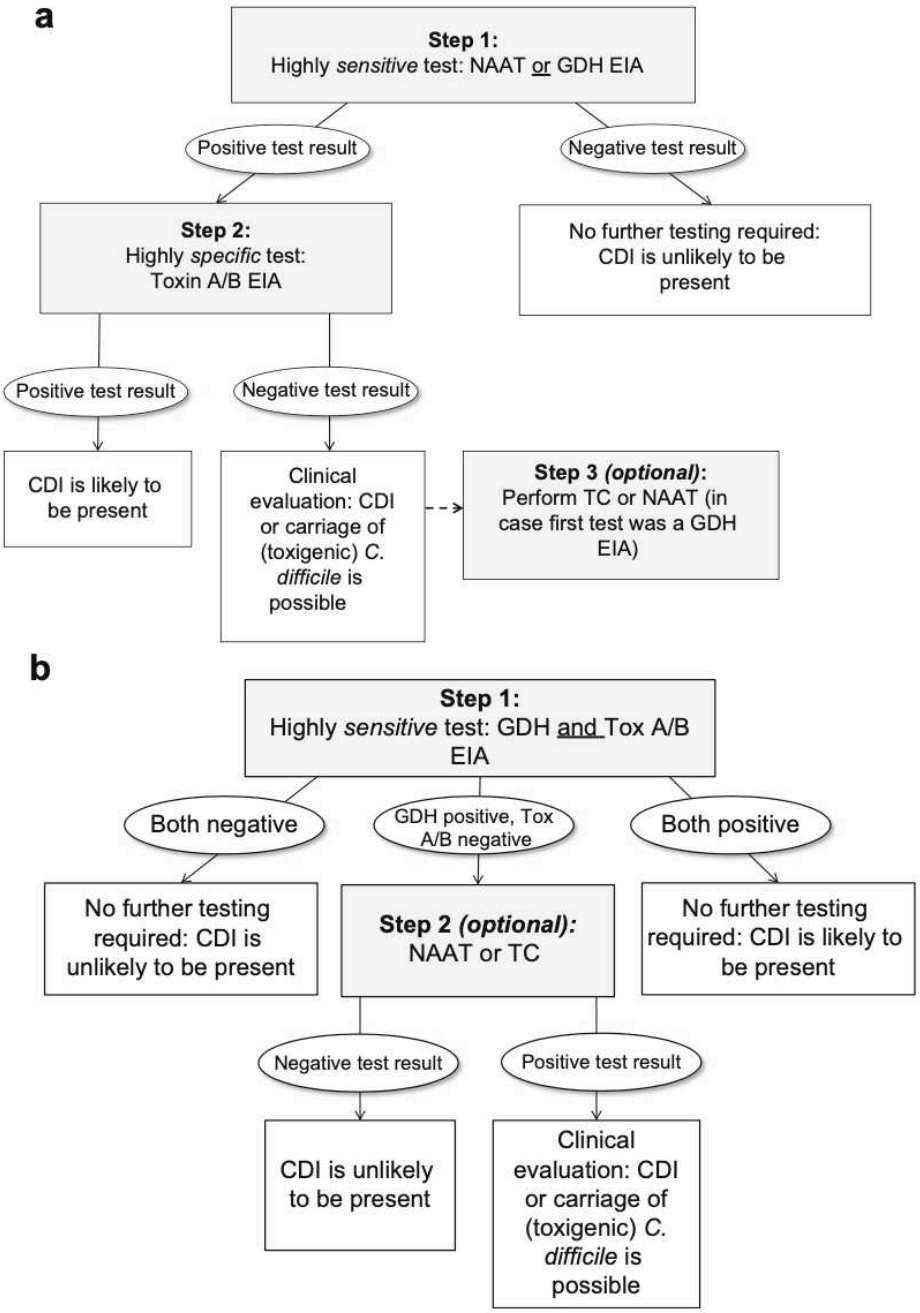

Figure 20. Algorithms for CDI testing as recommended by ESCMID guidelines. **a)** GDH or Tox A/B – NAAT/TC algorithm. **b)** GDH and Tox A/B – nAAT/TC algorithm[244].

Accurate diagnosis can be achieved with the current tests that have been developed, however the turnaround time remains long and the multi-steps not straightforward (as well as requiring lab equipment and trained personnel), leaving room for improvement in CDI diagnosis.

Immunoassays have been used for decades in diagnosis, but novel rapid diagnostic techniques based on recombinant antibodies (rAb) have demonstrated promising results in both research and clinical environments[245–247]. The main hurdle of antibodies relies on their production cost. Over the past few years, development of recombinant antibody (rAb) technologies tackled this issue by enabling a faster and more cost-effective approach for antibody production[248–252]. Indeed, *in vitro* antibody production based on display technologies (yeast display, ribosome display, phage display, and mammalian cell display) has the main advantage that these techniques can generate a large diversity (10^{12} – 10^{15}) with high transformation efficiency[253–255]. The rAb technologies allows the construction of large libraries of different antibody fragments. Indeed, several engineered formats based on antibodies have developed in the past decades such as fragment antigen-binding (Fab), single-chain fragment variable (scFv), minibodies, nanobodies and others (Fig. 21)[248–250,256–258].

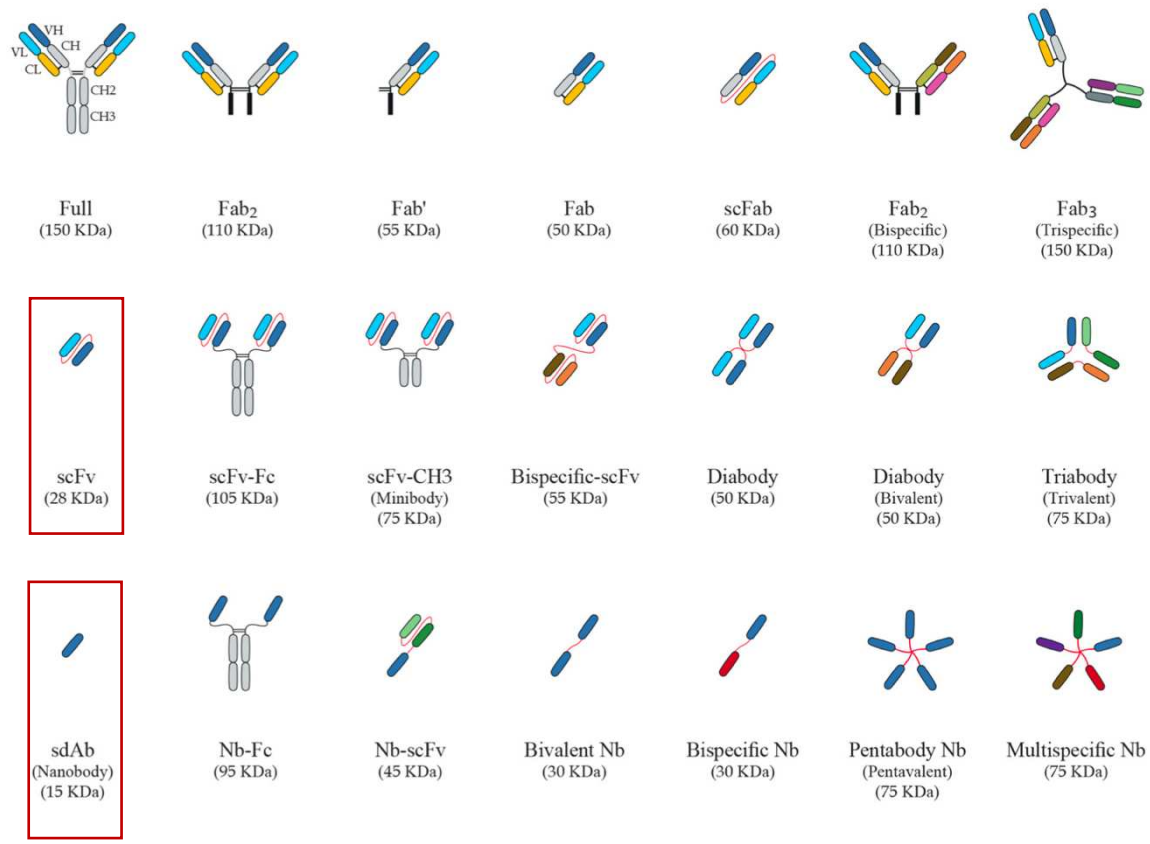

Figure 21. Schematic overview of antibody formats[257]. First line represents formats that derive of Fab, second line represents formats that derive from scFv and the third line represents formats that derive of nanobodies.

Successful tests based on rAbs have been developed for diagnosis of other bacterial infections such as *Porphyromonas gingivalis, Mycobacterium tuberculosis*[259,260].

For CDI, two commercial clinical biosensor kits have been introduced for CDI diagnosis. They can detect the GDH or whole cells in a few minutes[242]. Several other rapid methods for detection of toxins of *C. difficile* have been developed and some of them are highly rapid and sensitive but are not yet commercially available[261–263]. Future diagnosis of CDI will for sure benefit from the design of ultrasensitive methods using rAb technologies.

2. Treatment and prevention of CDI

Treatments for CDI depend on the severity of the infection. For an initial episode and a first recurrence, antibiotics are usually used while fecal microbiota transplantation (FMT) is restricted for recurrences. There is currently no recommended treatment in prophylaxis.

2.1. Antibiotics

When *C. difficile* infection was first described in 1935, no treatments were available. It is in 1979 that the efficacy of metronidazole and vancomycin was demonstrated on hamsters[264]. Fidaxomicin, a narrow-spectrum, oral macrocyclic antibiotic, was discovered in the late 1970s [265]. It has been approved in the United States in 2011 for the treatment of mild-to-moderate CDI and showed a recurrence rate (15.4%) lower than vancomycin (25.3%)[266]. It was the first new drug to be approved for CDI in over 25 years. Fidaxomicin is hydrolyzed in the colon in the active metabolite OP-1118 and has an absorption close to zero therefore retaining its full efficacy when it reaches the colon[267]. This molecule inhibits RNA polymerase and is specific to a few bacteria (efficacy has been demonstrated *in vitro* on *Mycobacterium tuberculosis* even

if its clinical use is limited to CDI[268]). To date, three cases of resistance have been reported (RCDF 2023, Paris). Contrary to vancomycin which is bacteriostatic, fidaxomicin is bactericidal. It inhibits the production of spores whereas vancomycin inhibits growth[269]. Fidaxomicin also inhibits toxins' production whereas vancomycin does not influence the toxins' production[267]. Finally, its impact on the microbiota has been partially evaluated and showed that there was no change in the *Bacteroides* quantity in the colon contrary to vancomycin[270]. However, this antibiotic is more expensive than the others (a 10-day course costs $3000 which is twice the cost of vancomycin and 300 times the cost of metronidazole)[271].

Oral metronidazole was recommended for initial CDI in mild/moderate disease in 2014 ESCMID guidelines while IDSA/SHEA 2017 guidelines advised metronidazole only for patients with an initial episode of non-severe CDI in places where vancomycin or fidaxomicin were unavailable[208,272]. These two organizations updated their guidelines in 2021 to recommend fidaxomicin over vancomycin for initial CDI, a first non-severe recurrence, and severe CDI[273]. A second or subsequent non-severe recurrence benefits from fidaxomicin according to IDSA/SHEA while ESCMID recommends FMT (Table 5).

Category	IDSA/SHEA 2021	ESCMID 2021
Initial episode, non severe	Fidaxomicin STD preferred[a] OR vancomycin[b]. If above agents are unavailable: metronidazole[c].	Fidaxomicin STD preferred[a] OR vancomycin[b]. If above agents are unavailable: metronidazole[c]. If high risk of recurrence, especially elderly hospitalized, consider EPFX[d] or adjunctive bezlotoxumab if fidaxomicin is unavailable.
First recurrence non-severe	Fidaxomicin STD[a] or EPFX[d] OR vancomycin tapered and pulsed regimen alternative[e] OR vancomycin[b] And adjunctive bezlotoxumab if prior episode within 6 months.	Fidaxomicin STD[a] if fidaxomicin is not used for initial episode of CDI OR Fidaxomicin STD[a] or vancomycin[b] with ajunctive bezlotoxumab OR vancomycin tapered and pusled regimen alternative[e] is acceptable alternative if other options are unavailable.
Second or subsequent recurrence non-severe	Fidaxomicin STD[a] or EPFX[d] OR vancomycin tapered and pusled regimen alternative[e] OR vancomycin[b] followed by rifaximin[f] and adjunctive bezlotoxumab if prior episode within 6 months. FMT: appropriate antibiotic treatment for at least two recurrences (i.e. three CDI episodes) should be tried prior offering FMT.	FMT: after pretreatment with fidaxomicin STD[a] or vancomycin[b] OR Fidaxomicin STD[a] OR vancomycin[b] with adjunctive bezlotoxumab OR vancomycin tapered and pusled regimen[e] is acceptable alternative if other options are unavailable.
Severe	Fidaxomicin STD[a] OR vancomycin[b] and adjunctive bezlotoxumab for primary CDI if other risk factors for recurrence (age >65years, immunocompromised host) or if episode in prior 6 months.	Fidaxomicin STD[a] OR vancomycin[b].
Severe-complicated 'fulminant'	Vancomycin[b] or by nasogastric tube and metronidazole[g] AND consider vancomycin per rectum if ileus present.	Fidaxomicin STD[a] OR vancomycin[b] and consider IV tigecycline[h]. Consult a surgeon.
Severe-complicated 'fulminant' refractory	No commentary in focused update.	Refer for surgery OR Consider rescue FMT if ineligible for surgery.

Table 5. Treatment recommendations for CDI, adapted from Bishop *et al.*[6] a: 200 mg 12 hourly for 10 days, b: 125 mg PO 6 hourly for 10 days, c: 500 mg PO 8 hourly for 10 – 14 days, d: extended-pulsed regimen, 200 mg PO 12 hourly for 5 days followed by 200 mh PO every other day for 20 days, e: 125 mg four times daily for 10 -14 days, two times daily for 7 days, once daily for 7 days, and then every 2 - 3 days for 2 - 8 weeks, f: 400 mg PO 8 hourly for 20 days, g: 500 mg IV 8 hourly, h: 100 mg load, then 50 mg 12 hourly.

For patients with a high risk of relapses (age, anterior episodes, hospitalized-associated CDI, following an antibiotic treatment), fidaxomicin is recommended in first line.

A novel fidaxomicin regimen, which extends administration of the regular dose from 10 to 25 days, have been evaluated for patients with recurrent CDI[274]. When administered in a prolonged period, a regimen called extended pulse-regimen, decreases recurrences, and microbiota recovery is facilitated. Consequently, this regimen is indicated for the first or subsequent recurrences.

2.2. Fecal microbiota transplantation (FMT)

FMT has been used to treat patients with pseudomembranous colitis for the last 50 years. FMT consists in an infusion of a donor feces into a patient's gastrointestinal lumen either by nasogastric tube, colonoscopy, or enema directly to the lower gut. Oral capsules have also been developed and proved to retain the same efficacy as colonoscopy or enema[275,276]. FMT theoretically works by recreating an equilibrated microbiota in patient intestine[277].

This technique results in a cure rate of approximately 90% in recurrent CDI[278]. Nood *et al.* demonstrated in 2013 that FMT could cure better (81%) than vancomycin with bowel lavage (31%) or vancomycin alone (23%) for the treatment of recurrent CDI[279]. Consequently, the FDA approved its clinical use for refractory CDI after at least two recurrences[280].

The limited utilization is due to lingering questions regarding its optimal timing, preparation, and route of delivery and the specific patient population that would benefit most from it. Moreover, the absence of data from large-scale clinical trials, the unappealing nature of the process, and the challenging procedure in screening potential fecal donors restricted its use. For now, tests are performed to prevent communicable diseases and the donor is generally chosen among family members of the patient so that the microbiota will be similar. Another limiting factor for the widespread adoption of this technique is the cost, which amounts to $1300 per treatment[240].

2.3. Microbiome therapies

The FDA has approved over the last two years two microbiome therapies. The first one, developed by the Swiss company Ferring Pharmaceuticals is a rectally administered microbiota-based product called Rebyota (RBX2660). This treatment is a suspension of stool coming from qualified donors. In a phase III clinical trial PUNCH CD3 including 267 patients, the ones who received standard of care antibiotic treatment followed by Rebyota had a 71% sustained clinical response versus 58% for the ones who received placebo[281].

The second microbiome therapy has been developed by Seres Therapeutics and Nestlé for the prevention of CDI recurrence CDI. The SER-109 drug, also called Vowst, is based on *Firmicutes* bacteria purified from healthy donor. In their phase III clinical trial ECOSPOR on 182 patients who had three or more episodes of CDI, standard of care antibiotic treatment was followed by SER-109 or placebo. 88% of the patients who received SER-109 had sustained clinical response at 8 weeks versus 60% for the patients who received the placebo[282].

2.4. Vaccines

Vaccines have been tested in preclinical animal models and clinical trials over the past decade but none of them have been approved by the Food and Drug Administration (FDA) yet. These vaccines needed either repetitive dosing, the use of formalin-induced detoxification, or were not enough stable[283]. The best candidate for now has been a vaccine able to elicit neutralizing antibodies against both toxins produced by *C. difficile*[284].

One vaccine went through phase I and consists of a recombinant fusion protein with relevant epitopes of toxins A and B. This vaccine was well tolerated and induced high antibody titers against toxins A and B[285] but as of now, no information has been given on a next phase. Sanofi-Pasteur developed a toxoid vaccine based on inactivated toxins A and B and went through phase II clinical trial, but the company has decided to stop the development following an analysis by the Independent Data Monitoring Committee[286,287]. They indeed concluded that the likelihood of the study meeting its primary objective was low. Finally, the most advanced vaccine is the one from Pfizer which developed a recombinant vaccine designed to elicit antibody responses against TcdA and TcdB. However, the primary endpoint was not reached at the end of Phase

III CLOVER clinical trial, as communicated in March 2022. They are currently analyzing the data in detail to decide what their next steps will be.

2.5. Antibodies

2.5.1. Approved monoclonal antibodies

Two human monoclonal antibodies -actoxumab targeting toxin A and bezlotoxumab targeting toxin B- have been tested in a hamster model and showed significant efficacy. Two phase III clinical trials evaluated their ability to reduce CDI recurrence in 2655 patients. Patients received oral antibiotics for primary or recurrent CDI with an infusion of either actoxumab, bezlotoxumab or placebo[288]. The addition of actoxumab did not improve efficacy but bezlotoxumab showed a reduction of recurrences compared with placebo (17% v 26/%). An ongoing phase III clinical trial is evaluating safety, tolerability, and efficacy of bezlotoxumab in children (NTC03182907).

No antibodies targeting the CDT toxin has been developed, while immunization of hamsters with TcdA and TcdB demonstrated that they did not have protection against strains that express CDT[148].

2.5.2. Towards new monoclonal antibodies for CDI

The technique of mAb production, known as hybridoma technology, was invented by Kohler and Milstein in 1975, who received the Nobel prize for this invention in 1984[289]. Since then, this technology has developed, with the engineering of the sequences to generate chimeric or humanized antibodies carrying the least mouse antigens, and therefore leading to less side effects when the antibodies are injected in humans (Fig. 22).

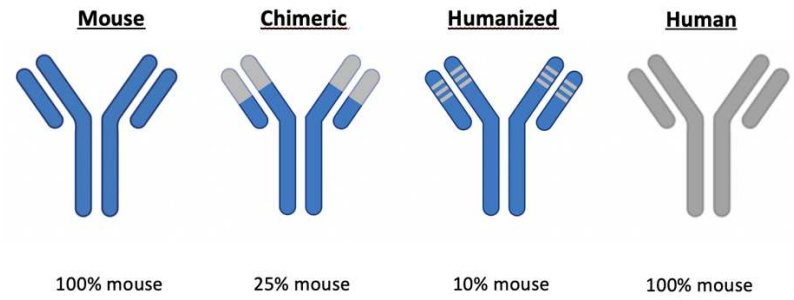

Figure 22. Schematic overview of mouse, chimeric, humanized, and human antibodies. Created with Biorender.com

Several other mAbs are still in development. One therapy based on humanized toxin-specific mAbs (PA-50 an anti-toxin A, PA-41 an anti-toxin B) showed a long-term survival in hamsters compared to vancomycin (95% *vs* 0%). Interestingly, combination of PA-50 and PA-41 was more effective than the combination of actoxumab and bezlotoxumab[290]. These are attractive candidates for a non-antibiotic therapy in CDI. These anti-toxin antibodies, used in combination with antibiotics such as vancomycin, also showed a decrease in recurrence[291]. Yang *et al.* went further by generating a bispecific single-domain antibody (sdAb) (highlighted in Fig. 4.2) targeting both toxins which showed high efficiency to treat severe CDI[292].

Another interesting application of antibodies in the treatment of CDI involves probiotic bacteria expressing antitoxin fragments. Andersen *et al.* assessed the expression of anti-toxins sdAb on the surface of four *Lactobacillus paracasei* strains. Two strains delayed death of hamsters when challenged with *C. difficile* spores, whereas no animal in the control group survived[151]. Interestingly, this team also administrated purified anti-TcdB VHH alone but did not observe any protection, likely due to VHH degradation in the GI tract. Indeed, expression of the antibodies on the surface of *Lactobacilli* was found to help preserving antibodies from degradation. A recent study in 2020 assessed the expression of a single tetra-specific antibody neutralizing both TcdA and TcdB by targeting four distinct toxin epitopes on the surface of *Saccharomyces boulardii*. This engineered probiotic neutralized both toxins and protected mice in both primary and rCDI models[293]. Other formats that are resistant to the harsh conditions of the upper gastrointestinal tract have been developed. Gastrobodies, which are antibody mimetics, were resilient to pepsin and hydrochloric acid. Phage selection of gastrobody libraries against the glucosyltransferase domain of TcdB highlighted molecules binding with high

affinities (K_D~10^{-9} M)[294]. These studies reveal complementary approach for the future of CDI treatment.

Finally, other targets besides the TcdA and TcdB toxins have been considered. The last toxin CDT is also a crucial pathogenicity factor[295]. sdAbs from phage libraries were constructed and could block enzymatic and cytotoxic activity of CDT[296]. Likewise, cell-surface components involved in the adherence to host gut tissues and colonization are of major interest. Among them are SLPs[28,297], flagella[298], or Cwp84[299]. Anti-SLPs antibodies are suggested to be a good choice for CDI treatment as they could inhibit bacterial motility *in vitro*, prolong survival of hamsters as well as decrease colonization of *C. difficile* in mice[300–302]. Anti-flagella antibodies also demonstrated to be interesting as single-chain variable fragments (scFv) (highlighted in Fig. 4.2) targeting FliC and FliD of *C. difficile* inhibited bacterial motility[303]. Components of the cell surface of *C. difficile* are interesting targets even if detailed studies remain to be performed.

2.6. Personalized medicine and CDI

Personalized medicine is based on the fact that each individual possesses nuanced and unique characteristics at the molecular, physiological and behavioral levels[304]. Consequently, the treatment, monitoring, and prevention of diseases in individuals should be tailored or personalized to their specific needs. This personalized approach becomes even more crucial in the case of CDI, considering the uniqueness of an individual's microbiota, which is shaped by distinct parameters. The microbiota plays a central role in fighting CDI, as demonstrated by the remarkably effective outcomes of FMT[277,305].

Moreover, antibiotic resistance is a main concern for prevention and treatment of CDI. Indeed, antibiotic resistance plays an important role in driving *C. difficile* epidemiology, and emergence of new types is often associated with new resistances[306]. Antibiotic resistance in *C. difficile* can be due to acquisition of genetic elements and alterations of the antibiotic target sites, as well as variations in metabolic pathways or biofilm production where antibiotics cannot penetrate and kill the bacteria easily. The multifactorial nature of antibiotic resistance and the rapid evolution of *C. difficile* epidemiology require development of alternative therapies to prevent and contain the spread of resistant strains and to ensure efficient therapy for CDI[306]. Phage therapies have been studied for CDI, but none of them led to the development of effective treatments for CDI.

As phages are not specific of all the strains of *C. difficile*, this development will only be valuable for certain ones[51,231].

Altogether, it could be interesting to explore new treatments that take into account *C. difficile* strain, antibiotic resistance profile and the unicity of each patient's microbiota.

- Several diagnostic methods have been developed for CDI but turnaround time remains long and accurate diagnosis requires multi-step algorithms.
- Treatment of CDI mainly rely on antibiotics.
- No vaccine has been approved for CDI.
- FMT is used in the case of multiple recurrences.
- One mAb targeting the toxin has been approved and its use is now recommended in combination with antibiotics for recurrences.

V. Objectives

With an incidence that is constantly increasing since the turn of the new millennium, the emergence of hypervirulent strains such as RT027, and rapid changes in strains involved in CDI, this infection remains an urgent threat to tackle. New strategies are needed to (i) reduce the consumption of antibiotics in the treatment of CDI and (ii) prevent *C. difficile* spread in health care institutions.

While *C. difficile* toxins have been largely studied, other virulence factors such as adhesins and surface proteins have focused a growing interest. These proteins are involved in colon localization, evasion of the immune system surveillance and are therefore playing a major role in the initiation of bacterial pathogenesis[307,308]. Among these proteins, one gained substantial interest: the Surface-Layer Protein A (SlpA). Composed of two subunits that are the High Molceular Weight (HMW SlpA) and the Low Molecular Weight (LMW SlpA), SlpA is central for maintaining bacterial membrane integrity and bacterial fitness. Of note, the LMW SlpA is the most external one. SlpA has been also involved in bacterial adhesion to enterocytes and is needed for successful colonization of the host[28,297]. While these data suggest that SlpA is crucial in the early stages of CDI, detailed analysis are still needed. S-layer proteins are immunogenic as anti-S-layer antibodies have been detected in sera from convalescents patients[43]. However, *C. difficile*-host antibodies interactions remain largely unexplored. Another point of interest is the high variability of the LMW SlpA across the different ribotypes of *C. difficile*, suggesting a mechanism to escape host immune surveillance[35]. Currently, five ribotypes (001, 002, 014, 078 and 027) account for more than 60% of CDI[170]. Nevertheless, fundamental research focused on one reference strain of *C. difficile i.e C. difficile 630,* missing other members of *C. difficile* family.

The aim of my PhD was to generate monoclonal antibodies that recognize surface-layer proteins of *Clostridioides difficile* and to evaluate their impact on the bacteria in the context of an infection.

The first part of this work was to generate the first mAbs recognizing the LMW of current clinical ribotypes 001, 002, 014, 027 and 078, and mAbs recognizing the LMW from the basic research strain 630. I undertook the characterization of their binding profiles in terms of affinity to the protein and binding to whole bacteria. These mAbs displayed various cross-specific

profiles for the different LMW and are tools that can be used in several assays to study or detect *C. difficile* bacteria such as ELISA, flow cytometry, microscopy, or histology to name a few. This work led to the following manuscript (to be submitted summer 2023), which is presented in chapter VI:

Lise Hunault, *et al.*

A monoclonal antibody collection for *Clostridioides difficile* typing

In preparation.

The second part of my thesis work aimed at identifying mAbs that could affect *C. difficile* physiology. For that, we focused on the reference strain *C. difficile* 630 and evaluated several mAbs we developed against *C. difficile* 630 LMW SlpA. We observed distinct effects on *C. difficile* physiology depending on the mAb we used. One mAb impaired bacterial growth and increased *C. difficile* sensitivity to stress agents. Two mAbs abolished toxin secretion suggesting that S-layer flexibility is hampered when *C. difficile* is coated with these mAbs. Finally, two mAbs increased biofilm formation, supporting a role for the S-layer in biofilm formation and structure. Altogether, this work provides important insights on the role of the S-layer in *C. difficile* fitness. These results also reveal the ambivalent effects of anti-S-layer antibodies, questioning the S-layer directed therapeutic approaches. This work is presented in the following article (to be submitted summer 2023), presented in chapter VII:

Lise Hunault, *et al.*

Anti-S-layer monoclonal antibodies impact *Clostridioides difficile* physiology

In preparation.

The last part of my PhD work is still ongoing and focuses on developing a rapid identification test "Quick-Ribodif". We took advantage of the anti-LMW mAb collection described in manuscript #1 to propose a new solution to track the spreading of *C. difficile* strains in healthcare settings and to enable a better surveillance of *C. difficile* epidemiology. Using

luciferase-based ELISA (LuLiSA[309]) we could detect *C. difficile* from the most frequent clinical ribotypes when spiked into a complex human microbiota from healthy donor stool samples. We are currently addressing the proof of concept using feces from CDI patients, with results that should be presented during the oral defense of this thesis. This ongoing work is presented in the following manuscript, inserted in chapter VIII:

Lise Hunault, *et al.*

'Quick-Ribodif': a quick and easy ribotyping test to follow *Clostridioides difficile* epidemiology

In preparation.

Results

VI. Construction of a monoclonal antibody collection for *C. difficile* typing

This first article describes the generation of LMW SlpA specific mAbs.

To generate mAbs, mice were immunized with the LMW SlpA of 6 ribotypes (previously recombinantly produced) and their splenocytes fused with myeloma cells to generate hybridoma. After screening, specific clones were selected and expanded.

Their binding profiles to the different LMW was then assessed by ELISA, and various cross-specificity profiles could be observed. The affinity was assessed by BLI and a range of affinities -from 10 pM to 100 nM- was determined.

Following these first characterizations, binding to the LMW at the surface of *C. difficile* was assessed by flow cytometry, by adapting a technique developed by Moor *et al*[310]. Binding to whole bacteria did not always correlate with binding to the recombinant protein, which can either be due to insufficient affinities or epitopes on the protein that are masked at the surface of the bacteria.

Related work to this chapter is presented after this first manuscript. It includes the characterization of a cross-specific mAb that recognized the LMW of the five clinical ribotypes R001, R002, R014, R027 and R078, homology percentages extracted from sequence alignments and of the LMW of these five clinical ribotypes as well as the LMW630, and the production and characterization of anti-FliC mAbs.

A monoclonal antibody collection for *C. difficile* typing

Lise Hunault[1,2,3], Patrick England[4], Frédéric Barbut[5,6], Bruno Iannascoli[1], Ophélie Godon[1], Bruno Dupuy[7], Lynn Macdonald[8], Guy Gorochov[2,†,#], Delphine Sterlin[2,†] and Pierre Bruhns[1,†,#].

†shared senior authorship

[1]Institut Pasteur, Université Paris Cité, INSERM UMR1222, Antibodies in Therapy and Pathology, 75015 Paris, France.

[2]Sorbonne Université, INSERM, CNRS, Centre d'Immunologie et des Maladies Infectieuses (CIMI-Paris), F-75013 Paris, France.

[3]Sorbonne Université, Collège doctoral, F-75005 Paris, France

[4]Institut Pasteur, Université Paris Cité, CNRS UMR3528, Plateforme de Biophysique Moléculaire, 75015 Paris, France.

[5]National Reference Laboratory for Clostridium difficile, Paris, France

[6]Université Paris Cité, INSERM UMR-1139, Paris, France.

[7]Institut Pasteur, Université Paris-Cité, UMR-CNRS 6047, Laboratoire Pathogenèse des Bactéries Anaérobies, 75015 Paris, France.

[8]Regneron Pharmaceuticals, Tarrytown, NY, USA.

To whom correspondence should be addressed:
pierre.bruhns@pasteur.fr, guy.gorochov@sorbonne-universite.fr, and delphine.sterlin@aphp.fr

ABSTRACT

Clostridioides difficile is the leading cause of antibiotic-associated diarrhea and pseudomembranous colitis in adults. Various *C. difficile* strains circulate currently, associated with different outcomes and antibiotic resistance profiles. However, most studies still focus on the reference strain 630 that does not circulate anymore, partly due to the lack of immunological tools to study current clinically relevant strains. Herein, we immunized mice expressing human variable antibody genes with the Low Molecular Weight (LMW) subunit of the surface layer protein SlpA from various *C. difficile* strains. Monoclonal antibodies purified from hybridomas bound LMW with high-affinity and whole bacteria from current *C. difficile* ribotypes with different cross-specificities. This first collection of anti-*C. difficile* mAbs represent valuable tools for basic research or diagnostic approaches.

KEYWORDS (5-10 WORDS)

Clostridioides difficile, monoclonal antibodies, S-layer, hybridomas

INTRODUCTION

C. difficile is an anaerobic, Gram-positive and spore-forming bacteria that is the main agent responsible for antibiotic-associated diarrhea and pseudomembranous colitis in adults[311]. In the past decades, there was a drastic increase in nosocomial *C. difficile* infection (CDI) with a significant burden of community-acquired CDI[307]. CDI epidemiology reflects *C. difficile* phylogenetic diversity with at least 86 distinct ribotypes reported worldwide, including hypervirulent lineages associated with increased transmission and mortality[56,59,168,169]. The latest epidemiology data worldwide reported that 5 ribotypes i.e., R001, R002, R014, R027 and R078, account for more than 60 % of the infections[170].

Whereas several advances such as fluorescent mutants and novel fingerprinting techniques have contributed to a new understanding of *C. difficile* diversity and physiology[312–314], basic research still relies on one single strain *i.e., C. difficile* 630 that derived from the clinical ribotype 012 and is not found in CDI patients anymore. An increasing number of studies has been performed on the hypervirulent ribotype 027, which caused major outbreaks in the United States and Europe at the end of the 2010s[171,172]. Other ribotypes remain largely unexplored even though some are associated with antibiotic resistance and increased severity[168], which can be partly explained by the lack of genetic and immunological tools to study these strains.

C. difficile surface is composed of adhesins e.g., the flagellar cap protein FliD, the flagellin FliC, the cell wall protein Cwp66, the surface layer protein SlpA, and the protease Cwp84[315]. SlpA is expressed on the bacterial surface of all ribotypes and plays a crucial role in the pathogenesis and virulence of *C. difficile* by mediating interactions with the host cells and the surrounding environment[50,297,299,301]. SlpA contains two biologically distinct entities, the high-molecular weight (HMW) and the low molecular weight (LMW) subunits that assemble on the bacterial surface into a paracrystalline lattice[37]. Sequence variations of SlpA have been reported for the LMW that correlate with the diversity of clinical isolates, whereas the HMW is less variable[28,316]. SlpA is highly immunogenic, meaning it can trigger an immune response in the host[43]. Antibodies against SlpA have been detected in the sera of patients infected with *C. difficile*, indicating its potential as a target for vaccine development[43,44].

In this work, we generated the first collection of mAbs that bind and discriminate predominant clinical ribotypes of *C. difficile*. Knock-in mice expressing human antibody variable genes for the heavy (V_H) and light chain (V_L)[317,318] were immunized with a collection

of recombinantly expressed LMW from five clinically relevant *C. difficile* ribotypes i.e., R001, R002, R014, R027 and R078. Hybridomas were generated and their corresponding IgG mAbs bound both recombinant LMW *in vitro* and LMW naturally expressed on the bacterial surface. At least one mAb was identified against each of the five ribotypes used for immunization, with 6 mAbs being cross-reactive between LMW subunits of two different *C. difficile* ribotypes. The reduced sequence identity of LMW between different *C. difficile* ribotypes[35] allows for specific identification of bacterial ribotypes by this anti-LMW mAb collection that represents a novel toolkit for *C. difficile* research.

RESULTS

LMW SlpA subunits from 5 predominant ribotypes of *C. difficile* i.e., R001, R002, R014, R027 and R078 (Fig.1a), were recombinantly produced from transformed *Escherichia coli coli* as his-tagged soluble proteins and affinity-purified. As anti-LMW antibodies may potentially be of therapeutic interest for the treatment of CDIs, we used knock-in mice in which the endogenous genes encoding the heavy chain variable domain (VH) and the kappa light chain variable domain (Vκ) were replaced by their human counterparts (Velocimmune)[317,318] with one modification, i.e., one allele of the endogenous Vκ locus was replaced by human Vκ segments, whereas the second allele of the endogenous Vκ locus was replaced by human Vλ segments to increase the variability at the kappa locus that represents 95% of antibodies in mice[319]. Thus, after hybridoma identification, cloning of these VH and VL into vectors containing human heavy and light chain constant domains, allows for direct development - *in fine* – of fully human anti-LMW mAbs. To generate hybridomas, mice were immunized at D0, D21 and D42 with 50 µg/mouse of each LMW (Fig. 1c). High anti-LMW IgG serum titers were obtained in all mice at day 42 (Fig.1d). Mice were boosted with all five LMW at equimolar ratio (Fig. 1c), and their spleen harvested 4 days later. Two different protocols were tested and gave similar results; one based on the similarity between the LMW – grouping two highly similar LMW in a single immunization; one based on their frequency in current CDI – grouping LMW corresponding to current clinical ribotypes in a single immunization (Supp. Fig.1). More than 700 hybridomas were generated and among them 100 hybridoma were found to secrete anti-LMW antibodies.

Among these 100 hybridomas, the 14 clones displaying the highest ratio of LMW binding by ELISA compared to IgG concentration in their culture supernatant were expanded and their antibodies purified. Their binding profiles towards the five recombinant LMW proteins were assessed by ELISA (Fig. 2a). 12 out of 14 (86%) significantly bound LMW-R001 with variable profiles, 1 out of 14 (7%) bound LMW-R002, 1 out of 14 (7%) bound LMW-R014, 6 out of 14 (43%) bound LMW-R078 and 11 out of 14 (78%) bound LMW-R027. Among the eleven LMW-R027-binding mAbs, four (36%) cross-reacted strongly with LMW-R001 (mAb SG8, TF1, TH4 and VA10) and one with both LMW-R001 and LMW-R078 (mAb RF12). mAb QE2 cross-reacted with four LMWs: LMW-R001, LMW-R014, LMW-R027 and LMW-R078. Among the three mAbs that did not recognize LMW-R027, mAb RA11 was

specific for LMW-R078, mAb UA5 cross-reacted with LMW-R001 and LMW-R002, and mAb SC6 cross-reacted with LMW-R001 and LMW-R078 (Fig. 2b).

We next evaluated the affinity of the mAbs displaying the strongest interactions with their respective targets i.e., LMW-R001, LMW-R002, LMW-R014, LMW-R078 and LMW-R027, by Bio Layer Interferometry (BLI), coupling IgGs to the sensors and keeping LMW antigens in solution. mAbs displayed equilibrium dissociation constant (K_D) values ranging more than 3 logs from 0.08 nM to 200 nM, which corresponds to low to very high-affinity antibodies (Fig. 3). We identified mAbs with a 1 nM affinity or better for all ribotypes, except for R014 that was only bound by mAb QE2 with a 9 nM affinity. Noticeably, cross-specific mAbs displayed different affinities for their targets, with systematically one ribotype bound with at least a 10-fold better affinity, except for mAb VA10 that bound LMW-R001 and LMW-R027 with comparable affinities.

As SlpA is the main component of the *C. difficile* surface, we investigated if this series of mAbs could also bind LMW when exposed naturally at the bacterial surface. Fixed *C. difficile* from the different ribotypes were used for bacterial flow cytometry (Fig. 4). Each ribotype could be significantly bound by at least one mAb. Consistent with the ELISA results (Fig. 2), monospecific anti-LMW mAbs (PH4, QD8, QH5, RD11 and TE8) and anti-LMW-R078-specific mAbs (RA11), bound to *C. difficile* R027 and R078 whole bacteria, respectively. However, cross-specific mAbs bound a restricted number of ribotypes by bacterial flow cytometry (Fig. 4) compared to ELISA (Fig. 2), indicating that their epitopes are hidden or inaccessible, or that their affinity is not sufficient for flow cytometry detection. Indeed, 3 out 8 cross-specific mAbs showed a restricted binding profile using flow cytometry, *e.g.,* QE2 mAb bound 4 distinct recombinant LMW ribotypes by ELISA but only 2 *C. difficile* ribotypes using flow cytometry. Table 1 summarizes the binding profiles of these mAbs to the LMW recombinant proteins and the LMW exposed at the bacterial surface for the five clinical ribotypes R001, R002, R014, R078, R027.

Finally, we studied the impact of LMW binding by the anti-LMW-R027 mAbs in an *in vitro* growth assay on *C. difficile* strain 027. Two monospecific mAbs for LMW-R027 (QD8 and QH5) and two cross-specific mAbs (VA10 and TH4) were tested for their impact on growth. Growth was followed over 24 hours with an isotype control IgG and showed an exponential phase followed by a plateau (Fig. 4c). Anti-LMW-R027 did not significantly alter growth, even though mAb VA10 had a tendency to delay growth, and mAb QD8 and, to a lesser extent, mAb QH5, a tendency to increase growth.

DISCUSSION

Herein, we report the first monoclonal antibody collection that targets a surface protein of *C. difficile.* Due to sequence variability in the low-molecular weight subunit of surface layer protein A, this mAb collection allows the detection of 5 different ribotypes of clinical interest. More than half the mAbs bound selectively to the bacterial surface of one of these ribotypes, whereas the cross-reactive mAbs bound to two different ribotypes. The relatively high affinity of the interaction (nanomolar range) allows to envision using these mAbs for various assays such as ELISA, flow cytometry, microscopy, or histology assays.

In this study we chose to immunize mice with the low-molecular weight subunit of surface layer protein A as it represents a major antigen of the *C. difficile* surface[320]. Although we found by alignment stretches of conserved residues between the five ribotype sequences we used[37], we could not identify any antibody cross-binding all five strains. The most cross-reactive anti-LMW mAbs recognized by bacterial flow cytometry only two different ribotypes. This suggests that conserved epitopes between LMW of different strains may not be dominant epitopes in terms of immunogenicity or may be hidden or poorly accessible to antibodies. Indeed, conserved amino acids have been implicated in the interaction between the LMW and the High Molecular Weight subunits which face inward toward the bacterial cell wall[38] and are therefore probably inaccessible to antibodies.

Mice were immunized sequentially with five different LMWs and boosted with a mix of all of them, leading to identification of mAbs to each of them. Varying the order of different LMWs in the immunization scheme did not significantly alter antibody titers for the various LMWs, except for LMW-R001 when injected with a farther ribotype. Antibodies binding SlpA have also been detected in the sera of patients infected with *C. difficile*, suggesting that, indeed, SlpA or its LMW subunit are immunogenic. Even though the knock-in mice we used produce antibodies with human variable domains[317,318], thus potentially resembling those found in infected patients, we did not identify antibodies that significantly alter bacterial growth in our *in vitro* assays. It remains unclear whether such antibodies exist in patients in remission or if other mechanisms are at play. Interestingly, 30% of relapsing *C. difficile* infections are not due to the initial infecting strain but to a different strain, acquired from an exogenous source[321]. Whether the sequence variability of LMW among *C. difficile* ribotypes is involved in this recurrence and escape from the host immune response remains to be investigated.

This novel series of anti-*C. difficile* mAbs contains three anti-LMW mAbs specifically recognizing hypervirulent ribotypes R027, bound by mAb TE8, R078 bound by mAb RA11, and R002 bound by mAb U5A. These three ribotypes have been associated with poor outcomes after infection[169,217,218]. Beyond *C. difficile* 630, the most studied *C. difficile* ribotype, this set of mAbs could help to study ribotypes R027, R078 and R002 by resorting to various assays (ELISA, flow cytometry, microscopy, histology, blotting). One could even propose targeted treatments, by coupling antibiotics to these mAbs (aka Antibody-Drug Conjugates, ADC) to reduce antibiotic doses.

Our study however has limitations. While it has recently been reported, using whole-genome sequencing, that diversity exists within a given ribotype[321], we only tested five ribotypes of *C. difficile*, each derived from a single clinical isolate. Therefore, more clinical isolates now remain to be tested to determine whether mAb specificity encompasses all known strains in each ribotype.

To our knowledge, these mAbs represent the first collection of antibodies against *C. difficile* surface protein SlpA. These mAbs bind LMW from different clinically relevant strains *i.e.,* LMW-R001, LMW-R002, LMW-R014, LMW-R027 and LMW-R078. These mAbs represent interesting probes to better understand *C. difficile* infection, pathogenesis, and epidemiology, but also to envision applications as tools for specific cargo delivery targeting *C. difficile*.

MATERIALS AND METHODS

Mice. Knock-in mice expressing human antibody variable genes for the heavy (V_H) and light chain (V_L) (VelocImmune) were described previously[317,318] and provided by Regeneron Pharmaceuticals to be bred at Institut Pasteur. All animal care and experimentation were conducted in compliance with the guidelines. The study, registered under #170043, was approved by the Animal Ethics committee CETEA (Institut Pasteur, Paris, France) and by the French Ministry of Research.

Production of recombinant LMW proteins. Recombinant *C. difficile* LMW-SLPs (LMW001, LMW002, LMW014, LMW078, LMW027, LMW630[35]) were produced as C-terminal 6xHis-tagged proteins from plasmid pET-28a(+) (TwistBiosciences, #69864). Plasmids were transformed into *E. coli* strain D43 and grown in NZY auto-induction lysogeny broth (LB) medium (NZYtech, #MB180). Bacteria were harvested by centrifugation and lysed using Precellys system according to manufacturer instructions (Bertin Technologies, *#P002511-PEVT0-A.0*). Recombinant LMW-SLP proteins from the soluble fraction were purified by affinity chromatography on Ni-agarose columns using an AKTA prime (GE Healthcare, #11001313). All proteins were dialyzed against 10 mM HEPES pH 7.5, 150 mM NaCl prior to analysis or long-term storage.

Production of LMW-specific monoclonal antibodies. VelocImmune mice were injected i.p. at day 0, 21 and 42 with 50 µg of each of five recombinant LMWs in alum mixed with 200 ng/mouse pertussis toxin (Sigma-Aldrich, #70323-44-3). ELISA was performed to measure serum responses to antigen (see methods below) and the 3 best immunized animals were boosted with the same antigen mix. Four days later, splenocytes were fused with myeloma cells P3X63Ag8 (ATCC, #TIB-9) using ClonaCell-HY Hybridoma Kit according to manufacturer's instructions (StemCell Technologies, #03800). Culture supernatants were screened using ELISA (see below) and antigen-reactive clones were expanded in RPMI-1640 complemented with 10% IgG-free Fetal Calf Serum (Sigma-Aldrich, #F1283) into roller bottles (Sigma-Aldrich, #CLS431344) at 37°C. After 14 days, supernatants were harvested by centrifugation at 2500 rpm for 30 min and filtered (0.2 µm). Antibodies were purified by protein A affinity chromatography (AKTA pure) as described previously[322].

ELISA assays. Maxisorp microtiter plates (Dutscher, #055260) were coated with a total of 0.3 µg per well of LMW recombinant proteins in carbonate-bicarbonate buffer (pH 9.6) for 2 hours at room temperature (RT). Free sites were blocked by a 2-hour incubation at RT with 1X-PBS 1% BSA. Plates were washed three times with 1X-PBS 0.05% Tween 20 (PBS-T) before being co-incubated with serum, supernatants or monoclonal antibodies at different concentrations (from 10^{-6} µg/mL to 10 µg/mL) for 1h at RT. After five washes, goat anti-mouse IgG-Fc fragment HRP conjugated antibody (Bethyl, dilution 1:20,000, #A90-131P) was added for 1h at RT followed by incubation with OPD (o-phenylenediamine dihydrochloride) revelation substrate for 10 min (Sigma-Aldrich, #P8287). Absorbances were analyzed at 492 vs 620 nm on an ELISA plate reader (Berthold).

Bio-layer interferometry. Biolayer interferometry assays were performed using Anti-Mouse Fc Capture biosensors on an Octet Red384 instrument (ForteBio, #18-5088). Monoclonal antibodies (10 µg/mL) were captured on the sensors at 25°C for 1,800 seconds. Biosensors were equilibrated for 10 minutes in 1x-PBS, 0,05% Tween 20, 0.1% BSA (PBS-BT) prior to measurement. Association was monitored for 1,200s in PBS-BT with LMW at a range of concentrations from 0.01 nM to 500 nM followed by dissociation for 1,200s in PBS-BT. Traces were reference sensor (sensors loaded with an unspecific mAb) subtracted and curve fitting was performed using a global 1:1 binding model in the HT Data analysis software 11.1 (ForteBio), allowing to determine K_D values.

Flow cytometry assays. mAb binding to whole bacteria was assessed by bacterial flow cytometry, as previously described[323]. Briefly, fixed *C. difficile* (10^6/condition) were stained with 5 µM Syto9 (Thermo Fisher Scientific, #S34854) in 0.9% NaCl for 30 min at RT. Bacteria were washed (10 min, 4,000g, 4°C) and resuspended in 1X PBS, 2% BSA and 0.02% Sodium Azide (PBA). Monoclonal antibodies were pre-diluted in PBA at 20 µg/mL and incubated for 30 min at 4°C. Bacteria were washed, and AF647 AffiniPure goat anti-mouse IgG (H+L) antibody or isotype control (Jackson ImmunoResearch, #115-605-003) were incubated for 30 min at 4°C. After washing, bacteria were resuspended in sterile 1X-PBS. Flow cytometry acquisition was performed on a MacsQuant cytometer (Miltenyi) and analyzed on FlowJo software (BD Biosciences). Staining index was calculated by subtracting the MFI of the isotype from the MFI of each condition with the anti-LMW mAbs, then divided by the MFI of the isotype.

Bacterial strains and culture conditions. *C. difficile* R001, R002, R014, R027, R078 strains were grown anaerobically (5% H2, 5% CO2, 90% N2) in TY medium (30 g/L tryptone, 20 g/L yeast extract). Bacteria were fixed in 4% paraformaldehyde (PFA) for 30 min and resuspended in 1X PBS, 10% glycerol before being stored at -80°C. All media and chemicals were purchased from Sigma-Aldrich.

Growth assays. Overnight *C. difficile* cultures were grown in TY broth and sub-cultured to an Optical Density at 600 nm (OD_{600nm}) of 0.05 in 200 µL of BHISG in 96-well flat bottom plates (Merck, #Z707902). Bacterial growth was followed for 24h or 18h with OD_{600nm} measurements every 30 min using GloMax Plate Reader (Promega). Anaerobia was maintained with a O_2 less sealing film (Sigma-Aldrich, #Z380059).

Statistical analysis. Growth and ELISA assays values were analyzed in Prism 8.0 (GraphPad, San Diego, CA). Statistical analysis was performed using two-way ANOVA test. A p value ≤ 0.05 was considered significant.

ACKNOWLEDGEMENTS

This work was funded by Fondation Janssen Horizon, the Institut National de la Santé et de la Recherche Médicale (INSERM) and the Institut Pasteur. LH is a doctoral fellow of Sorbonne Université. DS was a recipient of a poste d'accueil 2017 Institut Pasteur – Assistance Publique des Hôpitaux de Paris (APHP). Work in the G. Gorochov's team is supported by Institut National de la Santé et de la Recherche Médicale (INSERM), Sorbonne Université, Fondation pour la Recherche Médicale (FRM), Paris, France, program ''Investissement d'Avenir'' launched by the French Government and implemented by the Agence Nationale de la Recherche (ANR) with the reference COFIFERON ANR- 21-RHUS-08, by EU Horizon HLTH-2021-DISEASE-04 UNDINE project, programme DIM Ile de France thérapie cellulaire et génique and by the Département Médico-Universitaire de Biologie et Génomique Médicales (DMU BioGen), APHP, Paris, France.

AUTHORSHIP CONTRIBUTIONS

Experimental design, LH, DS and PB; Conducting experiments, LH, BI, OG; Data analyses and discussions: LH, PE, FB, BD, LM, GG, DS and PB. Writing (original draft), LH, DS and PB; Writing (review and editing), all authors.

COMPETING INTERESTS

Unrelated to the submitted work, P.B. received consulting fees from Regeneron Pharmaceuticals. The other authors declare no competing interests.

FIGURES

a

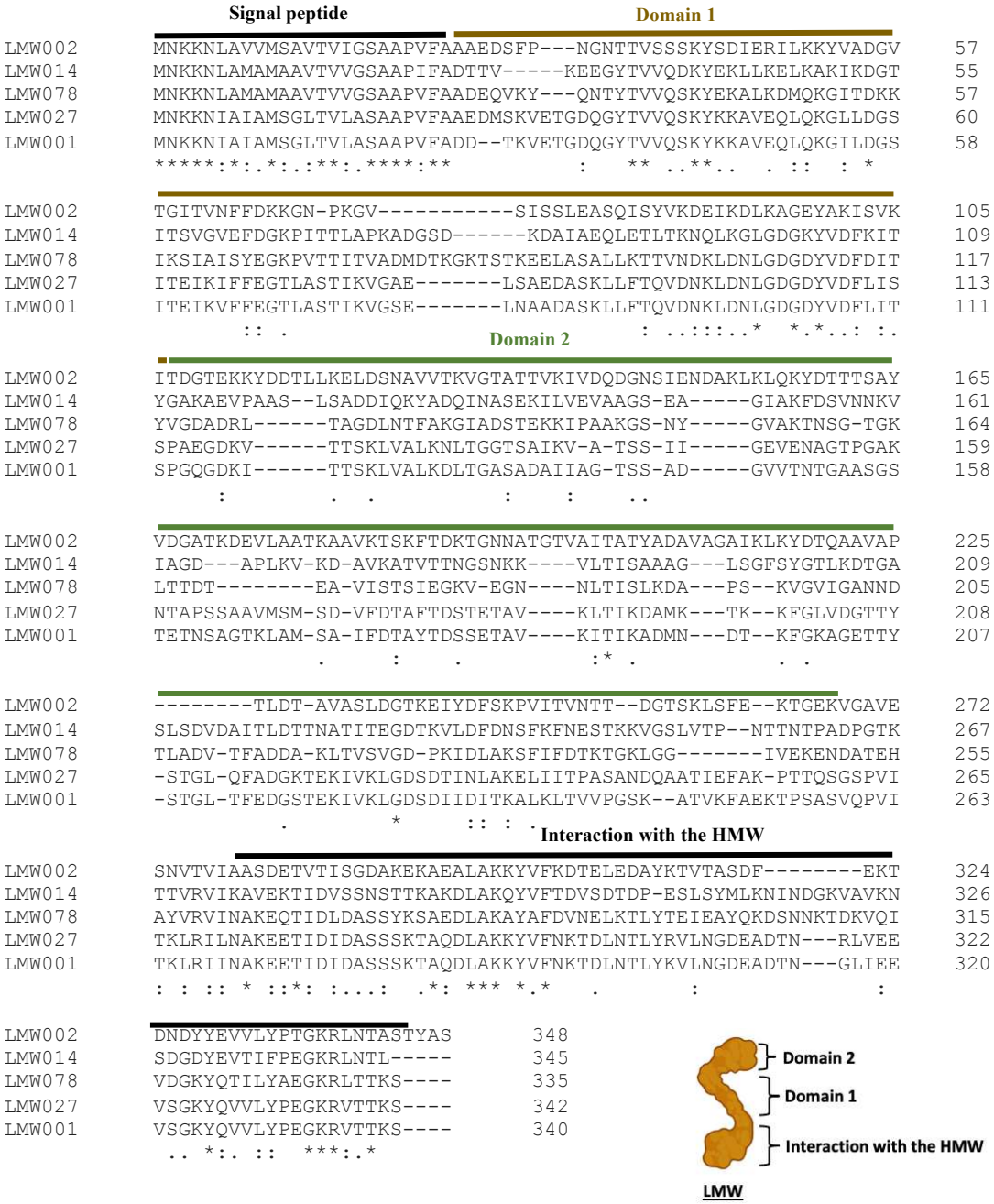

*** fully conserved residue**

: conservation between groups of strongly similar properties – roughly equivalent to scoring >0.5 in the Gonnet PAM 250 matrix

. conservation between groups of weakly similar properties – roughly equivalent to scoring <0.5 and >0 in the Gonnet PAM 250 matrix

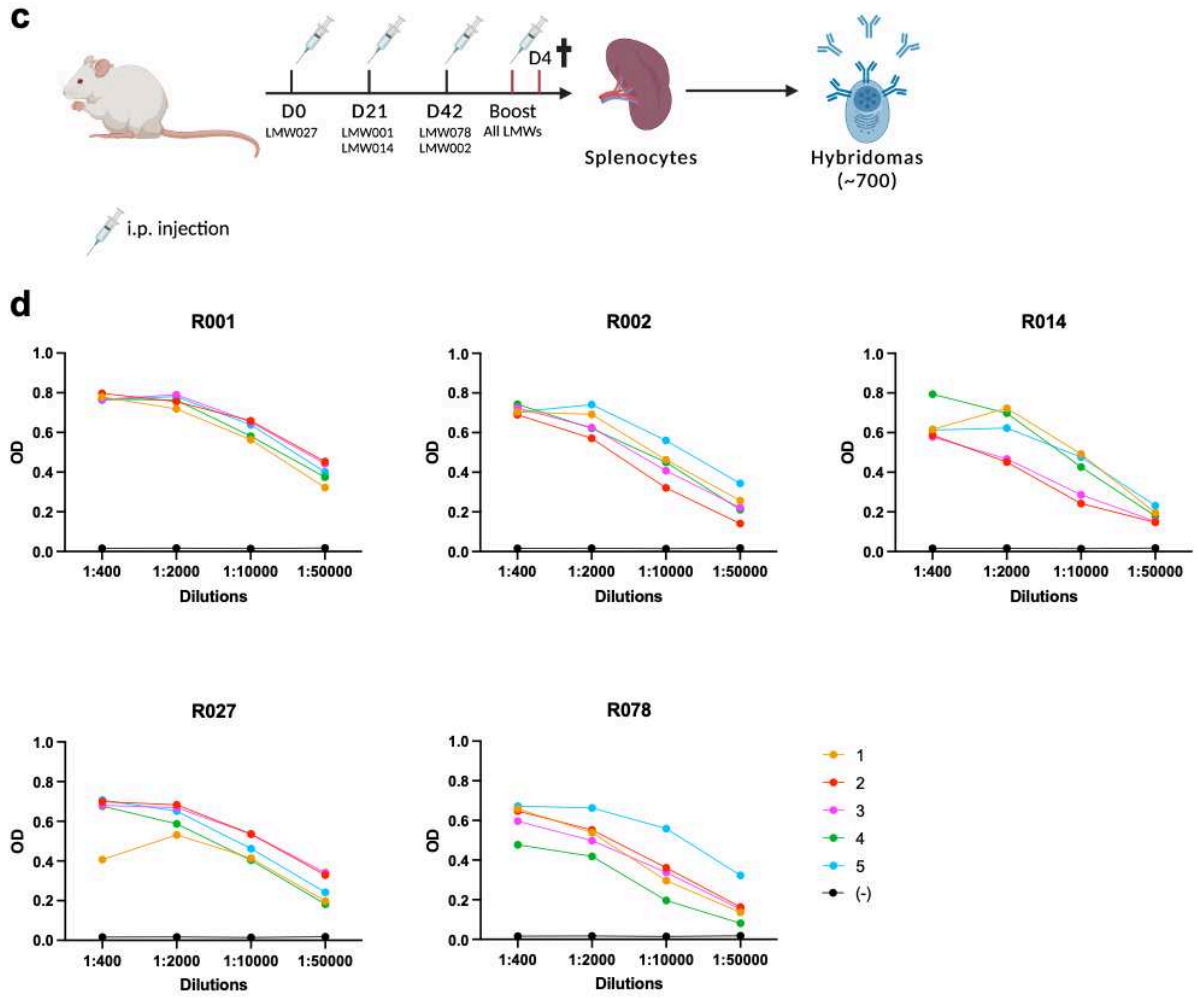

Figure 1: Generation of anti-LMW-specific hybridomas from immunized mice. (**a**) Sequence alignments of the LMW of five clinical ribotypes (LMW-R001, LMW-R002, LMW-R014, LMW-R027, LMW-R078) by ClustalOmega software. Conserved residues are indicated by *, . or :. Signal peptide, domain 1 and 2 and the domain that interacts with the HMW are indicated. (**b**) Generation of mice knock-in for the human variable VDJ segments in the endogenous variable heavy chain locus, and for the human variable VJ segments in the endogenous variable light chain kappa locus. (**c**) Protocol outline. Mice were immunized with LMW proteins according to the represented scheme combined to alum and *Bordetella pertussis* toxin. Four days after the last boost, spleens were collected and hybridoma generated. (**d**) Sera titers at day 42 of immunized mice for recombinant LMW-R001, LMW-R002, LMW-R014, LMW-R078, LMW-R027 measured by ELISA. OD values for several dilutions for mice #1, #3, #4, #6 and #7 are represented. Black curves represent sera titers naïve mouse.

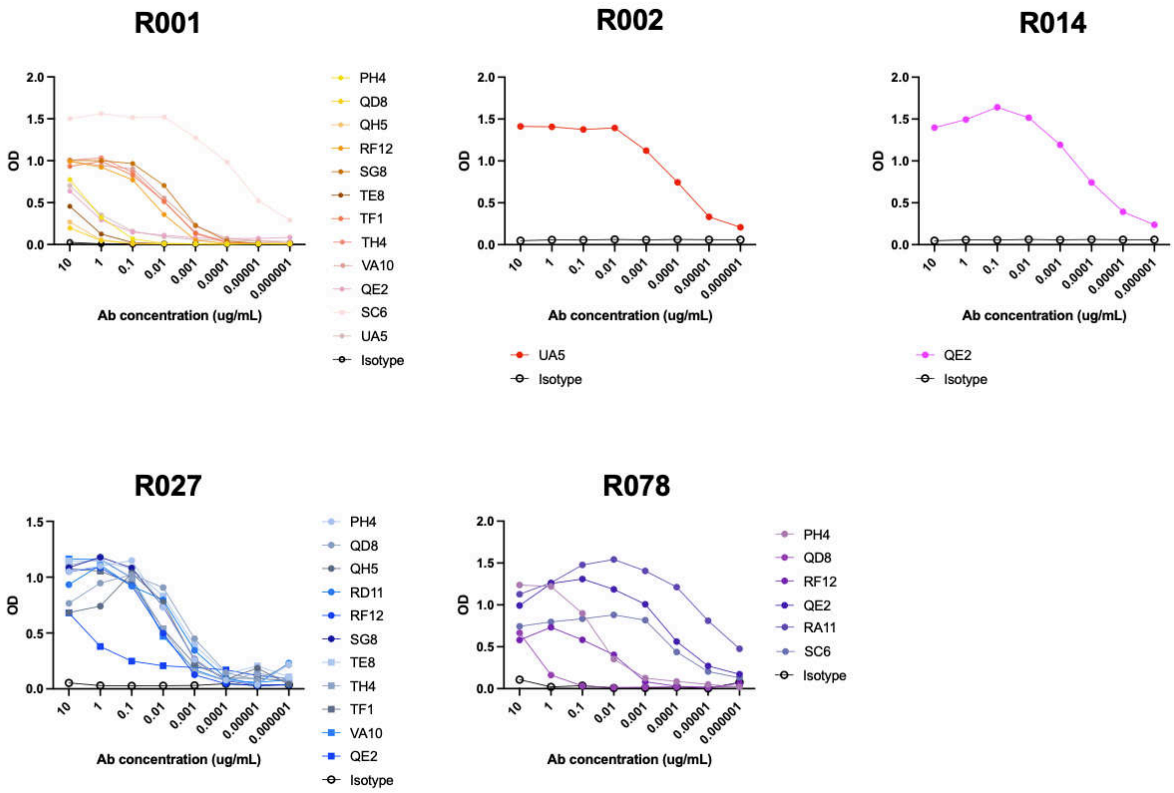

Figure 2: Specificities of anti-LMW mAbs. ELISA results (OD values 492 nm VS 620 nm) against recombinant LMW-R001, LMW-R002, LMW-R014, LMW-R078 and LMW-R027 of IgG mAbs at indicated concentrations. Black curves represent isotype controls.

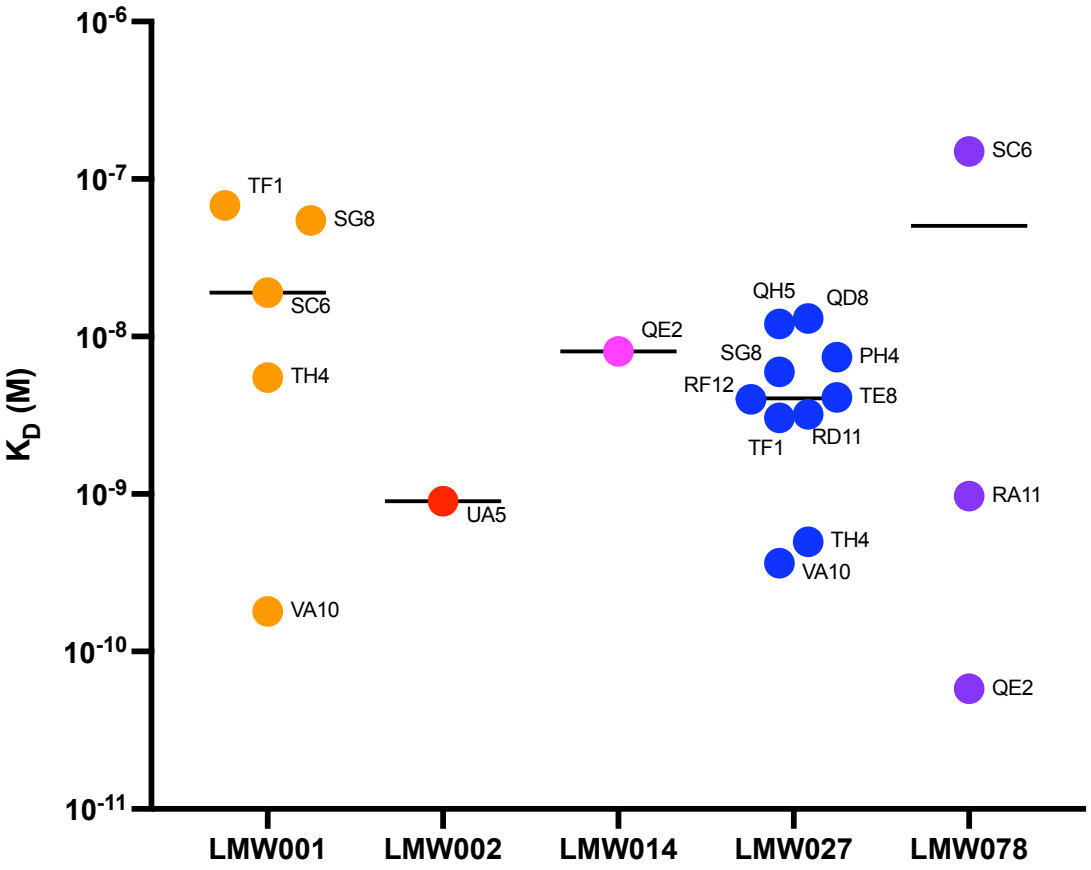

Figure 3: Affinities of mAbs for the LMW of five clinical ribotypes. Dissociation constant (K_D) values measured by BLI. Each dot represents the K_D value of one mAb (mAb name indicated) interacting with one LMW among LMW-R001, LMW-R002, LMW-R014, LMW-R078 and LMW-R027. Black bars represent median KD values of the group of mAbs binding one ribotype.

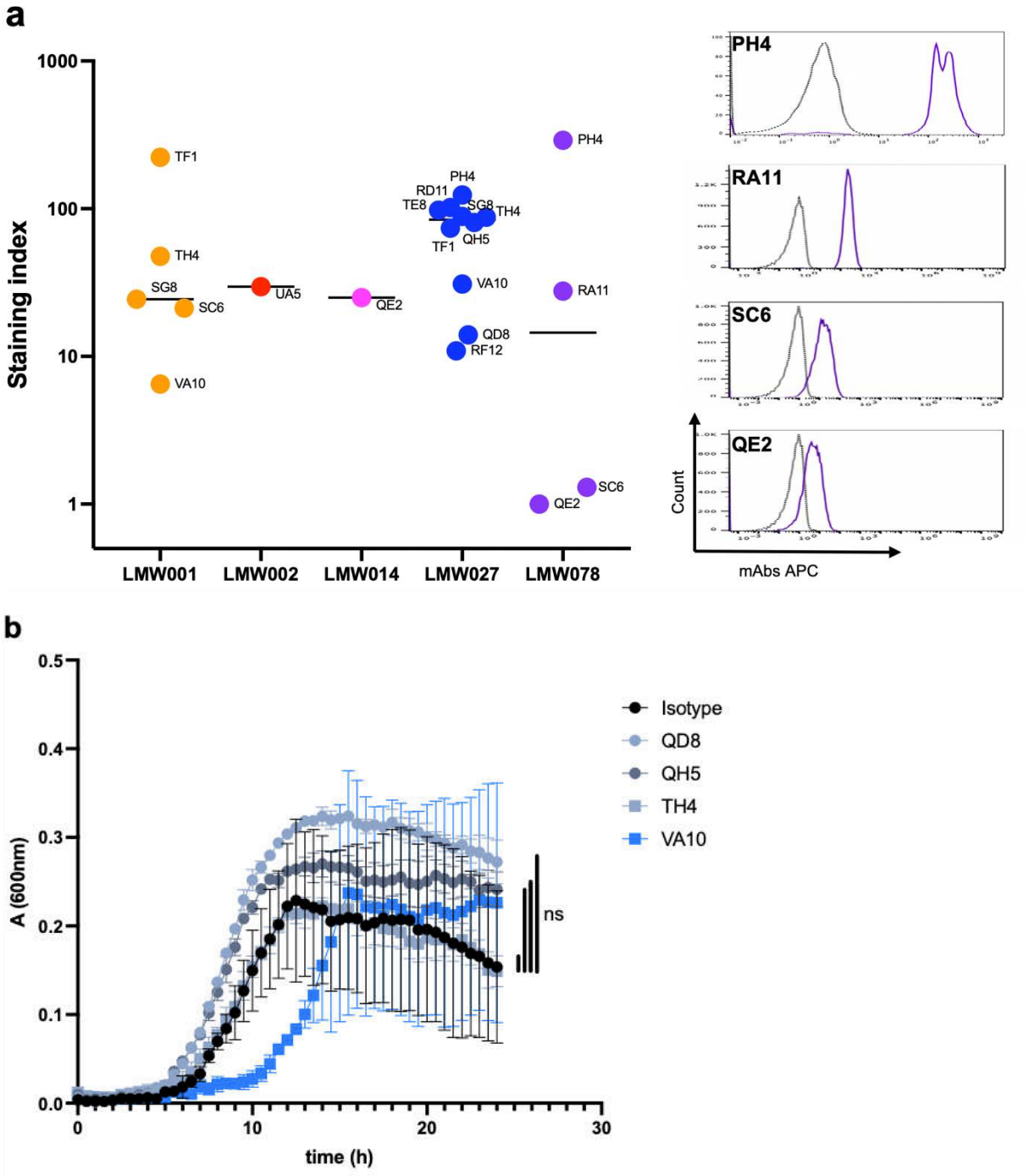

Figure 4: Binding of mAbs to LMWs expressed at the surface of *C. difficile* bacteria. (**a**) Flow cytometry analysis of mAbs binding to LMW of indicated *C. difficile* ribotypes. Results are displayed as staining index (*refer to methods section*) (left panel). Representative histograms of *C. difficile* R078 bound by anti-LMW078 mAbs (right panel). (**b**) Growth of *C. difficile* strain R027 in BHISG medium incubated with indicated anti-LMW027 mAb or with an unspecific IgG (isotype). Growth was followed continuously over 24h. Each dot represents

the mean of three technical replicates, and the bars indicate standard deviations. ns: non-significant.

Antibody	Ribotype				
	001	002	014	078	027
PH4	E			E/F	E/F
QD8	E			E	E/F
QH5	E				E/F
RD11					E/F
RF12	E			E	E/F
SG8	E/F				E/F
TE8	E				E/F
TF1	E/F				E/F
TH4	E/F				E/F
VA10	E/F				E/F
QE2	E		E/F	E/F	E
RA11				E/F	
SC6	E/F			E/F	
UA5	E	E/F			

Table 1: Summary table of mAbs binding profiles to LMW recombinant proteins and LMW expressed at the bacterial surface of *C. difficile* bacteria for five clinical ribotypes. E indicates binding by ELISA and F binding by flow cytometry. Blanks indicate absence of binding.

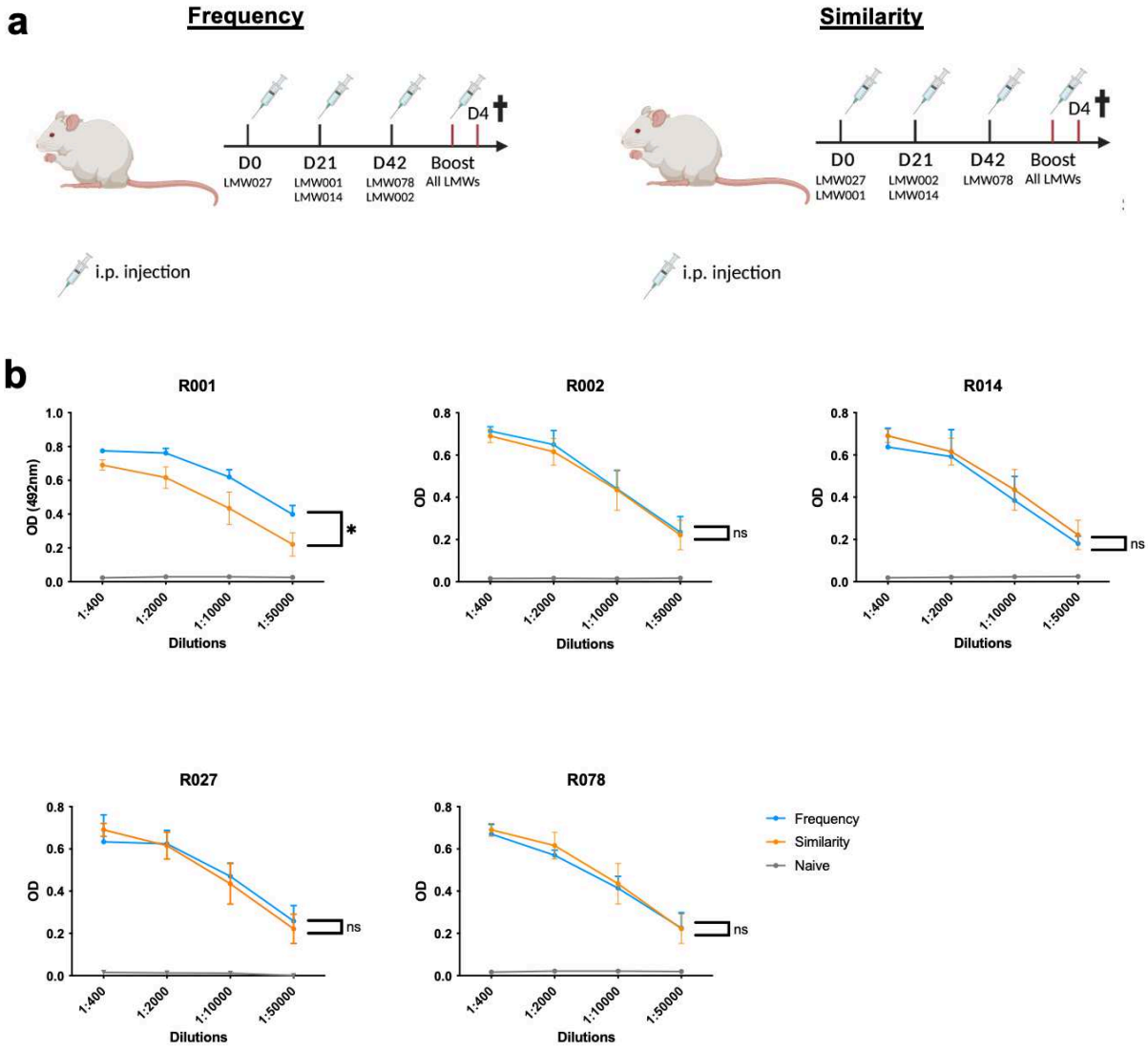

Figure S1. Comparison of two immunization protocols using recombinant LMWs. Mice were immunized following two different protocols termed "similarity" and "frequency". (**a**) In the "Frequency" protocol, mice are immunized with LMWs in the order of their frequency in current CDI and boosted with a mix of all five LMWs. In the "Similarity" protocol, mice are immunized with two highly similar LMW the same day and boosted with a mix of all five LMWs. (**b**) Dose response of sera titers of immunized mice from the protocols depicted in (a) are measured by ELISA against the indicated LMW ribotype. Data are presented as mean values (±SD) for each group of mice (n=5). ns: non-significant; *: $p<0.05$. Black curves represent sera from naive mice prior immunization.

Unpublished data associated to chapter VI

This data has been generated during the work on the mAb collection. However, to avoid adding to much negative data in the manuscript, we did not include it in the version that will be submitted.

Generation of cross-specific anti-LMW mAbs against the five clinical ribotypes R001, R002, R014, R027 and R078

We succeeded in generating one mAb, UF11 that was recognizing the LMW of the five clinical ribotypes R001, R002, R014, R078 and R027 (Fig. 1). Binding by ELISA could be seen until 1-0.1 µg/mL, suggesting medium affinities (~100 nm). However, this mAb could not bind to any LMW exposed at the surface of *C. difficile* from these five ribotypes. This suggests that this mAb recognizes a conserved epitope that is likely involved in LMW-HMW interaction, which is therefore hidden at the surface of the bacteria.

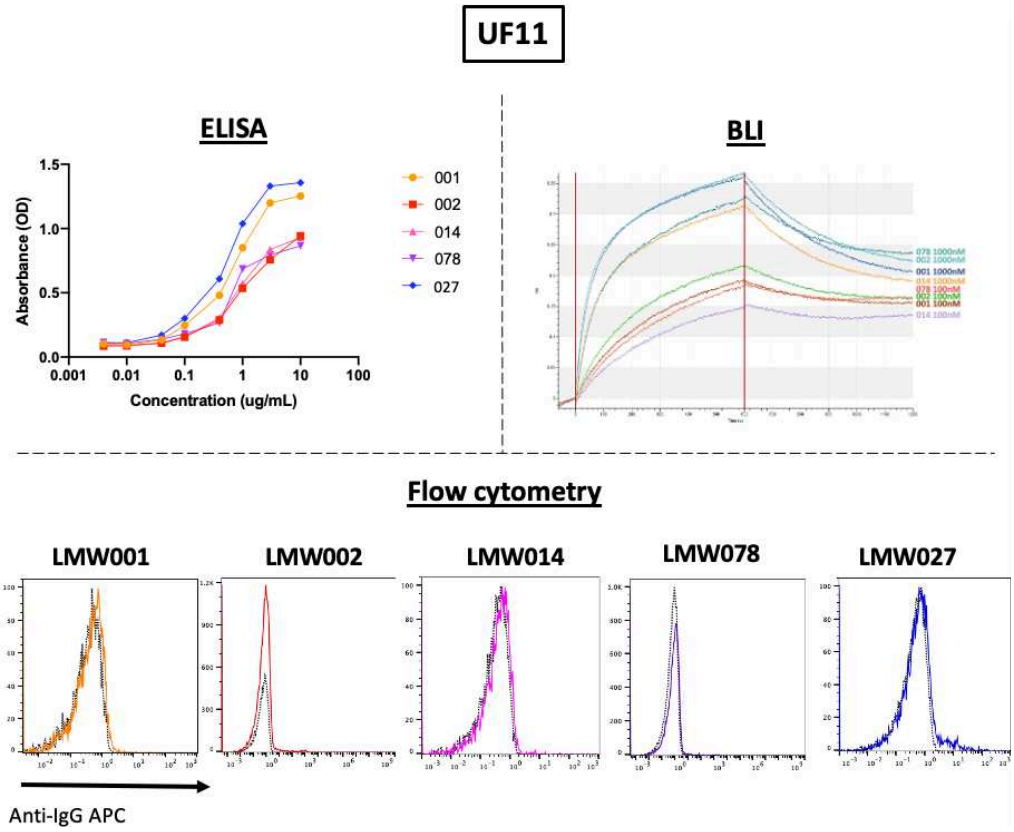

Figure 1. Binding of anti-LMW mAb UF11 to LMW recombinant proteins (top row) and whole bacteria (bottom row).

Homology between the LMW from ribotype R001, R002, R014, R027, R078 and strain 630

We aligned the different LMW sequences and found the highest homology percentage between the LMW-R027 and the LMW-R001, followed by the LMW-R078 and R014 (Fig. 4). This is in good agreement with the cross-specific binding profiles of the mAbs reported in this collection. Interestingly, the LMW630, which shares the least homology percentage with the other LMWs was not recognized by any of the cross-specific mAbs.

	630	002	014	078	2029	001
630	100	25.86	31.82	36.39	38.04	39.38
002	25.86	100	46.81	48.60	46.12	45.74
014	31.82	46.81	100	55.24	50.21	50.77
078	36.39	48.60	55.24	100	61.50	61.72
2029	38.04	46.12	50.21	61.50	100	88.86
001	39.38	45.74	50.77	61.72	88.86	100

Figure 2. Tree and percentage of homology between LMWs proteins.

Generation of monoclonal antibodies against *C. difficile* FliC protein

Introduction

C. difficile flagella are composed of a 39-kDa flagellin protein (FliC) and a 56-kDa flagellar cap protein (FliD)[324]. These two proteins have various biological functions that favor bacterial survival and host colonization[325]. Flagella are believed to play a direct role in *C. difficile* virulence via the modulation of toxin production by flagellar regulon[326], and an indirect role via TLR5 interaction[78], therefore favoring inflammation. FliC is more conserved across *C. difficile* strains than the LMW SlpA, with conservation (> 95%[327]) in the N and C termini and a central region that is more diverse[328]. We therefore decided to generate new monoclonal antibodies against FliC protein and evaluate their effect on bacterial fitness.

Materials and methods

Production of FliC recombinant protein. FliC recombinant protein was produced as described by Batah *et al*[78]. Briefly, *E. Coli* transformed with FliC (MRVNTNVSALIANNQMGRNVNGQSKSMEKLSSGVRIKRAADDAAGLAISEKMRAQ IKGLDQAGRNVQDGISVVQTAEGSLEETGNILQRMRTLSLQSANEINNTEEREKIADE LTQLKDEIERISSSTEFNGKKLLDGTSSTIRLQVGASYGTNVSGTSNNNNEIKIQLVNT ASIMASAGITTASIGSMKAGGTTGTDAAKTMVSSLDAALKSLNSSRAKLGAQQNRLE STQNNLNNTLENVTAAESRIRDTDVASEMVNLSKMNILVQASQSMLAQANQQPQGV LQLLLEHHHHHH) expression plasmid were cultured in LB medium supplemented with 40mg/mL kanamycin overnight at 37°C.

This preculture was expanded in 2L of the same medium until OD_{600nm} reached 0.8-1. Then FliC expression was induced with1 mM Isopropyl β-D-thiogalactoside (IPTG) for 4h. Cultures were spined down and pellet kept. FliC was purified on a His-Select Nickel Affinity Gel followed by SDS-PAGE.

Production of monoclonal antibodies against FliC. Monoclonal antibodies were produced as described in chapter VI by immunizing Balb/c mice with with 50 µg of recombinant FliC protein mixed with 200 ng/mouse pertussis toxin i.p. following the same scheme used to produce anti-LMW antibodies.

ELISA assays. 0.3 µg of FliC recombinant protein in carbonate buffer were coated on microtiter plates (Dutscher, France) 2h at room temperature and then ELISA assays were caried out as described in chapter VI.

Flow cytometry assay. *C. difficile* strains (ribotypes 001, 014, 078, 027 and 630) were obtained as part as a collaboration with BaPS' team (Université Paris-Saclay) and Dr. Bruno Dupuy's team (Institut Pasteur, Paris). Flow cytometry assay was conducted as described in chapter VI with anti-FliC mAbs at 10 µg/mL.

Western Blot (WB) assay. WB assays were done in collaboration with Dr Susanne Sievers' lab (University of Greiswald, Germany), according to their own protocol. Native FliC proteins were extracted from *C. difficile,* and WB performed with 10 µg/mL of anti-FliC mAbs.

Results

Flagella proteins are important for bacterial motility and have been identified as interacting with TLR5[78]. Therefore, we generated mAbs that recognize FliC, the dominant protein of *C. difficile* flagella to evaluate them as potential therapeutics. We first produced and purified FliC protein. As shown in Figure 1.a, purified fractions contained predominantly FliC protein (band around 35kDa -the molecular weight of FliC is 39kDa-). We then confirmed that our recombinant FliC protein was recognized by serum of rabbits immunized with different forms of FliC (flagellin extract and recombinant FliC obtained in other labs). As shown in Figure 1.b, our recombinant FliC protein was correctly recognized by both rabbit sera.

Balb/c mice were then immunized with recombinant FliC protein according to the following scheme (Fig. 1.c). Previous publications demonstrated FliC immunogenicity[78]. Accordingly, we observed significant anti-FliC antibody titers in mice serum, regardless of the adjuvant (Fig. 1.d). Splenocytes from two mice (676 and 848) were fused with myeloma cells to obtain hybridomas. After screening by ELISA, two hybridomas producing anti-FliC mAbs were expanded and their mAbs (1E11 and 2C3) purified.

Binding of these two anti-FliC mAbs was evaluated by ELISA towards the recombinant protein. As shown in Figure 2.a, binding to FliC was detectable until 1ng/mL suggesting high-affinity antibodies. We also confirmed by WB that both mAbs could bind to native FliC protein directly extracted from *C. difficile* bacteria (Fig. 2.b).

We then wanted to know whether these mAbs recognize *C. difficile* bacteria. To do so, we performed bacterial flow cytometry assay with both fixed bacteria (data not shown) and alive bacteria. While FliC protein is expressed and conserved across *C. difficile* ribotypes, we detected either very weak binding (R001, R014) or no binding (R078, R027 and 630) to bacteria (Fig. 2.c).

Discussion

We isolated two anti-FliC mAbs that recognize both recombinant and native FliC protein, but do not bind whole *C. difficile*. At this point, we cannot rule out that the conditions we used for our experiments were detrimental for FliC expression. Indeed, a genetic "flagellar" switch (on/off) controls production of flagella proteins during growth *in vitro* and modulate intestinal colonization *in vivo*[329,330]. However, we were not able to determine the ON/OFF orientation of the flagellar switch during *C. difficile* growth. Besides, bacterial flow cytometry protocol requires washing steps with spinning that can break the flagella. Moreover, vortexing, which is routinely used for bacterial resuspension after overnight culture, can remove flagella from the bacteria. To avoid washing steps and vortexing, we evaluate anti-FliC mAb binding to *C. difficile* using microscopy, but we could not see significant staining. An ongoing collaboration with Dr. Susanne Sievers' lab, which was able to detect *C. difficile* flagella using microscopy, should help us to conclude whether our mAbs bind whole flagella and not only recombinant FliC.

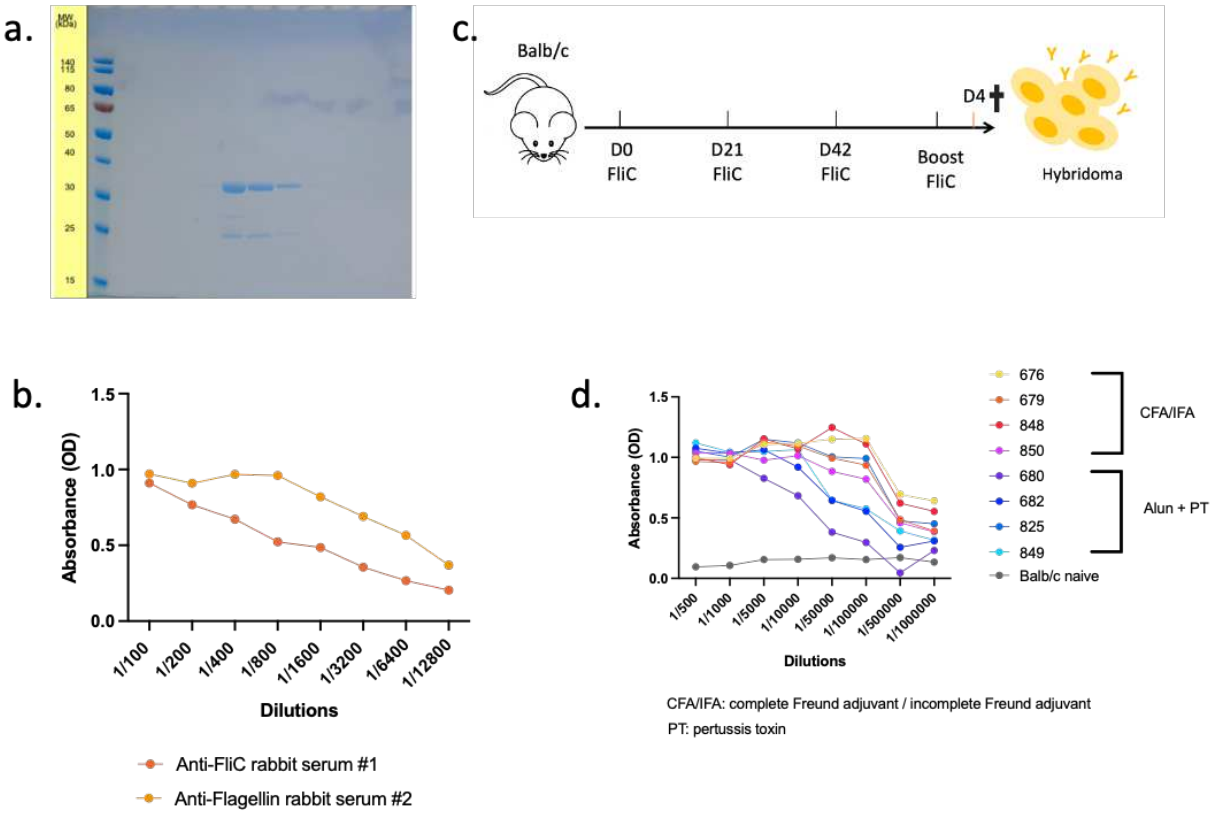

Figure 1. Generation of anti-FliC mAbs. a) SDS-PAGE of purified FliC recombinant protein. Lanes correspond to different elution fractions. **b)** Microtiter plates were coated with FliC protein before being co-incubated with anti-FliC sera at different dilutions. Detection of antibody binding FliC was performed using HRP conjugated anti-rabbit IgG Ab. **c)** Immunization schedule of Balb/c mice with FliC protein. **d)** Microtiter plates were coated with FliC proteins before being co-incubated with sera from immunized mice at different dilutions.

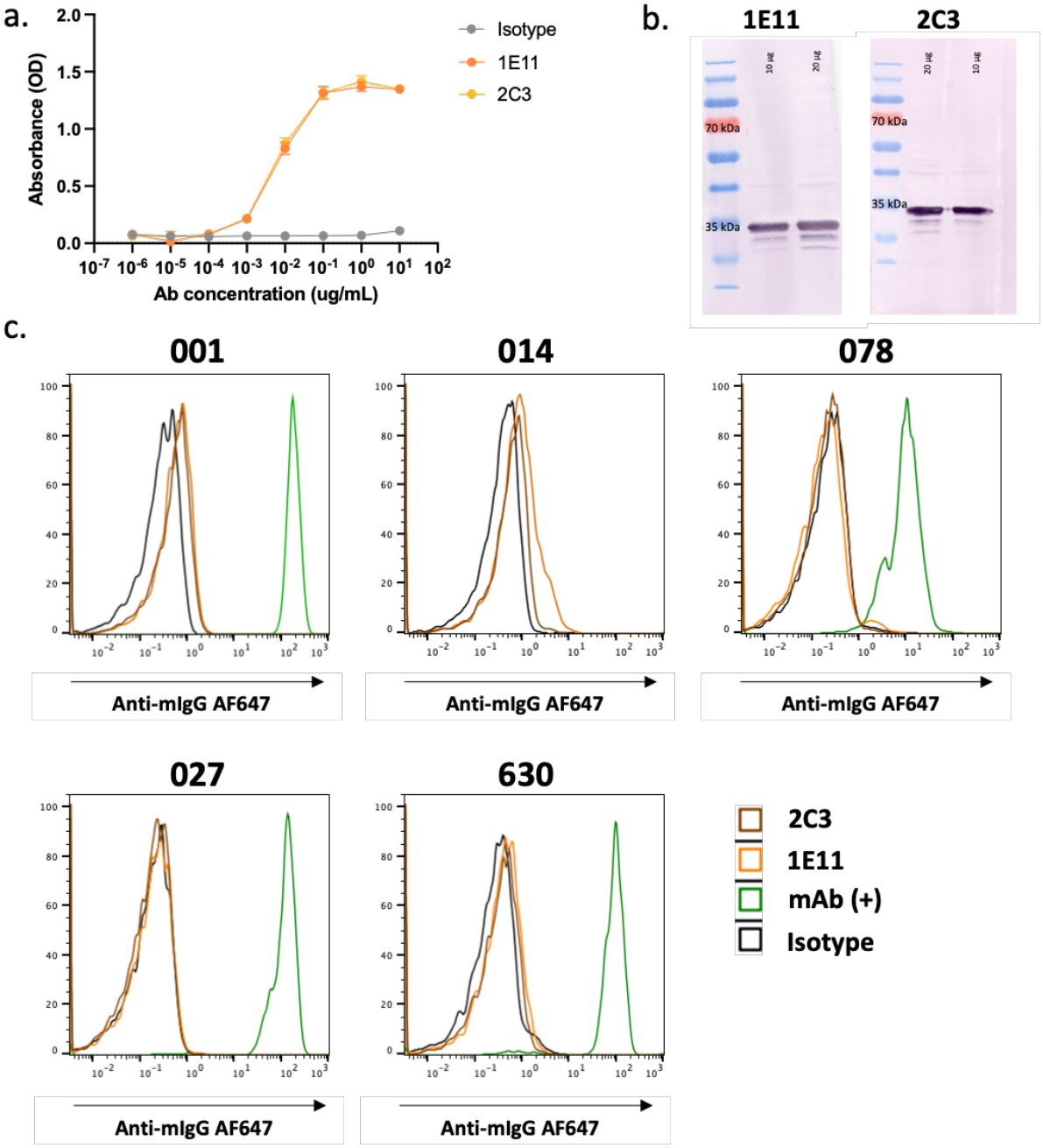

Figure 2. Characterization of anti-FliC mAbs. a) Microtiter plates were coated with FliC protein before being co-incubated with both purified mAbs (1E11 and 2C3) at different concentrations. Detection of mAbs was performed using HRP conjugated anti-mouse IgG Ab. **b)** Western blot analysis with native FliC proteins extracted from *C. difficile*. **c)** Anti-FliC mAbs binding profiles towards 5 different strains of *C. difficile* (R001, R014, R078, R027 and 630). Histograms showing mAb binding to *C. difficile* bacteria at 10 µg/mL.

VII. Anti-S layer monoclonal antibodies induce significant changes in *C. difficile* physiology

The second part of this work consisted in evaluating anti-LMW mAbs on the model strain of *C. difficile*: strain 630. To this end, we isolated anti-LMW630 mAbs and characterized their binding to the LMW by ELISA. We evaluated mAb affinity using BLI. The majority of the mAbs displayed medium to high affinities. Competitive assay was performed by BLI and showed that only 2 mAbs partially compete for the same epitope on the LMW.

Binding to the LMW at the surface of the bacteria was evaluated by flow cytometry on *C. difficile* (strain 630 and *C. difficile* ribotype 012) and on other commensal *Clostridium* species *C. butyricum* and *C. bifermentans*. No cross-reactivity for *C. difficile* of another ribotype or another specie was observed. We confirmed mAb binding to bacterial surface by microscopy, while mAb did not bind the surface of the spores. Finally, classical effector functions of these mAbs were evaluated. All anti-LMW mAbs increased phagocytosis compared to an unspecific mAb.

Having generated and characterized these anti-LMW mAbs, we next evaluated their effect on *C. difficile* physiology. Bacterial growth in presence of the mAbs was assessed and stinkingly, one mAb (NF10) inhibited the growth of *C. difficile* in a dose-dependent manner. Moreover, NF10 mAb restored *C. difficile* sensitivity to lysozyme. Interestingly, a synergistic effect between DCA and NF10 mAb was also observed, with an impact on growth more important in presence of these two molecules than the mAb alone. Impaired growth might be related to more bacterial lysis in presence of NF10 mAb, as quantified by the LDH released in *C. difficile* cultures.

The secretion of toxins was significantly modulated in presence of the anti-LMW mAbs, leading to contrasting effects. NF10 mAb increased toxins' secretion which can be related to the increase of lysis, while two other mAbs (KH2 and TG10) inhibited toxins' release. The precise mechanisms behind this inhibition remain to be investigated.

Lastly, biofilms' formation was evaluated in presence of anti-LMW mAbs. A first technique showed an increase of biofilms in presence of 2B7 mAb. To investigate more finely the impact on the structure of the biofilms, confocal microscopy was used. When examined with this

technique, biofilms in presence of NF10 and 2B7 appeared thicker, and with an increased biovolume and roughness.

Related work to this chapter is presented after this second manuscript. It includes adhesion assays to enterocytes that were performed in presence of anti-LMW mAbs, as well as the development of a gut-on-chip model to study *C. difficile* colonization and adhesion to enterocytes. Two *in vivo* assays evaluating anti-LMW mAbs in a CDI model using hamsters or axenic mice are finally presented and the results of these experiments discussed.

Anti-S-layer monoclonal antibodies impact *Clostridioides difficile* physiology

Lise Hunault[1,2,3], Emile Auria[4], Patrick England[5], Julien Deschamps[6], Romain Briandet[6], Vanessa Kremer[2,7], Bruno Iannascoli[2], Léo Vidal-Maison[1], Lynn Macdonald[8], Séverine Péchiné[9], Cécile Denève-Larrazet[9], Bruno Dupuy[4,†], Guy Gorochov[1,†,#], Pierre Bruhns[2,†,#] and Delphine Sterlin[1,†].

[1]Sorbonne Université, INSERM, CNRS, Centre d'Immunologie et des Maladies Infectieuses (CIMI-Paris), 75013 Paris, France

[2]Institut Pasteur, Université Paris-Cité, INSERM UMR1222, Antibodies in Therapy and Pathology, 75015 Paris, France

[3]Sorbonne Université, Collège doctoral, 75005 Paris, France

[4]Institut Pasteur, Université Paris-Cité, UMR-CNRS 6047, Laboratoire Pathogenèse des Bactéries Anaérobies, 75015 Paris, France

[5]Institut Pasteur, Université Paris Cité, CNRS UMR3528, Plateforme de Biophysique Moléculaire, 75015 Paris, France

[6]Université Paris-Saclay, INRAE, AgroParisTech, Institut Micalis, 78350 Jouy-en-Josas, France

[7]Inflammation, Microbiome and Immunosurveillance, Université Paris-Saclay, INSERM, 92290 Châtenay-Malabry, France

[8]Regneron Pharmaceuticals, Tarrytown, NY, USA

[9]Université Paris-Saclay, INRAE, AgroParisTech, Institut Micalis, Equipe Bactéries Pathogènes et Santé, 78350 Jouy-en-Josas, France

†shared senior authorship

To whom correspondence should be addressed:
pierre.bruhns@pasteur.fr, guy.gorochov@sorbonne-universite.fr

Abstract (250 words)

Clostridioides difficile (*C. difficile*), a Gram-positive anaerobic and spore-forming bacterium, is the leading cause of nosocomial antibiotic-associated diarrhea in adults and is characterized by high levels of recurrence and mortality. Surface-Layer Protein A (SlpA), the most expressed protein on bacterial surface, plays a crucial role in the early stages of infection although its role in *C. difficile* physiology is yet to be fully understood. Anti-S-layer antibodies have been identified in the sera of convalescent patients and correlate with improved outcome of *C. difficile* infection (CDI). However, the precise mechanisms of how anti-S-layer antibodies can confer protection to the host remain unknown. In this study, we report the first monoclonal antibodies (mAbs) targeting *C. difficile* S-layer. Characterization of these mAbs unravels important roles for S-layer protein in growth, toxin secretion, and biofilm formation with, surprisingly, opposite effects of different anti-SlpA mAbs on these functions. One anti-SlpA mAb impaired *C. difficile* growth and restored sensitivity to lysozyme-induced lysis. These findings suggest that anti-S-layer antibody responses may include protective and detrimental effects for the host, and provide important insights for designing adequate S-layer-targeting therapeutics.

Keywords (5-10 words)

Clostridioides difficile, monoclonal antibodies, S-layer, growth, biofilms, toxins, neutrophils

Introduction

Clostridioides difficile is an anaerobic, Gram-positive, and spore-forming bacteria, that is the leading agent responsible for nosocomial antibiotic-associated diarrhea and colitis in adults[1]. *C. difficile* infection (CDI) causes substantial morbidity and mortality with severe pseudomembranous colitis characterized by extensive colonic damage and intestinal inflammation. While CDI symptoms have largely been attributed to the bacterial toxins, a growing concern focused on *C. difficile* adhesins and surface proteins involved in gut colonization and evasion of the immune system surveillance. These proteins play a major role in triggering bacterial pathogenesis through interactions with Toll-Like Receptor 4 (TLR4) and inflammatory response induction[307,308]. Among these proteins, *C. difficile* Surface-layer protein A (SlpA) has gained substantial interest.

The *C. difficile* S-layer is composed of two main proteins *i.e.,* the High-Molecular Weight (HMW) and the Low-Molecular Weight (LMW) Surface Layer Proteins (SLPs) that derive from the common precursor SlpA. SlpA is first secreted and then cleaved by the cell wall cysteine protease Cwp84, releasing the two mature subunits HMW and LMW. These two subunits associate to form a stable heterodimeric complex, which is anchored to the cell wall by the HMW, with the LMW being the most external subunit. SlpA is secreted throughout the cytoplasmic membrane and constitutes an interwall reservoir, which is available to fill the gaps that form during growth or damage[37]. With the assembly of the S-layer at areas of newly synthesized peptidoglycan, *C. difficile* is able to maintain a stable S-layer that continually protects the cell. One astonishing characteristic of *C. difficile* S-layer is its compactness. With pores of only 10Å in diameter, it is more compact than other S-layers whose pores range from 30Å up to 100Å. This renders *C. difficile* impermeable to large molecules such as lysozyme[38], to which it is resistant.

The S-layer is crucial for bacterial integrity and *C. difficile* S-layer-null mutants display severe impaired physiological functions. They are highly sensitive to innate immune effectors such as lysozyme, show sporulation defects and produce less toxins *in vitro*[50]. *C. difficile*'s virulence and recurrence have been associated to its ability to form biofilms in the gut[72]. Biofilm formation is the differential process of planktonic cells to bacterial communities embedded into a thick enclosed matrix[331]. Cwp84 mutants with altered S-layer display an increased biofilm generation suggesting that intact S-layers prevent aggregation which is one of the first steps to generate biofilms[299]. As the predominant surface protein, *C. difficile* S-layer has also been implicated in attachment to intestinal cells both *in vitro* and *ex vivo*[45,297].

The S-layer is immunogenic, as anti-SLPs antibodies have been detected in the sera of convalescent patients and are associated with improved CDI outcome[44,154]. In animal models, passive immunization using anti-SlpA serum has been demonstrated to delay *C. difficile* colonization in mice[43], whereas active immunization with recombinant SlpA slightly prolonged survival of hamsters infected by *C. difficile*[332]. Additionally, anti-LMW nanobodies have been shown to decrease bacterial motility *in vitro*[302]. However, the extent to which anti-S-layer humoral responses interfere with *C. difficile* fitness and CDI pathogenesis remains unclear. No monoclonal antibodies (mAbs) targeting the S-layer that could be used to explore the role of SlpA *in vivo* have been reported so far.

Here, we generated and characterized the first anti-LMW mAbs to interrogate S-layer interactions with host immune response. We describe differential effects of anti-LMW mAbs on *C. difficile* physiology in terms of growth, toxin secretion, and biofilm formation *in vitro*. Our work deciphers interactions between antibodies and various epitopes of the S-layer with unexpectedly different outcomes, and describes further the role of *C. difficile* S-layer in bacterial fitness.

Results

Generation and characterization of high-affinity LMW-specific mAbs.

To interrogate the role of the S layer in *C. difficile* biology, we generated a collection of mAbs targeting the SlpA LMW, the most external subunit of *C. difficile* S-layer. As anti-LMW antibodies may potentially be of therapeutic interest for the treatment of *C. difficile* infections, we used knock-in mice in which the endogenous genes encoding the heavy chain variable domain (VH) and the kappa light chain variable domain (Vκ) were replaced by their human counterparts (Velocimmune)[317,318] with one modification: one allele of the endogenous Vκ locus was replaced by human Vκ segments, whereas the second allele of the endogenous Vκ locus was replaced by human Vλ segments to increase the variability at the kappa locus that represents 95% of antibodies in mice[319]. Thus, after hybridoma identification, cloning of these VH and VL into vectors containing human heavy and light chain constant domains, allows for direct development - *in fine* – of fully human anti-LMW mAbs. These mice but also BALB/c mice were immunized with recombinant LMW at D0, D21, D42 and four days before spleen collection, according to the schedule presented in Figure 1a. Anti-LMW hybridomas were generated from splenocytes of one Velocimmune and one BALB/c mouse, using ELISA as a screening method (Fig. 1a). Seven anti-LMW mAbs (all mouse IgG1) were identified that demonstrated a 10^{-1} to 10^{-2} µg/mL effective concentration 50 (EC_{50}) in an anti-LMW ELISA. mAbs NF10 and KH2 originated from the BALB/c mouse and possess mouse VH-VL sequences, whereas mAbs 1E2, 2B7, 2C4 and 4G4 originated from the Velocimmune mouse and possess human VH-VL sequences. For all mAbs, their VH-VL gene sequences displayed CDR3 length distributions from 10 to 20 residues (Table 1).

Bio-layer interferometry (BLI) experiments revealed a very large range of equilibrium dissociation constants (K_D) ranging from 32 pM to 7split 0 nM, corresponding to low to very-high affinity antibodies (Fig. 1c). The mAb with the worse affinity displayed a fast on/off profile with a high dissociation rate (k_{off}) of ~0.01 s^{-1}, whereas the two mAbs with the best affinities displayed a very low k_{off} of ~0.00003 s^{-1} (Table S1). To examine whether anti-LMW mAbs recognized overlapping or distinct epitopes on LMW, we designed a competitive BLI assay based on a pre-bound anti-LMW Ab as a competitor. Only two mAbs, KH2 and 2B7, partially competed for their binding to LMW (Fig. 1d). We therefore generated a set of mostly high-affinity anti-LMW mAbs that target 5 different and non-overlapping epitopes on *C. difficile* SlpA LMW.

Binding to *C. difficile* 630 vegetative cells.

Since the LMW is the most exposed S-layer protein of *C. difficile*, we next wanted to assess mAb binding to *C. difficile* whole bacteria. For this purpose, we used a previously reported bacterial flow cytometry assay[310]. Five out of the seven anti-LMW mAbs readily bound *C. difficile* 630 (Median Fluorescence Intensities (MFI) 100- to 1,000-fold higher compared to isotype control). mAb 2C4 poorly bound *C. difficile* 630 (MFI 5-fold higher compared to isotype) and mAb 4G4 very poorly if not at all (MFI 2.5-fold higher compared to isotype) (Fig. 2a). These results are mostly in agreement with the affinities of these mAbs for LMW, as mAb 4G4 possesses by far the worst affinity (70nM). mAb 2C4, however, should bind *C. difficile* in these conditions (K_D= 1.37nM) but its epitope may be partially inaccessible. Also, 2B7 that possesses a very high affinity (K_D= 67pM) displayed only a mild binding, 10x lower than that of NF10 that displays a similar affinity for LMW (K_D= 43pM). None of these 7 mAbs cross-reacted with commensal bacteria of the same genus i.e., *Clostridium bifermentans* and *Clostridium butyricum*, confirming their *C. difficile* specificity. In addition, none cross-reacted with a different ribotype (012) of *C. difficile* strain CD20-247, consistent with the low inter-strain homology of the LMWs (Fig. 2a).

LMW is expressed at the surface of vegetative forms, but not spores.

SlpA is expressed in the proteome of *C. difficile* spores, but whether the protein is exposed at the spores' surface remains unknown[41]. We therefore analyzed by microscopy the binding of the mAb with the best K_D and the highest staining index on bacteria i.e., mAb NF10, to spores as well as to the vegetative form of *C. difficile*. Anti-LMW mAb NF10 stained the vegetative form but did not stain spores (Fig. 2b), indicating that SlpA LMW is not expressed at the surface of *C. difficile* spores.

Anti-LMW mAbs enable *C. difficile* phagocytosis by neutrophils.

We next evaluated if SlpA LMW was a suitable target for enabling or increasing phagocytosis of *C. difficile* by neutrophils, as it might occur during CDI after epithelial breakdown by the toxins secreted by *C. difficile*[333] and invasion of the intestinal vili by bacteria and neutrophils[85]. We used a standard *in vitro* phagocytosis assay in which bacteria are fluorescently labeled, opsonized by anti-bacterial IgG mAbs and incubated with purified human neutrophils, and phagocytosis was measured by flow cytometry. All anti-LMW mAbs being of

the mouse IgG1 isotype, they are able to interact with human IgG receptors (FcγRs)[334] expressed by human neutrophils. As expected, we found that binding of all five anti-LMW mAbs with a significant staining index on bacteria (excluding mAbs 4G4 and 2C4 from this analysis) enabled neutrophil-dependent phagocytosis of *C. difficile* (Fig. 2c). Surprisingly, we found no correlation between phagocytosis and staining index by flow cytometry, with mAb 2B7 inducing very high phagocytosis and mAb KH2 very low phagocytosis. mAb 2B7 induced as much phagocytosis than a cocktail of mAbs NF10, KH2, 1E2, 2B7 and TG10 at equimolar ratio, suggesting a unique property of 2B7 or of its epitope to favor phagocytosis. Altogether, these results demonstrate that this set of five anti-LMW mAbs recognized *C. difficile* in a vegetative state and enhanced its phagocytosis by neutrophils.

C. difficile growth is inhibited solely by mAb NF10

The S-layer appears to be essential for *C. difficile* fitness as *de novo* S-layer proteins should be assembled during cell growth and division[37]. We investigated if targeting of SlpA LMW may impact bacterial growth. When growth was measured in suspension, mAb NF10 slowed down growth of *C. difficile* bacteria that could only reach ~50% of the plateau reached at 13 hours of culture in the presence of an isotype control (Fig. 3a). No other anti-LMW mAb had an effect on growth. A minimum concentration of 50 µg/mL mAb NF10 was however necessary to detect a statistically significant effect on growth (Supplemental Fig. 1a). The effect of NF10 mAb was specific to the *C. difficile* 630 strain as no effect was detected on a *C. difficile* strain belonging to another ribotype i.e., UK1 (Fig. 3b). These results underline a unique property of mAb NF10 or of its epitope to inhibit growth of *C. difficile* strain 630.

Bacterial lysis is promoted by mAb NF10

We next sought to determine how anti-LMW mAb NF10 impaired *C. difficile* growth. A pool of SlpA precursor was reported to be localized within the bacterial cell wall, available to repair openings in the S-layer during cell growth or damage[40]. We thus hypothesized that NF10 mAb could affect SlpA replacement in the S-layer, thereby promoting bacterial lysis. We therefore quantified the lactate dehydrogenase (LDH) released upon cell lysis during exponential growth phase in the presence of the NF10 mAb. We found significantly more LDH in supernatants of NF10-exposed bacterial cultures compared to isotype control-exposed bacterial cultures (Fig. 2c), supporting the hypothesis that NF10 mAb weakens the integrity of the bacterial membrane.

If the bacterial membrane integrity is compromised, it should become vulnerable to enzymes, in particular to lysozyme. Normal *C. difficile* is indeed highly resistant to lysozyme, a protein produced by Paneth cells in the small intestine and ascending colon in humans, unless it expresses SlpA mutants which leads to a slower growth in the presence of lysozyme[50]. Strikingly, high concentrations of NF10 (100 and 200 µg/mL) only partially inhibited growth of *C. difficile* in standard culture conditions but abrogated growth in the presence of lysozyme (Fig. 3d, Supplemental Fig. 1b). Moreover, low concentrations of NF10 (6.25 µg/ml to 25µg/mL)) that did not affect growth in standard culture conditions significantly inhibited growth in the presence of lysozyme. Bile acid, deoxycholate (DCA), plays also a major role in CDI[335] and can, at high dose, abrogate the growth of *C. difficile* bacteria[68]. Suboptimal concentrations of DCA (i.e., 25 µg/mL) , that only mildly affect growth in standard culture conditions[68], allowed mAb NF10 mAb to significantly inhibit growth (Fig. 3d, Supplemental Fig. 1c). Altogether, these results show that mAb NF10 can potentiate the detrimental effect of lysozyme or bile acid on C. difficile growth, with a synergistic effect of mAb NF10 with either component of the intestinal environment.

***C. difficile* toxin secretion is altered by anti-LMW mAbs.**

Even though *C. difficile* toxins are secreted through pores in the S-layer by a mechanism that is so far unknown[38], impaired toxin production has been reported in *C. difficile* SlpA-null mutants[50]. Consequently, we explored whether anti-LMW mAbs were able to alter toxin secretion *in vitro*. In our assay, *C. difficile* 630Δerm (Cd630Δ*erm*)- a spontaneous erythromycin sensitive derivative of the reference strain 630 – secreted ~18ng/mL at 24h and ~170ng/mL at 48h of TcdA, and ~1ng/mL at 24h and ~14ng/mL at 48h of TcdB (Fig. 4). As expected, the Pathogenicity locus (Paloc)-deficient *C. difficile* mutant (ΔPaloc)[336] that lacks the toxin A and toxin B genes did not secrete any detectable quantity of these two toxins. Incubation with mAb NF10, but not any other anti-LMW mAb, significantly increased TcdA and TcdB secretion (Median values; NF10 mAb *vs* isotype control: $C_{TcdA\text{-}24h}$= 31.9 *vs* 17.7 ng/mL, p=0.0008; $C_{TcdA\text{-}48h}$=335 *vs* 172 ng/mL, p<0.0001; $C_{TcdB\text{-}24h}$=2,5 *vs* 1.3 ng/mL, p=0.0428; $C_{TcdB\text{-}48h}$=27.4 *vs* 14.5 ng/mL; p=0.002). In contrast, mAbs KH2 and TG10 significantly reduced TcdA and TcdB secretion at 48h (Median values; KH2 mAb *vs* isotype control: $C_{TcdA\text{-}48h}$=45.1 vs 172 ng/mL, p=0.0002; $C_{TcdB\text{-}48h}$=4.2 vs 14.5 ng/mL, p=0.0119; TG10 mAb *vs* isotype control: $C_{TcdA\text{-}48h}$=51.2 vs 172 ng/mL, p<0.0001; $C_{TcdB\text{-}48h}$=5.9 vs 14.5 ng/mL, p=0.0507, ; KH2 mAb *vs* ΔPaloc: $C_{TcdA\text{-}48h}$= 45.1 vs < 3.7 ng/mL, p=0.2861; $C_{TcdB\text{-}48h}$=4.2 vs 0.05 ng/mL, p=0.1057 ;

TG10 mAb *vs* ΔPaloc: $C_{TcdA\text{-}48h}$ 51.2 vs < 3.7 ng/mL, p = 0.1129). Surprisingly, mAb 2B7 that partially the same epitope as mAb KH2 (Fig. 1D) and has a better affinity for LMW (Table 1) did not affect the secretion of either toxin ($C_{TcdA\text{-}24h}$=13.4 ng/mL, p=0.5071; $C_{TcdA\text{-}48h}$=117 ng/mL, p=0.5593; $C_{TcdB\text{-}24h}$=1.0 ng/mL, p=0.9866; $C_{TcdB\text{-}48h}$=16.3 ng/mL, p=0.8693). Together, these results indicate that even though anti-LMW mAbs NF10, KH2 and TG10 bind the same target on the *C. difficile* surface, they induce contrasting effects on toxin secretion that appears tightly epitope-dependent.

***C. difficile* biofilm formation is increased by anti-LMW mAbs NF10 and 2B7.**

C. difficile CWP84 mutants with altered S-layer were reported to have increased biofilm generation suggesting a role for SlpA in *C. difficile* biofilm formation. We therefore reasoned that biofilm formation could be modulated by constraining *C. difficile* S-layer with anti-LMW mAbs. The Cd630Δ*erm* strain demonstrated *in vitro* biofilm formation in plates[68] that appeared visually increased after mAb NF10 and mAb 2B7 incubation (Fig. 5a). By quantifying nucleic acids and proteins, we found a statistically significant increase after incubation with mAb 2B7 and a non-significant trend after incubation with mAb NF10 (increase in biofilm formation: 175%, p=0.0231 and 149%, p=0.1661, for 2B7 and NF10 respectively; Fig. 5b). To strengthen these results, we analyzed biofilm volume, thickness and roughness (aka unevenness of the biofilm surface) using confocal laser scanning microscopy on fluorescently-labeled *C. difficile* as previously reported[337]. Cd630Δ*erm* strain generated after 48h a biofilm of ~310,000 μm^3 with a main thickness of ~14 µm and a roughness of ~0.08 Arbitrary Units (Fig. 5c-d). Incubation with either mAb NF10 or mAb 2B7 induced a ~1.7-fold increase in biovolume, a ~2-fold increase in thickness and ~1.6-fold increase in roughness. These results highlight the contribution of SlpA LMW in the generation of biofilms, with epitope-dependent enhancement of biofilm generation revealed by two anti-LMW mAbs.

Discussion

C. difficile is a complex pathogen to study, being anaerobic and lacking tools i.e., antibodies, to investigate the contribution of its surface components to growth, adhesion, toxin secretion, infectivity, and biofilm generation among other of its properties. Herein, we identified the first series of anti-SlpA LMW mAbs and exploited them to demonstrate the contribution of LMW to growth, toxin secretion and biofilm generation, and its potential as a target for neutrophil-dependent phagocytosis. Interestingly, anti-LMW mAbs demonstrated various effects on *C. difficile* -sometimes opposite- depending on their epitope. The high-affinity anti-LMW mAb NF10 had multiple effects on *C. difficile* by dose-dependently impairing growth, and increasing susceptibility to lysis by lysozyme and bile acid, toxin secretion and biofilm generation. Anti-LMW mAbs KH2 and TG10 induced none of the effects but instead inhibited toxin secretion. This study reveals an epitope-dependent regulation of *C. difficile* biology by the low-molecular weight subunit of SlpA.

One of the most surprising features of these anti-LMW mAbs is their contrasting effects depending on the epitope they bind to. Antibodies and nanobodies targeting *C. difficile* S-layer have been proposed as attractive therapeutic agents[302,338]. Likewise, active and passive immunization strategies have been tested with varying degrees of success to prevent or treat CDI[300,332]. Our findings suggest that anti-S-layer polyclonal responses include both beneficial and detrimental antibodies. Thus, the precise definition of the epitope recognized (in this case, on the S-layer) and its effect on various *C. difficile* functions is of the outmost importance to design successful anti-S-layer therapeutic agents. Furthermore, even if a toxin-suppressing antibody might at first glance appear beneficial to the host, it might also facilitate biofilm formation and therefore promote recurrence. Our data prompt to test novel therapeutic agents not only on single episode CDI models, but on recurrence models, which consider biofilms as a reservoir for further infections.

The S-layer is an important component involved during bacterial growth since new S-layer must be continuously assembled when cells divide. While no previous study could evaluate the effect of targeting the *C. difficile* S-layer due to the lack of specific antibodies, a related study on *Bacillus anthracis* showed that anti-S-layer nanobodies attenuated bacterial growth[339], reminiscent of our findings with mAb NF10 on the growth of *C. difficile*. The authors showed that nanobodies inhibited S-layer *de novo* assembly with a full dissolution of S-layer polymers, which resulted in drastic morphological defects and S-layer disruption. In the same way, mAb NF10 may also prevent optimal S-layer compaction leading to morphological defects

(LH, preliminary data) and bacterial lysis. On the contrary, *C. difficile* S-layer null mutants did not show any growth defects[50], but were more susceptible to lysozyme and anti-microbial peptides such as LL-37. In our work, we also showed that mAb NF10 restored *C. difficile* sensitivity to lysozyme. As shown by Salgado *et al., C. difficile* S-layer forms a tightly compact barrier around the bacteria, impenetrable to large molecules[38]. Besides S-layer disruption, we propose that mAb NF10 interaction with *C. difficile* LMW allows for the import of large molecules *e.g.*, lysozyme (14kD), a promising process which could be used for specific drug delivery.

Toxin secretion is a major physiological process that confers its pathogenicity to the bacteria. Since CDI severity is caused by TcdA and TcdB toxins, regulation and mechanisms of tox(Majumdar & Govind, 2022)xtensively studied[340]. Toxin secretion occurs during stationary growth of the bacteria and is influenced by a variety of environmental factors such as availability of specific nutrients, temperature, and cell density[340–343]. However, how the toxins cross the *C. difficile* membrane and consequently how they interact with the S-layer without bacterial lysis remain open questions[38]. S-layer must create discrete pores to allow toxin export while maintaining bacterial integrity. Interestingly, three of our anti-LMW mAbs modulated toxin secretion: one increased it while two inhibited it, pointing towards a dual role of S-layer in toxin release. On the one hand, S-layer disruption by mAb NF10 may lead to a massive toxin release, on the other hand mAbs KH2 and TG10 may "rigidify" or "lock" the S-layer, thus abrogating toxin export. Consistent with our findings, mutants affecting *C. difficile* S-layer displayed these contrasting features[50,299,344]. Further functional and structural studies are needed to solve how SlpA impacts on import-export mechanisms *in C. difficile*.

Another aspect of *C. difficile* pathogenicity relies on its ability to forms biofilms, which have been associated with relapses[72]. Gut colonization and biofilm formation have been suggested to contribute to the pathogenesis and persistence of *C. difficile*[345]. Indeed, biofilm-like structures have been observed in CDI mouse models *in vivo*[71,346]. Analyses of *C. difficile* biofilm composition showed that extracellular DNA is an essential component and contributes to the development of biofilms. Of note, incubation with DNase I drastically reduced the biofilm biomass[347,348]. These data are in agreement with our hypothesis that mAb NF10-induced lysis facilitates biofilm formation by increasing the amount of extracellular DNA and proteins in the biofilm matrix. Beyond S-layer disruption and bacterial lysis, the extent to which S-layer proteins such as LMW are *per se* involved in biofilm formation remains unclear. Inhibition of

S-layer-mediated aggregation could also impact the early steps of biofilm formation, as has been demonstrated for *Lactobacillus helveticus M92*[349].

Our study has limitations. We studied biofilm formation and architecture in a closed system. As a recent study demonstrated that biofilms grown in well-plates and biofilms obtained in open systems harbor different characteristics in terms of cell-surface protein expression[350], it would be relevant to evaluate anti-LMW mAbs in other conditions. Moreover, knowing the precise LMW epitopes that are recognized by the mAb series we describe here could help to decipher the varying effects these have on *C. difficile* physiology. Secretory IgA have indeed been reported to shape functional microbial fitness depending on the antigen and epitopes recognized[351]. The absence of the D2 domain of the LMW in *C. difficile* has been shown to be sufficient to confer susceptibility to lysozyme, therefore indicating its crucial role in maintaining S-layer integrity[38]. We hypothesize that mAb NF10 interacts with an epitope in the D2 domain, thus impairing its function and therefore mimicking what has been found with the mutant lacking this domain.

In this work, we demonstrate that targeting of mAbs to the S-layer of *C. difficile* has multiple and contrasting effects on the physiology of the bacteria. This study provides insights on the function of the *C. difficile* S-layer and suggests ways to target and modify some of its physiological processes. Future fine-tuned work on mAbs recognizing a determined epitope on the S-layer, leading to a precise function such as impaired growth or decrease in toxin secretion, could lead to new therapeutic strategies for CDI.

Methods

Production of recombinant LMW proteins. Recombinant *C. difficile* LMW-630 was produced as C-terminal 6xHis-tagged proteins from plasmid pET-28a(+) (TwistBiosciences, #69864). Plasmids were transformed into *E. coli* strain D43 and grown in NZY auto-induction lysogeny broth (LB) medium (NZYtech, #MB180). Bacteria were harvested by centrifugation and lysed using Precellys system according to manufacturer instructions (Bertin Technologies, #P002511-PEVT0-A.0). Recombinant LMW-SLP proteins from the soluble fraction were purified by affinity chromatography on Ni-agarose columns using an AKTA prime (GE Healthcare, #11001313). Proteins were dialyzed against 10 mM HEPES pH 7.5, 150 mM NaCl prior to analysis or long-term storage.

Generation of monoclonal antibodies against LMW of *C. difficile* strain 630. Knock-in mice expressing human antibody variable genes for the heavy (VH) and kappa light chain (Vκ) (VelocImmune) were described previously[317,318] and provided by Regeneron Pharmaceuticals to be bred at Institut Pasteur. BALB/c mice and VelocImmune mice were injected at day 0, 21 and 42 with 50 µg of recombinant LMW630 mixed with 200 ng/mouse pertussis toxin (Sigma-Aldrich, MO, USA). Enzyme-linked immunosorbent assay was performed to measure serum responses to antigen (see methods below) and the 3 best immunized animals were boosted with the same mix. Four days later, splenocytes were fused with myeloma cells P3X63Ag8 (ATCC, France) using ClonaCell-HY Hybridoma Kit according to manufacturer's instructions (StemCell Technologies, Canada). Culture supernatants were screened using ELISA (see below) and antigen-reactive clones were expanded in serum IgG free RPMI-1640 (Sigma-Aldrich, MO, USA) into roller bottles (Sigma-Aldrich, MO, USA) at 37°C. After 14 days, supernatants were harvested by centrifugation at 2500 rpm for 30 min and filtered (0.2 µm). Antibodies were purified by protein A affinity chromatography (AKTA, Cytiva, Germany) as described previously[322].

ELISA assays. Maxisorp microtiter plates (Dutscher, France) were coated with 0.3 µg of LMW630 recombinant protein in carbonate buffer (Na_2CO_3/$NaHCO_3$) for 2 hours at room temperature (RT). Free sites were blocked by a 2-hour incubation at RT with 1X-PBS 1% BSA. Plates were washed three times with 1X-PBS 0.05% Tween 20 (PBS-T) before being co-incubated with serum, supernatants or mAbs at different concentrations (from 10^{-6} µg/mL to

10µg/mL) for 1h at RT. After five washes, goat anti-mouse IgG Heavy and Light Chain antibody HRP-conjugated (Bethyl, TX, USA, dilution 1:20 000) was added for 1h at RT followed by incubation with OPD substrate revealing reaction for 10 min (Sigma-Aldrich, MO, USA). Absorbances were analyzed at 495 *vs* 620 nm on an ELISA plate reader (Berthold, France).

Bio-layer interferometry. Biolayer interferometry assays were performed using Anti-Mouse IgG Fc Capture biosensors (18-5088) in an Octet Red384 instrument (ForteBio, USA). MAbs (10 µg/mL) were captured on the sensors at 25°C for 1800 seconds. Biosensors were equilibrated for 10 minutes in 1X-PBS, 0,05% Tween 20, 0.1% BSA (PBS-BT) prior to measurement. Association was monitored for 1200s in PBS-BT with LMW630 at a range of concentrations from 0.01 nM to 500 nM followed by dissociation for 1200s in PBS-BT. For epitope competition assays, sensors were further immersed in solutions containing mAbs at 10 µg/mL. Biosensor regeneration was performed by alternating 30s cycles of regeneration buffer (glycine HCl, 10 mM, pH 2.0) and 30s of PBS-BT for 3 cycles. Traces were reference sensor (sensors loaded with unspecifc mAb) subtracted and curve fitting was performed using a global 1:1 binding model in the HT Data analysis software 11.1 (ForteBio, USA), allowing to determine KD values.

IgH and IgL sequencing. Total RNA was extracted from murine splenocytes using NuceloSpin RNA plus kit (Macherey-Nagel, France) according to the manufacturer's instruction. cDNA were generated at 50°C for 60 min using random primers and SuperScript III Reverse Transcriptase (Invitrogen, MA, USA). The primer pairs for IgH and IgL, described in Supplemental Table 2 were used for amplification with GoTaq G2 polymerase (Promega, WI, USA). Amplification was performed by 35 cycles PCR each consisting of 94°C for 30 sec, 63°C for 30 sec, 72°C for 30 sec. At the end of the 35 cycles, samples were run for an additional 10 min at 72°C and analyzed by 1.5% agarose gel electrophoresis. PCR products were then sequenced by Eurofins (France) using 3' primers.

Flow cytometry assay. mAb binding to whole bacteria was assessed by bacterial flow cytometry assay, as previously described[310]. Briefly, fixed C. difficile (106/condition) were stained with 5 µM SYTO9 dye (Thermo Fisher Scientific, MA, USA) in 0.9% NaCl for 30 min at RT. Bacteria were washed (10 min, 4000g, 4°C) and resuspended in 1X PBS, 2% BSA and

0.02% Sodium Azide (PBA). Mabs were pre-diluted in PBA at 20 µg/mL and incubated for 30 min at 4◦C. Bacteria were washed, and AF647 AffiniPure goat anti-mouse IgG (H+L) antibody or isotype control (dilution 1:200, Jackson ImmunoResearch, PA, USA) were incubated for 30 min at 4◦C. After washing, bacteria were resuspended in sterile 1X-PBS. Flow cytometry acquisition was performed on a MacsQuant cytometer (Miltenyi, Germany) and analyzed on FlowJo software (BD Biosciences, CA, USA).

Isolation of human neutrophils. Human peripheral blood was collected on EDTA from healthy volunteers. Blood neutrophils were separated by negative magnetic selection (MACSxpress, Miltenyi Biotec, Germany) according to the manufacturer's instructions. After negative selection, the neutrophil-enriched suspension was recovered, and residual erythrocytes were further removed using the MACSxpress Erythrocyte Depletion kit (Miltenyi Biotec, Germany). The resulting neutrophil suspension was washed with HBSS (Sigma-Aldrich, MO, USA) and resuspended to an appropriate volume in HBSS (Ca2+/ Mg2+) + 2% fetal calf serum (Cytiva, Germany).

Phagocytosis assay. Human neutrophils were plated at a concentration of 8 x 10^5 cells/ml. Fixed *C. difficile* were incubated with one mAb at 20 µg/mL or a cocktail of mAbs NF10, KH2, 1E2, 2B7 and TG10 at equimolar ratio and stained with pHRodo dye (Thermo Fisher Scientific, MA, USA) following the manufacturer instructions. Mouse anti-rocuronium mAb (in house production) was used as isotype control. Bacteria were then incubated with neutrophils at a Multiplicity Of Infection (MOI) of 100 for 1.5h at 37°C (20,000 neutrophils for each condition). Flow cytometry acquisition was performed on a MacsQuant16 cytometer (Miltenyi, Germany) and analyzed on FlowJo software v10.8.1 (BD Biosciences, CA, USA).

Bacterial strains and culture conditions. *C. difficile* 630Δerm[352], a spontaneous erythromycin sensitive derivative of the reference strain 630, and *C. difficile* strain UK1[269] of ribotype 027 strains were grown anaerobically (5% H2, 5% CO2, 90% N2) in TY medium (30 g/L tryptone, 20 g/L yeast extract) or in Brain Heart Infusion (BHI) medium supplemented with 0.5% (w/v) yeast extract, 0.01 mg/mL cysteine and 100 mM glucose (BHISG). All media and chemicals were purchased from Sigma-Aldrich, MO, USA.

Growth assays, lysozyme resistance and quantification of lysis. Overnight *C. difficile* cultures were grown in TY broth, subcultured to an Optical Density at 600 nm (OD600nm) of 0.05 in 200 µL of BHISG or, when appropriate, BHISG supplemented with DCA (240 µM, Sigma-Aldrich, MO, USA) in 96-well flat bottom plates (Merck, Germany) and then grown for 24h or 18h with OD_{600nm} measurements every 30 min taken by GloMax Plate Reader (Promega, WI, USA). Anaerobiosis was maintained with a O_2-less sealing film (Sigma-Aldrich, MO, USA). Where appropriate, lysozyme (1 mg/mL) was added after 2.5h of growth. Experiments were performed at least in triplicate. For lysis quantification, LDH was measured in 13h-culture supernatants using CytoTox 96 Non-Radioactive cytotoxicity assay according to manufacturer instructions (Promega, WI, USA).

Biofilm assays. Overnight cultures of *C. difficile* 630Δerm grown in TY medium were diluted to 1:100 into fresh BHISG containing the desired supplements (240 µM DCA, 0.2 mg/mL mAbs). 1 mL of diluted cultures were added in 24-well plates (polystyrene tissue culture-treated plates, Costar, USA). Then, plates were incubated at 37°C in an anaerobic environment for 48h. Biofilm biomass was measured using an established method[68]. Briefly, biofilms were washed with 1X-PBS and stained with crystal violet for 5 min. After washing, crystal violet was resuspended in ethanol and OD_{600nm} measured.

Confocal Laser Scanning Microscopy (CLSM). Biofilms were grown in 96-well plates (Microclear, Greiner Bio-one, France) in BHISG supplemented with DCA (240 µM) and anti-LMW630 mAbs as described above. After 48h, supernatants were carefully removed by pipetting and biofilms were fixed with 4% paraformaldehyde (Sigma-Aldrich, MO, USA). Biomass was then stained with SYTO9 dye (Life Technologies, USA) at a final concentration of 20 µM. Dye were incubated for 30 min before CLSM imaging/analysis. Z-stacks of horizontal plane images were acquired in 1 µm steps using a Leica SP8 AOBS inverted laser scanning microscope (CLSM, LEICA Microsystems, Wetzlar, Germany) at the INRAE MIMA2 platfo(*ISC MIMA2 INRAE*, n.d.)5572348210007727E12)[353]. At least two stacks of images were acquired randomly on three independent samples at 800 Hz with a x63 water objective (N.A.=1.2). Fluorophores were excited, then their emissions were captured as prescribed by the manufacturer.

Analysis of CLSM biofilm images. Z-stacks from the CLSM experiments were analyzed with the BiofilmQ software[354] to extract quantitative geometric descriptors of biofilms structures. Images were all treated with the same process in each fluorescence channel. First, the images were denoised by convolution (dxy=5 and dz=3), then they were segmented into two classes with an OTSU thresholding method with a sensitivity of 2. The detected signal was then declumped in 3.68 µm cubes and small objects were removed with a threshold of ($0.5\mu m^3$) to clean the remaining noise. Exported data were analyzed in the software Imaris to generate biofilm 3D projections and in GraphPad prism to generate quantitative graphs.

Toxin A & B assays. *C. difficile* 630Δerm and 630ΔermΔPaloc were grown in 6-well plates containing 2 mL of TY medium for either 24h or 48h. Absorbances at 600 nm were measured, then cultures were harvested and centrifuged at 4,000 rpm for 5 min. Toxins were assessed in supernatants using ELISA. Maxisorb microtiter plates (Dutscher, France) were coated with 5 µg/mL of anti-TcdB capture antibody (BBI solutions, Madison, WI) or anti-TcdA capture antibody (Novus Biological, CO, USA). Purified toxin A and B were used as standards. Supernatants were added for 1h30 at RT. After washing, anti-toxin B biotinylated antibody (BBI solutions, Madison, WI) followed by high sensitivity Streptavidin-HRP conjugate (ThermoFisher, Waltham, MA), or anti-toxin A HRP-conjugated antibody (LSBio, WA, USA) signal was detected with TMB substrate (ThermoFisher, Waltham, MA) at 450nm using a ELISA plate reader (Berthold, France). Toxin concentrations were normalized with OD_{600nm} values for each well.

Statistical analysis. Growth, LDH, toxins and biofilm' assays values were analyzed in Prism 8.0 (GraphPad, San Diego, CA). Statistical analysis was performed using one-way ANOVA test followed by a Dunnett's multiple comparison test. A p value ≤ 0.05 was considered significant.

Acknowledgements

This work was funded by Fondation Janssen Horizon, the Institut National de la Santé et de la Recherche Médicale (INSERM) and the Institut Pasteur. LH is a doctoral fellow of Sorbonne Université. DS was partly supported by a poste d'accueil 2017 Institut Pasteur – Assistance Publique des Hôpitaux de Paris (APHP) and by the Agence Nationale de la Recherche (ANR) program Résilience-Covid- 19 MUCOVID. Work in the G. Gorochov's team is supported by Institut National de la Santé et de la Recherche Médicale (INSERM), Sorbonne Université, Fondation pour la Recherche Médicale (FRM), Paris, France, program ''Investissement d'Avenir'' launched by the French Government and implemented by the Agence Nationale de la Recherche (ANR) with the reference COFIFERON ANR- 21-RHUS-08, by EU Horizon HLTH-2021-DISEASE-04 UNDINE project, programme DIM Ile de France thérapie cellulaire et génique and by the Département Médico-Universitaire de Biologie et Génomique Médicales (DMU BioGen), APHP, Paris, France.

Competing Interests: Unrelated to the submitted work, P.B. received consulting fees from Regeneron Pharmaceuticals. The other authors declare no competing interests.

Figures

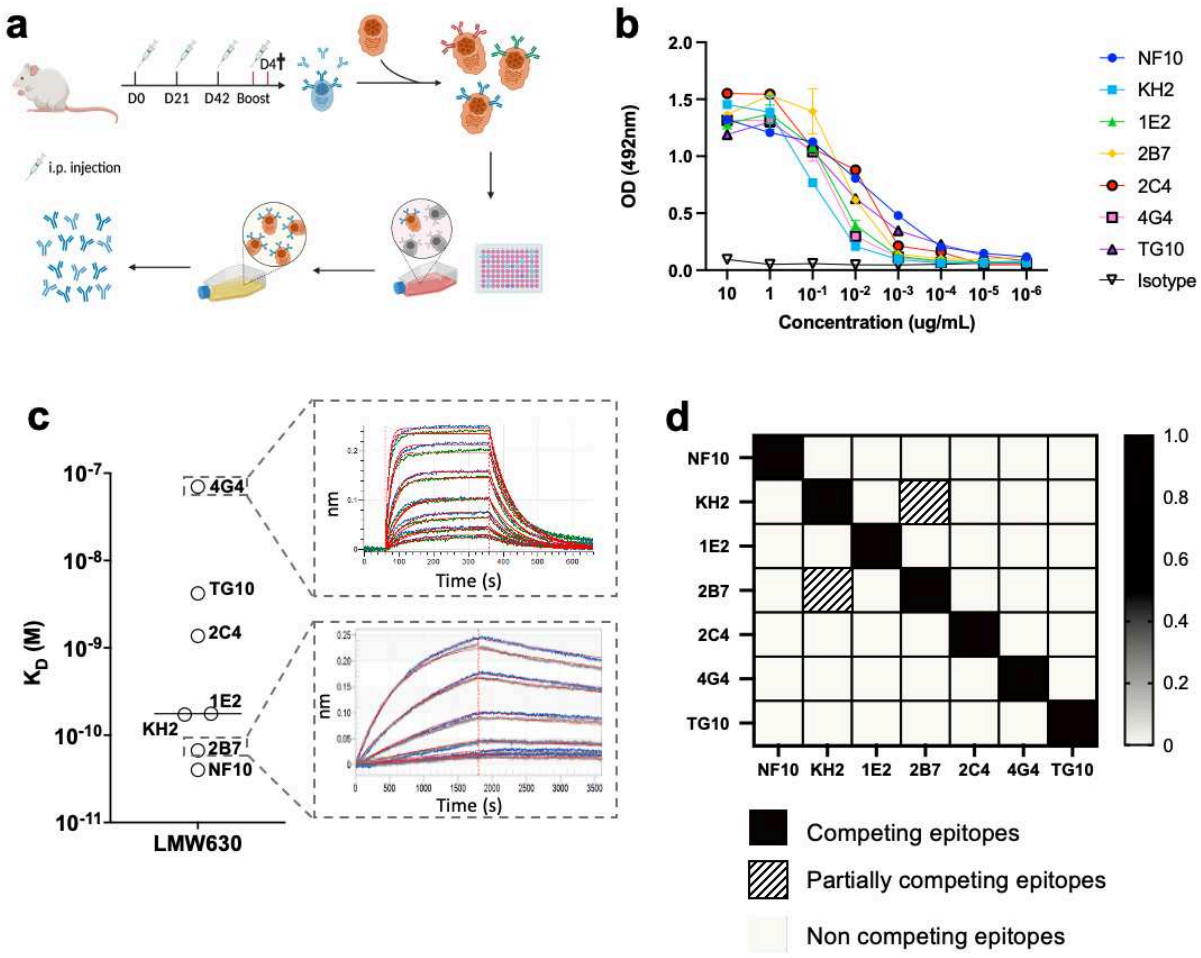

Figure 1: High-affinity anti-LMW mAbs bind distinct epitopes a. Schematic view of immunization, hybridoma generation and screening for obtention of anti-LMW mAbs. **b.** Mab binding to recombinant LMW measured by ELISA at indicated concentrations. Dark curve represents isotype control. **c.** Affinities towards LMW determined by Bio-Layer Interferometry. Representative sensorgrams of one low (4G4) and one high-affinity (2B7) mAb. Antibody concentration from 500 nM to 8 nM for 4G4 and from 2 nM to 0.02 nM for 2B7 were tested, as shown from top to bottom. Blue curves represent raw data while red curves represent fitting with a 1:1 antibody:antigen model. **d.** Summary table representing the results of BLI-based competitive of anti-LMW mAbs towards LMW.

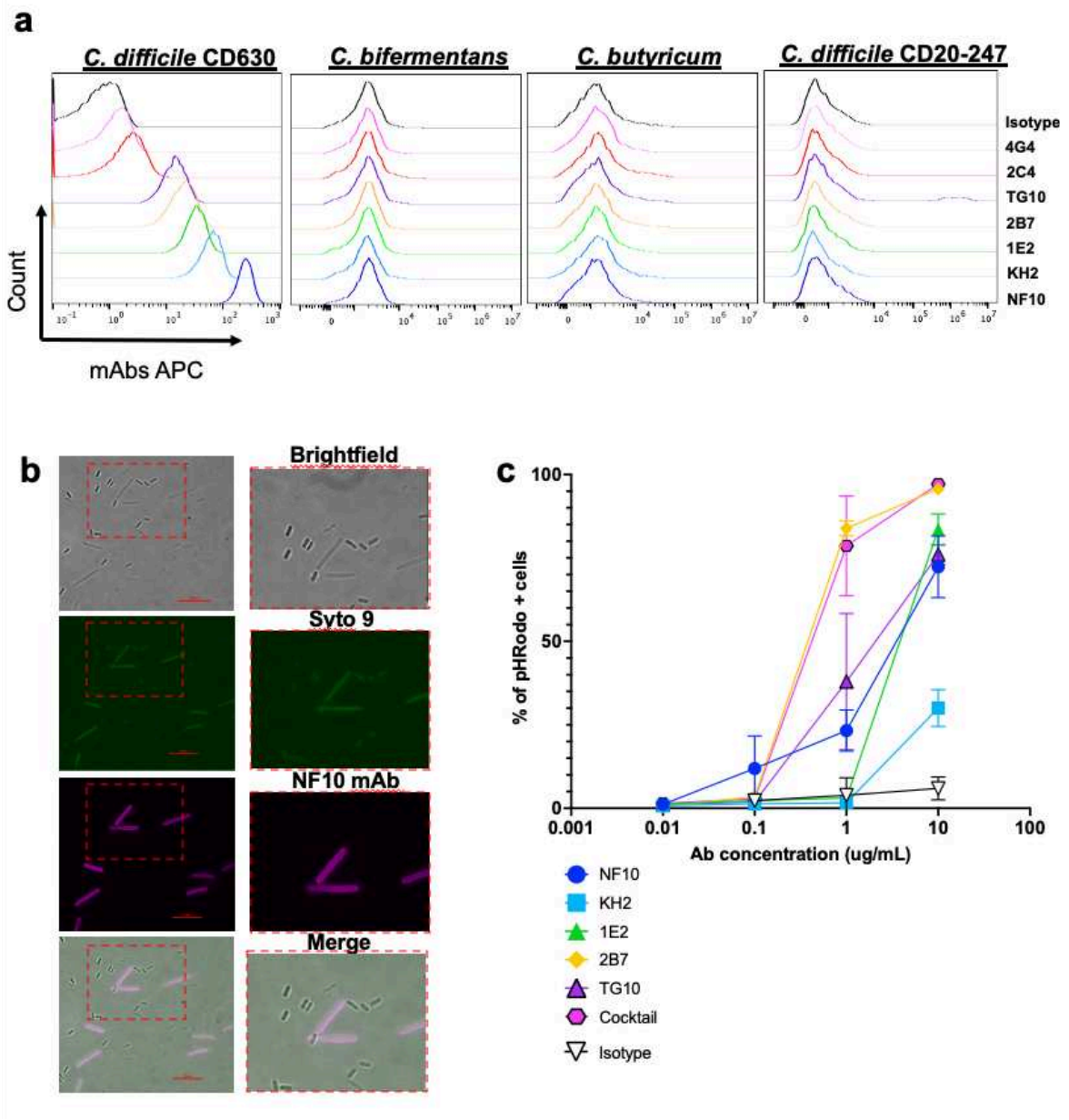

Figure 2: Anti-LMW mAbs bind vegetative *C. difficile* cells and enhance phagocytosis. a. Flow cytometry analysis of mAbs binding to indicated *C. difficile* strains and other *Clostridium* species (CD20-247 R012). Black curve corresponds to isotype control. **b.** Representative view of mAb binding to *C. difficile* vegetative cells but not to spores. DNA from vegetative cells and spores was labeled with SYTO9 while mAb-coated bacteria were stained with AF647-conjugated anti-mouse IgG antibody. Merged staining was presented on the right panel. Analysis was performed by confocal microscopy. **c.** Percentage of neutrophils that have phagocytosed *C. difficile*-opsonized by the indicated mAb or a cocktail of mAbs NF10, KH2, 1E2, 2B7 and TG10 at equimolar ratio, after 60 min and assessed by flow cytometry. Data represent mean + SEM of n = 3 technical replicates. Experiment was performed with at least 2 biological replicates.

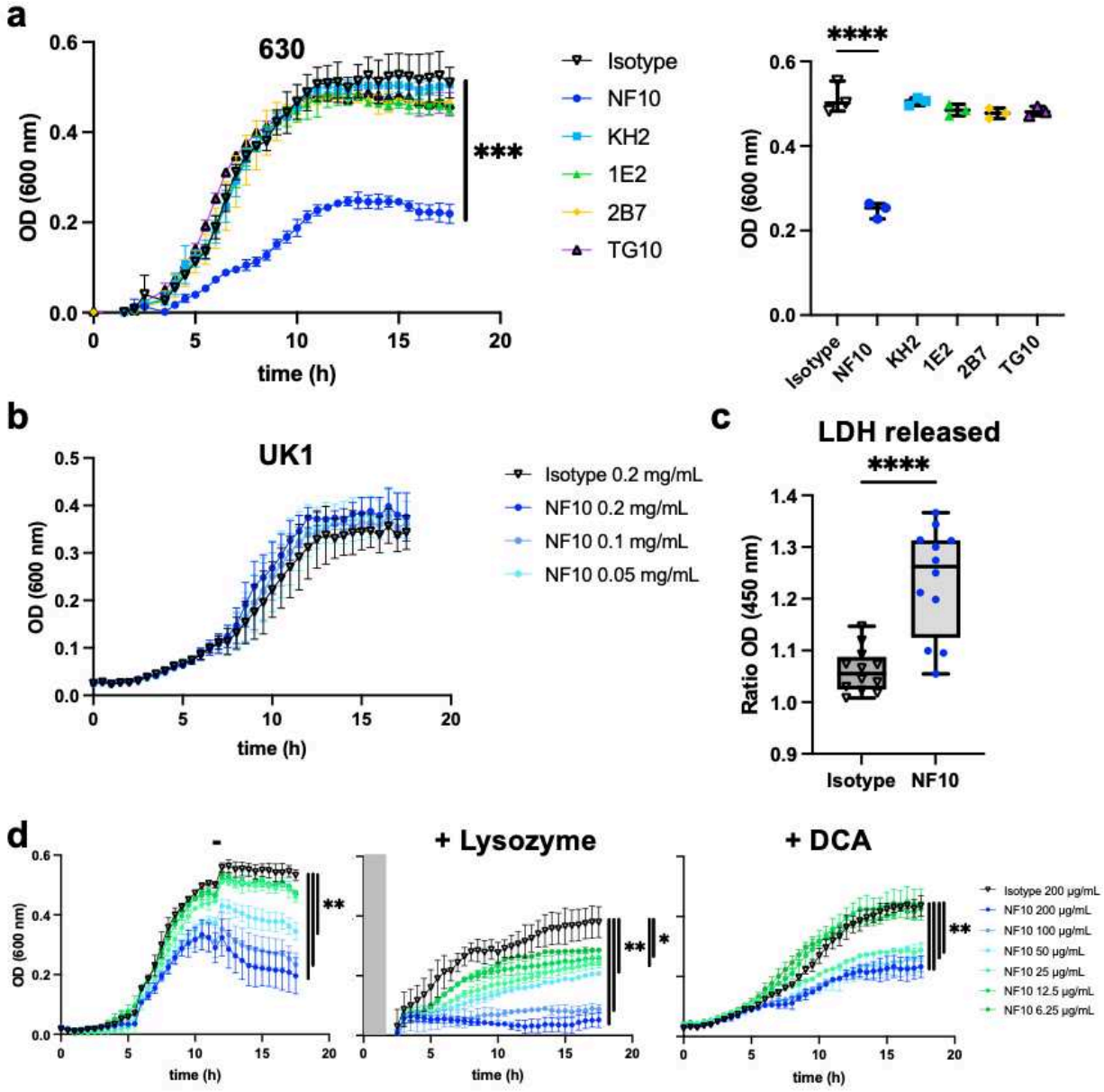

Figure 3: Effect on growth of anti-LMW mAbs and sensitivity to lysozyme and DCA. Cultures of *C. difficile* 630Δerm were inoculated at an OD_{600nm} of 0.05 and grown anaerobically at 37°C with OD_{600nm} measurements every 30 min. **a.** Effect of anti-LMW mAbs was assessed on growth. Left panel represents growth curves until 18h with measurements every 30 min for all anti-LMW mAbs and isotype. Right panel represents quantitative analysis at 13h for all anti-LMW mAbs and isotype. **b.** Effect of NF10 mAb was assessed on *C. difficile* UK1 strain growth at different concentrations. Data are presented as means and standard deviations from three technical replicates. **c.** LDH activity in the supernatant was normalized to condition without antibodies. The interquartile boxplots show medians (middle line), and the whiskers indicate minimal and maximal values. Asterisks indicate statistical significance calculated with a one-

way ANOVA test followed by a Dunnett's multiple comparison test (****p < 0.0001). Experiments were performed with two biological replicates in six technical replicates. **d.** Cultures of *C. difficile* 630Δerm incubated with different concentrations of NF10 mAb were monitored in combination with lysozyme (500 µg/ml), which was added after 2.5h growth or DCA (240 µM). Isotype control (dark lines) was included in all experiments. Data are presented as mean values (±SD) from three technical replicates. Asterisks indicate statistical significance with a two-way ANOVA test (ns: not significant; * p < 0.05, ** p < 0.01, *** p < 0.001, and **** p < 0.0001).

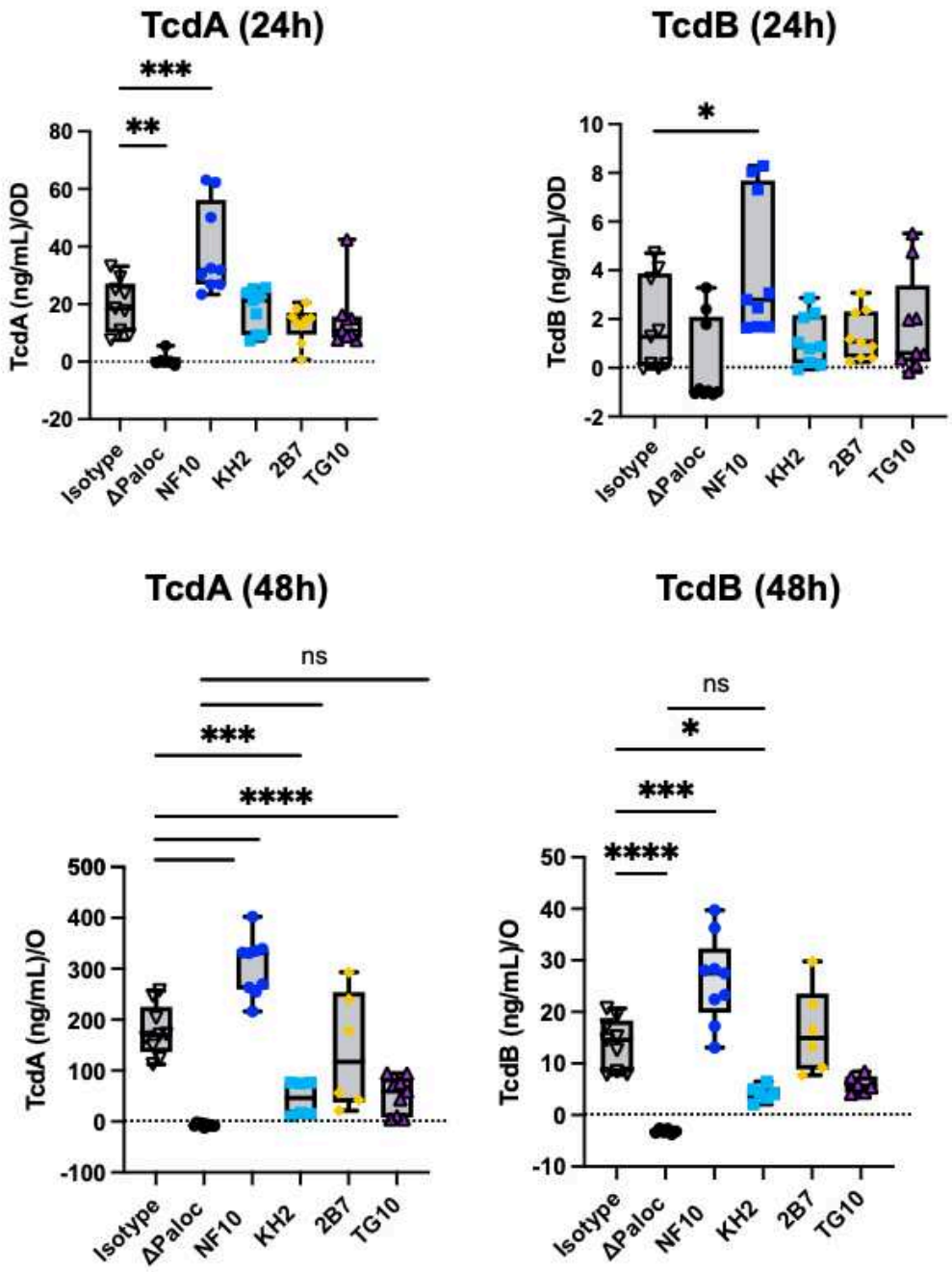

Figure 4: Anti-LMW mAbs modulate *C. difficile* toxin secretion. Quantification of TcdA or TcdB toxin secretion in Cd630Δerm in the presence of anti-LMW mAbs or isotype control. Cd630ΔermΔPaloc mutant strain has been tested as a negative control. Toxin titers in culture supernatants were determined at 24h and 48h by ELISA. Boxplots show medians (middle line) and interquartile range, and the whiskers indicate minimal and maximal values of three replicates. Asterisks indicate statistical significance calculated with a one-way ANOVA test followed by a Dunnett's multiple comparison test (ns: not significant; * $p < 0.05$, * $p< 0.01$, *** $p < 0.001$, and **** $p < 0.0001$).

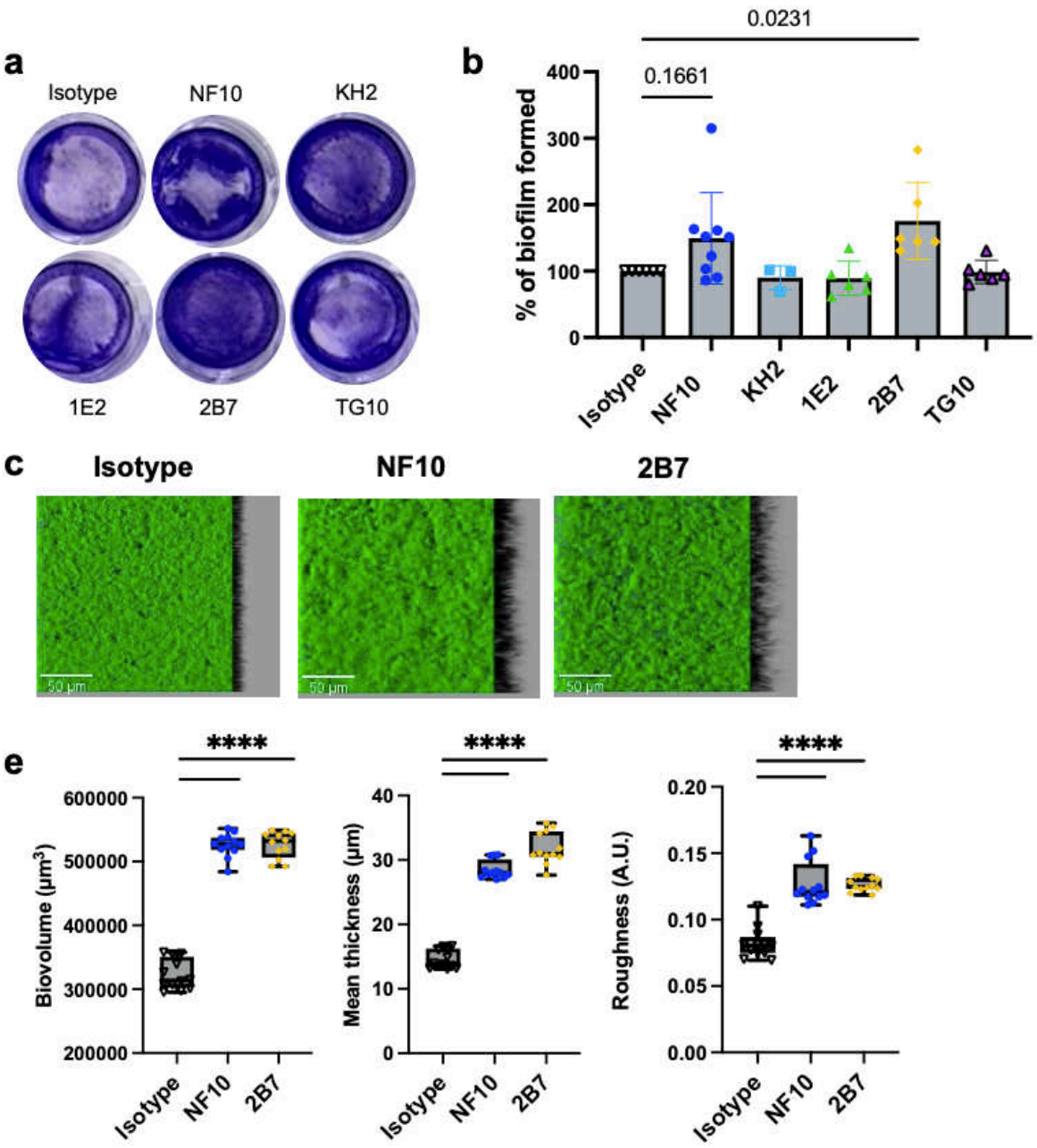

Figure 5: Anti-LMW mAbs influence *C. difficile* biofilm formation. Biofilm formation with Cd630Δ*erm* strain was assayed in BHISG medium supplemented with 240 µM DCA. **a**. Representative pictures of biofilm formed in the presence of indicated mAbs after crystal violet staining. **b**. Biofilm biomass was assessed by absorbance at 600nm. Histograms show medians (middle line) and whiskers indicate standard deviation of at least three independent experiments. **c.** Visualization mAbs-coated Cd630Δ*erm* biofilms stained with SYTO9. Z-stacks were analyzed with BiofilmQ. CLSM images are representative of three independent biological replicates. For each image, the virtual shadow projection of the biofilm is shown in dark on the right. **d**. Quantitative analyses were performed with BiofilmQ to measure the biovolume,

thickness and roughness of the biofilms. The interquartile boxplots show medians (middle line) and the whiskers indicate minimal and maximal values of three replicative samples. Asterisks indicate statistical significance with a one-way ANOVA test followed by a Dunnett's multiple comparison test (****p < 0.0001).

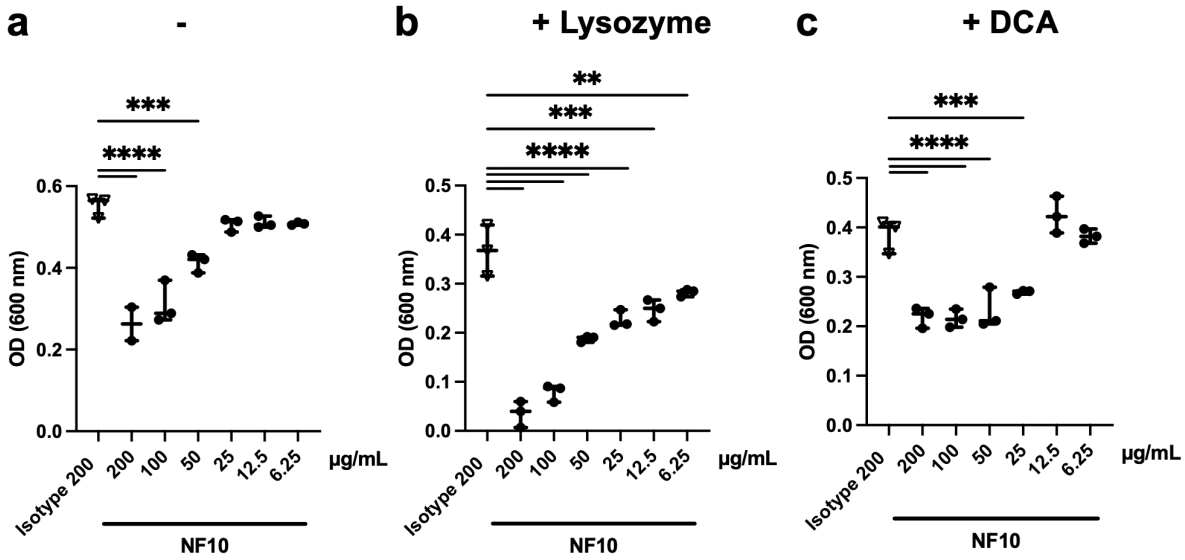

Figure S1 (related to Figure 3). Cultures of *C. difficile* 630Δerm incubated with different concentrations of NF10 mAb were monitored in combination with lysozyme (500 µg/ml), which was added after 2.5h growth or DCA (240 µM). Isotype control was included in all experiments. The boxplots show medians (middle line) and the whiskers indicate min and maximal values at 13 hours. Asterisks indicate statistical significance with a one-way ANOVA test followed by a Dunnett's multiple comparison test (ns: not significant; * p < 0.05, ** p < 0.01, *** p < 0.001, and **** p < 0.0001).

	IgH				IgL			Affinity		
mAbs	V	J	D	CDR3 Length (a.a)	V	J	CDR3 Length (a.a)	Kd (pM)	kon (1/Ms)	koff (1/s)
NF10	V1S22*01	J1*01	D6-1*01	13	V6-15*01	J1*01	11	43	7,00E+05	3,00E-05
KH2	V5-4*02	J3*01	D5-1*01	10	V14-111*01	J1*01	11	172	1,31E+05	2,25E-05
1E2	V1-46*01	J3*02	D6-13*01	16	V3-21*02	J2*01	14	176	2,00E+05	3,53E-05
2B7	V3-48*03	J4*02	D1-7*01	15	V9-49*02	J1*01	16	67	1,42E+06	9,46E-05
2C4	V3-20*01	J4*02	D3-16*02	11	V7-46*01	J2*01	12	1370	4,48E+05	3,23E-04
4G4	V3-33*01	J4*02	D1-26*01	16	V1-17*01	J2*01	12	70000	2,22E+05	1,56E-02
TG10	V2-70*15	J6*02	D1-7*01	19	V1-5*03	J1*01	11	4200	3,02E+05	1,22E-03

Table S1 (related to Figure 1): Ig gene analysis and kinetic parameters of anti-LMW mAbs. V(D)J families were obtained by blasting the sequences on IMGT data base and kinetic parameters determined using the BLI analysis software.

PCR step	Primer Name	5' - 3' Sequence
Balb/c Igh	5′ MsVHE	GGGAATTCGAGGTGCAGCTGCAGGAGTCTGG
	3' allmouse gamma	CKYGGTSYTGCTGGCYGGGTG
Balb/c Igk	5′ mVkappa	GAYATTGTGMTSACMCARWCTMCA
	3′ mCκ	GATGGTGGGAAGATGGATACAGTT
Balb/c Igl	5′ mVλ1/2	CAGGCTGTTGTGACTCAG
	5′ mVλx	CAACTTGTGCTCACTCAG
	3′ mCλ outer	GTACCATYTGCCTTCCAGKCCACT
VelocImmune Igh	5′LVH1	ACAGGTGCCCACTCCCAGGTGCAG
	5′LVH3	AAGGTGTCCAGTGTGARGTGCAG
	5′LVH4/6	CCCAGATGGGTCCTGTCCCAGGTGCAG
	5′LVH5	CAAGGAGTCTGTTCCGAGGTGCAG
	3' allmouse gamma	CKYGGTSYTGCTGGCYGGGTG
VelocImmune Igk	5′ L Vk 1/2	ATGAGGSTCCCYGCTCAGCTGCTGG
	5′ L Vk 3	CTCTTCCTCCTGCTACTCTGGCTCCCAG
	5′ L Vk 4	ATTTCTCTGTTGCTCTGGATCTCTG
	CG069	AAGAAGCACACGACTGAGGCAC
VelocImmune Igl	5′ L Vl 1	GGTCCTGGGCCCAGTCTGTGCTG
	5′ L Vl 2	GGTCCTGGGCCCAGTCTGCCCTG
	5′ L Vl 3	GCTCTGTGACCTCCTATGAGCTG
	5′ L Vl 4/5	GGTCTCTCTCSCAGCYTGTGCTG
	5′ L Vl 6	GTTCTTGGGCCAATTTTATGCTG
	5′ L Vl 7	GGTCCAATTCYCAGGCTGTGGTG
	5′ L Vl 8	GAGTGGATTCTCAGACTGTGGTG
	CG269	CACCAGTGTGGCCTTGTTAGTCTC

Table S2: Primers for Ig gene amplification of BALB/c and VelocImmune mice.

Unpublished data associated work to chapter VII

Evaluation of *C. difficile* adhesion to enterocytes

Introduction

In CDI, while tissue damage is primarily induced by the two toxins TcdA and TcdB, the first step remains the colonization of the epithelium. The role of bacterial adherence to the mucosa has been studied by several teams which have shown that *C. difficile* S-layer was involved in the adhesion to enterocytes in various models[28,297]. These models were based on 2D *in vitro* assays using intestinal epithelial cell lines such as Caco-2 cells that derived from a human colorectal adenocarcinoma. Indeed, pre-incubation of *C. difficile* with anti-HMW or anti-LMW serum prior to association with Caco-2 cells showed a diminution in adherence of *C. difficile*. In line with these results, we assessed if our anti-LMW mAbs could inhibit *C. difficile* adhesion.

Materials and methods

Adhesion assay on Caco-2 cells. Caco-2 cells were grown in DMEM with 15% FBS and 1% Non-Essential Amino Acids until they were polarized. The cells were then seeded into 24-well plates (25,000 cells/well) and were cultivated for 14 days by changing media every two days. The day before the experiment, *C. difficile* 630 was grown overnight in BHI. Bacteria were quantified then pre-incubated with various concentrations of anti-LMW mAbs for 30 min in anaerobia. MAb-coated bacteria were added to Caco-2 cells and incubated at 37°C in anaerobia for 1h. After 1h, co-cultures were washed gently twice with 1X-PBS, cells were lysed with saponin lysis buffer on ice for 14 min and *C. difficile* bacteria were numbered on BHI agar with 5% sheep blood after 24-48h of growth.

Transwell adhesion assay. Caco-2 and HT29-MTZ cells were grown in DMEM supplemented with 10% FBS. 10^5 cells/well were seeded on the membrane of Transwell™ plates at a 4:1 ratio Caco-2 : HT29-MTZ. Media was changed every 3 days for 21 days. The day before the experiment, *C. difficile* 630 was grown overnight in BHI. *C. difficile* were quantified and pre-incubated with various concentrations of anti-LMW mAbs for 30 min in anaerobia. Bacteria were then added on the membrane of the transwell plates containing the cells and incubated at 37°C in hypoxia (4% O_2, 5% CO_2) for 2h. Cells were washed two times with 1X-PBS, collected

and spined at 11,000rpm for 10 min. Cellular suspensions were homogenized and seeded on BHI agar. *C. difficile* colonies were numbered after 24h-48h.

Results

To assess functional abilities of our mAbs, we worked in collaboration with the BaPS team (Paris-Saclay University) directed by Pr. Claire Janoir. They have developed an *in vitro* assay which measure *C. difficile* adhesion to intestinal cells (Caco-2 cells). Using this assay, we sought to determine whether anti-LMW mAbs were able to inhibit *C. difficile* adhesion to intestinal cells. We first wanted to reproduce already published results with serum containing anti-SlpA and anti-LMW630 antibodies. In line with these results, we found a decrease of *C. difficile* adhesion with both polyclonal anti-SlpA and anti-LMW antibodies (50% and 40% respectively, Fig. 1.a).

We then evaluated all anti-LMW630 mAbs. However, we were not able to demonstrate a significant inhibition of adhesion compared to a non-relevant mAb, likely due to a huge intra- and inter-assay variability (Fig. 1.b). Consequently, we tried to reduce the variability and hypothesized that *C. difficile* strain may impact assay robustness.

We tested four strains from different ribotypes of *C. difficile*, some known to have a better adhesion than the strain 630. We observed slight differences between the four strains we tested (Fig. 1.c). However, these differences were not significant enough and did not help in reducing the variability.

Results from Bruno Dupuy's lab (data not shown) showed later than *C. difficile* adhesion is facilitated on cells that secrete mucus (model using Caco-2 cells and HTX-29 in transwell or intestine-on-chip) and that bacterial cells are wrapped up in mucin. We thus decided to use this model to look again at *C. difficile* adhesion in presence of our anti-LMW mAbs.

We confirmed an increased adhesion of *C. difficile* to enterocytes using this new model, with less than one log of difference between inoculum and adherent bacteria (Fig. 2). However, we did not observe inhibition of *C. difficile* 630 adhesion neither with anti-LMW630 mAbs, nor with an anti-SlpA polyclonal serum (Fig. 2).

Altogether, these results suggested that LMW is not necessary for *C. difficile* adhesion to enterocytes.

Conclusion

In these studies, we did not find any inhibition of *C. difficile* adhesion in two *in vitro* models. One could speculate that the epitopes targeted by the mAbs are not involved in the *C. difficile* adhesion to enterocytes. Another hypothesis is that blocking several epitopes might be required to abolish adhesion, which could explain the results obtained with polyclonal sera[28,297,300]. Of note, mAbs tested in a cocktail did not affect adhesion. Contrary to previous reports, our results argued that the S-layer is not involved in *C. difficile* interactions with epithelium, which is largely mediated by mucin. One could hypothesize that surface glycoproteins or peptidoglycan are required for this binding.

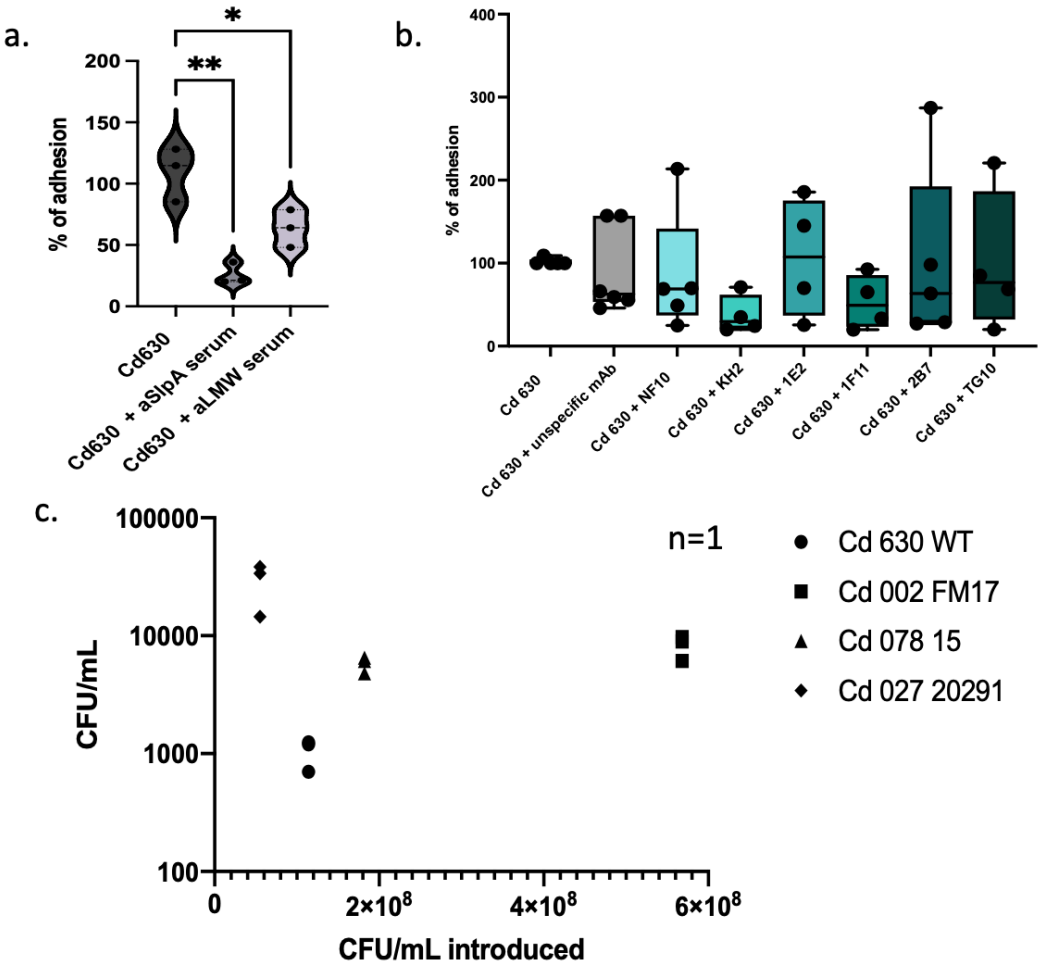

Figure 1. *C. difficile* adherence to Caco-2 cells. a) *C. difficile* strain 630 incubated with a 1:1000 dilution of anti-SlpA or anti-LMW serum prior to association with Caco-2 cells. Data were converted in percentage of adherence. **b)** *C. difficile* strain 630 incubated with 50ug/mL of anti-LMW630 mAbs or with non-specific mAb (anti-TNP). Data were converted in percentage of adherence and each

experiment was done in triplicate. **c)** *C. difficile* strains 630, 002, 078 and 027 incubated directly with Caco-2 cells.

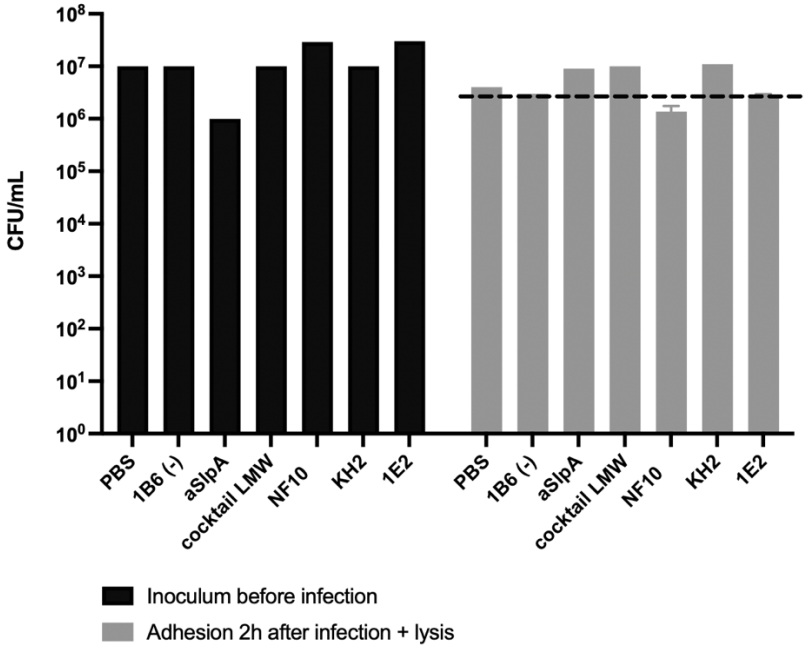

Figure 2. *C. difficile* adherence to Caco-2 + HT29-MTX cells. *C. difficile* strain 630 incubated with a 1:100 dilution of anti-SlpA or anti-LMW serum, or 0.2mg/mL anti-LMW630 mAbs (NF10, KH2 and 1E2) or with non-specific mAb (anti-Rocuronium, 1B6).

Development of an organ-on-chip model to study *C. difficile* infection

Introduction

The classical assays to study CDI and particularly adhesion to enterocytes commonly relies on the use of 2D-well plates that have the major drawback of not recapitulating the 3D structure of the intestine. Transwell models are a bit better in the fact that the 3D structures are more developed with the presence of polarized cells, but several parameters of the intestine environment remain unmet such as lateral flow and the peristaltic movement[355]. On the other hand, animal models are costly and sometimes too complex to be used to study some parameters of the infection. In the case of CDI, hamsters' model is too virulent compared to CDI in humans and axenic mice do not develop symptoms when infected with *C. difficile*. We therefore decided to take advantage of the intestine-on-chips developed by the Emulate® company to generate a new *in vitro* model to study *C. difficile* adhesion to enterocytes.

Materials and methods

Preparation and seeding of the chips. Chips were prepared and seed with Caco-2 cells according to the protocol described by *Ingber et al*[356].

Infection of the chips. Bacteria were grown overnight as described in chapter VII and resuspended in 50 µL of PBS-1X. 10^5 to 10^7 bacteria were then inoculated into the chips and adhesion was performed for 2 hours. After these 2 hours, chips were flushed with PBS-1X to remove non-adherent bacteria, fixed with PFA 4%, and stored at 4°C in PBS-1X until further analysis.

Bacteria Staining in the chips. Chips were cut into slices of 300 µm with vibratome and stained with NF10 mAb followed by AF647 AffiniPure goat anti-mouse IgG (H+L) antibody (dilution 1:200, Jackson ImmunoResearch, PA, USA). Images were acquired with a Nikon confocal microscope. For bacteria staining before infection, Syto9 or CFSE FITC at 10 µM were added for 30 min at RT and washed with PBS supplemented with 10% FBS. Bacteria were resuspended in 1X-PBS.

Results

Emulate® gut-on-chips can be seed with Caco-2 cells or organoids and replicate mechanical, structural, and pathophysiological properties of the human gut (Fig 1.a).

We first wanted to evaluate whether *C. difficile* bacteria would adhere to Caco-2 cells and which bacterial concentration would be optimal. Four different Multiplicity Of Infection (MOI) were tested and as revealed by microscopy bacteria could be seen in the chip with Caco-2 cells (Fig 1.b). No unspecific binding was shown with only the secondary antibody (data not shown). More bacteria have been detected in the MOI of 1000 than of 10 (Fig 1.c), however further quantification is needed.

We then wanted to optimize a staining protocol to follow *C. difficile* colonization in real time without having to stop the experiments at define timepoints and having to cut and stain the chips to assess the colonization. We tested several dyes, such as Syto9 that appeared to leak into the Caco-2 cells (Fig. 1.d). We then optimized a protocol using CFSE FITC that allowed bacteria staining without leakage into the enterocytes (Fig. 1.e).

Conclusion

In this part, we started the development of an *in vitro* model that recapitulate intestinal mechanical properties. We were able to demonstrate *C. difficile* adherence to Caco-2 cells in this model and found that 10^7 bacterial/chip seemed to be the best concentration to look at the colonization. Moreover, we optimized a staining protocol to follow the colonization of *C. difficile* in real time in the chips. Future developments include establishment of the infection under hypoxia conditions that recapitulate the O_2 concentrations in the gut. This work was followed by *Meza-Torres et al*. (manuscript in preparation).

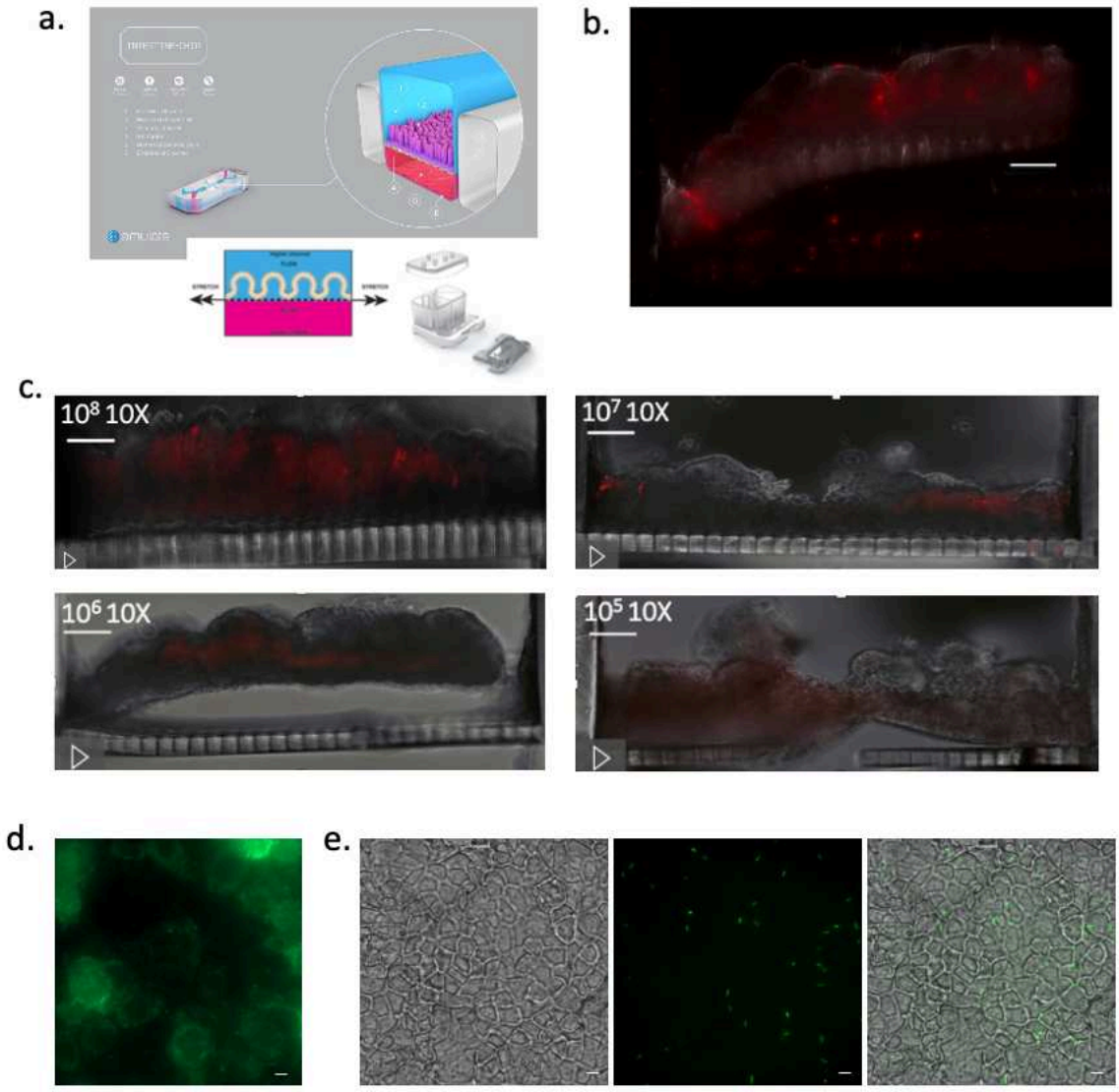

Figure 1. *C. Difficile* infection in Intestine-on-Chip. **a)** Photographs of the Intestine-Chip and scheme of a frontal plane of an Intestine-on-Chip central channel. Upper channel is blue and lower channel is pink. These top and bottom channels are separated by a porous membrane and are fluidically independents. The lateral arrows represent lateral stretching that mimic intestinal peristalsis. **b)** Representative view of a *C. difficile*- infected chip after 1h of bacterial exposure. Scale bar represents 100 µm. **c)** Representative views of a *C. difficile*-infected chips after 1h of bacterial exposure using four different MOI. Scale bars represent 100µm. Staining of bacteria in B and C was done using anti-mouse AF647 secondary antibody. **d)** Staining of *C. difficile* with Syto9 followed by infection in the chips. Scale bars represent 30 µm. **e)** Staining of *C. difficile* with CFSE FITC followed by infection in the chips. Scale bars represent 30 µm.

In vivo evaluation of anti-LMW mAbs in a hamster model of *C. difficile* infection

Introduction

Two *in vivo* models are generally used to study CDI: a virulent model in hamsters and a colonization model in mice[300,357]. The hamster model mimics CDI in humans as antibiotics are first administered to induce a dysbiosis in the microbiota followed by a challenge with *C. difficile* spores that give to hamster symptoms that resemble the ones in humans with diarrheas and death[332]. Hamsters are extremely sensitive to CDI and die within two days if no treatment is administered. It is therefore the most used model to test new vaccination and therapeutic strategies. A prolonged survival of hamsters is the readout of experiments. It is however more virulent compared to the infection in humans since the mortality rate turns around 5 to 10%[230]. For our first *in vivo* assay, we decided to assess if our mAbs had such a significant impact on the infection that they would allow a prolonged hamsters' survival.

Materials and methods

***In vivo* assay.** Hamsters were weighted and then treated with clindamycin 50 mg/kg by gavage à D-5 infection. At D0, hamsters were infected with 1000 spores of *C. difficile* diluted in water by gavage. Monoclonal antibodies were administered 6h before the infection, 17h and 24h after the infection by gavage at 16 mg/kg or the day of the infection by intra-peritoneal (i.p.) injection at 50 mg/kg (Fig. 1.a). Two anti-LMW mAbs were evaluated in this assay: NF10 and 1E2. Control groups included one group of hamsters that did not received any antibodies (group 1) and another one that received an unspecific antibody (group 2 and 5). One group received passive immunization by anti-LMW630 NF10 mAb (group 3), one by anti-LMW630 1E2 mAb (group 4) and one by unspecific mAb (group 2) by gavage, and 3 other groups received the same mAbs i.p. (groups 5, 6, 7 respectively). Mabs administered by gavage were diluted in 0.1 M sodium carbonate buffer, pH 9.6 as described by O'Brien *et al*[332]. Hamsters were weighted and their feces were collected at D-5 and D2.

Quantification of *C. difficile* in hamsters' feces. Feces were resuspended at 10 mg/mL in 1X-PBS and different dilutions were plated on BD Clostridium difficile agar with 7% sheep blood

(Becton Dickinson, NJ, USA) supplemented with sodium taurocholate 0.1%. The Colony Forming Unit (CFU/g feces) count of *C. difficile* vegetative cells and spores were determined by enumerating colonies after two days in anaerobic culture at 37°C.

ELISA with fecal waters. Feces were resuspended in 1X-PBS (1g for 2mL) and spined for 10 min at 4000g. Then supernatants were collected and spined for 10min at 4000g. Anti-LMW mAbs were assessed in the latter supernatant, also named fecal water. 0.3 µg of LMW630 protein or goat anti-mouse IgG-Fc (ThermoFisher Scientific, MA, USA) at 1:10,000 in carbonate buffer were coated on microtiter plates (Dutscher, France) 2h at room temperature and then ELISA assays were carried out as described in chapter VI by adding Day 2 fecal water.

Results

We took advantage of the hamster model routinely used by our collaborators from the BaPS team (Paris-Saclay University) to test the effects of two anti-LMW630 mAbs *in vivo*. In order to optimize mAbs delivery in colon, we administered our mAbs via two routes of administration: one by gavage as previously described with anti-SlpA serum[332], or one by intra-peritoneal injection as previously done with Bezlotoxumab[357], the anti-toxin B mAb (Fig 1a). To follow CDI, we collected feces and monitored animal survival. After two days, all the hamsters were dead in all groups (Fig 1.b), suggesting that anti-LMW630 mAbs did not confer protection in this virulent CDI model. In addition, *C. difficile* count in day 2 feces were similar between treated and control groups meaning that mAbs did not significantly hamper *C. difficile* colonization (Fig. 1.c). Then, we wanted to assess anti-LMW mAbs delivery and concentration in colon. While we detected residual mouse IgG antibodies in hamster fecal waters at Day 2 (Fig. 1.d, left panel), no anti-LMW specificity was measured in fecal waters from treated animals (Fig. 1.d, right panel) questioning mAbs integrity in colon.

Conclusion

No protection was seen in a survival model of CDI with our anti-LMW mAbs. Since the hamsters are extremely sensitive to *C. difficile* toxins, we wondered if we could not see an effect because this model was too virulent and if we could have seen something with a less virulent model, closer to CDI in humans.

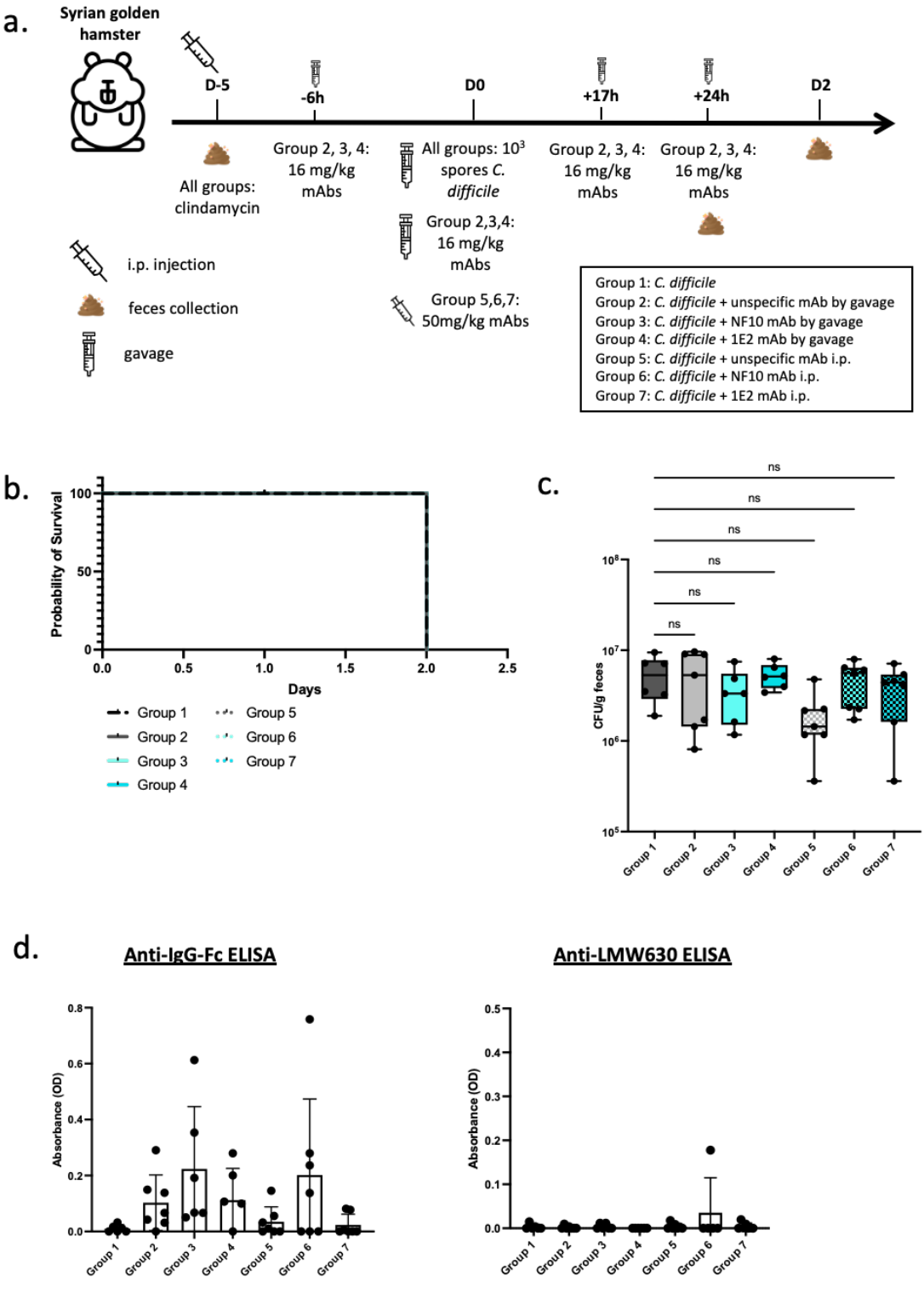

Figure 1. Anti-LMW630 mAbs did not protect hamsters against CDI. a) Passive immunization protocol. Before *C. difficile* challenge, hamsters received clindamycin to disrupt the intestinal microbiota at D-5. Then, hamsters were orally challenged by 10^3 spores of *C. difficile* 630. Feces were collected 24h and 48h after the infection. Control groups included a group that did not received any antibodies (group 1) and two groups that received an unspecific mAb either by gavage (group 2) or i.p.

(group 5). Animals received a total of 50mg/kg of mAbs, either in one-time i.p. on day 0, or in 4 times by gavage at -6h, D0, +17h and +24h. One group received passive immunization by gavage with anti-LMW630 NF10 mAb (group 3), one by anti-LMW630 1E2 mAb (group 4), and 2 other groups received the same mAbs but i.p. (group 6 and 7). **b)** Kaplan-Meier survival analysis after passive immunization. **c)** *C. difficile* spores and vegetative cells quantification in hamsters' feces (CFU/mL) for the 7 groups. **d)** Binding interactions of hamsters' fecal waters to goat anti-mouse IgG-Fc or LMW630 recombinant proteins.

In vivo evaluation of anti-LMW mAbs in a mice model of *C. difficile* infection

Introduction

Given anti-LMW effects on *C. difficile* growth, we hypothesized that anti-LMW may impact early steps of CDI. We therefore decided to evaluate anti-LMW mAbs in a second model of CDI *i.e.* axenic mice that are mostly used to study *C. difficile* colonization, without any competition with other commensal bacteria[358]. Of note, axenic mice are not sensitive to *C. difficile* toxins and generally do not develop any symptoms when infected with the bacteria.

Materials and methods

***In vivo* assay.** C3H axenic mice were weighted, and their blood sampled the day before *C. difficile* challenge. Three groups of mice were formed: the first one that did not receive any antibodies (group1), a second one that received an unspecific mAb (group 2) and a third one that received anti-LMW mAbs in a cocktail (group 3). 14 hours before the infection, anti-LMW mAbs in a cocktail containing four mAbs (NF10, KH2, 1E2, 2B7, TG10) were given by oral route at 10 mg/kg (Fig. 1.a). At D0, 500 *C. difficile* spores were administered by gavage. 1 mg of mAbs was administered by gavage along with 30 mg/kg of mAb i.p. 24 hours and 48 hours after, mAbs were given by gavage at 10 mg/kg. Feces were collected at 4h, 8h, 12h, 24h, 34h, 48h, D3, D8 and D14. Mice were euthanized at D14, and their large and small intestine recovered.

Quantification of *C. difficile* in mice's feces. Numbering was done as described previously in '*In vivo* evaluation of anti-LMW mAbs in a hamster model of *C. difficile* infection' paragraph.

ELISA. Fecal waters were prepared, and ELISA were performed as described in '*In vivo* evaluation of anti-LMW mAbs in a hamster model of *C. difficile* infection' paragraph.

Flow cytometry analysis. Feces were resuspended in 1X-PBS (1g for 2mL) and spined for 10 min at 4000g. Supernatant was removed, and pellet dissolved in 200 µL of PBS. Intestinal bacteria were recovered in supernatants after centrifugation (800g for 10 min at 4°C). These bacteria were stained with anti-mouse IgG AF647 (dilution 1:200, Jackson ImmunoResearch,

UK) for 30 min at 4°C, washed with 1X-PBS and resuspended in 100 µL of 1X-PBS. Flow cytometry acquisition was performed on a MacsQuant16 cytometer (Miltenyi, Germany) and analyzed on FlowJo software v10.8.1 (BD Biosciences, CA, USA).

Results

We took advantage of the axenic CDI mice model routinely used by our collaborators from the BaPS team (Paris-Saclay University) to test the effects of anti-LMW mAbs on *C. difficile* colonization *in vivo*. To follow bacterial colonization in mice, we quantify *C. difficile* in feces at different time points. *C. difficile* colonize axenic mice in 24 hours, with a linear progression between 0 and 24h and a plateau of 10^8 CFU/g feces that is reached after 24h. No significant differences could be seen in terms of colonization between the 3 groups of mice. We observed a slight delay at 12h for the group which received the anti-LMW630 mAbs cocktail but nothing significant (Fig. 1.b).

Given the lack of anti-LMW mAbs on *C. difficile* colonization, we wanted to verify mAb concentration in mice colon. We therefore looked for anti-LMW mAbs in fecal waters 3h and 12h after *C. difficile* challenge. Using ELISA, we were not able to detect a significant amount of anti-LMW mAbs. We then hypothesized that mAbs were not free but bound to bacteria. We evaluated mAb binding to *C. difficile* by flow cytometry. While we observed 45% of mAb-coated bacteria in treated group, untreated and control groups harbored similar binding profiles questioning staining specificity (Fig 1.d).

Conclusion

No difference in terms of colonization was found in a model of CDI using axenic mice and an anti-LMW mAb cocktail. However, we were not able to demonstrate mAb presence and integrity, neither in in fecal waters, nor on bacterial surface. We then wondered if another format of antibodies, such as secretory IgA (sIgA) would be more resistant to the harsh intestinal conditions. Encapsulating antibodies with gastro-resistant polymers could also be a way to circumvent this problem.

Moreover, it could be interesting to test anti-LMW mAbs in a model with a controlled microbiota (such as the OMM12 model[359]) to be closer to CDI in humans, or to evaluate the mAbs in a relapse model of CDI. Indeed, relapses are one of the main issues of CDI and

therapeutic molecules are generally evaluated for their impact to reduce these relapses, as it was done for the bezlotoxumab[288].

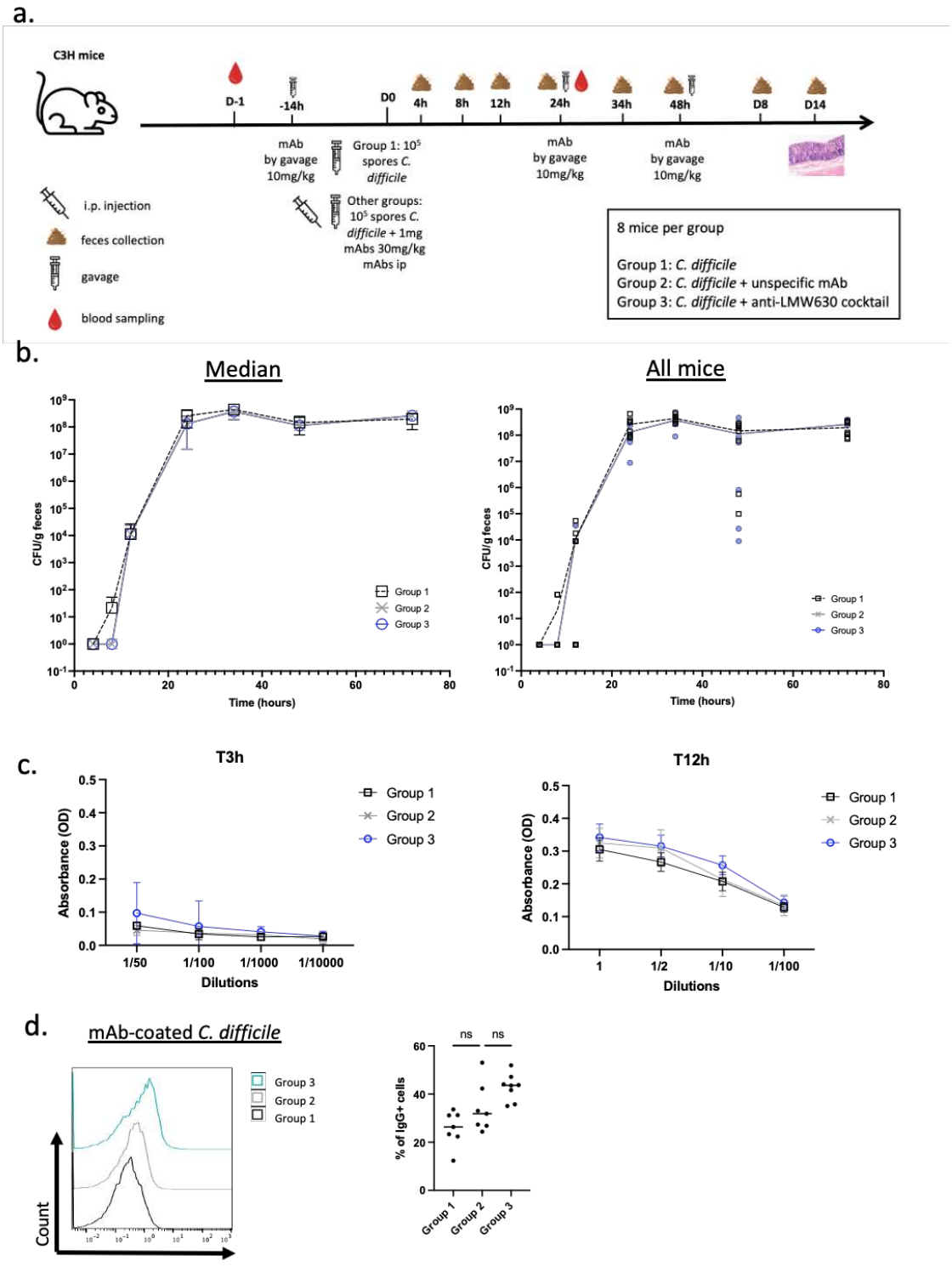

Figure 1. Anti-LMW630 mAbs did not delay colonization in an axenic mice model of CDI. a) Passive immunization protocol. Animals received a total of 50mg/kg of mAbs, by gavage at -14h, D0,

+12h and +24h at 10 mg/kg and 1 mg by i.p at D0. Mice were orally challenged by 500 *C. difficile* 630 spores. Feces were collected at 4h, 8h, 12h, 24h, 34h, 48h, D3, D8, D14. **b)** Quantification in CFU/mL of *C. difficile* in mice's feces for the 3 groups. Left panel represents median while right panel represents each mouse. **c)** Binding interactions of mice's fecal waters to LMW630 recombinant protein. **d)** Evaluation of mAb binding to fecal bacteria. Representative flow cytometry plot of mAb binding to *C. difficile* (left) and mAb-cotaed *C. difficile* frequencies in untreated, control and treated groups (right).

VIII. Development of new methods to ribotype *C. difficile*

The last part of this work took advantage of the high specificity of the anti-LMW mAbs produced. Indeed, most of them were specific of only one ribotype of *C. difficile*, thus having the potential to be valuable epidemiological tools.

A first part of this work focused on the hypervirulent ribotype 027. Anti-LMW027 mAb specificity was evaluated towards several R027 *C. difficile* strains and other ribotypes. Recognition of all the strains of the ribotype 027 could be demonstrated while some cross-specificity for other ribotypes was observed for certain mAbs. Then, binding to healthy human microbiota by anti-LMW mAbs was assessed and no cross-reactivity could be observed. Finally, flow cytometry was used to try and detect *C. difficile* in a complex microbiota and detection could be seen until 1:100 000 ratio (*C. difficile* vs microbiota).

Encouraged by these results, we started a collaboration with the diagnostic platform of Pasteur Institute. We developed a rapid identification test based on a highly sensitive bioluminescent method (LuLISA). A prototype of the test was designed by the diagnostic platform.

We then selected the best anti-LMW027 mAb, for which we could see the highest sensitivity to detect *C. difficile*. This mAb was not reacting with other ribotype of *C. difficile* and could detect *C. difficile* in a complex microbiota.

This work was extended to other ribotypes as the ribotype R027 is not circulated heavily in France anymore. Anti-LMW001 and anti-LMW014 mAb binding to various strains of *C. difficile* was evaluated.

Related work to this chapter is presented after this third manuscript. We present an assay using flow cytometry on clinical strains of *C. difficile* to evaluate if strains with the same ribotype can be recognized by anti-LMW mAbs. Cross-reactivity of anti-LMW mAbs with healthy human microbiota was also evaluated, and detection of *C. difficile* in a complex human microbiota was finally performed using this same technique.

‘Quick-Ribodiff’: a rapid and easy ribotyping test to follow *C. difficile* epidemiology

Lise Hunault, et al.

Ongoing study

Abstract

Clostridioides difficile (*C. difficile*), a Gram-positive anaerobic and spore-forming bacterium, is a member of the human gut microbiota and is the leading cause of nosocomial infectious diarrhea in adults following antibiotic treatment. Despite improvements in basic knowledge of this bacterium as well as the laboratory techniques to study it and follow the appearance and dissemination of the strains, epidemiology of CDI continues to challenge. Data are lacking for all the developing countries and one main limitation to follow CDI epidemiology is the lack of a quick and easy test that can determine the ribotype of *C. difficile*. To address this issue, we took an interest on the SlpA (Surface-Layer Protein A) protein, which is the most expressed protein on the surface of *C. difficile* and used its variability to develop a rapid identification test "Quick-Ribodif" for diagnostic and epidemiological monitoring purposes. The proof of concept of this test has been completed.

Keywords (5-10 words)

Clostridioides difficile, monoclonal antibodies, S-layer, ribotyping

Introduction

C. difficile is an anaerobic bacterium, Gram-positive and spore-forming rod, that is the main nosocomial agent responsible for antibiotic-associated diarrhea in adults[311]. In severe cases, *C. difficile* can lead to pseudomembranous colitis and death. *C. difficile* infection (CDI) is associated with an increased length of hospital stay and health care costs. Total annual CDI-attributable expenses have been estimated to $6.3 billion per case in US[160].

Rapid diagnosis, surveillance of emerging strains, transmission lines are needed to control CDI burden. Indeed, in countries where the incidence of CDI significantly dropped, a comprehensive national surveillance program has been implemented, with the standardization of diagnostic approach, sampling, and reporting. However, incidence rates still vary widely between

countries and capacity for surveillance and diagnosis remain highly variable from a country to another[220,232,233]. As of now, there is no rapid and sensitive approach for *C. difficile* surveillance, diagnosis and typing that would allow the estimation of the total burden of CDI in each country. With the rise of new hypervirulent ribotypes associated with increased CDI severity and higher recurrence rate such as ribotype R027, *C. difficile* strains need to be characterized beyond the species level. Typing methods enable identification of clusters and cross-transmission routes that prompt infection control measures in health care facilities. Moreover, it helps to track hypervirulent and new emergent strains in order to enhance the global surveillance.

The main typing method to identify *C. difficile* ribotypes is currently PCR ribotyping that discriminate strains of *C. difficile* based on differences in the ribosomal 16-23S interspace regions. PCR ribotyping require culture and isolation of the micro-organism, which can be drawn-out and labor intensive. Consequently, *C. difficile* typing is usually restricted to national reference centers. One quick and easy test had been developed to track the hypervirulent ribotype R027 directly from stool. However, GeneXpert assay had the main drawback of being expensive even for hospitals in developed countries[360]. This led to a restrict usage and therefore suboptimal following of the epidemiology compared to what could have been theoretically achieved with this technique. An ideal test would be one that detect *C. difficile* ribotype directly from patients' feces, in a few minutes. This quick and easy test would not require trained personnel and could consequently be performed in developing countries that do not possess heavy lab equipment and qualified personnel to perform PCR ribotyping.

In this work, we reported development of a rapid and easy-to-perform ribotyping test "Quick-Ribodiff" using a luciferase-linked immunosorbent assay (LuLISA), which retained high sensitivity and specificity. This LuLISA allows bioluminescent detection of various *C. difficile* R027 strains in complex microbiota using an anti-LMW monoclonal antibody, which displays a high affinity. We established a proof-of-concept for the hypervirulent strain R027 and extended our analysis for one frequent ribotype in France *i.e.* R001.

Results

Development of a LuLISA assay to detect *C. difficile R027*

To develop a LuLISA assay for *C. difficile* detection, we built on our anti-LMW mAb collection and the experience of the diagnostic platform of Pasteur Institute[309]. We designed a sandwich ELISA where we use the same anti-LMW mAb, but with different Fc portions, as capture and

detection antibody. Finally, an anti-human IgG VHH linked to a luciferase is used for revelation (Fig 3.a).

This LuLISA assay has been miniaturized, and can be sell as a quick, easy, and cheap commercial assay. A first prototype shown in Fig 3.b. has been designed by the platform. Of note, result reports are released within 15 minutes, and can be retrieved with the USB port (Fig 3.b).

Anti-LMW mAbs specifically detect *C. difficile* in a complex microbiota in a LuLISA assay.

Based on the collection of Hunault *et al.,* the four anti-LMW027 mAbs with the highest affinities (PH4, RD11, SG8 and VA10) were selected and tested using the LuLISA described above. We prepared serial dilutions in buffer of *C. difficile* R027 or *C. difficile* 630 as negative control. As expected, a concentration-dependent signal appeared only for the samples containing R027 strain with 3 out of 4 antibodies tested (RD11, VA10 and PH4). RD11 displayed the lowest detection limit (10^4 compared to 10^5 bacteria/mL for PH4 and VA10, Fig. 2.a). We further determined RD11 specificity by screening four *C. difficile* strains belonging to other common ribotypes (R001, R002, R014 and R078). No signal was detected for the other ribotypes (Fig. 2.b), confirming RD11 specificity.

To build a quick ribotyping test, we aimed to detect *C. difficile* bacteria directly in the feces of CDI patients. To this end, we mixed *C. difficile* R027 within two healthy human microbiotas in a series of 10-fold dilutions and assessed the detection limit in this complex environment. *C. difficile* was detectable at concentrations as low as 10^4 bacteria/mL (Figure 2.c). Strikingly, detection limit was similar in microbiota or buffer used for serial dilutions. Altogether, these results indicate that the Quick-Ribodiff LuLISA has a high specificity and sensitivity and could potentially be used to detect *C. difficile* in stool from CDI patients.

Discussion

In this work, we reported a proof-of-concept for the specific detection of *C. difficile* R027 in complex microbiota by LuLISA. Using RD11 mAb, detection limit reached 10^4 bacteria/mL. Quick-Ribodiff LuLISA presents the main advantages to be miniaturized, cost-effective and esay-to perform. Moreover, results are obtained directly from the feces in less than 15 min, compared to approximately 6 days for common PCR ribotyping methods[361].

The detection limit is a crucial performance characteristic of diagnostic tests. Current methods for *C. difficile* detection in feces showed detection limit of 10^6 CFU/g feces for Toxin Enzyme Immunoassays, 10^4 CFU/g feces for culture, and 10^5 to $10^{2.4}$ CFU/g feces for real-time PCR[362,363]. Although the comparison of detection limits is hindered by the use of different units, it appears that Quick-Ribodiff will be sensitive enough to detect *C. difficile* in patients' stool samples. Indeed, previous studies that enumerate intestinal populations of *C. difficile* in CDI and asymptomatic patients reported an average count of 10^4-10^5 CFU/g feces[362]. *C. difficile* abundance may vary according to the composition of intestinal microbial communities, as well as some extrinsic factors such as the environment or the host immune state[364].

Interestingly, since we produced anti-LMW mAbs recognizing other ribotypes of *C. difficile*, we looked at the detection of *C. difficile* strain 630 by LuLISA (Sup. Data. 1). Among the two anti-LMW630 mAbs tested (NF10 and KH2), only NF10 detected *C. difficile* by LuLISA assay with a high specificity (Fig. Sup 1.a). Whole *C. difficile* bacteria was detectable in two human microbiotas at concentrations as low as 10^3 – 10^4 bacteria/mL. This detection limit was 10-times lower than the one found with anti-LMW027 mAb. Of note, NF10 affinity is also 10-times higher than RD11. One could speculate that increasing mAb detection affinity would improve LuLISA sensitivity. A way to improve affinity would be to generate nanobodies and select the best binders after consecutive rounds of selection. Moreover, nanobodies are easier and more cost-effective to produce than mAb[258].

Our work faces limitations. The first one is that the proof of concept was performed with healthy microbiota spiked with *C. difficile*. Validation with samples from CDI patients is thus required. The ribotype 027 is an hypervirulent ribotype that led to the latest epidemies in the USA[365], but it is not mainly found in France. Currently, recruitment of CDI patients is ongoing in several hospitals in the North of France where R027 strain is circulating[366]. In parallel, we have also extended LuLISA for detection of R001 *C. difficile* (Fig). Using RF10 mAb, we reached a similar detection limit as R027, without cross-reactivity. Four patients infected with *C. difficile* R001 (a kind gift of Pr Frédéric Barbut, *C. difficile* National Reference Center) have been selected and experiments are currently performed.

Intra-ribotype variability has been described[321]. It will remain to define whether LuLISA would detect various strains belonging to the same ribotype. Parallel experiments using flow cytometry provided promising results about pan-ribotype detection (see unpublished data following). Besides, more than 86 ribotypes have been described in recent epidemiological

studies[168]. To address *C. difficile* diversity, a larger collection of anti-LMW mAbs should be include in Quick-Ribodiff LuLISA.

Despite its limitations, this study provides evidence that LuLISA showed a high specificity and sensitivity to detect *C. difficile* in human microbiota. This test could be used in combination with toxin-targeted diagnostic tests to provide a quicker and more accurate test than the ones currently commercialized. It could also be used to detect *C. difficile* in the environment and in the food chain where specific ribotypes are redundantly found (such as the ribotype 078 in pigs)[186,188].

Materials & Methods

Production of mAbs against LMWs. Murine mAbs against LMW-R001, LMW-R027 and LMW630 were produced as described in Hunault *et al.,* manuscripts in preparation #1 and #2. MAb V_H and V_L sequences (proprietary information) were cloned into pUC19-Igγ1, pUC-kappa and pUC-lambda-expressing vectors (a kind gift from Hugo Mouquet, Institut Pasteur, Paris) by SynbioTechnologies (NJ, USA) to obtain chimeric mAbs. Recombinant mAb production was performed as described in Balbino *et al.,*[322].

LuLISA assay. LuLISA assay were performed in collaboration with the diagnostic platform of Pasteur Institute, according to their protocol[309]. MAbs were used at 10 µg/mL for coating and primary recognition of bacteria. Signal of the wells without bacteria were used as reference wells.

Prototype design and conception. Prototype and conception of Quick-Ribodiff test was done by the diagnostic platform of Pasteur Institute.

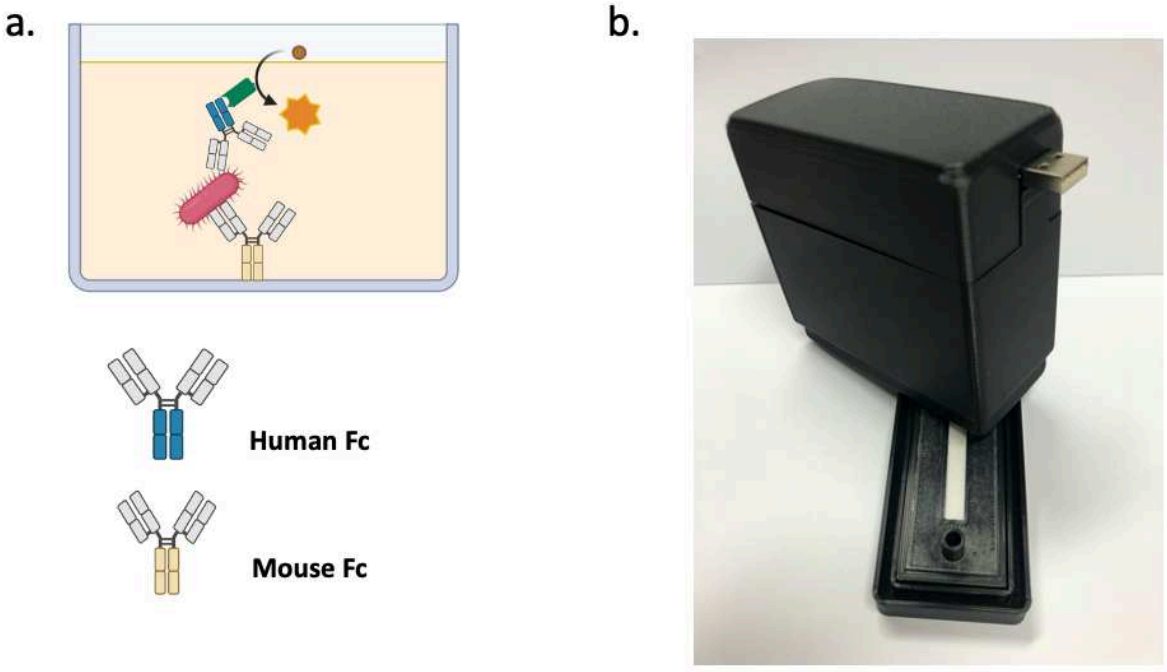

Figure 1: Detection of *C. difficile* by LuLISA. a. Cartoon representation showing anti-LMW mAbs bound to *C. difficile.* Anti-human IgG VHH- luciferase is depicted in green. **b.** Prototype of 'Quick-Ribodiff'.

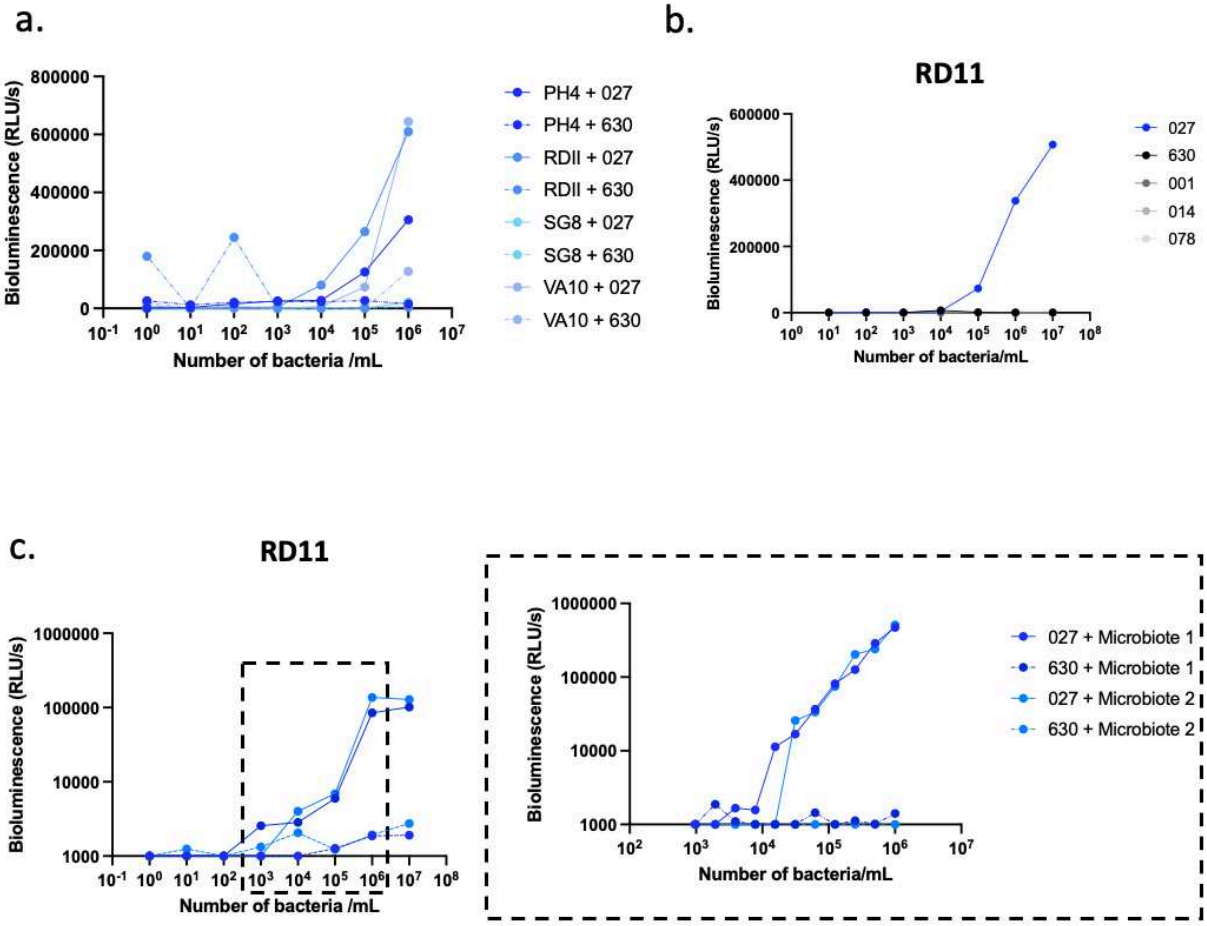

Figure 2: Anti-LMW027 mAbs detect *C. difficile* R027 in a complex human microbiota by LuLISA. a. Detection of whole *C. difficile* R027 by LuLISA. Strain 630 is used as a negative control. **b.** Detection of whole *C. difficile* bacteria from ribotypes 001, 014, 078, 027 and strain 630 with RD11 mAb by LuLISA. **c.** Detection of *C. difficile* in two healthy human microbiotas with RD11 mAb. RLU: Relative Luminescence Units.

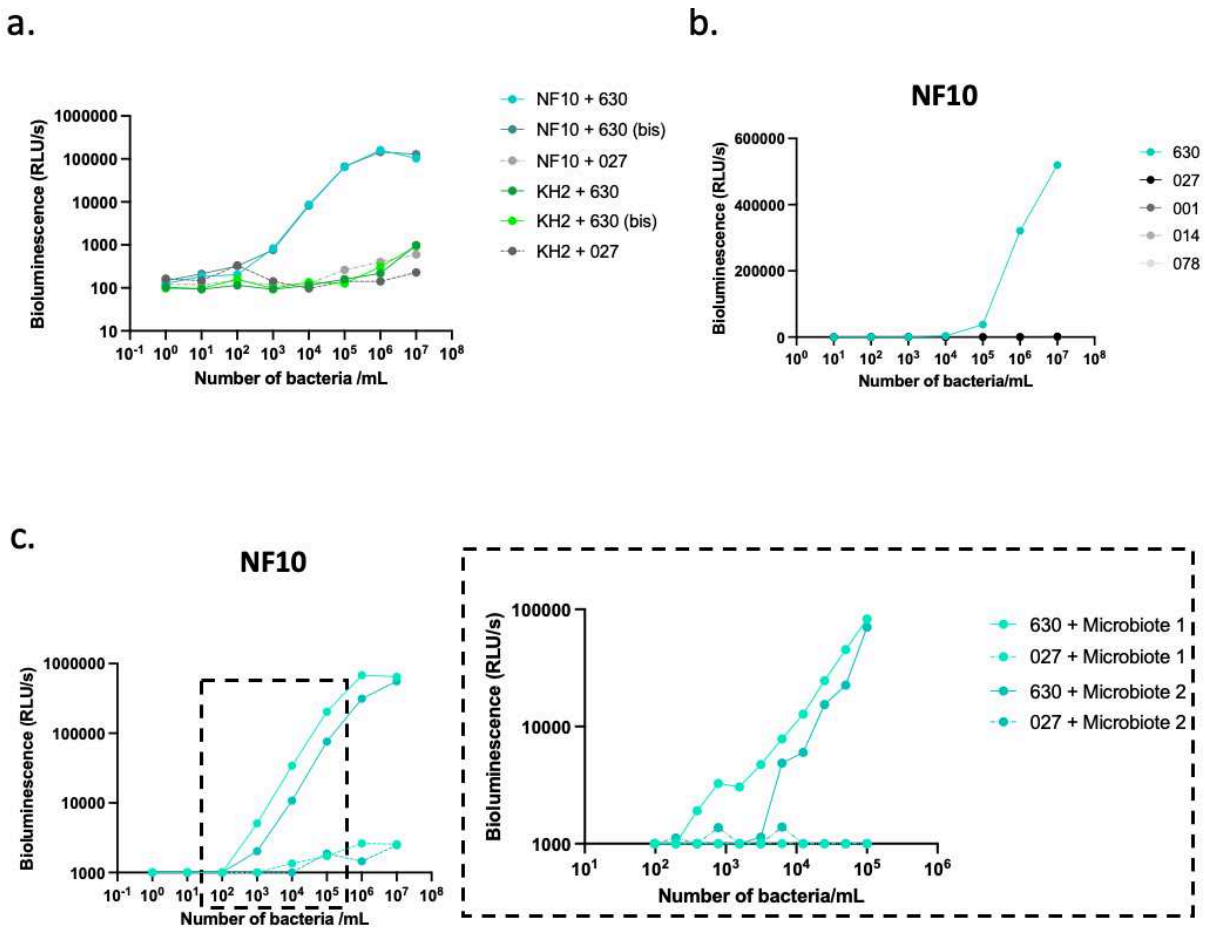

Supplementary figure 1: Anti-LMW630 mAbs detect *C. difficile* 630 in a complex human microbiota by LuLISA. a. Detection of whole *C. difficile* 630 by LuLISA. *C. difficile* R027 is used as a negative control. **b.** Detection of whole *C. difficile* bacteria from ribotypes 001, 014, 078, 027 and strain 630 with NF10 mAb by LuLISA. **c.** Detection of *C. difficile* in two healthy human microbiota with NF10 mAb. RLU: Relative Luminescence Units.

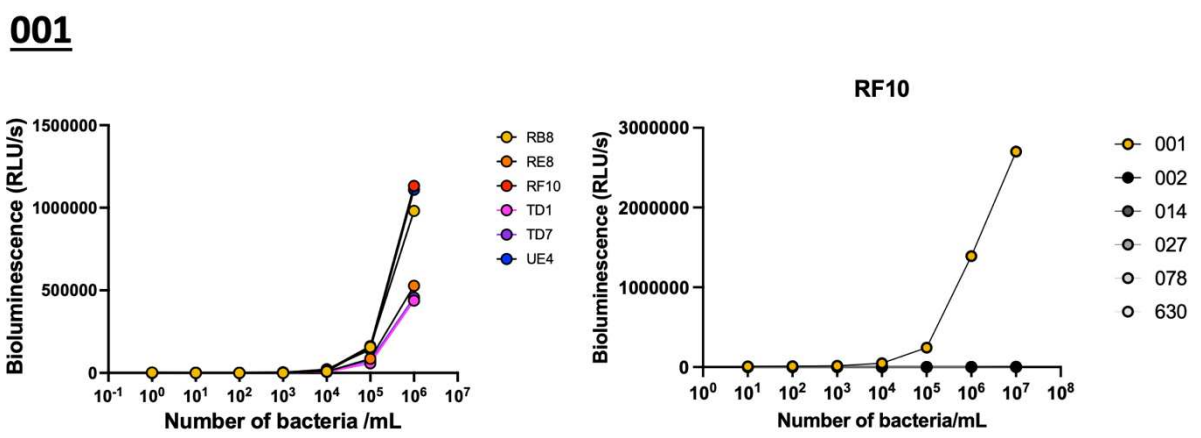

Supplementary figure 2: Anti-LMW001 mAbs detect *C. difficile* R001 by LuLISA. a. Detection of whole *C. difficile* R001 with anti-LMW001 mAbs by LuLISA. **b.** Detection of whole *C. difficile* bacteria from ribotype 001, 002, 014, 078, 027 and strain 630 with RF10 mAb by LuLISA. RLU: Relative Luminescence Units.

Unpublished data associated to chapter VIII

Identification of *C. difficile* ribotype with anti-LMW mAbs using flow cytometry

Introduction

C. difficile harbors different ribotypes, some of them driving large CDI epidemics[170,366]. Ribotyping of *C. difficile* is generally done with PCR typing[215]. In this work, we took advantage of ribotype-specific anti-LMW mAbs to test whether it is possible to determine the ribotype of clinical strains by flow cytometry. Binding to species of healthy microbiota was also evaluated, as well as the abilities of anti-LMW mAbs to detect *C. difficile* in a complex microbiota.

Materials and methods

Production of monoclonal antibodies against LMWs. Mabs against LMW-R001, LMW-R027, LMW014 and LMW630 were produced as described in Hunault *et al*.

Flow cytometry assay. Flow cytometry assay were performed as described in chapter VI with fixed *C. difficile* at 10^6 bacteria/well. The various strains of fixed *C. difficile* (R001, R027 and 630) were obtained from Pr. Frédéric Barbut at Saint-Antoine Hospital.

Results

Anti-LMW mAbs detect *C. difficile* in a complex microbiota.

We previously showed that surface-layer protein such as Low Molecular Weight (LMW) is an appropriate antibody target to discriminate *C. difficile* strains. Based on chapter VI mAbs collection, a total of 7 anti-LMW027 mAbs were produced and purified (n=7). We first assessed mAb binding to six *C. difficile* clinical strains of ribotype R027 (CD16-059, CD12-175, CD21-013, CD13-129, CD20-070, CD21-035) using flow cytometry. All the mAbs recognized a substantial fraction of the six tested strains (Fig. 1.a). We observed homogeneous mAb binding profiles for five strains (>80% of mAb-coated bacteria; CD16-059, CD12-175, CD21-013, CD13-129, CD20-070) while mAbs bound only a fraction of cultured CD21-035 strain suggesting that LMW exposure varied within the strain.

We then extended our analysis to other ribotypes to evaluate mAb specificity. We first focused on R001 and R078 strains, known to share strong similarity with ribotype R027 (Chapter VI). One mAb (PH4) weakly bound R078 strains (<10 %) whereas two mAbs (SG8 and TH4) recognized a substantial fraction (>50%) of R001 strains (Fig 1a). We then tested a frequent ribotype in Europe, R002. No cross-specificity was observed for one R002 strain (Fig 1a).

We then wanted to assess mAb cross-specificity towards commensal species of healthy human microbiota. Indeed, microbiota contains thousands of different species, and some chemical motifs can be shared among different bacteria. To this end, we tested four fecal microbiotas obtained from healthy individuals[323]. No cross-reactivity was detected for any of the mAbs with the microbiota CER201 and CER203. A small fraction of the microbiota CER213 (from 0.5 to 6%) was bound by 4 mAbs (PH4, QD8, RD11 and TE8). Likewise, all the mAbs except QD8 recognized a small fraction of the microbiota CER232 (from 2% to 3.4%, Fig 1b). For these two microbiotas, a cross-reactivity with other species can be envisioned, or an asymptomatic carriage of *C. difficile* (colonization can reach up to 15% in healthy individuals[367]).

We next decided to evaluate if our mAbs could detect *C. difficile* bacteria among a complex human microbiota in order to develop a ribotyping test directly from patients' stools. Hence, we mixed different ratios of *C. difficile* R027 into healthy microbiota and assessed *C. difficile* detection by flow cytometry (Fig 1.c). Detection by two anti-LMW mAbs (QH5 and TE8) that did not cross-react with other ribotypes of *C. difficile* could be observed until 1:1000 ratio for microbiota 1, and 1:100 for microbiota 2.

In this part, we showed that the mAbs we generated recognize various clinical strains of the ribotype 027. Out of the seven anti-LMW027 mAbs, one mAb (QH5) demonstrated no cross-reactivity with other *C. difficile* ribotypes or gut commensals.

This work was extended to frequent ribotypes in France *i.e.* R001 (Fig 2.a) and R014 (Fig. 2.b). Six anti-LMW mAbs were recognizing the ribotype 001 and among the five clinical strains we tested (CD18-095, CD17-185, CD20-060, CD16-048, CD18-247), we observed homogeneous mAb binding profiles for three strains (>50% of mAb-coated bacteria; CD18-095, CD17-185, CD16-048) while mAbs bound only a fraction of cultured CD20-060 and CD18-247 strains (<15%) suggesting that LMW exposure varied within the strain (Fig 1.a). No cross-specificity was observed for 3 clinical strains of ribotype 002 (CD18-103, CD15-354, CD19-035, <4% mAb-coated bacteria), 4 strains of ribotype 014 (CD20-199, CD20-191, CD19-238, CD19-176, <7%) and 4 strains of ribotype 078 (CD20-252, CD19-232, CD16-079, CD15-364, <1%).

Six anti-LMW mAbs were recognizing the ribotype 014 and among the four clinical strains we tested (CD20-199, CD20-191, CD19-238, CD19-176), 2 of them were recognized by all the antibodies (from 15% to 86%) except SB1 which did not stain any strain from ribotype 014 (<7%), and SA3 which did not stain CD20-191 strain (<5%, Fig 1.b). Two strains (CD20-199 and CD19-238) were not stained by any antibody (<2%). No cross-specificity was observed for 3 clinical strains of ribotype 002 (CD18-103, CD15-354, CD19-035, <10%) and 4 strains of ribotypes 078 (CD20-252, CD19-232, CD16-079, CD15-364, 1%). Some cross-specificity was seen for ribotype 001. UA2 and TE10 mAbs were recognizing CD19-095 strain (>18%), UB10, UA2 and TE10 mAbs were recognizing CD17-185 (>90%), UA2 mAb was recognizing CD20-060 (12.6%), and UB10 and UA2 were recognizing CD16-048 strain (>90%).

Conclusion

In this work, we show that anti-LMW mAbs can be used to determine the ribotype of *C. difficile* by flow cytometry and that some mAbs did not cross-react with other ribotypes. These mAbs were overall not cross-reacting heavily with healthy species of the microbiota and could detect *C. difficile* in a complex microbiota, suggesting that they could be used for diagnostic or epidemiology monitoring.

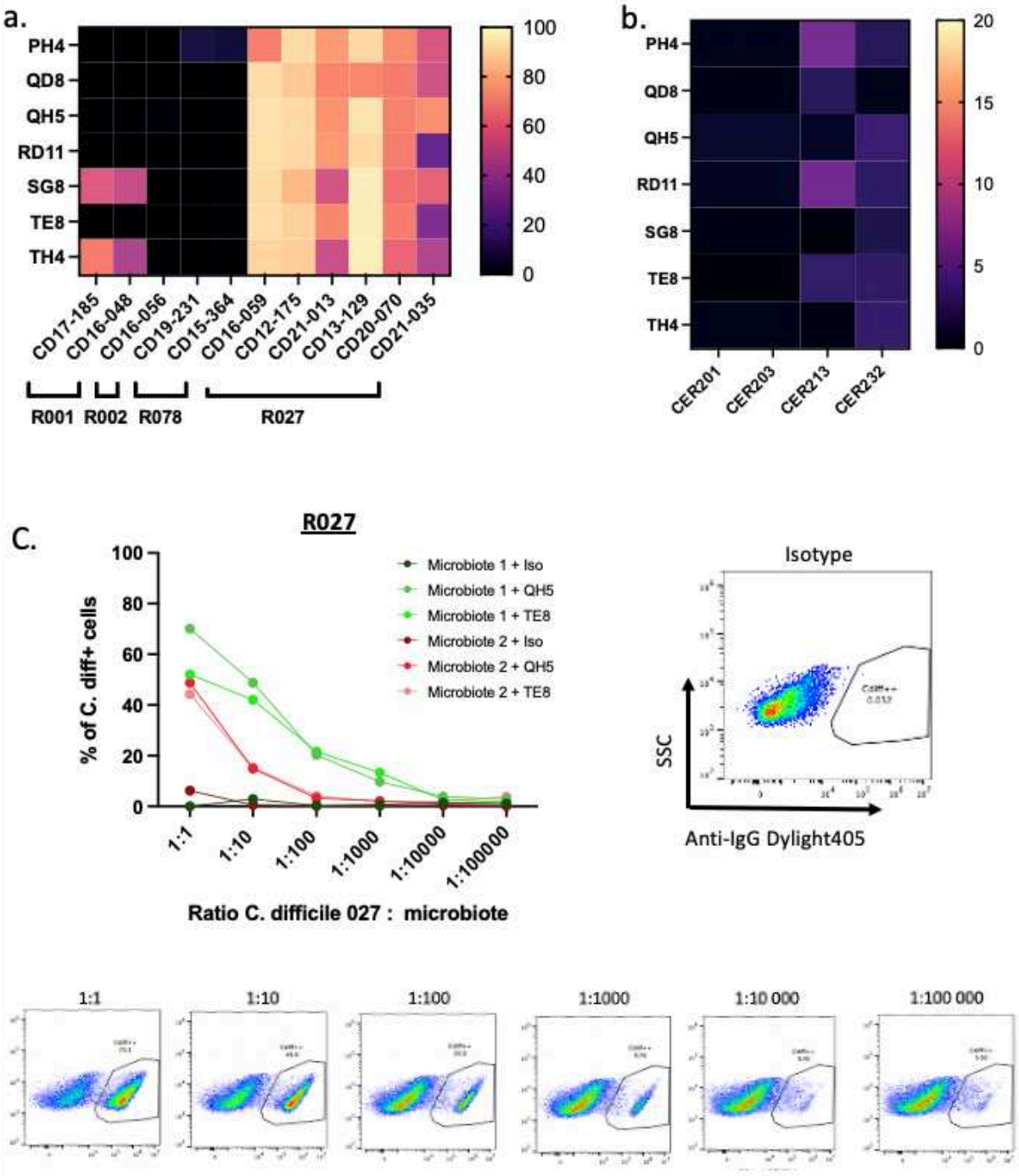

Figure 1: Anti-LMW027 mAbs recognize *C. difficile* in a complex human microbiota with flow cytometry. a. Heat map showing mAb positive fraction (%). *C. difficile* clinical strains from ribotypes R001, R002, R078 or R027. **b.** Heat map showing the percentage of the healthy human microbiota recognized by the anti-LMW027 mAbs. **c.** Binding profiles of anti-LMW027 mAbs to *C. difficile* spiked into healthy microbiota. Percentages of bacteria in healthy microbiota recognized by anti-LMW027 mAbs are shown. mAbs are used at 10 µg/mL for the all the experiments.

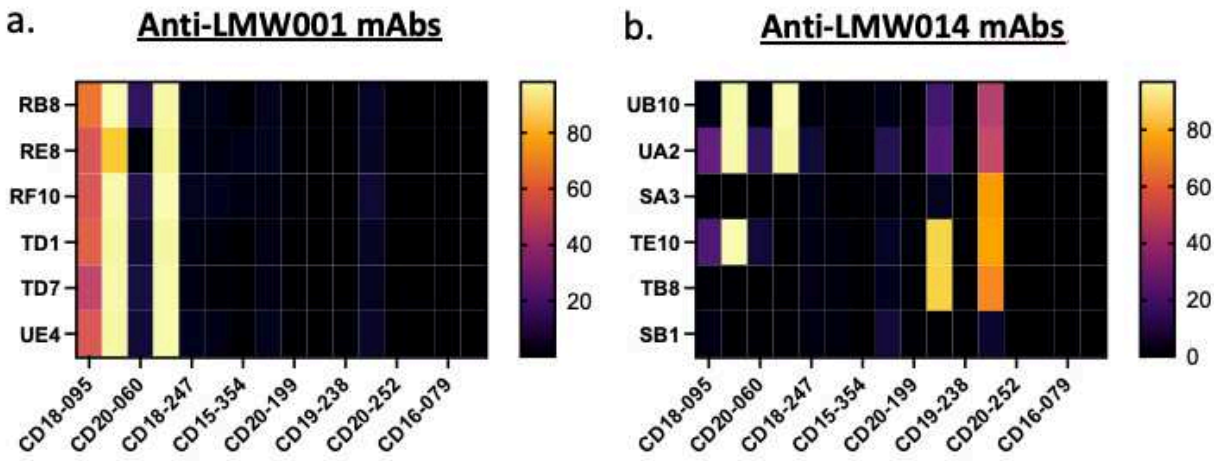

Figure 2: Anti-LMW001 and anti-LMW014 mAbs recognize various clinical strains of *C. difficile*. **a.** Heat map showing mAb positive fraction (%) with anti-LMW001 mAbs. **b.** Heat map showing mAb positive fraction (%) with anti-LMW014 mAbs. *C. difficile* clinical strains are classified as R001, R002, R078 or R027. mAbs are used at 10 µg/mL.

Discussion and perspectives

1. Strategies to generate anti-SlpA mAbs and questions of cross-specificity

The initial stage to generate monoclonal antibodies involves producing the antigen that the antibodies will be target. Antigen can be produced through two methods: direct extraction from their natural source[368,369] or recombinant production if their sequence is known. Recombinant expression involves competent bacteria that will absorb the DNA and use their molecular machinery to produce the protein along with their other ones[370]. In our work to generate monoclonal antibodies against surface-layer proteins of *C. difficile*, first attempts were made using a recombinant SlpA (data not shown). These first monoclonal antibodies however had relatively low affinities and were not able to stain the bacteria by flow cytometry. Several hypotheses could explain these results. Alum was used as the sole adjuvant and might not be sufficient to stimulate the immune response. This adjuvant is the most widely used and has proven safety record. It is cost-effective and compatible with a variety of antigens[371]. Alum activate DCs and macrophages leading to Th2 immune responses. A way to improve its adjuvanticity is to use TLR agonists[372,373] or opioid antagonists, as it has been done with naloxone[374]. Indeed, inhibition with naxolone shifted the immune response towards a Th1 profile which is more favorable for vaccine efficacy[375]. Generation of low affinity antibodies could also be due to the fact that the precursor SlpA was not immunogenic enough to generate B cells expressing high affinity antibodies. The immune response against SlpA has not been extensively studied; nonetheless, it has been demonstrated that humans develop an immune response against SlpA. Moreover, vaccination with SlpA, along with cholera toxin as an adjuvant, has been shown to induce a local and systemic humoral immune response in mice and hamsters[43]. The affinities of the antibodies produced, both in humans and in animal models, remain an open question.

This problem was solved in our case by adding the pertussis toxin in the immunization mix. We also moved to S-layer crude extracts *i.e.* containing both LMW and HWM subunits, from six *C. difficile* ribotypes in order to generate pan-ribotypes antibodies. However, we could not isolate cross-specific antibodies directed towards the LMW by immunizing with the SlpA of various ribotypes. The HMW is highly conserved across strains, whereas the LMW is not[35]. Explanations point towards a mechanism of evolution that protect the bacteria against the immune response generated towards the LMW. Indeed, antibodies produced against one

ribotype are not able to recognize another one and bacteria that have a mutated S-layer will not be recognized by the antibodies[154]. Recently, it has also been shown that the SlpA was a phage-receptor[51]. This can also explain why strains of *C. difficile* that have a different S-layer are selected through evolution, by escaping the recognition and infection by phages. Therefore, we hypothesized that immunizing with S-layer extracts from different *C. difficile* strains would drive the immune response towards the most conserved part *i.e.* the HMW subunit. Consequently, we finally produced 6 recombinant LMWs: LMW-R001, LMW-R002, LMW-R014, LMW-R078 and LMW-R027, LMW630 and used them in combination to immunize mice. We succeeded with this immunization scheme to generate cross-specific antibodies recognizing the 5 clinical ribotypes R001, R002, R014, R078 and R027. The different immunization schemes that we used, and the antibodies respectively produced are summarized in Figure 23.

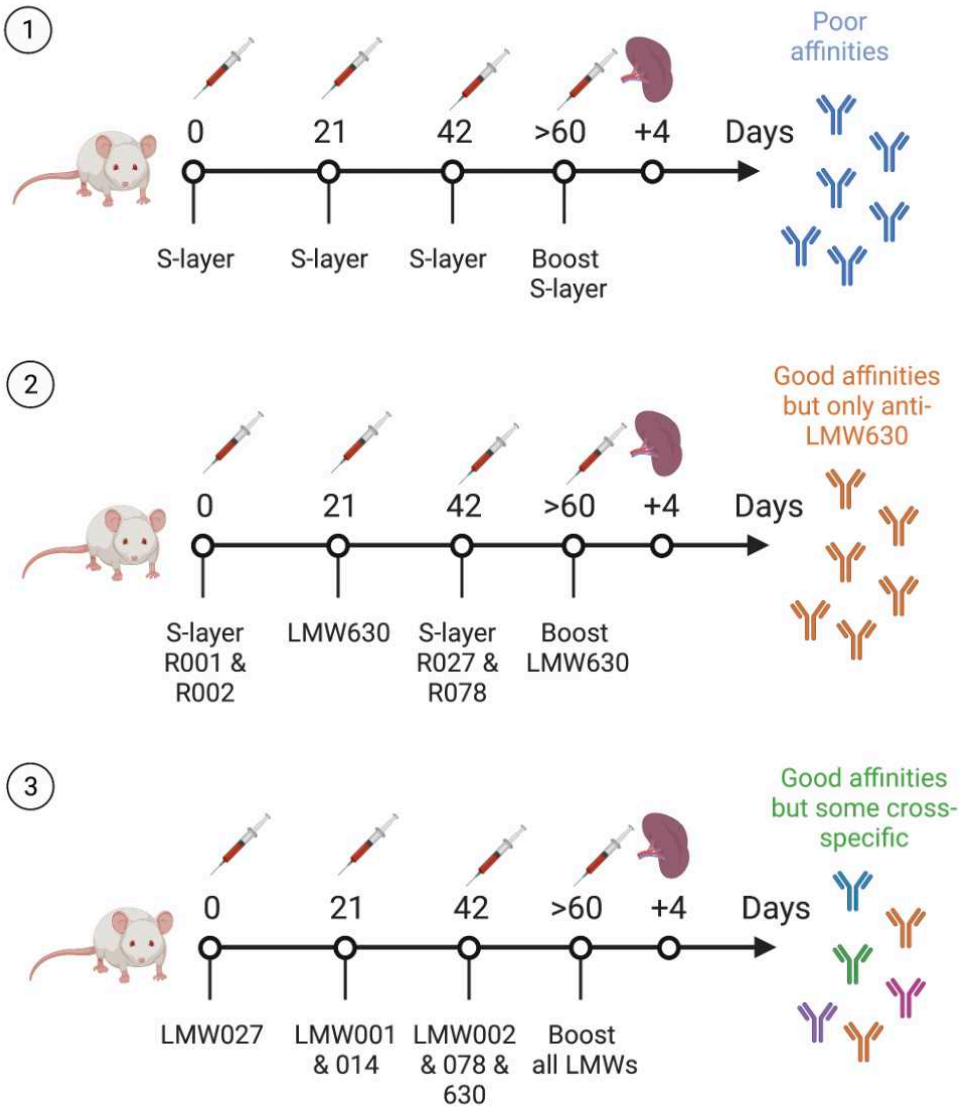

Figure 23. Immunization schemes to generate anti-LMW mAbs.

In our third round of immunization with the 6 LMWs, we were able to detect and isolate cross-specific antibodies. Indeed, the LMW SlpA carry certain regions that are conserved across the different ribotypes. The first one corresponds to the signal peptide, the second one is responsible for the attachment to the HMW, and the last one has been hypothesized to be involved in the attachment to enterocytes, by interacting with a receptor that is so far unknown[316]. Overall, the sequences of the LMWs from the 5 different ribotypes we studied are dissimilar with very few conserved stretches, making conserved linear epitopes rare among these proteins. Sequence alignment of the LMWs we produced are represented in Figure 24.

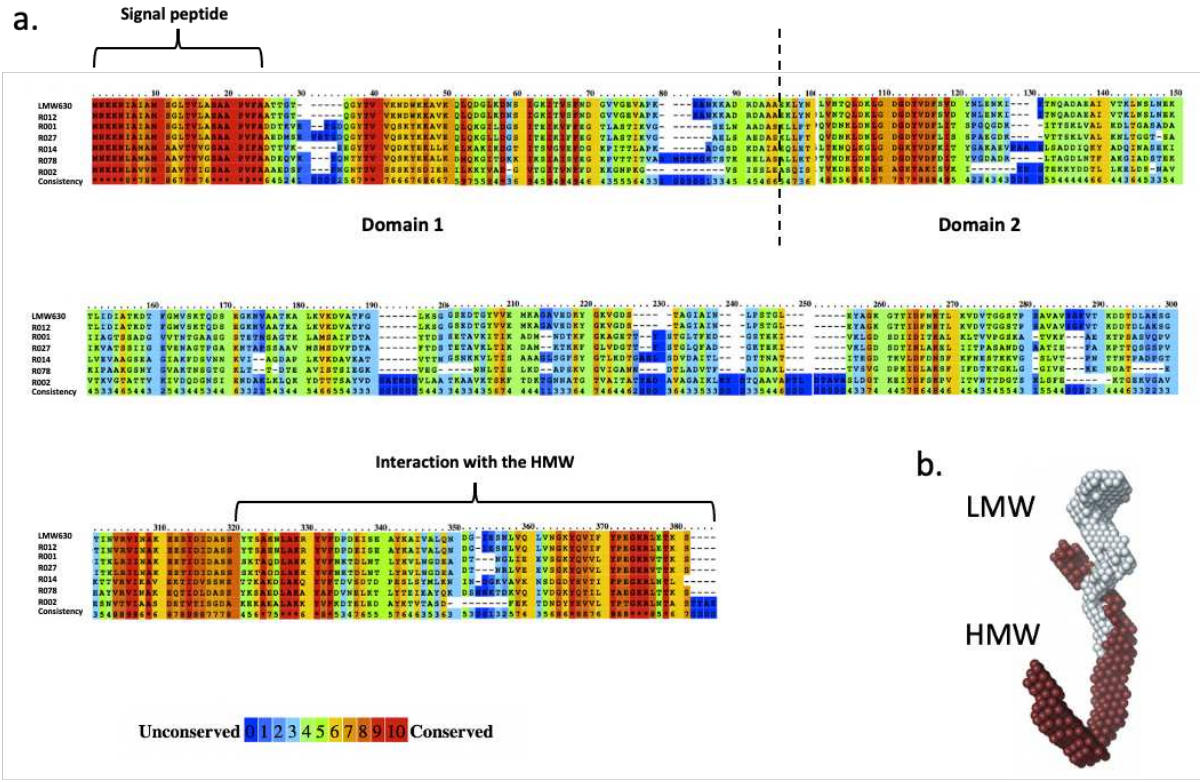

Figure 24. LMW sequences and interaction with the HMW. **a)** Alignments of LMW sequences from ribotypes R001, R002, R012, R014, R078, R027 and strain 630 of *C. difficile* using Clustal Omega software. Dash line represents the separation between domain 1 and 2. **b)** Small-angle X-ray scattering structure of the LMW/HMW complex from *C. difficile* CD630[37].

The majority (n=63, 67%) of the mAbs produced was unsurprisingly monospecific, but we could isolate 24 clones recognizing 2 LMWs, 2 mAbs recognizing 3 LMWs, 3 recognizing 4

LMWs and even 2 that were recognizing 5 LMWs (Fig. 25). We observed that mAb cross-specific profiles were coherent with the phylogenetic tree of the LMW (Chapter VI). Indeed, a majority of mAbs recognizing two LMWs bound the LMW-R001 and LMW-R027 which share the highest percentage of homology, followed by the LMW-R078. Interestingly, no cross-specific mAbs recognizing the LMW630 and another LMW could be generated. This can be explained by the low percentage of homology shared between the LMW630 and the other LMW (between 25 and 40%). Indeed, the *C. difficile* 630 is initially derived from the clinical ribotype R012, but its wide use as a reference model has driven major modifications, which could question about its adequacy for the study of "real world" *C. difficile*[376].

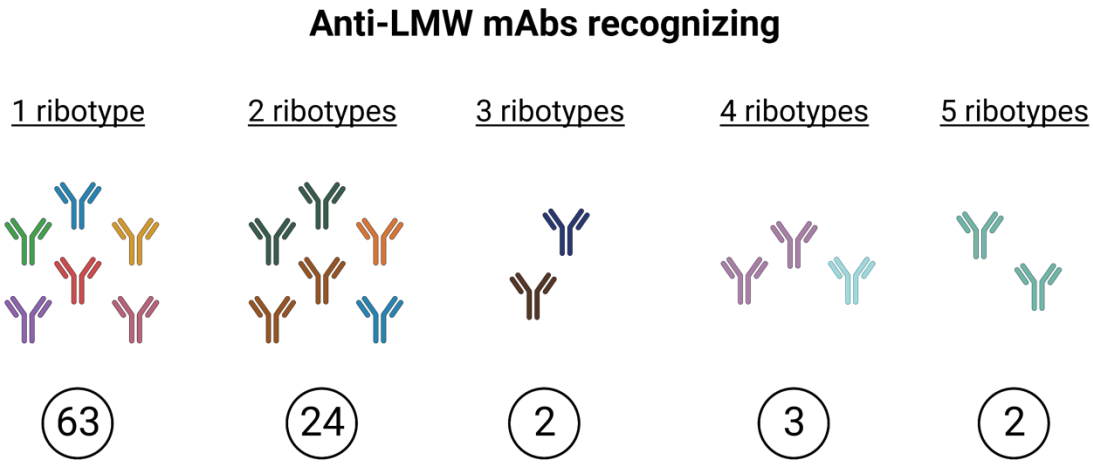

Figure 25. Schematic representation of the different anti-LMW mAbs obtained, classified by the number of *C. difficile* ribotypes they recognize. Circled numbers indicate the number of mAbs in each category.

Cross-specificity profiles towards the different LMW recombinant proteins evaluated by ELISA were only partially reproduced when binding to whole bacteria was examined by flow cytometry. Several mAbs loose one or two ribotype specificities when observed by flow cytometry. Even more interestingly, no binding to bacterial surface was observed for the two mAbs that bound five different LMWs using ELISA. A first explanation can be found in the various affinity towards the protein. An antibody with a low affinity can be detected in an assay using recombinant protein such as ELISA but will not be detected in a flow cytometry assay[377]. Indeed, this could be observed in more details when doing BLI measurements. For QE2 mAb, binding to the LMW014 was of nanomolar affinity whereas binding to LMW001 was of

micromolar affinity. Consistently, *C. difficile* R014 was stained by this antibody by flow cytometry while R014 was not (Fig. 26).

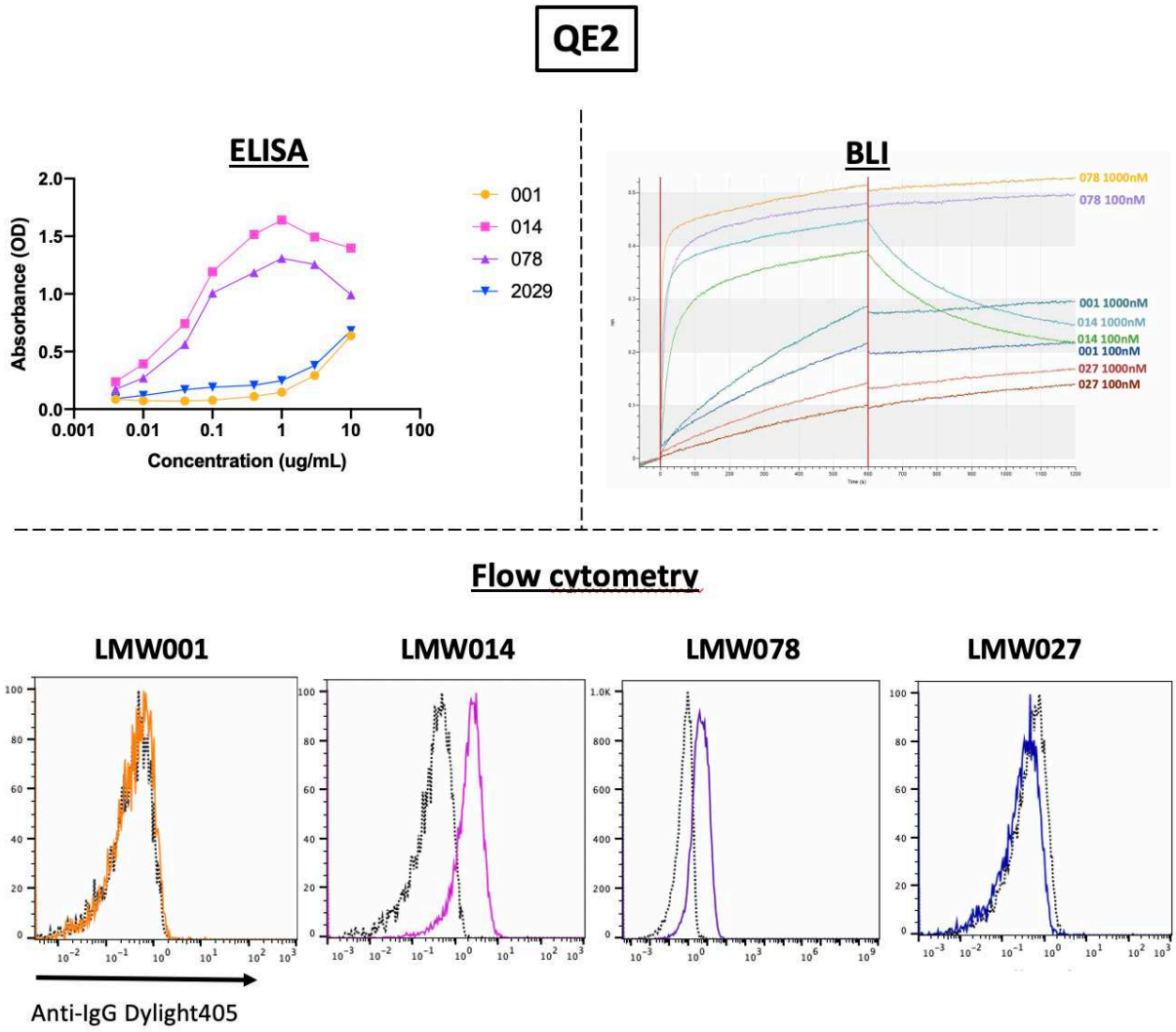

Figure 26. Binding of anti-LMW mAb QE2 to LMW recombinant proteins (top row) and whole bacteria (bottom row).

A second explanation resides in the different conformations of the protein when binding is evaluated with recombinant proteins or with whole bacteria. The arrangement and position of the protein may vary between these different setups, and the protein will also be less flexible when bound at the bacterial surface than when bound on plastic wells[378]. Antigen-antibody interaction will therefore differ. Moreover, low affinity combined to a slight change in antigen conformation can result in a total loss of binding. Finally, the epitopes that are accessible to B cells when mounting an immune response with a recombinant protein vary from the ones

exposed on the surface of the whole bacteria. Indeed, some of these epitopes are hidden at the bacterial surface because they are engaged in other functions such as binding with another protein (in our case the HMW SlpA for instance). We believe that the two mAbs recognizing all five LMWs recombinantly produced bind a cryptic epitope of the LMW, hidden from or inaccessible to mAbs when expressed at bacterial surface. Moreover, conserved regions of the LMW between strains are: the one involved with the binding to the HMW, and the other one to enterocytes. We think that our immunization strategies led in part to the development of cross-specific mAbs directed towards the region involved in the binding with the HMW, that is therefore not accessible by antibodies at the bacterial surface.

Consequently, a future perspective to obtain cross-specific anti-LMW mAbs would be to use peptides that correspond to the region one wants to generate antibodies against. For instance, it seems that the D2 domain of the LMW plays a central role for various physiological functions of *C. difficile*[38]. Production of conserved peptides of this domain and immunization of mice with a combination of peptides and recombinant LMWs may result in antibodies recognizing a crucial part of the protein, with a cross-specificity for various strains of *C. difficile*. This cross-specificity would be necessary to generate a therapeutic molecule that target different strains of *C. difficile*.

2. Deciphering the role of the S-layer in physiological functions of *C. difficile*

In our study to evaluate anti-LMW mAbs on various physiological functions of *C. difficile* bacterium, one anti-LMW mAb (clone NF10) impaired bacterial growth. We wondered if the effect was similar to the one observed on *Bacillus anthracis* with anti-S-layer nanobodies (Nbs)[339]. In this study, the bacteria could not divide properly when coated with the Nbs. The authors further showed that *de novo* assembly of the S-layer was inhibited by the Nbs, with a full dissolution of the polymers in minutes. In our case, one could speculate that NF10 mAb breaks up the LMW/HMW complexes when they are formed, preventing *C. difficile* bacteria to fill the gaps that form in the S-layer. In line with this hypothesis and *B. anthracis* work, we observed remarkable morphological defects of *C. difficile* in presence of NF10 mAb (unpublished data): bacteria appeared smaller, more aggregated, and less motile (quantification of these parameters are ongoing).

Contrary to the effects of mAb NF10 on *C. difficile*, the mutants generated by Kirk *et al.* that lack the S-layer entirely showed a slight delay upon entry into stationary phase but did not affect growth rate[50]. However, these mutants were extremely hard to generate as they happened at a frequency $< 1 \times 10^{-9}$, mainly indicating that the S-layer is crucial for the viability of the bacteria. For the ones that could be viable, one can wonder whether the selective pressure was so drastic that they had to use alternative pathways and find a way to substitute the function of the S-layer with other components of the membrane. The distinct ribotype (R027) studied by Kirk *et al* is another limitation to find parallels between our two studies.

Bacteria were also more susceptible to stress agents *i.e.* lysozyme and bile salt deoxycholate when coated by NF10 mAb. These results were also found with the mutants lacking the S-layer[50]: they were more susceptible to lysozyme and to anti-microbial peptide LL-37. As shown by Salgado *et al.,* the S-layer of *C. difficile* forms a tight layer around the bacteria, which gain in flexibility when growth and division happen[38]. Coating the bacteria with anti-LMW mAbs during its growth could lead to a disruption of the processes that maintain bacterial integrity, therefore increasing susceptibility to large molecules that could not initially penetrate through it.

We observed that anti-LMW mAbs have opposite effects on toxins' secretion. For 4 mAbs, impact on toxin production had either no effect, decreased toxin secretion by a mechanism that

remains unknown, or increased toxin secretion that we linked to an increase of lysis. Toxins' production happend during stationary growth of the bacteria, with a TcdA:TcdB ratio between 2:1 and 3:1[379,380] and are usually secreted between 16 and 72h of growth[381]. In the host, toxin production occurs after colonization and proliferation of the bacteria. However, how the toxins go through the membrane of the bacteria and consequently what are the interactions with the S-layer to liberate the toxin without lysis of the bacteria remains an open question[38]. Several key players as well as various hypothesis have been proposed. The holin-like (Govind & Dupuy, 2012b)to play a major role[343] but recent work suggested that it is not the only component involved in toxin secretion (unpublished data, Rassemblement *Clostridioides Difficile* France (RCDF) 2023). The existence of an endolysin allowing passage through the cell membrane and peptidoglycan is hypothesized but remains to be identified (unpublished data, RCDF 2023). We hypothesize a mechanism in which anti-LMW mAbs restrain the S-layer, preventing the endolysin to form a passage through the bacterial membrane. Another explanation could be that anti-LMW mAbs via their binding to S-layer interact with some regulation or metabolic pathways involved in toxin secretion. Indeed, production of TcdA and TcdB is not a continuous process and occurs in response to various environmental conditions such as availability of specific nutrients, temperature, cell density, phage infection, presence of antibiotics, some of these processes involving interaction with the S-layer[343,382,383]. More studies are now needed to understand the precise relation of *C. difficile* S-layer and the secretion of toxins.

Coating bacteria with anti-LMW mAbs modify the volume and the structure of the biofilms formed. Increase of biofilm formation has also been observed with mutants lacking Cwp84. Lack of Cwp84 led to an aberrant retention of uncleaved SlpA in the cell wall, which resulted in an altered S-layer[39]. However, increase of biofilm formation was dependent on the ribotype as a Cwp84 mutant in strain R20291 showed reduced biofilm formation[384] whereas in strain 630 this same mutant showed an increase in biofilm formation[299]. The precise role of the S-layer in biofilm formation nonetheless remains to be precisely elucidated. Aggregation of the bacteria is a simple explanation of how biofilms could be modified, and this has been shown with *Lactobacillus helveticus* M92 (*L. helveticus*) as removal of the S-layer produced a decrease in autoaggregation and in coaggregation of *L. helveticus* M92 with *Salmonella Typhimurium FP1*[349]. SLP from aggregative *L. kefiri* strains has been demonstrated to mediate coaggregation with *Saccharomyces lypolitica*[385]. One could speculate that anti-LMW mAbs facilitate *C. difficile* aggregation. Two states of the S-layer can be envisioned: one that would favor

aggregation and the other one bacterium in individual state. These two states would be depending on environmental conditions and in our case, the presence of anti-LMW mAbs. Moreover, we suggest that by promoting bacterial lysis, NF10 mAb facilitates biofilm formation by increasing the amount of extracellular DNA and proteins in the environment. Indeed, extracellular DNA has been demonstrated to be an essential component of the *C. difficile* biofilm matrix, as incubation with DNase I reduced the biomass[386]. Finally, several other proteins are involved in biofilm formation such as flagella or type IV pili[345]. One can speculate that these surface proteins are affected by the presence of antibodies and that steric hindrance impacts their classical role in biofilm formation.

Biofilms formed by bacteria have gained a substantial interest over the years as the models to study and the techniques to visualize them have developed[387]. In this project, two techniques were used to study biofilm formation. While the results were overall reproducible between these two methods, some differences could be noted. The first one performed in microtiter plates followed by staining of the biomass is the most commonly used. This method is versatile and high throughput but nonetheless suffers from a lack of sensitivity and reproducibility[388]. The second method we used was still using microtiter plates, but quantification of the biofilms was done with fluorescent probes. Sensitivity and reproducibility were indeed better with this method. However, both these two methods look at biofilms formed at the bottom of well plates without flow which is far from the reality of the digestive track. A perspective of this part of work would therefore be to study the biofilms in reactors. Several methods have been developed such as the drip flow biofilm reactor[389] or rotary biofilm reactors[388]. These methods overcome the problem of sedimentation in microtiter wells and can better mimic the intestinal flow.

The effects of anti-LMW mAbs on *C. difficile* are summarized in Figure 27.

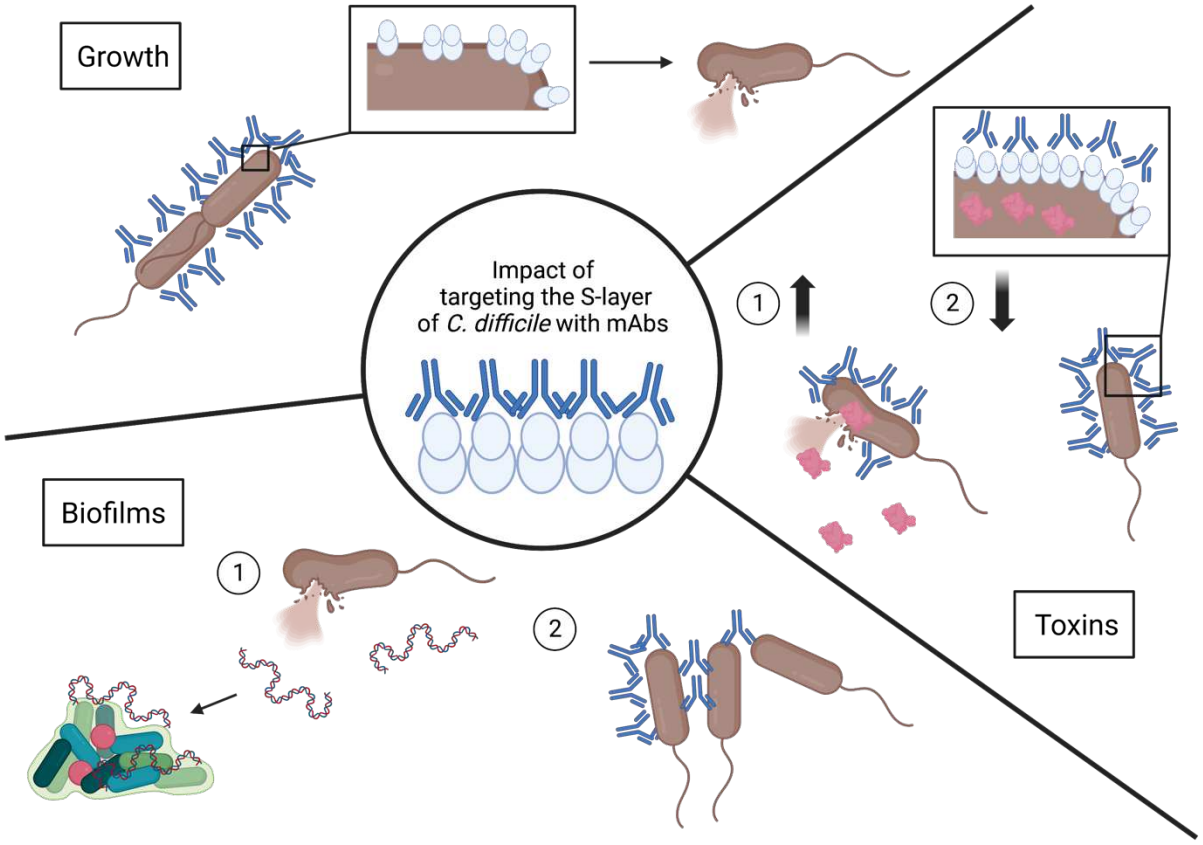

Figure 27. Mechanisms of action of anti-LMW mAbs on: **growth** for which anti-LMW mAbs can impair S-layer reconstruction during division resulting in daughter cell that can lyse more promptly; **toxins** for which an increase can be due to release by lysis and a decrease by inability of the toxins to go through the S-layer because of lack of flexibility imposed by anti-LMW mAbs; **biofilms** in which lysis releases eDNA used for the extracellular matrix to increase biofilm formation or antibody-mediated aggregation can help biofilm formation.

3. From animal to human *ex vivo* models to study CDI

Animal models are central in research to understand physiological processes and recapitulate infections that take place in humans. In the case of CDI, several animal models have been developed to study various aspects such as colonization, disease pathophysiology, intoxication, transmission, recurrence, efficacy testing of potential therapeutics and the impact of strain variability on all these factors[390–392]. A crucial point of these models is that disease pathogenesis observed in infected animals mirror the key pathological features seen in humans. An important factor in animal models for CDI is that -except for axenic mice-, induction of the disease requires pretreatment with antibiotics to induce dysbiosis in the microbiota. We first tested our anti-LMW mAbs in hamsters, which is the gold standard to test new therapeutics for CDI. Indeed, they are very sensitive to the infection. After induction of dysbiosis in their microbiota, *C. difficile* colonize and secrete toxins that kill the animals within two days if no treatment is administered. No protection could however be observed after i.p. injection and gavage with the anti-LMW mAb cocktail we identified (Chapter VII, unpublished data). With this model, toxins are the predominant factors since hamsters are extremely sensitive to them. Therefore, the impact that could have been expected with the mAbs such as a delay in colonization, removal of the bacteria when the microbiota reconstitutes could not be easily evaluated in this fast and acute model. Indeed, one could speculate that if the inflammatory response in response to the toxins has started before the mAbs have a significant effect on the infection, the hamsters will still die no matter the impact of anti-LMW mAbs.

Following these results, we shifted to another animal model based on mice to assess the effect of anti-LMW mAbs on colonization. Axenic mice generally do not develop any symptoms at all and, therefore, serve as an excellent model to study the colonization or parameters linked to colonization[358,393]. No change in colonization could however be seen after i.p. injection and gavage with the anti-LMW mAb cocktail we identified with this model (Chapter VII, unpublished data). Another solution that may be explored is a mouse model with controlled microbiota, such as the OMM12 model that have a defined microbial community composed of 12 different species[359,394]. This model is closer to CDI in humans without adding all the complexity of a conventional rodent microbiota, and could be used to test our anti-LMW mAb cocktail in the future.

Anti-LMW mAbs could also be evaluated in a model of relapsing CDI. Indeed, relapse rate is the readout currently used for novel therapeutics in human CDI. Bezlotoxumab clinical trials were based on relapses as primary endpoint[288]. Indeed, this antibody did not have an impact on the duration of diarrhea. Fidaxomicin efficiency has also been compared to vancomycin in terms of relapses[266]. This readout is coherent with the fact that relapses are the main burden of CDI and made us wonder if we used the most appropriate readout to evaluate our anti-LMW mAbs. CDI mice models have also been developed to assess relapse frequency[395]. Disease relapse in mice resembles the one seen in human in terms of clinical symptoms and is induced by administering an antibiotic cocktail to mice that have recovered from a primary infection followed by another challenge with spores. One limitation of this model is nonetheless that it corresponds more to a reinfection than a real relapse due to *C. difficile* bacteria that would still be present in the microbiota and under certain conditions would cause new symptoms.

Another hypothesis to explain the lack of effect of our anti-LMW mAb cocktail on CDI is that they did not reach the intended place. We looked at the presence of antibodies in the feces of both hamsters and mice, but we were not able to detect free fecal antibodies. We then hypothesized that all the antibodies were bound to bacteria, but again, antibody-coated bacteria were not detected using flow cytometry in feces. One explanation we envisioned was that at least part of the antibodies was degraded or/and their binding ability altered when they were ingested by gavage and went through the stomach and the intestine. Indeed, to treat gastro-intestinal infections, antibodies must reach the right place in the intestine. However, this environment is extremely harsh for molecules, and protein-based targeting reagents are rapidly inactivated in the upper gastrointestinal tract. Hydrocholoric acid in gastric juice denatures proteins and activates pepsin[294]. Therefore, proteins are rapidly denatured and hydrolyzed to peptides following entry to the stomach[396].

The IgG format we used might also not be the most adequate one, as IgA is the most predominant isotype found at the intestine mucosa. IgA plays a crucial role in clearing bacterial infections. Indeed, IgA-mediated cross-linking has been shown to enchain daughter cells of *Salmonella typhimurium* bacteria, therefore preventing their separation after division, and leading to a clumping mechanism that is dependent on growth[397]. During my PhD, IgA1 and IgA2[358] anti-LMW mAbs were attempted to be produced but the yield did not exceed hundreds of micrograms in our hands. IgA are notoriously difficult to produce and glycosylation of IgA pose(RReinhart et al., 2012; Woof & Russell, 2011)Reinhart et al., 2012; Woof & Russell,

2011). We attempted to produce a less glycosylated and stabilized IgA2 version[399] of anti-LMW mAbs but the yield was nor significantly improved. The large dose of mAbs required for the models made us choose IgG as we could obtain tens of milligrams per production, but it was probably an unwise decision. The most appropriate format would have been secretory IgA (sIgA), that would more closely resemble host immunity against *C. difficile* toxins[400].[417] One perspective of this work would be to produce NF10 mAb, which showed an effect on *C. difficile in vitro,* in the sIgA format and to test them *in vivo* in an appropriate model as it has been discussed before.

If sufficient sIgA cannot be produced, other formats can be considered. Indeed, administering therapeutics orally is gaining a major interest. Compared to intravenous injections, orally administered drugs have the potential to reduce side effects for GI diseases. For instance, vancomycin is not absorbed when administered orally and is therefore only active in the intestine -which is ideal for CDI- but side effects such as nephropathies have been linked with intravenous administration of vancomycin when this route is necessary to treat other diseases[401]. To create a successful therapeutic for an intestinal disease, mAbs must be encapsulated into low pH and pepsin-resistant vehicles.(Gbassi & Vandamme, 2012)tarting to develop[402]. Moreover, different formats have been developed to specifically deliver biomolecules in the intestine such as gastrobodies[294]. These scaffolds, by retaining stability at low pH and being protease-resistant, are therefore really promising for the development of intestine-targeted drugs.

Animal models have limitations, and some of these limitations directly impacted our work. It is therefore crucial to develop other *in vitro* or *ex vivo* models that recapitulate closely CDI both to study this infection and to develop new therapeutic molecules. To study *C. difficile* interaction with the host epithelium, several organ-on-chips models have been developed. Such models rely on three-dimensional organoids, which are formed through *ex vivo* cultures of organ cells to mimic the architecture of the source tissue[355]. Alternatively, two-dimensional monolayers can be derived from fragmented 3D organoids and plated onto extracellular matrix-coated wells called transwell plates[403]. These models have been developed to allow extended co-culture of human epithelial cells with oxygen-sensitive bacterial species[404]. The latest enables longer cultures times compared to 3D organoids and can even form villus-like structures. However, its main drawback is the absence of fluid flow and peristalsis-like motion which are two major components of the intestinal environment. This has led to the development of gut-on-chip models that usually contain two channels that represent gut lumen and blood

vessels, separated by a semi-permeable membrane where epithelial cells can be grown[405]. Each channel can be perfused with distinct culture media and the most recent developments enable transluminal hypoxia gradients for the cultures of strict anaerobes such as *C. difficile*[404]. This last gut-on-chip model is the one that we used to monitor adhesion and colonization of *C. difficile in vitro*. Preliminary work using Caco-2 cells showed that *C. difficile* could indeed adhere to the epithelium and divide. Staining with a fluorochrome to track bacteria in real time was established (Unpublished data associated to chapter VII). This work was on hold until an incubator allowing hypoxia was installed. Indeed, *C. difficile* being a strict anaerobe, this condition is required to ensure growth and colonization of the epithelium by the pathogen. The work of Dr. Jazmin Meza-Torres (manuscript in preparation) uses this system to study adherence of *C. difficile* to enterocytes and the role of CDT in this process. Future developments will certainly ameliorate this technology to bring it closer to physiological conditions. These include further developments of the microscopy staining to follow live bacteria and different markers, or inclusion of immune cells below the epithelial layer to recapitulate the host immune response during CDI. Establishment of microbiota in the intestine-on-chip before infecting them with *C. difficile* bacteria is also crucial to recapitulate the complex interactions between this pathogen and the host microbiota. Furthermore, the presence of biofilms may vary depending on the selected source of epithelial cells, despite their crucial role in CDI pathogenesis[346,406]. Hence careful consideration should be given to their presence during the development of more accurate models.

4. On *C. difficile* variability: from the development of a quick ribotyping test for epidemiology to considerations on personalized medicine

The ribotyping test that we developed "Quick-Ribodiff" (manuscript #3), is based on anti-LMW mAbs that are specific of one ribotype among the 5 ribotypes we investigated. Some inter-ribotype variability has been reported previously[321] but we found that the LMW is overall conserved across clinical isolates of the same ribotype and is therefore a promising candidate to distinguish different ribotypes of *C. difficile*. We nonetheless express some concerns for the ribotype R014. Indeed, recognition by anti-LMW mAbs varied drastically between clinical isolates, suggesting higher intra-ribotype variability, at least on the LMW. The main advantage of mAbs is that they can be used in quick and miniaturized detection tests[407]. Here, we took advantage of the high affinity of the anti-LMW mAbs to build a ribotyping test that -*in fine*- could be used by untrained personnel, without any heavy lab equipment, allowing for the implementation of this test worldwide, with a substantial interest for developing countries.

As of now, the proof of concept was obtained for a few ribotypes: 001, 014 and 027. Ribotype 027 has been extensively studied because of its hypervirulence and the increase of cases it provoked in 2003 in the USA. However, if it has spread to France territory, it is now only found in some specific areas such as the North of France. In Paris, this ribotype is rare, and the two most common ribotypes are 001 and 014. For these reasons, we first focused our efforts on these three ribotypes. Of note, we also tested the anti-LMW630 mAbs on the clinical ribotype R012 from which R630 is derived. As discussed in chapter VIII, we did not find any binding of the anti-LMW630 mAbs to the four R012 clinical isolates strains we tested. These results state once again that *C. difficile* strain 630 is a model strain used in research and that it has derived substantially from the infecting R012 strains responsible for current CDIs.

A commercial development of the "Quick-Ribodiff" test could go into two directions, either as a companion test of the other existing diagnostic tests that detect the GDH or the toxins, or as a stand-alone test on a chip containing detection mAbs for dozens of *C. difficile* ribotypes. Quick-Ribodiff test should allow a more precise diagnostic of CDI and potentially enable tailored treatment based on the infecting strain in the future. Quick-Ribodiff could also be used solely for epidemiological surveillance purposes, in humans or animals. In the case of one ribotype being predominant, as it is the case in pigs with ribotype 078, it could be interesting to have a quick ribotyping test that could detect it[186]. Besides, Quick-Ribodiff test could be adapted to various sources of environmental contamination. Bacterial contamination in manures

or food could indeed be traced and monitored with such a test. This could lighten the burden of the *Clostridium* national reference centers that are currently ribotyping for the whole territory. This type of test will not replace the PCR ribotyping currently performed by the national centers but can come as a first-line assay. By detecting the most frequent ribotypes, reference centers might have more time to focus on the rare and atypic ribotypes.

The immunization strategies we developed indeed enable a quick generation of high-affinity anti-LMW mAbs. Similar chips have already been developed to detect multiple bacteria[408], and no technical difficulty is foreseen. The cost of antibody production in the IgG format for the test may be considered a limitation, as it is more costly than the production of small(er) molecules. To anticipate this hurdle, we started to generate VHHs based on the VH sequences of the anti-LMW mAbs. VHHs are produced by prokaryotic cells instead of eukaryotes and therefore their production is more scalable and less expensive. Engineering of VHHs allow rounds of selection to improve affinity, but it is not guaranteed that detection of the LMWs can be solely performed by a VHH based on a VH region without the contribution of its cognate VL region.

One major limitation of our work is that we produced anti-LMW mAbs targeting "only" 5 ribotypes that account for 60% of CDI. As a result, some strains of *C. difficile* will not be detected with these first mAbs, leading to the question of how many ribotypes an epidemiological test should be able to detect. Should additional mAbs detecting additional ribotypes be generated and included in the test?

Generation of a cross-specific mAb that could recognize various strains of *C. difficile* was not highly successful as only a maximum of two ribotypes could be recognized by anti-LMW mAbs. This lack of cross-specificity renders difficult to imagine anti-LMW mAb as a new treatment for CDI as their production cost is much higher than the one of antibiotics. Without a substantial benefit for the patient by using anti-bacterial mAbs, antibiotics will continue to be used as a first line of treatment. Nonetheless, since certain *C. difficile* strains are associated with increased severity, relapses and resistance, it could be interesting to explore new treatments as monoclonal antibodies for such strains. The high specificity of mAbs and development of various engineering and coupling techniques allows them to be exploited to deliver small molecules such as antimicrobial peptides at a precise site. For instance, antibody-drug conjugates containing an anti-neoplastic drug mitomycin C was used to treat bacterial biofilms of *Staphylococcus aureus* formed on implant[409]. One can therefore imagine that the high

specificity and affinity of these anti-LMW mAbs could be exploited via the engineering of antibody-drug conjugates.

Finally, in the case of CDI, the microbiota plays a crucial role in fighting against this infection, as it has been shown by the remarkably efficient results of fecal microbiota transplantation[277,305]. Personalized medicine is based on the fact that each individual possesses nuanced and unique characteristics at the molecular, physiological and behavioral levels[304]. Consequently, treating an individual with a disease, as well as monitoring or preventing the disease should be tailored or 'personalized' to that individual. In the case of CDI, the unique characteristic of an individual is all the truer when considering its microbiota, that is shaped with unique parameters. New treatments that take advantage of each person's microbiota could be developed for CDI. The two microbiome therapies that have been approved over the past two years go in that direction[281,282]. Moreover, antibiotic resistance is another increasing problem. Phage-therapy could be part of the solution but as of now, phages targeting *C. difficile* proved to be ribotype specific[51]. This type of treatment might therefore be of interest in the concept of personalized medicine in which the strain a patient is infected with is known, along with its unique genetic and environmental characteristics.

Conclusion

In this work, we have generated the first collection of mAbs that recognize the LMW SlpA, a protein that is expressed at the surface of *C. difficile* bacteria. These anti-LMW mAbs recognize several clinical ribotypes of *C. difficile*, as well as the model strain used in research *C. difficile* 630. This mAb collection harbors different cross-specific profiles. Their affinities for the protein were precisely determined, as well as their binding to whole bacteria. These mAbs are of interest as research tools to detect different strains of *C. difficile*, and can be used in ELISA, flow cytometry, microscopy, and histology assay. Particularly, these mAbs could detect *C. difficile* in a complex human microbiota using flow cytometry.

These anti-LMW mAbs were then used to decipher the role of the S-layer in various physiological processes of the bacteria such as the growth, susceptibility to stress agents, toxin secretion, and biofilm formation. We showed that some anti-LMW mAbs can impair bacterial growth and increase sensitivity to lysozyme. Impaired growth in presence of anti-LMW mAb NF10 was accentuated in the presence of the bile acid DCA, that is known to be a stress agent for *C. difficile*. Toxin secretion in presence of some anti-LMW mAbs was found to be either increased or decreased depending on the mAb. Anti-LMW mAb NF10, that impaired *C. difficile* growth, increased toxin secretion, an effect that was related to increased lysis of the bacteria. Two other mAbs (KH2 and TG10), that did not have an impact on growth, inhibited toxin secretion. The mechanisms behind this inhibition remain to be elucidated. Biofilm formation and structure were modified in presence of anti-LMW mAbs, as biovolume, thickness and roughness were increased for anti-LMW mAbs NF10 and 2B7. Altogether, this part of my PhD work provides indirect but important insights on the role of S-layer in *C. difficile* fitness. These results also reveal the ambivalent effects of anti-S-layer antibodies, questioning the S-layer directed therapeutic approaches. Precise determination of the epitopes that are recognized by these anti-LMW mAbs could deepen this work and lead to the generation of antibodies targeting a precise site of the S-layer crucial for the bacteria and beneficial to treat CDI.

We also took advantage of the anti-LMW mAbs collection to develop a rapid identification test "Quick-Ribodif" for diagnostic and epidemiological monitoring purposes. We specifically detected *C. difficile* from the most frequent clinical ribotypes among a complex human microbiota. Feces of *C. difficile* infected patients are being collected by our clinical

collaborators, and detection of the *C. difficile* ribotype(s) using the Quick-Ribodif test will soon be performed.

Other parts of my work investigated the adhesion of *C. difficile* to enterocytes in presence of anti-LMW mAbs. No clear effect on the adhesion could be seen in two different *in vitro* models, questioning the role of the S-layer in adhesion to cells that secrete mucus, as well as the ability of anti-LMW mAb to inhibit the interaction between bacteria and host cell. No survival was seen in a hamster lethal model of *C. difficile* infection following mAb administration and no delay of colonization was observed in a model using axenic mice, but questions remain regarding the ability of anti-LMW mAbs to actually reach and bind *C. difficile* in the colon of these animals in the administration mode and mAb format we chose.

References

1. Hall, I. C. & O'Toole Elizabeth. Intestinal flora in new-born infatns: with a description of a new pathogenic anaerobe, bacillus difficilis. *American Journal of Diseases of Children* **49**, 390–402 (1935).
2. Silhavy, T. J., Kahne, D. & Walker, S. The bacterial cell envelope. *Cold Spring Harbor perspectives in biology* vol. 2 Preprint at https://doi.org/10.1101/cshperspect.a000414 (2010).
3. Martínez-Meléndez, A., Cruz-López, F., Morfin-Otero, R., Maldonado-Garza, H. J. & Garza-González, E. An Update on Clostridioides difficile Binary Toxin. *Toxins (Basel)* **14**, 305 (2022).
4. CDC. *Emerging Infections Program Healthcare-Associated Infections-Community Interface Report: Clostridioides difficile infection, 2019 Surveillance Catchment Areas Case Definition*. https://www.cdc.gov/hai/eip/Annual-CDI-Report-2019.html.
5. Cohen, S. H. *et al.* Clinical Practice Guidelines for Clostridium difficile Infection in Adults: 2010 Update by the Society for Healthcare Epidemiology of America (SHEA) and the Infectious Diseases Society of America (IDSA). *Infect Control Hosp Epidemiol* **31**, 431–455 (2010).
6. Bishop, E. J. & Tiruvoipati, R. Management of Clostridioides difficile infection in adults and challenges in clinical practice: review and comparison of current IDSA/SHEA, ESCMID and ASID guidelines. *The Journal of antimicrobial chemotherapy* vol. 78 21–30 Preprint at https://doi.org/10.1093/jac/dkac404 (2022).
7. Kelly, C. P. & LaMont, J. T. Clostridium difficile — More Difficult Than Ever . *New England Journal of Medicine* **359**, 1932–1940 (2008).
8. Krutova, M. *et al.* How to: Surveillance of Clostridium difficile infections. *Clinical Microbiology and Infection* vol. 24 469–475 Preprint at https://doi.org/10.1016/j.cmi.2017.12.008 (2018).
9. Gerding, D. N., Johnson, S., Peterson, L. R., Mulligan, M. E. & Silva, J. Clostridium Difficile-Associated Diarrhea and Colitis. *Infect Control Hosp Epidemiol* **16**, 459–477 (1995).
10. Heeg, D., Burns, D. A., Cartman, S. T. & Minton, N. P. Spores of Clostridium difficile Clinical Isolates Display a Diverse Germination Response to Bile Salts. *PLoS One* **7**, e32381- (2012).
11. Kuehne, S. A. *et al.* The role of toxin A and toxin B in Clostridium difficile infection. *Nature* **467**, 711–713 (2010).
12. Howerton, A., Ramirez, N. & Abel-Santos, E. Mapping interactions between germinants and Clostridium difficile spores. *J Bacteriol* **193**, 274–282 (2011).
13. Kang, J. D. *et al.* Bile Acid 7α-Dehydroxylating Gut Bacteria Secrete Antibiotics that Inhibit Clostridium difficile: Role of Secondary Bile Acids. *Cell Chem Biol* **26**, 27-34.e4 (2019).
14. Sorg, J. A. & Sonenshein, A. L. Bile Salts and Glycine as Cogerminants for *Clostridium difficile* Spores. *J Bacteriol* **190**, 2505–2512 (2008).
15. Winston, J. A. & Theriot, C. M. Impact of microbial derived secondary bile acids on colonization resistance against Clostridium difficile in the gastrointestinal tract. *Anaerobe* **41**, 44–50 (2016).
16. Cho, I. & Blaser, M. J. The human microbiome: At the interface of health and disease. *Nature Reviews Genetics* vol. 13 260–270 Preprint at https://doi.org/10.1038/nrg3182 (2012).

17. Walter, J. & Ley, R. The Human Gut Microbiome: Ecology and Recent Evolutionary Changes. *Annu Rev Microbiol* **65**, 411–429 (2011).
18. Nord, C. E., Kager, L. & Anders, H. *Impact of Antimicrobial Agents on the Gastrointestinal Microflora and the Risk of Infections*.
19. Chang, J. Y. *et al.* Decreased Diversity of the Fecal Microbiome in Recurrent Clostridium difficile—Associated Diarrhea. *J Infect Dis* **197**, 435–438 (2008).
20. Ridlon, J. M., Kang, D. J., Hylemon, P. B. & Bajaj, J. S. Bile acids and the gut microbiome. *Curr Opin Gastroenterol* **30**, 332–338 (2014).
21. Gerbino, E., Carasi, P., Mobili, P., Serradell, M. A. & Gómez-Zavaglia, A. Role of S-layer proteins in bacteria. *World Journal of Microbiology and Biotechnology* vol. 31 1877–1887 Preprint at https://doi.org/10.1007/s11274-015-1952-9 (2015).
22. Brouwer, M. S. M. *et al.* Horizontal gene transfer converts non-toxigenic Clostridium difficile strains into toxin producers. *Nat Commun* **4**, 2601 (2013).
23. Jank, T. & Aktories, K. Structure and mode of action of clostridial glucosylating toxins: the ABCD model. *Trends Microbiol* **16**, 222–229 (2008).
24. Stiles, B., Wigelsworth, D., Popoff, M. & Barth, H. Clostridial Binary Toxins: Iota and C2 Family Portraits. *Front Cell Infect Microbiol* **1**, (2011).
25. Di Bella, S., Ascenzi, P., Siarakas, S., Petrosillo, N. & di Masi, A. Clostridium difficile toxins A and B: Insights into pathogenic properties and extraintestinal effects. *Toxins* vol. 8 Preprint at https://doi.org/10.3390/toxins8050134 (2016).
26. Aktories, K., Papatheodorou, P. & Schwan, C. Binary Clostridium difficile toxin (CDT) - A virulence factor disturbing the cytoskeleton. *Anaerobe* **53**, 21–29 (2018).
27. Roberts, A. P. & Mullany, P. *Clostridium dii cile Methods and Protocols Second Edition Methods in Molecular Biology 1476*. http://www.springer.com/series/7651.
28. Merrigan, M. M. *et al.* Surface-Layer Protein A (SlpA) is a major contributor to host-cell adherence of clostridium difficile. *PLoS One* **8**, (2013).
29. Messner, P., Steiner, K., Zarschler, K. & Schäffer, C. S-layer nanoglycobiology of bacteria. *Carbohydrate Research* vol. 343 1934–1951 Preprint at https://doi.org/10.1016/j.carres.2007.12.025 (2008).
30. Houwink, A. L. & Le Poole, J. B. . *Physikalische Verhandlungen* **3**, (1952).
31. Sleytr, U. B., Sa´ra, M., Pum, D., Schuster, B. & Messner, P. Polyamides and Complex Proteinaceous Matrices I. *Biopolymers* **7**, 285–338 (2002).
32. Pum, D., Breitwieser, A. & Sleytr, U. B. Patterns in nature—S-layer lattices of bacterial and archaeal cells. *Crystals* vol. 11 Preprint at https://doi.org/10.3390/cryst11080869 (2021).
33. Schäffer, C. & Messner, P. *Glycobiology of surface layer proteins*. (2001).
34. Kawata, T., Takeoka, A., Takumi, K. & Masuda, K. Demonstration and preliminary characterization of a regular array in the cell wall of Clostridium difficile. *FEMS Microbiol Lett* **24**, 323–328 (1984).
35. Calabi, E. *et al. Molecular characterization of the surface layer proteins from Clostridium difficile*. *Molecular Microbiology* (2001).
36. Takeoka A, Takumi K, Koga T & Kawata T. Purification and characterization of S layer proteins from Clostridium difficile. *Gen Microbiol.* **137**, 261–267 (1991).
37. Fagan, R. P. *et al.* Structural insights into the molecular organization of the S-layer from Clostridium difficile. *Mol Microbiol* **71**, 1308–1322 (2009).
38. Lanzoni-Mangutchi, P. *et al.* Structure and assembly of the S-layer in C. difficile. *Nat Commun* **13**, (2022).
39. Kirby, J. M. *et al.* Cwp84, a Surface-associated Cysteine Protease, Plays a Role in the Maturation of the Surface Layer of Clostridium difficile. *Journal of Biological Chemistry* **284**, 34666–34673 (2009).

40. Oatley, P., Kirk, J. A., Ma, S., Jones, S. & Fagan, R. P. Spatial organization of Clostridium difficile S-layer biogenesis. *Sci Rep* **10**, (2020).
41. Lawley, T. D. *et al.* Proteomic and genomic characterization of highly infectious Clostridium difficile 630 spores. *J Bacteriol* **191**, 5377–5386 (2009).
42. Pantosti, A., Cerquetti, M., Viti, F., Ortisi, G. & Mastrantonio, P. Immunoblot analysis of serum immunoglobulin G response to surface proteins of Clostridium difficile in patients with antibiotic-associated diarrhea. *J Clin Microbiol* **27**, 2594–2597 (1989).
43. Bruxelle, J. F. *et al.* Immunogenic properties of the surface layer precursor of Clostridium difficile and vaccination assays in animal models. *Anaerobe* **37**, 78–84 (2016).
44. Mizrahi, A., Bruxelle, J. F., Péchiné, S. & Le Monnier, A. Prospective evaluation of the adaptive immune response to SlpA in Clostridium difficile infection. *Anaerobe* **54**, 164–168 (2018).
45. Emanuela, C., Franco, C., D, P. A. & F, F. N. Binding of Clostridium difficile Surface Layer Proteins to Gastrointestinal Tissues. *Infect Immun* **70**, 5770–5778 (2002).
46. DiRita, V. J. *et al.* Role of FliC and FliD Flagellar Proteins of Clostridium difficile in Adherence and Gut Colonization. *Infect Immun* **69**, 7937–7940 (2001).
47. Hennequin, C., Janoir, C., Barc, M. C., Collignon, A. & Karjalainen, T. Identification and characterization of a fibronectin-binding protein from Clostridium difficile. *Microbiology (N Y)* **149**, 2779–2787 (2003).
48. Ternan, N. G., Jain, S., Srivastava, M. & McMullan, G. Comparative Transcriptional Analysis of Clinically Relevant Heat Stress Response in Clostridium difficile Strain 630. *PLoS One* **7**, e42410- (2012).
49. Waligora, A. J. *et al.* Characterization of a cell surface protein of Clostridium difficile with adhesive properties. *Infect Immun* **69**, 2144–2153 (2001).
50. Kirk, J. A. *et al.* New class of precision antimicrobials redefines role of Clostridium difficile S-layer in virulence and viability. *Sci Transl Med* **9**, (2017).
51. Royer, A. L. M. *et al.* Clostridioides difficile S-Layer Protein A (SlpA) Serves as a General Phage Receptor. *Microbiol Spectr* (2023) doi:10.1128/spectrum.03894-22.
52. Kyne, L., Sougioultzis, S., McFarland, L. V & Kelly, C. P. Underlying Disease Severity as a Major Risk Factor for Nosocomial Clostridium difficile Diarrhea. *Infect Control Hosp Epidemiol* **23**, 653–659 (2002).
53. Johnson, S. Recurrent Clostridium difficile infection: A review of risk factors, treatments, and outcomes. *Journal of Infection* vol. 58 403–410 Preprint at https://doi.org/10.1016/j.jinf.2009.03.010 (2009).
54. Schutze, G. E. *et al. Clostridium difficile* Infection in Infants and Children. *Pediatrics* **131**, 196–200 (2013).
55. Slimings, C. & Riley, T. V. Antibiotics and hospital-acquired Clostridium difficile infection: update of systematic review and meta-analysis. *J Antimicrob Chemother* **69**, 881–91 (2014).
56. Furuya-Kanamori, L. *et al.* Comorbidities, Exposure to Medications, and the Risk of Community-Acquired Clostridium difficile Infection: a systematic review and meta-analysis. *Infect Control Hosp Epidemiol* **36**, 132–41 (2015).
57. Leonard, J., Marshall, J. K. & Moayyedi, P. Systematic review of the risk of enteric infection in patients taking acid suppression. *Am J Gastroenterol* **102**, 2047–56; quiz 2057 (2007).
58. Kwok, C. S. *et al.* Risk of Clostridium difficile infection with acid suppressing drugs and antibiotics: meta-analysis. *Am J Gastroenterol* **107**, 1011–9 (2012).

59. Deshpande, A. *et al.* Risk factors for recurrent Clostridium difficile infection: a systematic review and meta-analysis. *Infect Control Hosp Epidemiol* **36**, 452–60 (2015).
60. Lübbert, C. *et al.* Immunsuppressive Behandlung als Risikofaktor für das Auftreten einer Clostridium-difficile-Infektion (CDI). *Z Gastroenterol* **51**, 1251–1258 (2013).
61. Negrut, N. *et al.* Risk Factors Associated with Recurrent Clostridioides difficile Infection. *Healthcare* **8**, 352 (2020).
62. McFarland LV, Elmer GW & Surawicz CM. Breaking the cycle: treatment strategies for 163 cases of recurrent Clostridium difficile disease. *Am J Gastroenterol* **97**, 1768–75 (2002).
63. Song, J. H. & Kim, Y. S. Recurrent Clostridium difficile Infection: Risk Factors, Treatment, and Prevention. *Gut Liver* **13**, 16–24 (2019).
64. *Recurrences of Clostridium difficile Diarrhea Not Caused by the Original Infecting Organism*. https://academic.oup.com/jid/article/159/2/340/902560.
65. Eyre, D. W. *et al.* Whole-Genome Sequencing Demonstrates That Fidaxomicin Is Superior to Vancomycin for Preventing Reinfection and Relapse of Infection With Clostridium difficile. *J Infect Dis* **209**, 1446–1451 (2014).
66. Castro-Córdova, P. *et al.* Entry of spores into intestinal epithelial cells contributes to recurrence of Clostridioides difficile infection. *Nat Commun* **12**, (2021).
67. Deakin, L. J. *et al.* The Clostridium difficile spo0A gene is a persistence and transmission factor. *Infect Immun* **80**, 2704–2711 (2012).
68. Dubois, T. *et al.* A microbiota-generated bile salt induces biofilm formation in Clostridium difficile. *NPJ Biofilms Microbiomes* **5**, (2019).
69. Crowther, G. S. *et al.* Development and validation of a chemostat gut model to study both planktonic and biofilm modes of growth of Clostridium difficile and human microbiota. *PLoS One* **9**, (2014).
70. Buckley, A. M., Spencer, J., Candlish, D., Irvine, J. J. & Douce, G. R. Infection of hamsters with the UK clostridium difficile ribotype 027 outbreak strain R20291. *J Med Microbiol* **60**, 1174–1180 (2011).
71. Soavelomandroso, A. P. *et al.* Biofilm structures in a mono-associated mouse model of Clostridium difficile infection. *Front Microbiol* **8**, (2017).
72. Meza-Torres, J., Auria, E., Dupuy, B. & Tremblay, Y. D. N. Wolf in sheep's clothing: Clostridioides difficile biofilm as a reservoir for recurrent infections. *Microorganisms* vol. 9 Preprint at https://doi.org/10.3390/microorganisms9091922 (2021).
73. Sansonetti, P. J. War and peace at mucosal surfaces. *Nature Reviews Immunology* vol. 4 953–964 Preprint at https://doi.org/10.1038/nri1499 (2004).
74. Péchiné, S. & Collignon, A. Immune responses induced by Clostridium difficile. *Anaerobe* **41**, 68–78 (2016).
75. Vohra, P. & Poxton, I. R. Induction of cytokines in a macrophage cell line by proteins of *Clostridium difficile*. *FEMS Immunol Med Microbiol* **65**, 96–104 (2012).
76. Rumbo, M., Nempont, C., Kraehenbuhl, J. P. & Sirard, J. C. Mucosal interplay among commensal and pathogenic bacteria: Lessons from flagellin and Toll-like receptor 5. *FEBS Letters* vol. 580 2976–2984 Preprint at https://doi.org/10.1016/j.febslet.2006.04.036 (2006).
77. Yoshino, Y. *et al.* Clostridium difficile flagellin stimulates toll-like receptor 5, and toxin B promotes flagellin-induced chemokine production via TLR5. *Life Sci* **92**, 211–217 (2013).
78. Batah, J. *et al.* Clostridium difficile flagella predominantly activate TLR5-linked NF-κB pathway in epithelial cells. *Anaerobe* **38**, 116–124 (2016).

79. Yu, H. *et al.* Cytokines Are Markers of the Clostridium difficile-Induced Inflammatory Response and Predict Disease Severity. *Clinical and Vaccine Immunology* **24**, (2017).
80. Kim, J. M. *et al.* Differential Expression and Polarized Secretion of CXC and CC Chemokines by Human Intestinal Epithelial Cancer Cell Lines in Response to *Clostridium difficile* Toxin A. *Microbiol Immunol* **46**, 333–342 (2002).
81. Gotshal, D., Azrad, M., Hamo, Z., Nitzan, O. & Peretz, A. IL-16 and BCA-1 Serum Levels Are Associated with Disease Severity of C. difficile Infection. *Pathogens* **10**, 631 (2021).
82. Wu, X., Lai, X., Tu, H., Zou, H. & Cao, J. Elevated serum CXCL10 in patients with Clostridium difficile infection are associated with disease severity. *Int Immunopharmacol* **72**, 92–97 (2019).
83. Wang, L., Cao, J., Li, C. & Zhang, L. Chemokine CXCL13 expression was up-regulated in Clostridium difficile infection. *Cytokine* **88**, 232–240 (2016).
84. Wershil, B. K., Castagliuolo, I. & Pothoulakis, C. Direct evidence of mast cell involvement in Clostridium difficile toxin a—induced enteritis in mice☆☆☆. *Gastroenterology* **114**, 956–964 (1998).
85. El Feghaly, R. E. *et al.* Markers of intestinal inflammation, not bacterial burden, correlate with clinical outcomes in clostridium difficile infection. *Clinical Infectious Diseases* **56**, 1713–1721 (2013).
86. Geiger, T. L. *et al.* Nfil3 is crucial for development of innate lymphoid cells and host protection against intestinal pathogens. *Journal of Experimental Medicine* **211**, 1723–1731 (2014).
87. Abt, M. C. *et al.* Innate Immune Defenses Mediated by Two ILC Subsets Are Critical for Protection against Acute Clostridium difficile Infection. *Cell Host Microbe* **18**, 27–37 (2015).
88. Ryan, A. *et al.* A Role for TLR4 in Clostridium difficile Infection and the Recognition of Surface Layer Proteins. *PLoS Pathog* **7**, e1002076- (2011).
89. Ausiello, C. M. *et al.* Surface layer proteins from Clostridium difficile induce inflammatory and regulatory cytokines in human monocytes and dendritic cells. *Microbes Infect* **8**, 2640–2646 (2006).
90. Lowenthal, A., Sande, M. Van & Karcher, D. THE DIFFERENTIAL DIAGNOSIS OF NEUROLOGICAL DISEASES BY FRACTIONATING ELECTRO-PHORETICALLY THE CSF ?-GLOBULINS. *J Neurochem* **6**, 51–56 (1960).
91. Swain, S. L. T Cell Subsets and the Recognition of MHC Class. *Immunol Rev* **74**, 129–142 (1983).
92. KISIELOW, P. *et al.* Ly antigens as markers for functionally distinct subpopulations of thymus-derived lymphocytes of the mouse. *Nature* **253**, 219–220 (1975).
93. Shiku, H. *et al.* Expression of T-cell differentiation antigens on effector cells in cell-mediated cytotoxicity in vitro. Evidence for functional heterogeneity related to the surface phenotype of T cells. *Journal of Experimental Medicine* **141**, 227–241 (1975).
94. Cantor, H. & Boyse, E. A. Functional subclasses of T-lymphocytes bearing different Ly antigens. I. The generation of functionally distinct T-cell subclasses is a differentiative process independent of antigen. *Journal of Experimental Medicine* **141**, 1376–1389 (1975).
95. Ehrlich, P. Nobel Lecture, December 11, 1908. *Elsevier* 1901–1921 (1967).
96. von Behring, E. & Kitasato, S. Ueber das zutandekommen der diphtherie-immunitat und der tetanus-immunitat bei thieren. *Deutsche Medizinsche Wochenschrift* **16**, 1113–114 (1890).

97. Tiselius, A. & Kabat, E. A. AN ELECTROPHORETIC STUDY OF IMMUNE SERA AND PURIFIED ANTIBODY PREPARATIONS. *Journal of Experimental Medicine* **69**, 119–131 (1939).
98. FLEISCHMAN, J., PORTER, R. & PRESS, E. THE ARRANGEMENT OF THE PEPTIDE CHAINS IN γ-GLOBULIN. *Biochemical Journal* **88**, 220–228 (1963).
99. Antibody. *Britannica* (2023).
100. Porter, R. R. The hydrolysis of rabbit γ-globulin and antibodies with crystalline papain. *Biochemical Journal* **73**, 119–127 (1959).
101. Edelman, G. M. & Poulik, M. D. STUDIES ON STRUCTURAL UNITS OF THE γ-GLOBULINS. *Journal of Experimental Medicine* **113**, 861–884 (1961).
102. Dreyer, W. J. & Bennett, J. C. The molecular basis of antibody formation: a paradox. *Proceedings of the National Academy of Sciences* **54**, 864–869 (1965).
103. Edelman, G. M. *et al.* THE COVALENT STRUCTURE OF AN ENTIRE γG IMMUNOGLOBULIN MOLECULE. *Proceedings of the National Academy of Sciences* **63**, 78–85 (1969).
104. HOOD, L. & EIN, D. Immunoglobulin Lambda Chain Structure: Two Genes, One Polypeptide Chain. *Nature* **220**, 764–767 (1968).
105. Delves PJ, M. S. B. D. R. I. *Roitt's essential immunology*. (2017).
106. Janeway CA Jr, T. P. W. M. et al. *Immunobiology: The Immune System in Health and Disease.* (2001).
107. Woof, J. M. & Russell, M. W. Structure and function relationships in IgA. *Mucosal Immunol* **4**, 590–597 (2011).
108. Rowe, D. S. & Fahey, J. L. A NEW CLASS OF HUMAN IMMUNOGLOBULINS. *Journal of Experimental Medicine* **121**, 185–199 (1965).
109. Heremans, J. F., Heremans, M.-Th. & Schultze, H. E. Isolation and description of a few properties of the β2A-globulin of human serum. *Clinica Chimica Acta* **4**, 96–102 (1959).
110. Ishizaka, K., Ishizaka, T. & Hornbrook, M. M. Physicochemical properties of reaginic antibody. V. Correlation of reaginic activity wth gamma-E-globulin antibody. *J Immunol* **97**, 840–53 (1966).
111. Cruse MD PhD, J. M. & Lewis, R. E. *Atlas of Immunology*. (CRC Press, 2010). doi:10.1201/EBK1439802687.
112. Tomasi, T. B., Tan, E. M., Solomon, A. & Prendergast, R. A. CHARACTERISTICS OF AN IMMUNE SYSTEM COMMON TO CERTAIN EXTERNAL SECRETIONS. *Journal of Experimental Medicine* **121**, 101–124 (1965).
113. Toraño, A., Tsuzukida, Y., Liu, Y. S. & Putnam, F. W. Location and structural significance of the oligosaccharides in human Ig-A1 and IgA2 immunoglobulins. *Proceedings of the National Academy of Sciences* **74**, 2301–2305 (1977).
114. Bonner, A., Almogren, A., Furtado, P. B., Kerr, M. A. & Perkins, S. J. The Nonplanar Secretory IgA2 and Near Planar Secretory IgA1 Solution Structures Rationalize Their Different Mucosal Immune Responses. *Journal of Biological Chemistry* **284**, 5077–5087 (2009).
115. Mistry, D. & Stockley, R. A. IgA1 protease. *Int J Biochem Cell Biol* **38**, 1244–1248 (2006).
116. Jonard, P. P. *et al.* Secretion of immunoglobulins and plasma proteins from the jejunal mucosa. Transport rate and origin of polymeric immunoglobulin A. *Journal of Clinical Investigation* **74**, 525–535 (1984).
117. Berth, M., Delanghe, J., Langlois, M. & De Buyzere, M. Reference values of serum IgA subclasses in caucasian adults by immunonephelometry. *Clin Chem* **45**, 309–10 (1999).

118. Pakkanen, S. H. *et al.* Expression of Homing Receptors on IgA1 and IgA2 Plasmablasts in Blood Reflects Differential Distribution of IgA1 and IgA2 in Various Body Fluids. *Clinical and Vaccine Immunology* **17**, 393–401 (2010).
119. Chiba, M., Ohta, H., Yagisawa, H. & Masamune, O. IgA1 & IgA2 distribution in the intestine. *Gastroenterol Jpn* **22**, 18–23 (1987).
120. Ladjeva, I., Peterman, J. H. & Mestecky, J. IgA subclasses of human colostral antibodies specific for microbial and food antigens. *Clin Exp Immunol* **78**, 85–90 (1989).
121. HALPERN, M. S. & KOSHLAND, M. E. Novel Subunit in Secretory IgA. *Nature* **228**, 1276–1278 (1970).
122. Krugmann, S., Pleass, R. J., Atkin, J. D. & Woof, J. M. Structural requirements for assembly of dimeric IgA probed by site-directed mutagenesis of J chain and a cysteine residue of the alpha-chain CH2 domain. *J Immunol* **159**, 244–9 (1997).
123. Mora, J. R. *et al.* Generation of Gut-Homing IgA-Secreting B Cells by Intestinal Dendritic Cells. *Science (1979)* **314**, 1157–1160 (2006).
124. Lemke, A. *et al.* Long-lived plasma cells are generated in mucosal immune responses and contribute to the bone marrow plasma cell pool in mice. *Mucosal Immunol* **9**, 83–97 (2016).
125. Duc, M., Johansen, F.-E. & Corthésy, B. Antigen Binding to Secretory Immunoglobulin A Results in Decreased Sensitivity to Intestinal Proteases and Increased Binding to Cellular Fc Receptors. *Journal of Biological Chemistry* **285**, 953–960 (2010).
126. Crottet, P. & Corthésy, B. Secretory component delays the conversion of secretory IgA into antigen-binding competent F(ab')2: a possible implication for mucosal defense. *J Immunol* **161**, 5445–53 (1998).
127. Newcomb, R. W., Normansell, D. & Stanworth, D. R. A Structural Study of Human Exocrine IgA Globulin. *The Journal of Immunology* **101**, 905–914 (1968).
128. Stadtmueller, B. M. *et al.* The structure and dynamics of secretory component and its interactions with polymeric immunoglobulins. *Elife* **5**, (2016).
129. Brandtzaeg, P. The Mucosal Immune System and Its Integration with the Mammary Glands. *J Pediatr* **156**, S8–S15 (2010).
130. Brandtzaeg, P. Secretory IgA: Designed for Anti-Microbial Defense. *Front Immunol* **4**, (2013).
131. Yoshida, M. *et al.* Human Neonatal Fc Receptor Mediates Transport of IgG into Luminal Secretions for Delivery of Antigens to Mucosal Dendritic Cells. *Immunity* **20**, 769–783 (2004).
132. Roopenian, D. C. & Akilesh, S. FcRn: the neonatal Fc receptor comes of age. *Nat Rev Immunol* **7**, 715–725 (2007).
133. Rosekrans, P. C., Meijer, C. J., van der Wal, A. M., Cornelisse, C. J. & Lindeman, J. Immunoglobulin containing cells in inflammatory bowel disease of the colon: a morphometric and immunohistochemical study. *Gut* **21**, 941–947 (1980).
134. Fanning, L. J., Connor, A. M. & Wu, G. E. Development of the Immunoglobulin Repertoire. *Clin Immunol Immunopathol* **79**, 1–14 (1996).
135. Hozumi, N. & Tonegawa, S. Evidence for somatic rearrangement of immunoglobulin genes coding for variable and constant regions. *Proceedings of the National Academy of Sciences* **73**, 3628–3632 (1976).
136. Nemazee, D. Receptor editing in lymphocyte development and central tolerance. *Nat Rev Immunol* **6**, 728–740 (2006).
137. Briney, B., Inderbitzin, A., Joyce, C. & Burton, D. R. Commonality despite exceptional diversity in the baseline human antibody repertoire. *Nature* **566**, 393–397 (2019).

138. Market, E. & Papavasiliou, F. N. V(D)J Recombination and the Evolution of the Adaptive Immune System. *PLoS Biol* **1**, e16 (2003).
139. Teng, G. & Papavasiliou, F. N. Immunoglobulin somatic hypermutation. *Annu Rev Genet* **41**, 107–20 (2007).
140. Chi, X., Li, Y. & Qiu, X. V(D)J recombination, somatic hypermutation and class switch recombination of immunoglobulins: mechanism and regulation. *Immunology* **160**, 233–247 (2020).
141. Stavnezer, J. Immunoglobulin class switching. *Curr Opin Immunol* **8**, 199–205 (1996).
142. Viscidi, R. *et al.* Serum Antibody Response to Toxins A and B of Clostridium difficile. *Journal of Infectious Diseases* **148**, 93–100 (1983).
143. Kelly, C. P., Pothoulakis, C., Orellana, J. & Lamont, J. T. *Human Colonic Aspirates Containing Immunoglobulin A Antibody to Clostridium dificile Toxin A Inhibit Toxin A-Receptor Binding*.
144. Eglow, R. *et al.* Diminished Clostridium difficile toxin A sensitivity in newborn rabbit ileum is associated with decreased toxin A receptor. *Journal of Clinical Investigation* **90**, 822–829 (1992).
145. Al-Jumaili, I. J., Shibley, M., Lishman, A. H. & Record, C. O. Incidence and origin of Clostridium difficile in neonates. *J Clin Microbiol* **19**, 77–78 (1984).
146. Shim, J. O. *Clostridium difficile* in Children: To Treat or Not to Treat? *Pediatr Gastroenterol Hepatol Nutr* **17**, 80 (2014).
147. Kyne, L., Warny, M., Qamar, A. & Kelly, C. P. Association between antibody response to toxin A and protection against recurrent Clostridium difficile diarrhoea. *The Lancet* **357**, 189–193 (2001).
148. Secore, S. *et al.* Development of a Novel Vaccine Containing Binary Toxin for the Prevention of Clostridium difficile Disease with Enhanced Efficacy against NAP1 Strains. *PLoS One* **12**, e0170640 (2017).
149. Johal, S. S. *et al.* Colonic IgA producing cells and macrophages are reduced in recurrent and non-recurrent Clostridiun difficile associated diarrhoea. *J Clin Pathol* **57**, 973–979 (2004).
150. Qiu, H. *et al.* Novel Clostridium difficile Anti-Toxin (TcdA and TcdB) Humanized Monoclonal Antibodies Demonstrate In Vitro Neutralization across a Broad Spectrum of Clinical Strains and In Vivo Potency in a Hamster Spore Challenge Model. *PLoS One* **11**, e0157970 (2016).
151. Andersen, K. K. *et al.* Neutralization of Clostridium difficile Toxin B Mediated by Engineered Lactobacilli That Produce Single-Domain Antibodies. *Infect Immun* **84**, 395–406 (2016).
152. Cole, L. E. *et al.* Deciphering the domain specificity of C. difficile toxin neutralizing antibodies. *Vaccine* **37**, 3892–3901 (2019).
153. Cerquetti, M., Pantosti, A., Stefanelli, P. & Mastrantonio, P. Purification and characterization of an immunodominant 36 kDa antigen present on the cell surface of Clostridium difficile. *Microb Pathog* **13**, 271–279 (1992).
154. Drudy, D. *et al.* Human antibody response to surface layer proteins in *Clostridium difficile* infection. *FEMS Immunol Med Microbiol* **41**, 237–242 (2004).
155. Péchiné, S., Janoir, C. & Collignon, A. Variability of Clostridium difficile surface proteins and specific serum antibody response in patients with Clostridium difficile-associated disease. *J Clin Microbiol* **43**, 5018–5025 (2005).
156. Bomers, M. K. *et al.* Using a dog's superior olfactory sensitivity to identify Clostridium difficile in stools and patients: proof of principle study. *BMJ : British Medical Journal* **345**, e7396 (2012).

157. Bartlett, J. G. *Narrative Review: The New Epidemic of Clostridium difficile-Associated Enteric Disease*. www.annals.org (2006).
158. Guery, B., Galperine, T. & Barbut, F. Clostridioides difficile: Diagnosis and treatments. *The BMJ* vol. 366 Preprint at https://doi.org/10.1136/bmj.l4609 (2019).
159. Lessa, F. C. *et al.* Burden of Clostridium difficile Infection in the United States . *New England Journal of Medicine* **372**, 825–834 (2015).
160. Zhang, S. *et al.* Cost of hospital management of Clostridium difficile infection in United States—a meta-analysis and modelling study. *BMC Infect Dis* **16**, 447 (2016).
161. Zimlichman, E. *et al.* Health Care–Associated Infections. *JAMA Intern Med* **173**, 2039 (2013).
162. Kuijper, E. J., Coignard, B. & Tüll, P. Emergence of Clostridium difficile-associated disease in North America and Europe. *Clinical Microbiology and Infection* **12**, 2–18 (2006).
163. Le Monnier, A. *et al.* Hospital cost of Clostridium difficile infection including the contribution of recurrences in French acute-care hospitals. *Journal of Hospital Infection* **91**, 117–122 (2015).
164. Grube, R. *et al.* Ökonomische Auswirkungen einer Clostridium-difficile-Enterokolitis in deutschen Krankenhäusern auf der Basis von DRG-Kostendaten. *Z Gastroenterol* **53**, 391–397 (2015).
165. Wiegand, P. N. *et al.* Clinical and economic burden of Clostridium difficile infection in Europe: a systematic review of healthcare-facility-acquired infection. *Journal of Hospital Infection* **81**, 1–14 (2012).
166. Asensio, A. *et al.* The impact of Clostridium difficile infection on resource use and costs in hospitals in Spain and Italy: a matched cohort study. *International Journal of Infectious Diseases* **36**, 31–38 (2015).
167. Wilcox, M. H., Cunniffe, J. G., Trundle, C. & Redpath, C. Financial burden of hospital-acquired Clostridium difficile infection. *Journal of Hospital Infection* **34**, 23–30 (1996).
168. Herbert, R. *et al.* Two-year analysis of Clostridium difficile ribotypes associated with increased severity. *Journal of Hospital Infection* **103**, 388–394 (2019).
169. Miller, M. *et al.* Health care-associated clostridium difficile infection in Canada: Patient age and infecting strain type are highly predictive of severe outcome and mortality. *Clinical Infectious Diseases* **50**, 194–201 (2010).
170. Couturier, J., Davies, K., Gateau, C. & Barbut, F. Ribotypes and New Virulent Strains Across Europe. in 45–58 (2018). doi:10.1007/978-3-319-72799-8_4.
171. Freeman, J. *et al.* The changing epidemiology of Clostridium difficile infections. *Clinical Microbiology Reviews* vol. 23 529–549 Preprint at https://doi.org/10.1128/CMR.00082-09 (2010).
172. Kuehne, S. A. *et al.* Importance of Toxin A, Toxin B, and CDT in Virulence of an Epidemic Clostridium difficile Strain. *J Infect Dis* **209**, 83–86 (2014).
173. Public Health England. Clostridium difficile ribotyping network (cdrn) for england and northern ireland. *Report* (2013).
174. Cheng, A. C. *et al.* Control of fluoroquinolone resistance through successful regulation, Australia. *Emerg Infect Dis* **18**, 1453–1460 (2012).
175. Eyre, D. W. *et al.* Emergence and spread of predominantly community-onset Clostridium difficile PCR ribotype 244 infection in Australia, 2010 to 2012. *Eurosurveillance* **20**, (2015).
176. Collins, D. A., Hawkey, P. M. & Riley, T. V. Epidemiology of Clostridium difficile infection in Asia. *Antimicrob Resist Infect Control* **2**, 21 (2013).

177. Martin, J. S. H., Monaghan, T. M. & Wilcox, M. H. Clostridium difficile infection: Epidemiology, diagnosis and understanding transmission. *Nature Reviews Gastroenterology and Hepatology* vol. 13 206–216 Preprint at https://doi.org/10.1038/nrgastro.2016.25 (2016).
178. Davies, K. A. *et al.* Underdiagnosis of Clostridium difficile across Europe: the European, multicentre, prospective, biannual, point-prevalence study of Clostridium difficile infection in hospitalised patients with diarrhoea (EUCLID). *Lancet Infect Dis* **14**, 1208–1219 (2014).
179. *2018 Annual report for the emerging infections program for Clostridioides difficile infection.*
180. Guh, A. Y. *et al.* Trends in U.S. Burden of *Clostridioides difficile* Infection and Outcomes. *New England Journal of Medicine* **382**, 1320–1330 (2020).
181. Khanna, S. *et al.* The epidemiology of community-acquired clostridium difficile infection: A population-based study. *American Journal of Gastroenterology* **107**, 89–95 (2012).
182. Romano, V. *et al.* Toxigenic Clostridium difficile PCR Ribotypes from Wastewater Treatment Plants in Southern Switzerland. *Appl Environ Microbiol* **78**, 6643–6646 (2012).
183. Romano, V. *et al.* Prevalence and Genotypic Characterization of *Clostridium difficile* From Ruminants in Switzerland. *Zoonoses Public Health* **59**, 545–548 (2012).
184. Koene, M. G. J. *et al.* Clostridium difficile in Dutch animals: their presence, characteristics and similarities with human isolates. *Clinical Microbiology and Infection* **18**, 778–784 (2012).
185. Avberšek, J., Pirš, T., Pate, M., Rupnik, M. & Ocepek, M. Clostridium difficile in goats and sheep in Slovenia: Characterisation of strains and evidence of age-related shedding. *Anaerobe* **28**, 163–167 (2014).
186. Avbersek, J. *et al.* Diversity of Clostridium difficile in pigs and other animals in Slovenia. *Anaerobe* **15**, 252–255 (2009).
187. Zidaric, V., Zemljic, M., Janezic, S., Kocuvan, A. & Rupnik, M. High diversity of Clostridium difficile genotypes isolated from a single poultry farm producing replacement laying hens. *Anaerobe* **14**, 325–327 (2008).
188. Rodriguez Diaz, C., Seyboldt, C. & Rupnik, M. Non-human C. difficile Reservoirs and Sources: Animals, Food, Environment. in 227–243 (2018). doi:10.1007/978-3-319-72799-8_13.
189. Schneeberg, A., Rupnik, M., Neubauer, H. & Seyboldt, C. Prevalence and distribution of Clostridium difficile PCR ribotypes in cats and dogs from animal shelters in Thuringia, Germany. *Anaerobe* **18**, 484–488 (2012).
190. Orden, C. *et al.* Recreational sandboxes for children and dogs can be a source of epidemic ribotypes of *Clostridium difficile*. *Zoonoses Public Health* **65**, 88–95 (2018).
191. Álvarez-Pérez, S., Blanco, J. L., Harmanus, C., Kuijper, E. J. & García, M. E. Prevalence and characteristics of Clostridium perfringens and Clostridium difficile in dogs and cats attended in diverse veterinary clinics from the Madrid region. *Anaerobe* **48**, 47–55 (2017).
192. Diab, S. S., Songer, G. & Uzal, F. A. Clostridium difficile infection in horses: A review. *Vet Microbiol* **167**, 42–49 (2013).
193. Bandelj, P. *et al.* Prevalence and molecular characterization of Clostridium difficile isolated from European Barn Swallows (Hirundo rustica) during migration. *BMC Vet Res* **10**, 40 (2014).
194. Bandelj, P. *et al.* Zero prevalence of Clostridium difficile in wild passerine birds in Europe. *FEMS Microbiol Lett* **321**, 183–185 (2011).

195. Bojesen, A. M., Olsen, K. E. P. & Bertelsen, M. F. Fatal enterocolitis in Asian elephants (Elephas maximus) caused by Clostridium difficile. *Vet Microbiol* **116**, 329–335 (2006).
196. Álvarez-Pérez, S. *et al.* Shedding of Clostridium difficile PCR ribotype 078 by zoo animals, and report of an unstable metronidazole-resistant isolate from a zebra foal (Equus quagga burchellii). *Vet Microbiol* **169**, 218–222 (2014).
197. Pasquale, V. *et al.* Isolation and characterization of Clostridium difficile from shellfish and marine environments. *Folia Microbiol (Praha)* **56**, 431–437 (2011).
198. Skraban, J., Dzeroski, S., Zenko, B., Tusar, L. & Rupnik, M. Changes of poultry faecal microbiota associated with Clostridium difficile colonisation. *Vet Microbiol* **165**, 416–424 (2013).
199. Schneeberg, A. *et al.* Clostridium difficile Genotypes in Piglet Populations in Germany. *J Clin Microbiol* **51**, 3796–3803 (2013).
200. Alvarez-Perez, S. *et al.* Prevalence of Clostridium difficile in diarrhoeic and non-diarrhoeic piglets. *Vet Microbiol* **137**, 302–305 (2009).
201. Burt, S. A., Siemeling, L., Kuijper, E. J. & Lipman, L. J. A. Vermin on pig farms are vectors for Clostridium difficile PCR ribotypes 078 and 045. *Vet Microbiol* **160**, 256–258 (2012).
202. Andrés-Lasheras, S. *et al.* Presence of *Clostridium difficile* in pig faecal samples and wild animal species associated with pig farms. *J Appl Microbiol* **122**, 462–472 (2017).
203. Borriello, S. P., Honour, P., Turner, T. & Barclay, F. Household pets as a potential reservoir for Clostridium difficile infection. *J Clin Pathol* **36**, 84–87 (1983).
204. Hofer, E., Haechler, H., Frei, R. & Stephan, R. Low Occurrence of Clostridium difficile in Fecal Samples of Healthy Calves and Pigs at Slaughter and in Minced Meat in Switzerland. *J Food Prot* **73**, 973–975 (2010).
205. Eckert, C., Burghoffer, B. & Barbut, F. Contamination of ready-to-eat raw vegetables with Clostridium difficile in France. *J Med Microbiol* **62**, 1435–1438 (2013).
206. Bauer, M. P. & Kuijper, E. J. Potential Sources of Clostridium difficile in Human Infection. *Infect Dis Clin North Am* **29**, 29–35 (2015).
207. Janezic, S., Ocepek, M., Zidaric, V. & Rupnik, M. Clostridium difficile genotypes other than ribotype 078 that are prevalent among human, animal and environmental isolates. *BMC Microbiol* **12**, 48 (2012).
208. McDonald, L. C. *et al.* Clinical Practice Guidelines for Clostridium difficile Infection in Adults and Children: 2017 Update by the Infectious Diseases Society of America (IDSA) and Society for Healthcare Epidemiology of America (SHEA). *Clinical Infectious Diseases* **66**, 987–994 (2018).
209. Stoesser, N. *et al.* Epidemiology of Clostridium difficile in infants in Oxfordshire, UK: Risk factors for colonization and carriage, and genetic overlap with regional C. Difficile infection strains. *PLoS One* **12**, (2017).
210. von Müller, L. *et al.* Epidemiology of Clostridium difficile in Germany based on a single center long-term surveillance and German-wide genotyping of recent isolates provided to the advisory laboratory for diagnostic reasons. *International Journal of Medical Microbiology* **305**, 807–813 (2015).
211. Krutova, M. *et al.* Molecular characterisation of Czech Clostridium difficile isolates collected in 2013–2015. *International Journal of Medical Microbiology* **306**, 479–485 (2016).
212. Van Dorp, S. M. *et al.* Clinical and Microbiological Characteristics of Clostridium difficile Infection Among Hospitalized Children in the Netherlands. *Clinical Infectious Diseases* **64**, 192–198 (2017).

213. Bidet, P., Barbut, F., Lalande, V., Burghoffer, B. & Petit, J.-C. Development of a new PCR-ribotyping method for *Clostridium difficile* based on ribosomal RNA gene sequencing. *FEMS Microbiol Lett* **175**, 261–266 (1999).
214. Indra, A. *et al.* Characterization of Clostridium difficile isolates using capillary gel electrophoresis-based PCR ribotyping. *J Med Microbiol* **57**, 1377–1382 (2008).
215. Fawley, W. N. *et al.* Development and Validation of an Internationally-Standardized, High-Resolution Capillary Gel-Based Electrophoresis PCR-Ribotyping Protocol for Clostridium difficile. *PLoS One* **10**, e0118150 (2015).
216. Rupnik, M., Avesani, V., Janc, M., von Eichel-Streiber, C. & Delmée, M. A Novel Toxinotyping Scheme and Correlation of Toxinotypes with Serogroups of *Clostridium difficile* Isolates. *J Clin Microbiol* **36**, 2240–2247 (1998).
217. Loo, V. G. *et al. A Predominantly Clonal Multi-Institutional Outbreak of Clostridium difficile-Associated Diarrhea with High Morbidity and Mortality*. vol. 8 www.nejm.org (2005).
218. Clifford McDonald, L. *et al. An Epidemic, Toxin Gene-Variant Strain of Clostridium difficile*. *n engl j med* vol. 353 www.nejm.org (2005).
219. Burns, K. *et al.* Infection due to C. difficile ribotype 078: first report of cases in the Republic of Ireland. *Journal of Hospital Infection* **75**, 287–291 (2010).
220. Bauer, M. P. *et al.* Clostridium difficile infection in Europe: a hospital-based survey. *The Lancet* **377**, 63–73 (2011).
221. Plankaova, A. *et al.* Clostridioides difficile infections were predominantly driven by fluoroquinolone-resistant Clostridioides difficile ribotypes 176 and 001 in Slovakia in 2018–2019. *Int J Antimicrob Agents* **62**, 106824 (2023).
222. Magnusson, C. *et al.* Characterization of a *Clostridioides difficile* outbreak caused by PCR ribotype 046, associated with increased mortality. *Emerg Microbes Infect* **11**, 850–859 (2022).
223. Collins, J. *et al.* Dietary trehalose enhances virulence of epidemic Clostridium difficile. *Nature* **553**, 291–294 (2018).
224. Nicholas, A. *et al.* Molecular epidemiology and antimicrobial susceptibility of Clostridium difficile isolates from two Korean hospitals. *PLoS One* **12**, e0174716 (2017).
225. Shin, B.-M. *et al.* Multicentre study of the prevalence of toxigenic Clostridium difficile in Korea: results of a retrospective study 2000–2005. *J Med Microbiol* **57**, 697–701 (2008).
226. Lee, J.-H., Lee, Y., Lee, K., Riley, T. V. & Kim, H. The changes of PCR ribotype and antimicrobial resistance of Clostridium difficile in a tertiary care hospital over 10 years. *J Med Microbiol* **63**, 819–823 (2014).
227. Byun, J.-H. *et al.* A nationwide study of molecular epidemiology and antimicrobial susceptibility of Clostridioides difficile in South Korea. *Anaerobe* **60**, 102106 (2019).
228. Senoh, M. *et al.* Predominance of PCR-ribotypes, 018 (smz) and 369 (trf) of Clostridium difficile in Japan: a potential relationship with other global circulating strains? *J Med Microbiol* **64**, 1226–1236 (2015).
229. Spigaglia, P., Barbanti, F., Dionisi, A. M. & Mastrantonio, P. *Clostridium difficile* Isolates Resistant to Fluoroquinolones in Italy: Emergence of PCR Ribotype 018. *J Clin Microbiol* **48**, 2892–2896 (2010).
230. Walker, A. S. *et al.* Relationship between bacterial strain type, host biomarkers, and mortality in clostridium difficile infection. *Clinical Infectious Diseases* vol. 56 1589–1600 Preprint at https://doi.org/10.1093/cid/cit127 (2013).
231. Fujimoto, K. & Uematsu, S. Phage therapy for Clostridioides difficile infection. *Front Immunol* **13**, (2022).

232. Kola, A. *et al.* Survey of clostridium difficile infection surveillance systems in Europe, 2011. *Eurosurveillance* **21**, (2016).
233. de Noordhout, C. M. *et al.* Burden of salmonellosis, campylobacteriosis and listeriosis: A time series analysis, Belgium, 2012 to 2020. *Eurosurveillance* **22**, 6–18 (2017).
234. *European surveillance of Clostridium difficile infections. Surveillance protocol version 2.3*. (2017).
235. Paola Mastrantonio & Maja Rupnik. Updates on Clostridium difficile in Europe. (2018).
236. Eyre, D. W. & Walker, A. S. Clostridium difficile surveillance: Harnessing new technologies to control transmission. *Expert Review of Anti-Infective Therapy* vol. 11 1193–1205 Preprint at https://doi.org/10.1586/14787210.2013.845987 (2013).
237. Fawley, W. N. & Wilcox, M. H. An enhanced DNA fingerprinting service to investigate potential Clostridium difficile infection case clusters sharing the same PCR ribotype. *J Clin Microbiol* **49**, 4333–4337 (2011).
238. He, M. *et al.* Emergence and global spread of epidemic healthcare-associated Clostridium difficile. *Nat Genet* **45**, 109–113 (2013).
239. Planche, T. & Wilcox, M. Reference assays for Clostridium difficile infection: one or two gold standards? *J Clin Pathol* **64**, 1–5 (2011).
240. Carey-Ann, B. D. & Carroll, K. C. Diagnosis of Clostridium difficile Infection: an Ongoing Conundrum for Clinicians and for Clinical Laboratories. *Clin Microbiol Rev* **26**, 604–630 (2013).
241. Delmée, M. Laboratory diagnosis of Clostridium difficile disease. *Clinical Microbiology and Infection* **7**, 411–416 (2001).
242. Raeisi, H., Azimirad, M., Asadzadeh Aghdaei, H., Yadegar, A. & Zali, M. R. Rapid-format recombinant antibody-based methods for the diagnosis of Clostridioides difficile infection: Recent advances and perspectives. *Frontiers in Microbiology* vol. 13 Preprint at https://doi.org/10.3389/fmicb.2022.1043214 (2022).
243. Crobach, M. J. T. *et al.* European Society of Clinical Microbiology and Infectious Diseases: update of the diagnostic guidance document for Clostridium difficile infection. *Clinical Microbiology and Infection* **22**, S63–S81 (2016).
244. Crobach, M. J. T., Baktash, A., Duszenko, N. & Kuijper, E. J. Diagnostic Guidance for C. difficile Infections. in 27–44 (2018). doi:10.1007/978-3-319-72799-8_3.
245. Byrne, H., Conroy, P. J., Whisstock, J. C. & O'Kennedy, R. J. A tale of two specificities: bispecific antibodies for therapeutic and diagnostic applications. *Trends Biotechnol* **31**, 621–632 (2013).
246. Alibeiki, M., Golchin, M. & Tabatabaei, M. Development of a double-recombinant antibody sandwich ELISA for quantitative detection of epsilon toxoid concentration in inactivated Clostridium perfringens vaccines. *BMC Vet Res* **16**, 361 (2020).
247. Hwang, Y.-C. *et al.* Monoclonal antibodies for COVID-19 therapy and SARS-CoV-2 detection. *J Biomed Sci* **29**, 1 (2022).
248. Raeisi, H., Safarnejad, M. R. & Sadeghkhani, F. A new single-chain variable fragment (scFv) antibody provides sensitive and specific detection of citrus tristeza virus. *J Virol Methods* **300**, 114412 (2022).
249. Fouladi, M. *et al.* Selection of a fully human single domain antibody specific to Helicobacter pylori urease. *Appl Microbiol Biotechnol* **103**, 3407–3420 (2019).
250. Shali, A. *et al.* Generation and screening of efficient neutralizing single domain antibodies (VHHs) against the critical functional domain of anthrax protective antigen (PA). *Int J Biol Macromol* **114**, 1267–1278 (2018).

251. Xu, C. *et al.* Construction of an Immunized Rabbit Phage Display Library for Selecting High Activity against *Bacillus thuringiensis* Cry1F Toxin Single-Chain Antibodies. *J Agric Food Chem* **65**, 6016–6022 (2017).
252. Alfaleh, M. A. *et al.* Phage Display Derived Monoclonal Antibodies: From Bench to Bedside. *Front Immunol* **11**, (2020).
253. Høydahl, L. S. *et al.* Multivalent pIX phage display selects for distinct and improved antibody properties. *Sci Rep* **6**, 39066 (2016).
254. Kunamneni, A., Ogaugwu, C., Bradfute, S. & Durvasula, R. Ribosome Display Technology: Applications in Disease Diagnosis and Control. *Antibodies* **9**, 28 (2020).
255. Willats, W. G. T. Phage display: practicalities and prospects. *Plant Mol Biol* **50**, 837–854 (2002).
256. Rangnoi, K., Jaruseranee, N., O'Kennedy, R., Pansri, P. & Yamabhai, M. One-Step Detection of Aflatoxin-B1 Using scFv-Alkaline Phosphatase-Fusion Selected from Human Phage Display Antibody Library. *Mol Biotechnol* **49**, 240–249 (2011).
257. Raeisi, H. *et al.* Application of recombinant antibodies for treatment of Clostridioides difficile infection: Current status and future perspective. *Front Immunol* **13**, (2022).
258. Van Bockstaele, F., Holz, J.-B. & Revets, H. The development of nanobodies for therapeutic applications. *Curr Opin Investig Drugs* **10**, 1212–24 (2009).
259. Skottrup, P. D. *et al.* Diagnostic evaluation of a nanobody with picomolar affinity toward the protease RgpB from Porphyromonas gingivalis. *Anal Biochem* **415**, 158–167 (2011).
260. Ferrara, F. *et al.* Using Phage and Yeast Display to Select Hundreds of Monoclonal Antibodies: Application to Antigen 85, a Tuberculosis Biomarker. *PLoS One* **7**, e49535 (2012).
261. Gite, S. *et al.* A Rapid, Accurate, Single Molecule Counting Method Detects Clostridium difficile Toxin B in Stool Samples. *Sci Rep* **8**, 8364 (2018).
262. Wilson, D. H. *et al.* The Simoa HD-1 Analyzer: A Novel Fully Automated Digital Immunoassay Analyzer with Single-Molecule Sensitivity and Multiplexing. *SLAS Technol* **21**, 533–547 (2016).
263. Pollock, N. R. Ultrasensitive Detection and Quantification of Toxins for Optimized Diagnosis of Clostridium difficile Infection. *J Clin Microbiol* **54**, 259–264 (2016).
264. Bartlett, J. G., Chang, T. W., Moon, N. & Onderdonk, A. B. Antibiotic-induced lethal enterocolitis in hamsters: studies with eleven agents and evidence to support the pathogenic role of toxin-producing Clostridia. *Am J Vet Res* **39**, 1525–30 (1978).
265. Johnson AP. Drug evaluation: OPT-80, a narrow-spectrum macrocyclic antibiotic. *Curr Opin Investig Drugs* **8**, 168–173 (2007).
266. Louie, T. J. *et al.* Fidaxomicin versus Vancomycin for Clostridium difficile Infection. *New England Journal of Medicine* **364**, 422–431 (2011).
267. Koon, H. W. *et al.* Fidaxomicin and OP-1118 Inhibit Clostridium difficile Toxin A- and B-Mediated Inflammatory Responses via Inhibition of NF-κB Activity. *Antimicrob Agents Chemother* **62**, (2018).
268. Boyaci, H. *et al.* Fidaxomicin jams Mycobacterium tuberculosis RNA polymerase motions needed for initiation via RbpA contacts. *Elife* **7**, (2018).
269. Babakhani, F. *et al.* Fidaxomicin Inhibits Spore Production in Clostridium difficile. *Clinical Infectious Diseases* **55**, S162–S169 (2012).
270. Louie, T. J. *et al.* Fidaxomicin Preserves the Intestinal Microbiome During and After Treatment of Clostridium difficile Infection (CDI) and Reduces Both Toxin Reexpression and Recurrence of CDI. *Clinical Infectious Diseases* **55**, S132–S142 (2012).

271. Bartsch, S. M., Umscheid, C. A., Fishman, N. & Lee, B. Y. Is Fidaxomicin Worth the Cost? An Economic Analysis. *Clinical Infectious Diseases* **57**, 555–561 (2013).
272. Debast, S. B., Bauer, M. P. & Kuijper, E. J. European Society of Clinical Microbiology and Infectious Diseases: Update of the Treatment Guidance Document for Clostridium difficile Infection. *Clinical Microbiology and Infection* **20**, 1–26 (2014).
273. Johnson, S. *et al.* Clinical Practice Guideline by the Infectious Diseases Society of America (IDSA) and Society for Healthcare Epidemiology of America (SHEA): 2021 Focused Update Guidelines on Management of *Clostridioides difficile* Infection in Adults. *Clinical Infectious Diseases* **73**, e1029–e1044 (2021).
274. Guery, B. *et al.* Extended-pulsed fidaxomicin versus vancomycin for Clostridium difficile infection in patients 60 years and older (EXTEND): a randomised, controlled, open-label, phase 3b/4 trial. *Lancet Infect Dis* **18**, 296–307 (2018).
275. Kao, D. *et al.* Effect of Oral Capsule– vs Colonoscopy-Delivered Fecal Microbiota Transplantation on Recurrent *Clostridium difficile* Infection. *JAMA* **318**, 1985 (2017).
276. Verdier, C. *et al.* An Oral FMT Capsule as Efficient as an Enema for Microbiota Reconstruction Following Disruption by Antibiotics, as Assessed in an In Vitro Human Gut Model. *Microorganisms* **9**, 358 (2021).
277. Kelly, C. P. Fecal Microbiota Transplantation — An Old Therapy Comes of Age. *New England Journal of Medicine* **368**, 474–475 (2013).
278. Burke, K. E. & Lamont, J. T. Clostridium difficile infection: A worldwide disease. *Gut and Liver* vol. 8 1–6 Preprint at https://doi.org/10.5009/gnl.2014.8.1.1 (2014).
279. van Nood, E. *et al.* Duodenal Infusion of Donor Feces for Recurrent Clostridium difficile . *New England Journal of Medicine* **368**, 407–415 (2013).
280. Tariq, R., Pardi, D. S., Bartlett, M. G. & Khanna, S. Low Cure Rates in Controlled Trials of Fecal Microbiota Transplantation for Recurrent Clostridium difficile Infection: A Systematic Review and Meta-analysis. *Clinical Infectious Diseases* **68**, 1351–1358 (2019).
281. Khanna, S. *et al.* Efficacy and Safety of RBX2660 in PUNCH CD3, a Phase III, Randomized, Double-Blind, Placebo-Controlled Trial with a Bayesian Primary Analysis for the Prevention of Recurrent Clostridioides difficile Infection. *Drugs* **82**, 1527–1538 (2022).
282. Feuerstadt, P. *et al.* SER-109, an Oral Microbiome Therapy for Recurrent *Clostridioides difficile* Infection. *New England Journal of Medicine* **386**, 220–229 (2022).
283. Lee, B. Y. *et al.* The potential value of Clostridium difficile vaccine: An economic computer simulation model. *Vaccine* **28**, 5245–5253 (2010).
284. Smits, W. K., Lyras, D., Lacy, D. B., Wilcox, M. H. & Kuijper, E. J. Clostridium difficile infection. *Nat Rev Dis Primers* **2**, 16020 (2016).
285. Bézay, N. *et al.* Safety, immunogenicity and dose response of VLA84, a new vaccine candidate against Clostridium difficile, in healthy volunteers. *Vaccine* **34**, 2585–2592 (2016).
286. Clements, J. D. *et al.* Safety and Immunogenicity of Increasing Doses of aClostridium difficile Toxoid Vaccine Administered to Healthy Adults. *Infect Immun* **69**, 988–995 (2001).
287. de Bruyn, G. *et al.* Defining the optimal formulation and schedule of a candidate toxoid vaccine against Clostridium difficile infection: A randomized Phase 2 clinical trial. *Vaccine* **34**, 2170–2178 (2016).
288. Wilcox, M. H. *et al.* Bezlotoxumab for Prevention of Recurrent *Clostridium difficile* Infection. *New England Journal of Medicine* **376**, 305–317 (2017).

289. KÖHLER, G. & MILSTEIN, C. Continuous cultures of fused cells secreting antibody of predefined specificity. *Nature* **256**, 495–497 (1975).
290. Marozsan, A. J. *et al.* Protection Against Clostridium difficile Infection With Broadly Neutralizing Antitoxin Monoclonal Antibodies. *J Infect Dis* **206**, 706–713 (2012).
291. Lowy, I. *et al.* Treatment with Monoclonal Antibodies against *Clostridium difficile* Toxins. *New England Journal of Medicine* **362**, 197–205 (2010).
292. Yang, Z. *et al.* A Novel Multivalent, Single-Domain Antibody Targeting TcdA and TcdB Prevents Fulminant Clostridium difficile Infection in Mice. *J Infect Dis* **210**, 964–972 (2014).
293. Chen, K. *et al.* A probiotic yeast-based immunotherapy against *Clostridioides difficile* infection. *Sci Transl Med* **12**, (2020).
294. Wicke, N., Bedford, M. R. & Howarth, M. Gastrobodies are engineered antibody mimetics resilient to pepsin and hydrochloric acid. *Commun Biol* **4**, (2021).
295. Eckert, C. *et al.* Prevalence and pathogenicity of binary toxin–positive Clostridium difficile strains that do not produce toxins A and B. *New Microbes New Infect* **3**, 12–17 (2015).
296. Unger, M. *et al.* Selection of Nanobodies that Block the Enzymatic and Cytotoxic Activities of the Binary Clostridium Difficile Toxin CDT. *Sci Rep* **5**, 7850 (2015).
297. Calabi, E., Calabi, F., Phillips, A. D. & Fairweather, N. F. Binding of Clostridium difficile surface layer proteins to gastrointestinal tissues. *Infect Immun* **70**, 5770–5778 (2002).
298. Stevenson, E., Minton, N. P. & Kuehne, S. A. The role of flagella in Clostridium difficile pathogenicity. *Trends Microbiol* **23**, 275–282 (2015).
299. Pantaléon, V. *et al.* The Clostridium difficile Protease Cwp84 Modulates both Biofilm Formation and Cell-Surface Properties. *PLoS One* **10**, e0124971 (2015).
300. Péchiné, S. *et al.* Diminished intestinal colonization by Clostridium difficile and immune response in mice after mucosal immunization with surface proteins of Clostridium difficile. *Vaccine* **25**, 3946–3954 (2007).
301. Ní Eidhin, D. B., O'Brien, J. B., McCabe, M. S., Athié-Morales, V. & Kelleher, D. P. Active immunization of hamsters against *Clostridium difficile* infection using surface-layer protein. *FEMS Immunol Med Microbiol* **52**, 207–218 (2008).
302. Kandalaft, H. *et al.* Targeting surface-layer proteins with single-domain antibodies: a potential therapeutic approach against Clostridium difficile-associated disease. *Appl Microbiol Biotechnol* **99**, 8549–8562 (2015).
303. Shirvan, A. N. & Aitken, R. Isolation of recombinant antibodies directed against surface proteins of Clostridium difficile. *Brazilian Journal of Microbiology* **47**, 394–402 (2016).
304. Goetz, L. H. & Schork, N. J. Personalized medicine: motivation, challenges, and progress. *Fertility and Sterility* vol. 109 952–963 Preprint at https://doi.org/10.1016/j.fertnstert.2018.05.006 (2018).
305. de Groot, P. F., Frissen, M. N., de Clercq, N. C. & Nieuwdorp, M. Fecal microbiota transplantation in metabolic syndrome: History, present and future. *Gut Microbes* vol. 8 253–267 Preprint at https://doi.org/10.1080/19490976.2017.1293224 (2017).
306. Wiuff, C., Banks, A.-L., Fitzpatrick, F. & Cottom, L. The Need for European Surveillance of CDI. in 13–25 (2018). doi:10.1007/978-3-319-72799-8_2.
307. Poxton, I. R., McCoubrey, J. & Blair, G. The pathogenicity of Clostridium difficile. *Clinical Microbiology and Infection* **7**, 421–427 (2001).
308. Péchiné, S., Bruxelle, J. F., Janoir, C. & Collignon, A. Targeting Clostridium difficile Surface Components to Develop Immunotherapeutic Strategies Against Clostridium difficile Infection. *Front Microbiol* **9**, (2018).

309. Goyard, S. *et al.* A highly sensitive bioluminescent method for measuring allergen-specific IgE in microliter samples. *Allergy: European Journal of Allergy and Clinical Immunology* vol. 75 2952–2956 Preprint at https://doi.org/10.1111/all.14365 (2020).
310. Moor, K. *et al.* Analysis of bacterial-surface-specific antibodies in body fluids using bacterial flow cytometry. *Nat Protoc* **11**, 1531–53 (2016).
311. Giles, J. & Roberts, A. Clostridioides difficile: Current overview and future perspectives. in *Advances in Protein Chemistry and Structural Biology* vol. 129 215–245 (Academic Press Inc., 2022).
312. Oliveira Paiva, A. M., Friggen, A. H., Douwes, R., Wittekoek, B. & Smits, W. K. Practical observations on the use of fluorescent reporter systems in Clostridioides difficile. *Antonie Van Leeuwenhoek* **115**, 297–323 (2022).
313. Donnelly, M. L. *et al.* Development of a Dual-Fluorescent-Reporter System in Clostridioides difficile Reveals a Division of Labor between Virulence and Transmission Gene Expression. *mSphere* **7**, e0013222 (2022).
314. Buckley, A. M. *et al.* Lighting Up Clostridium Difficile: Reporting Gene Expression Using Fluorescent Lov Domains. *Sci Rep* **6**, 23463 (2016).
315. Péchiné, S., Denève-Larrazet, C. & Collignon, A. Clostridium difficile Adhesins. in 91–101 (2016). doi:10.1007/978-1-4939-6361-4_7.
316. Eidhin, D. N., Ryan, A. W., Doyle, R. M., Walsh, J. B. & Kelleher, D. Sequence and phylogenetic analysis of the gene for surface layer protein, slpA, from 14 PCR ribotypes of Clostridium difficile. *J Med Microbiol* **55**, 69–83 (2006).
317. Macdonald, L. E. *et al.* Precise and in situ genetic humanization of 6 Mb of mouse immunoglobulin genes. *Proceedings of the National Academy of Sciences* **111**, 5147–5152 (2014).
318. Murphy, A. J. *et al.* Mice with megabase humanization of their immunoglobulin genes generate antibodies as efficiently as normal mice. *Proceedings of the National Academy of Sciences* **111**, 5153–5158 (2014).
319. Chen, J. *et al.* B cell development in mice that lack one or both immunoglobulin kappa light chain genes. *EMBO J* **12**, 821–830 (1993).
320. Péchiné, S. *et al.* Immunological properties of surface proteins of Clostridium difficile. in *Journal of Medical Microbiology* vol. 54 193–196 (2005).
321. Knight, D. R. *et al.* Genomic epidemiology and transmission dynamics of recurrent Clostridioides difficile infection in Western Australia. *Eur J Clin Microbiol Infect Dis* **42**, 607–619 (2023).
322. Balbino, B. *et al.* The anti-IgE mAb omalizumab induces adverse reactions by engaging Fcγ receptors. *Journal of Clinical Investigation* **130**, 1330–1335 (2020).
323. Fadlallah, J. *et al.* Synergistic convergence of microbiota-specific systemic IgG and secretory IgA. *J Allergy Clin Immunol* **143**, 1575-1585.e4 (2019).
324. Tasteyre, A. *et al.* Molecular characterization of fliD gene encoding flagellar cap and its expression among Clostridium difficile isolates from different serogroups. *J Clin Microbiol* **39**, 1178–1183 (2001).
325. Tasteyre, A., Barc, M. C., Collignon, A., Boureau, H. & Karjalainen, T. Role of FliC and FliD flagellar proteins of Clostridium difficile in adherence and gut colonization. *Infect Immun* **69**, 7937–7940 (2001).
326. Dingle, T. C., Mulvey, G. L. & Armstrong, G. D. Mutagenic analysis of the clostridium difficile flagellar proteins, flic and flid, and their contribution to virulence in hamsters. *Infect Immun* **79**, 4061–4067 (2011).
327. Tasteyre, A. *et al. Phenotypic and Genotypic Diversity of the Flagellin Gene (fliC) among Clostridium difficile Isolates from Different Serogroups*. *JOURNAL OF CLINICAL MICROBIOLOGY* (2000).

328. Aliramezani, A., Talebi, M. & Douraghi, M. Polymorphisms in the genes encoding surface associated proteins of Clostridioides difficile isolates. *Infection, Genetics and Evolution* **86**, (2020).
329. Anjuwon-Foster, B. R. & Tamayo, R. A genetic switch controls the production of flagella and toxins in Clostridium difficile. *PLoS Genet* **13**, (2017).
330. Trzilova, D., Warren, M. A. H., Gadda, N. C., Williams, C. L. & Tamayo, R. Flagellum and toxin phase variation impacts intestinal colonization and disease development in a mouse model of *Clostridioides difficile* infection. *Gut Microbes* **14**, (2022).
331. Tremblay, Y. D. N., Hathroubi, S. & Jacques, M. [Bacterial biofilms: their importance in animal health and public health]. *Can J Vet Res* **78**, 110–6 (2014).
332. O'Brien, J. B. *et al.* Passive immunisation of hamsters against Clostridium difficile infection using antibodies to surface layer proteins. *FEMS Microbiol Lett* **246**, 199–205 (2005).
333. Jose, S. & Madan, R. Neutrophil-mediated inflammation in the pathogenesis of Clostridium difficile infections. *Anaerobe* **41**, 85–90 (2016).
334. Wang, Y. *et al.* Specificity of mouse and human Fcgamma receptors and their polymorphic variants for IgG subclasses of different species. *Eur J Immunol* **52**, 753–759 (2022).
335. Usui, Y. *et al.* Impact of deoxycholate on Clostridioides difficile growth, toxin production, and sporulation. *Heliyon* **6**, e03717 (2020).
336. Cohen, S. H., Tang, Y. J. & Silva, Jr. , J. Analysis of the Pathogenicity Locus in *Clostridium difficile* Strains. *J Infect Dis* **181**, 659–663 (2000).
337. Bridier, A. & Briandet, R. Contribution of Confocal Laser Scanning Microscopy in Deciphering Biofilm Tridimensional Structure and Reactivity. in 255–266 (2014). doi:10.1007/978-1-4939-0467-9_18.
338. Lawry, B. M. *et al.* Species-Specific Detection of C. difficile Using Targeted Antibody Design. *Anal Chem* **90**, 13475–13482 (2018).
339. Fioravanti, A. *et al.* Structure of S-layer protein Sap reveals a mechanism for therapeutic intervention in anthrax. *Nature Microbiology* vol. 4 1805–1814 Preprint at https://doi.org/10.1038/s41564-019-0499-1 (2019).
340. Majumdar, A. & Govind, R. Regulation of Clostridioides difficile toxin production. *Current Opinion in Microbiology* vol. 65 95–100 Preprint at https://doi.org/10.1016/j.mib.2021.10.018 (2022).
341. Girinathan, B. P., Ou, J., Dupuy, B. & Govind, R. Pleiotropic roles of Clostridium difficile sin locus. *PLoS Pathog* **14**, e1006940 (2018).
342. Ciftci, Y., Girinathan, B. P., Dhungel, B. A., Hasan, M. K. & Govind, R. Clostridioides difficile SinR' regulates toxin, sporulation and motility through protein-protein interaction with SinR. *Anaerobe* **59**, 1–7 (2019).
343. Govind, R. & Dupuy, B. Secretion of Clostridium difficile toxins A and B requires the holin-like protein TcdE. *PLoS Pathog* **8**, e1002727 (2012).
344. Bradshaw, W. J., Kirby, J. M., Roberts, A. K., Shone, C. C. & Acharya, K. R. Cwp2 from Clostridium difficile exhibits an extended three domain fold and cell adhesion in vitro. *FEBS J* **284**, 2886–2898 (2017).
345. Vuotto, C., Donelli, G., Buckley, A. & Chilton, C. Clostridium difficile Biofilm. in 97–115 (2018). doi:10.1007/978-3-319-72799-8_7.
346. Normington, C. *et al.* Biofilms harbour Clostridioides difficile, serving as a reservoir for recurrent infection. *NPJ Biofilms Microbiomes* **7**, 16 (2021).
347. Semenyuk, E. G. *et al.* Spore Formation and Toxin Production in Clostridium difficile Biofilms. *PLoS One* **9**, e87757 (2014).

348. Dawson, L. F., Valiente, E., Faulds-Pain, A., Donahue, E. H. & Wren, B. W. Characterisation of Clostridium difficile Biofilm Formation, a Role for Spo0A. *PLoS One* **7**, e50527 (2012).
349. Beganović, J. *et al.* Functionality of the S-layer protein from the probiotic strain Lactobacillus helveticus M92. *Antonie Van Leeuwenhoek* **100**, 43–53 (2011).
350. Brauer, M. *et al.* What's a Biofilm?—How the Choice of the Biofilm Model Impacts the Protein Inventory of Clostridioides difficile. *Front Microbiol* **12**, (2021).
351. Rollenske, T. *et al.* Parallelism of intestinal secretory IgA shapes functional microbial fitness. *Nature* **598**, 657–661 (2021).
352. Hussain, H. A., Roberts, A. P. & Mullany, P. Generation of an erythromycin-sensitive derivative of Clostridium difficile strain 630 (630Δerm) and demonstration that the conjugative transposon Tn916ΔE enters the genome of this strain at multiple sites. *J Med Microbiol* **54**, 137–141 (2005).
353. ISC MIMA2 INRAE.
354. Hartmann, R. *et al.* Quantitative image analysis of microbial communities with BiofilmQ. *Nat Microbiol* **6**, 151–156 (2021).
355. Ewin, D., Birch, W. D. & Moura, I. B. In vitro models to study Clostridioides difficile infection: Current systems and future advances. *Current Opinion in Gastroenterology* vol. 39 23–30 Preprint at https://doi.org/10.1097/MOG.0000000000000893 (2023).
356. Kim, H. J. & Ingber, D. E. Gut-on-a-Chip microenvironment induces human intestinal cells to undergo villus differentiation. *Integrative Biology* **5**, 1130 (2013).
357. Babcock, G. J. *et al.* Human monoclonal antibodies directed against toxins A and B prevent Clostridium difficile-induced mortality in hamsters. *Infect Immun* **74**, 6339–6347 (2006).
358. Reeves, A. E., Koenigsknecht, M. J., Bergin, I. L. & Young, V. B. Suppression of Clostridium difficile in the Gastrointestinal Tracts of Germfree Mice Inoculated with a Murine Isolate from the Family Lachnospiraceae. *Infect Immun* **80**, 3786–3794 (2012).
359. Eberl, C. *et al.* Reproducible Colonization of Germ-Free Mice With the Oligo-Mouse-Microbiota in Different Animal Facilities. *Front Microbiol* **10**, 2999 (2019).
360. Senok, A. *et al.* Detection of clostridium difficile antigen and toxin in stool specimens: Comparison of the C. difficile quik chek complete enzyme immunoassay and GeneXpert C. difficile polymerase chain reaction assay. *Saudi Journal of Gastroenterology* **23**, 259 (2017).
361. van Rossen, T. M. *et al.* Simultaneous detection and ribotyping of Clostridioides difficile, and toxin gene detection directly on fecal samples. *Antimicrob Resist Infect Control* **10**, 23 (2021).
362. Matsuda, K. *et al.* Sensitive Quantification of Clostridium difficile Cells by Reverse Transcription-Quantitative PCR Targeting rRNA Molecules. *Appl Environ Microbiol* **78**, 5111–5118 (2012).
363. van den Berg, R. J. *et al.* Prospective Multicenter Evaluation of a New Immunoassay and Real-Time PCR for Rapid Diagnosis of *Clostridium difficile* -Associated Diarrhea in Hospitalized Patients. *J Clin Microbiol* **43**, 5338–5340 (2005).
364. Zhang, L. *et al.* Insight into alteration of gut microbiota in Clostridium difficile infection and asymptomatic C. difficile colonization. *Anaerobe* **34**, 1–7 (2015).
365. Giancola, S. E., Williams, R. J. & Gentry, C. A. Prevalence of the Clostridium difficile BI/NAP1/027 strain across the United States Veterans Health Administration. *Clinical Microbiology and Infection* **24**, 877–881 (2018).
366. Blanckaert, K. *et al.* Infections à Clostridium difficile PCR-ribotype 027 (ICD) : épidémiologie et gestion des risques. *Antibiotiques* **9**, 274–277 (2007).

367. KATO, H. *et al.* Colonisation and transmission of Clostridium difficile in healthy individuals examined by PCR ribotyping and pulsed-field gel electrophoresis. *J Med Microbiol* **50**, 720–727 (2001).
368. Delvallez, M., Carlier, Y., Bout, D., Capron, A. & Martin, G. R. Purification of a surface-specific soluble antigen from Listeria monocytogenes. *Infect Immun* **25**, 971–7 (1979).
369. Syuto, B. & Matsumoto, M. Purification of a protective antigen from a saline extract of Pasteurella multocida. *Infect Immun* **37**, 1218–26 (1982).
370. Fox, J. L. & Klass, M. Antigens produced by recombinant DNA technology. *Clin Chem* **35**, 1838–42 (1989).
371. Kool, M., Fierens, K. & Lambrecht, B. N. Alum adjuvant: Some of the tricks of the oldest adjuvant. *Journal of Medical Microbiology* vol. 61 927–934 Preprint at https://doi.org/10.1099/jmm.0.038943-0 (2012).
372. Steinhagen, F., Kinjo, T., Bode, C. & Klinman, D. M. TLR-based immune adjuvants. *Vaccine* **29**, 3341–3355 (2011).
373. Duthie, M. S., Windish, H. P., Fox, C. B. & Reed, S. G. Use of defined TLR ligands as adjuvants within human vaccines. *Immunol Rev* **239**, 178–196 (2011).
374. Jazani, N. H. *et al.* Naloxone and alum synergistically augment adjuvant activities of each other in a mouse vaccine model of Salmonella typhimurium infection. *Immunobiology* **216**, 744–751 (2011).
375. SACERDOTE, P., GASPANI, L. & PANERAI, A. E. The Opioid Antagonist Naloxone Induces a Shift from Type 2 to Type 1 Cytokine Pattern in Normal and Skin-Grafted Mice. *Ann N Y Acad Sci* **917**, 755–763 (2006).
376. Collery, M. M. *et al.* What's a SNP between friends: The influence of single nucleotide polymorphisms on virulence and phenotypes of clostridium difficile strain 630 and derivatives. *Virulence* **8**, 767–781 (2017).
377. Slack, E., Balmer, M. L., Fritz, J. H. & Hapfelmeier, S. Functional Flexibility of Intestinal IgA – Broadening the Fine Line. *Front Immunol* **3**, (2012).
378. Ngai, P. K., Ackermann, F., Wendt, H., Savoca, R. & Bosshard, H. R. Protein A antibody-capture ELISA (PACE): an ELISA format to avoid denaturation of surface-adsorbed antigens. *J Immunol Methods* **158**, 267–76 (1993).
379. Martin-Verstraete, I., Peltier, J. & Dupuy, B. The Regulatory Networks That Control Clostridium difficile Toxin Synthesis. *Toxins (Basel)* **8**, 153 (2016).
380. Hundsberger, T. *et al.* Transcription Analysis of the Genes tcdA-E of the Pathogenicity Locus of Clostridium Difficile. *Eur J Biochem* **244**, 735–742 (1997).
381. Darkoh, C., DuPont, H. L., Norris, S. J. & Kaplan, H. B. Toxin Synthesis by Clostridium difficile Is Regulated through Quorum Signaling. *mBio* **6**, (2015).
382. Matamouros, S., England, P. & Dupuy, B. Clostridium difficile toxin expression is inhibited by the novel regulator TcdC. *Mol Microbiol* **64**, 1274–88 (2007).
383. Karlsson, S. *et al.* Expression of Clostridium difficile toxins A and B and their sigma factor TcdD is controlled by temperature. *Infect Immun* **71**, 1784–93 (2003).
384. Thapa, T. *et al.* Multiple Factors Modulate Biofilm Formation by the Anaerobic Pathogen Clostridium difficile. *J Bacteriol* **195**, 545–555 (2013).
385. Golowczyc, M. A. *et al.* Interaction between Lactobacillus kefir and Saccharomyces lipolytica isolated from kefir grains: evidence for lectin-like activity of bacterial surface proteins. *J Dairy Res* **76**, 111–6 (2009).
386. Semenyuk, E. G. *et al.* Analysis of Bacterial Communities during Clostridium difficile Infection in the Mouse. *Infect Immun* **83**, 4383–4391 (2015).
387. Relucenti, M. *et al.* Microscopy Methods for Biofilm Imaging: Focus on SEM and VP-SEM Pros and Cons. *Biology (Basel)* **10**, 51 (2021).

388. Azeredo, J. *et al.* Critical review on biofilm methods. *Critical Reviews in Microbiology* vol. 43 313–351 Preprint at https://doi.org/10.1080/1040841X.2016.1208146 (2017).
389. Goeres, D. M. *et al.* A method for growing a biofilm under low shear at the air–liquid interface using the drip flow biofilm reactor. *Nat Protoc* **4**, 783–788 (2009).
390. Hutton, M. L., Mackin, K. E., Chakravorty, A. & Lyras, D. Small animal models for the study of Clostridium difficile disease pathogenesis. *FEMS Microbiology Letters* vol. 352 140–149 Preprint at https://doi.org/10.1111/1574-6968.12367 (2014).
391. Lawley, T. D. & Young, V. B. Murine models to study Clostridium difficile infection and transmission. *Anaerobe* **24**, 94–7 (2013).
392. Best, E. L., Freeman, J. & Wilcox, M. H. Models for the study of Clostridium difficile infection. *Gut Microbes* **3**, 145–67 (2012).
393. Pawlowski, S. W. *et al.* Murine Model of *Clostridium difficile* Infection with Aged Gnotobiotic C57BL/6 Mice and a BI/NAP1 Strain. *J Infect Dis* **202**, 1708–1712 (2010).
394. Brugiroux, S. *et al.* Genome-guided design of a defined mouse microbiota that confers colonization resistance against Salmonella enterica serovar Typhimurium. *Nat Microbiol* **2**, 16215 (2016).
395. Chen, X. *et al.* A Mouse Model of Clostridium difficile–Associated Disease. *Gastroenterology* **135**, 1984–1992 (2008).
396. Lee, V. H. Enzymatic barriers to peptide and protein absorption. *Crit Rev Ther Drug Carrier Syst* **5**, 69–97 (1988).
397. Moor, K. *et al.* High-avidity IgA protects the intestine by enchaining growing bacteria. *Nature* **544**, 498–502 (2017).
398. Reinhart, D., Weik, R. & Kunert, R. Recombinant IgA production: single step affinity purification using camelid ligands and product characterization. *J Immunol Methods* **378**, 95–101 (2012).
399. Lohse, S. *et al.* An Anti-EGFR IgA That Displays Improved Pharmacokinetics and Myeloid Effector Cell Engagement *In Vivo*. *Cancer Res* **76**, 403–417 (2016).
400. Corthésy, B. Multi-Faceted Functions of Secretory IgA at Mucosal Surfaces. *Front Immunol* **4**, (2013).
401. Luque, Y. *et al.* Vancomycin-Associated Cast Nephropathy. *Journal of the American Society of Nephrology* **28**, 1723–1728 (2017).
402. Gbassi, G. K. & Vandamme, T. Probiotic Encapsulation Technology: From Microencapsulation to Release into the Gut. *Pharmaceutics* **4**, 149–163 (2012).
403. Wang, Y. *et al.* Self-renewing Monolayer of Primary Colonic or Rectal Epithelial Cells. *Cell Mol Gastroenterol Hepatol* **4**, 165-182.e7 (2017).
404. Zhang, J. *et al.* Primary Human Colonic Mucosal Barrier Crosstalk with Super Oxygen-Sensitive Faecalibacterium prausnitzii in Continuous Culture. *Med* **2**, 74-98.e9 (2021).
405. Ashammakhi, N. *et al.* Gut-on-a-chip: Current progress and future opportunities. *Biomaterials* **255**, 120196 (2020).
406. Frost, L. R., Cheng, J. K. J. & Unnikrishnan, M. Clostridioides difficile biofilms: A mechanism of persistence in the gut? *PLoS Pathog* **17**, e1009348 (2021).
407. Saleem, M. & Kamal, M. Monoclonal antibodies in clinical diagnosis: A brief review application. *Afr J Biotechnol* **7**, 923–925 (2008).
408. Jin, J. *et al.* A real-time LAMP-based dual-sample microfluidic chip for rapid and simultaneous detection of multiple waterborne pathogenic bacteria from coastal waters. *Analytical Methods* **13**, 2710–2721 (2021).

409. Tvilum, A. *et al.* Antibody-Drug Conjugates to Treat Bacterial Biofilms via Targeting and Extracellular Drug Release. *Advanced Science* (2023) doi:10.1002/advs.202301340.

Annexes

Annex 1: The cell wall lipoprotein CD1687 acts as a DNA binding protein during deoxycholate-induced biofilm formation in *Clostridioides difficile*

Emile Auriaa, Lise Hunaultb,c, Patrick Englandd, Marc Monote, Juliana Pipoli Da Fonsecae, Mariette Matondof, Magalie Duchateauf, Yannick D.N. Tremblayg and Bruno Dupuya#

a Institut Pasteur, Université Paris-Cité, UMR-CNRS 6047, Laboratoire Pathogenèse des Bactéries Anaérobies, F-75015 Paris, France
b Sorbonne Université, INSERM, CNRS, Centre d'Immunologie et des Maladies Infectieuses (CIMI-Paris), F-75013 Paris, France
c Institut Pasteur, Université Paris-Cité, INSERM UMR1222, Unit of Antibodies in Therapy and Pathology, Paris, France

d Plateforme de Biophysique Moléculaire, Institut Pasteur, CNRS UMR3528, Paris, France.
e Plateforme technologique Biomics, Institut Pasteur, Paris, France
f Plateforme Proteomic, Institut Pasteur, France
g University of Saskatchewan: Saskatoon, SK, CA

NPJ Biofilms and Microbiomes (2023)9:24 ; https://doi.org/10.1038/s41522-023-00393-5

npj biofilms and microbiomes

www.nature.com/npjbiofilms

ARTICLE OPEN

Check for updates

The cell wall lipoprotein CD1687 acts as a DNA binding protein during deoxycholate-induced biofilm formation in *Clostridioides difficile*

Emile Auria[1], Lise Hunault[2,3], Patrick England[4], Marc Monot[5], Juliana Pipoli Da Fonseca[5], Mariette Matondo[6], Magalie Duchateau[6], Yannick D. N. Tremblay[7] and Bruno Dupuy[1]✉

The ability of bacterial pathogens to establish recurrent and persistent infections is frequently associated with their ability to form biofilms. *Clostridioides difficile* infections have a high rate of recurrence and relapses and it is hypothesized that biofilms are involved in its pathogenicity and persistence. Biofilm formation by *C. difficile* is still poorly understood. It has been shown that specific molecules such as deoxycholate (DCA) or metronidazole induce biofilm formation, but the mechanisms involved remain elusive. In this study, we describe the role of the *C. difficile* lipoprotein CD1687 during DCA-induced biofilm formation. We showed that the expression of *CD1687*, which is part of an operon within the *CD1685-CD1689* gene cluster, is controlled by multiple transcription starting sites and some are induced in response to DCA. Only CD1687 is required for biofilm formation and the overexpression of CD1687 is sufficient to induce biofilm formation. Using RNAseq analysis, we showed that CD1687 affects the expression of transporters and metabolic pathways and we identified several potential binding partners by pull-down assay, including transport-associated extracellular proteins. We then demonstrated that CD1687 is surface exposed in *C. difficile*, and that this localization is required for DCA-induced biofilm formation. Given this localization and the fact that *C. difficile* forms eDNA-rich biofilms, we confirmed that CD1687 binds DNA in a non-specific manner. We thus hypothesize that CD1687 is a component of the downstream response to DCA leading to biofilm formation by promoting interaction between the cells and the biofilm matrix by binding eDNA.

npj Biofilms and Microbiomes (2023)9:24; https://doi.org/10.1038/s41522-023-00393-5

INTRODUCTION

Gastrointestinal infections are a major public health issue. In high-income countries, the Gram-positive spore-forming anaerobe *Clostridioides difficile* is the leading cause of nosocomial diarrhea and colitis in adults receiving antibiotic treatments[1,2]. Moreover, *C. difficile* infections (CDI) can be persistent, which is a major challenge in the management of CDI following anti-*C. difficile* antibiotic treatment. Recurrent CDI occur in more than 20% of patients that receive antibiotics to treat their first CDI episode and this rate increases following new episodes[3,4]. The causes of recurrences have not been fully elucidated. Recurrence can be caused by either reinfection with a new strain or relapse with the same strain, suggesting that *C. difficile* can persist in the gastrointestinal tract[5]. Relapses were initially correlated with *C. difficile* ability to sporulate during the infection and resist antibiotic treatment[6,7]. However, relapses are also hypothesized to be associated with the persistence of *C. difficile* as a biofilm[8,9]. Persistent and chronic infections caused by different pathogens are known to be associated with biofilm formation[10]. It is estimated that at least 60% of all nosocomial and chronic bacterial infections are biofilm-associated[11]. In support of this hypothesis, *C. difficile* was recently showed to integrate biofilms formed by the colonic microbiota and this biofilm acted as a reservoir for persistence and recurrence in a laboratory model of CDI[9].

Biofilms are structured communities of microorganisms associated with surfaces and encased in a self-produced extracellular matrix, which varies between bacterial species[12]. *C. difficile* can form biofilms as a single species or with other bacteria on various abiotic surfaces and several in vitro systems[9,13–15]. Moreover, *C. difficile* can integrate in vivo multi-species communities during a mouse infection, suggesting its ability to integrate mucosal biofilms[16]. In addition, *C. difficile* can form patchy glycan-rich biofilm-like structures in a mono-associated mouse model[17]. Although *C. difficile* can integrate multi-species biofilms in the gastrointestinal tract, there is limited knowledge on the biology of *C. difficile* biofilm formation in response to the gastrointestinal environment. During an infection, pathogens encounter several environmental factors including the presence of antibiotics, bile salts, osmotic pressure and varying nutrient sources and these are known to be important signals for biofilm formation during colonization[18,19]. Interestingly, *C. difficile* would face different challenges during dysbiosis as it changes the nutritional environment, bile salt metabolism, and osmotic and oxidative/nitrosative stresses[20]. Any of these factors could induce biofilm formation. For example, sub-inhibitory concentrations of antibiotics used to treat CDI enhance biofilm formation in vitro[21,22]. Furthermore, we recently demonstrated that sub-inhibitory concentrations of the secondary bile salt deoxycholate (DCA) enhances *C. difficile* biofilm formation[15]. In the DCA-induced biofilm, vegetative cells are protected from the toxicity of DCA as well as antibiotics and antimicrobial peptides[15]. We showed that biofilms induced by DCA are formed due to metabolic adaptation and reprogramming

[1]Institut Pasteur, Université Paris-Cité, UMR-CNRS 6047, Laboratoire Pathogenèse des Bactéries Anaérobies, F-75015 Paris, France. [2]Institut Pasteur, Université Paris-Cité, INSERM UMR1222, Unit of Antibodies in Therapy and Pathology, Paris, France. [3]Sorbonne Université, INSERM, CNRS, Centre d'Immunologie et des Maladies Infectieuses (CIMI-Paris), F-75013 Paris, France. [4]Plateforme de Biophysique Moléculaire, Institut Pasteur, CNRS UMR3528, Paris, France. [5]Plateforme Technologique Biomics, Institut Pasteur, Paris, France. [6]Plateforme Proteomic, Institut Pasteur, Paris, France. [7]Department of Biochemistry, Microbiology and Immunology, University of Saskatchewan, Saskatoon, SK, Canada. ✉email: bruno.dupuy@pasteur.fr

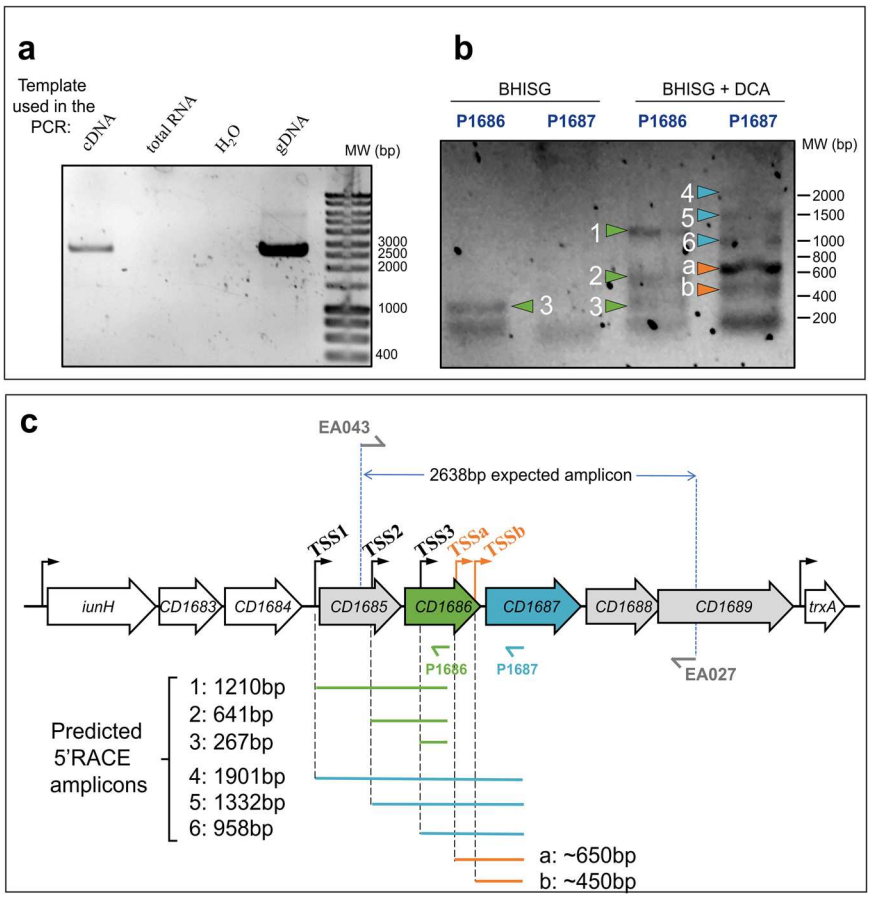

Fig. 1 The *CD1685-CD1689* cluster in *C. difficile* strain 630Δ*erm* forms an operon with multiple transcription start sites. a.RT-PCR performed with primers EA043 and EA027 (Supplementary Table 1) from various nucleic acid templates. cDNA was obtained using the EA027 primer with total RNA extracted from 48 h biofilms grown in BHISG supplemented with DCA (240 µM). **b** 5'RACE results from amplification of the poly-guanylated cDNA obtained, respectively, with the EA021 and EA018 primers (Supplementary Table 1), then the P1686 or P1687 primers along with the universal amplification primer (AAP) from the 5'RACE kit. The RNA was extracted from 48 h cell cultures grown under biofilm-inducing conditions (BHISG + 240 µM DCA) or non-biofilm-inducing conditions (BHISG). **c** Organization of the *CD1685-CD1689* cluster, the location of the primers used for RT-PCR and the amplicons from the 5'RACE results using the P1686 or P1687 primers (amplicon sizes were predicted from the TSS identified by Soutourina et al. (2020) and Fuchs et al. (2021). TSS: Transcriptional Start Site; cDNA: complementary DNA; gDNA: genomic DNA. Blots in **a** and **b** derive from the same experiments and were not processed.

that are dependent on the available nutrients and excreted metabolites. Overall, excreted pyruvate is critical for the induction of biofilm formation[23].

In addition to environmental factors inducing biofilm formation, several cellular factors, including cell surface components and regulators, have been shown to influence biofilm formation by *C. difficile*[24]. Among the genes that were upregulated in response to DCA, a gene encoding a lipoprotein (CD1687) is essential for biofilm formation in response to DCA[15]. The aim of this study was to characterize the role of CD1687 during biofilm formation by *C. difficile* in response to DCA. We demonstrated that CD1687 is exposed and active at the surface of the bacteria and that it binds DNA in vitro. This suggests that CD1687 acts as a protein anchoring the cells to the extracellular DNA (eDNA) present in the biofilm matrix.

RESULTS

Genes of the *CD1685-CD1689* locus form an operon but multiple transcription start site control their expression

In previous transcriptomic experiments, we observed that the majority of genes in the *CD1685-CD1689* cluster were upregulated in the 48 h DCA-induced biofilm formed by *C. difficile* strain 630Δ*erm*[15,23]. However, inactivation of CD1687 but not CD1688 prevented DCA-induced biofilm formation. To verify that the *CD1685-CD1689* genes formed an operon, RT-PCR experiments were performed with RNA extracted from cells grown under biofilm-inducing conditions (BHISG with 240 µM DCA). We observed a unique transcript spanning *CD1685* to *CD1689* suggesting the presence of at least one polycistronic mRNA at this locus (Fig. 1a). We then performed qRT-PCR to confirm that the five genes were upregulated at 48 h in the presence of DCA and only small difference in the fold changes were seen (Supplementary Figure 1a).

When looking at our previous RNAseq experiments, we observed a mapping bias of the sequencing reads favouring CD1687, CD1688, and CD1689 (Supplementary Figure 1b). Interestingly, recent analyses predicted three transcription starting sites (TSS) for the *CD1685-CD1689* locus: one upstream of the *CD1685* gene (TSS1), one upstream the *CD1686* gene (TSS2), and one in the coding sequence of *CD1686* (TSS3)[25,26] (Fig. 1c). To confirm the existence of multiple TSS, 5'-RACE experiments were performed with total RNA extracted from cells grown for 48 h in BHISG with DCA (i.e., biofilm-inducing) or without DCA (i.e., non-biofilm inducing). The initial reverse transcriptions were performed with two primers annealing either the coding sequence of *CD1686* (P1686) or the coding sequence of *CD1687* (P1687) (Fig. 1b, c). In the absence of DCA, only one amplicon was

observed, which is associated with the TSS inside *CD1686*. This amplicon was detectable when the P1686 primer was used but not with the P1687 primer. In the presence of DCA, we observed amplicons corresponding to the three predicted TSS with either primer (P1686 or P1687) and two additional amplicons were detected with P1687. This suggests that these two additional TSS (TSSa and TSSb; Fig. 1c) are active in the presence of DCA and one of these (TSSa) appears to be the most active of all TSS (Fig. 1b). Each amplicon was sequenced (Supplementary Table 2) and the location of TSS1, TSS2, and TSS3 closely matched their predicted location. However, high variation of the sequences for TSSa and TSSb made it difficult to identify their exact location. Overall, the transcription of the *CD1685-CD1689* operon is initiated from multiple TSS in the presence of DCA, suggesting that multiple factors are integrated to regulate the expression of the *CD1685-1689* operon to reflect the state of the bacterial population.

Overexpressing CD1687 induces biofilm formation in the absence of DCA

We previously inactivated *CD1687* using the Clostron system[15] but this approach is known to have some limitations. To confirm that only *CD1687* was required for biofilm formation, deletion of *CD1686*, *CD1687,* and *CD1688-CD1689* were generated (Supplementary Figure 2a). As observed before, only the deletion of *CD1687* negatively affected biofilm formation and complementation restore the phenotype (Supplementary Figure 2bc). Interestingly, deletion of *CD1686* removed TSS3, TSSa and TSSb suggesting that TSS1 and/or TSS2 are sufficient for the transcription of CD1687 in the presence of DCA resulting in biofilm formation.

Since CD1687 is required for DCA-induced biofilm formation and previously localized in the cell wall fraction[15], we hypothesized that CD1687 is a DCA-sensing protein. To test this hypothesis, we verified the ability of CD1687 to directly interact with DCA using surface plasmon resonance. We showed that CD1687 can interact with DCA (Supplementary Figure 3). However, the dissociation constant is high (Kd of 1.65 ± 0.58 mM), and the estimated stoichiometry of the interaction is 5 ± 1 DCA molecules for one CD1687 protein, which implies that the interaction is not specific.

Interestingly, we observed an increase in biofilm formation in the presence and, to a certain extent, in the absence of DCA when the Δ*1687* mutant was complemented with an inducible plasmid-borne CD1687 (pDIA6920) (Supplementary Figure 2C). Although the increase was not significant, it suggested that CD1687 could induce biofilm formation in the absence of DCA. To test this hypothesis, pDIA6920 was introduced in the wild-type strain and its ability to form biofilm in the absence of DCA was evaluated with and without the addition of the inducer ATC. When CD1687 was overexpressed, a stronger biofilm was detectable at 24 h and 48 h (Fig. 2). Taken together, our results suggest that CD1687 expression is critical for biofilm formation which does not require DCA for its activity.

CD1687 affects the expression of several transporter and metabolic priorities

As CD1687 is essential for DCA-induced biofilm formation and its overexpression can induce biofilm formation in the absence of DCA, we sought to identify genes whose expression is modified in the presence of CD1687 during the biofilm formation process. To do so, we performed two transcriptomic analyses: one comparing the wild type and the *Δ1687* mutant grown in presence of DCA for 24 h, and the second comparing the wild type containing either the CD1687 inducible plasmid (pDIA6920) or an empty vector, both grown in the absence of DCA and in the presence of ATC as an inducer for 24 h.

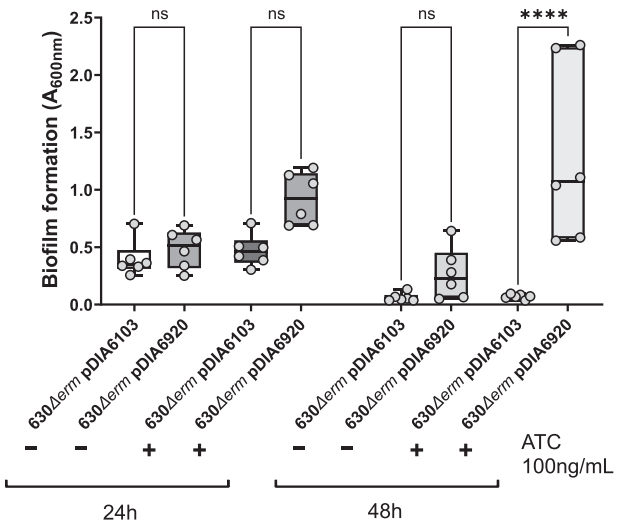

Fig. 2 Overexpression of CD1687 induces biofilm formation in the absence of DCA. Biofilms formation was assayed 24 h or 48 h after inoculation in BHISG +/− ATC (100 ng/mL) with the wild-type strain (630Δ*erm*) containing either a control empty vector (pDIA6103) or the vector allowing the expression of CD1687 under the inducible P_{tet} promoter (pDIA6920). Each data point represents an independent biological replicate composed of 2 to 4 technical replicates. The boxplot used to represent quantitative data figure the median, minimum, maximum, and upper and lower quartiles. Asterisks indicate statistical significance with a one-way ANOVA test followed by a Tukey's multiple comparison test (ns: not significant; ****$p < 0.0001$).

A total of 527 genes had a significant differential expression with a fold change <0.5 or >2 in the wild-type strain compared to the *Δ1687* mutant under biofilm-inducing conditions (+DCA) (Fig. 3). In the presence of DCA, CD1687 seems to mainly downregulate the cell wall reticulation (*vanY2Y3*) as well as several uncharacterized regulators (Supplementary Figure 4, Supplementary Table 3). There seems to be a shift in membrane transporters that may result in an increase in the importation of branched-chain amino acids, iron, and a change in sugar transport (Supplementary Table 3). In terms of metabolism, the cells shift from the utilization of succinate (*CD2338-CD2344*), the Wood-Ljungdahl pathway, and the biosynthesis of aromatic amino acids to the fermentation of acetoin, leucine, branched chain amino acids and glycine (Supplementary Figure 4, Supplementary Table 3).

When CD1687 was overexpressed, 809 genes were differentially expressed, 343 genes were upregulated and 466 were downregulated (Fig. 3). As described in Supplementary Figure 4, changes in gene expression indicate a shift in transporters, metabolism, and regulation. Specifically, the expression of several sugar transporters is increased whereas the expression of the branched chain amino acids, methionine, alanine, and glycine transporters is downregulated (Supplementary Table 3). In terms of metabolism, genes involved in acetoin utilization, Stickland fermentations involving aromatic amino acids or leucine, the Wood-Ljungdahl pathway, and the pentose phosphate pathway are upregulated as well as those involved in the biosynthesis of several amino acids such as histidine, isoleucine, valine, and cysteine (Supplementary Table 3). The *dltABCD* operon is upregulated suggesting an increase of the D-alanylation of the teichoic acids (*dltABCD*). Interestingly, we noted that the gene cluster encoding the flagellum and genes associated with sporulation were upregulated.

When we compared both transcriptomic analyses, few genes overlapped between both analyses. Only 69 genes changed in the same direction whereas 47 genes were regulated in opposite direction (Fig. 3). The remaining 1220 genes were differentially expressed only under either condition (Fig. 3). The genes that

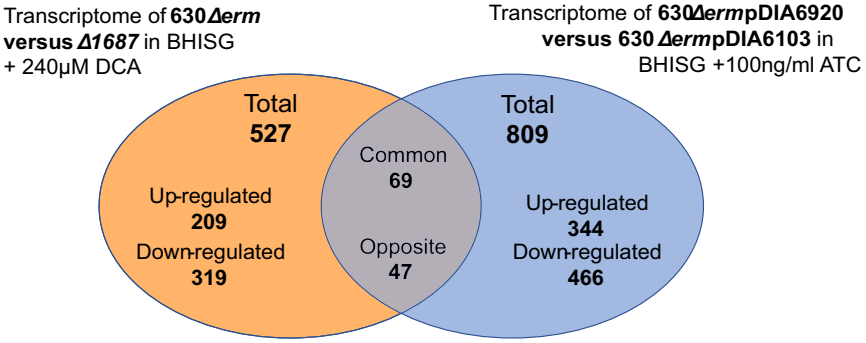

Fig. 3 Differences in gene expression in the two transcriptomics experiments. Venn diagram of the genes differentially regulated in the two transcriptomics experiments performed in this study (Supplementary Table 4).

were regulated in both conditions include those involved in cysteine synthesis (*cysE*, *cysK*), leucine utilization in Stickland fermentation (*hadABCI*), acetoin fermentation (*acoABCL*), cell wall proteins (*cwp9*, *cwp12*), some transporters (*alsT* transporting alanine or glycine, *rbsK* transporting ribose) and regulation (*sinRR'*). Overall, this suggests that CD1687 induces metabolic re-organization, including those occurring in response to DCA that leads to biofilm formation[23].

However, these changes do not fully align with our previous analyses[23]. We previously observed that DCA causes the up-regulation of gene involved in butanoate, lactate, and acetate fermentations, a shift in Stickland fermentations from the use of aromatic amino acids to the use of branched chain amino acids and glycine, and the down-regulation of genes involved in glycolysis, glucose intake, and sporulation[23]. These changes were not observed when CD1687 was overexpressed suggesting that CD1687 is not involved in those processes or does not mediate the immediate response to DCA. CD1687 is probably part of the downstream response and may interact with other proteins to promote these changes.

CD1687 interacts with several cell wall proteins

Given that CD1687 is a cell wall protein[15] that does not have a transmembrane domain but probably anchored to the cell surface membrane via a myristoyl anchor[27], we hypothesized that CD1687 induces transcriptional changes by transmitting external signals by interacting with membrane proteins. To find these potential proteins, we performed a pull-down assay using crude extracts of *C. difficile* cells overexpressing a C-terminal hexahistidine-tagged CD1687 in BHISG without DCA (Supplementary Table 5). They were compared to control extracts collected from a *C. difficile* mutant *Δ1687* with the empty vector in the same conditions. Among the 43 proteins identified only in the test samples and not in the control samples, which included the CD1687 protein (Supplementary Table 5), four are predicted to be membrane proteins and include a component of sugar transporter (CD2667) and a sodium symporter (CD2693). We also identified four proteins that belong to the large family of solute-binding proteins associated with ABC transporters and one nucleotide phosphodiesterase (CD0689). These five proteins could be involved in signal transport and cellular response leading adaptation in different environmental conditions[28,29]. Among the membrane proteins, we also found a putative lipoprotein (CD0747) and a LCP (LytR-CpsA-Psr) family protein (CD2766) involved in the cell wall polysaccharide assembly[30]. We noted that only one encoding gene of protein partners (CD0037) was upregulated in both transcriptomes (Supplementary Table 5), which is typically localized in the cytoplasm. Since most of the membrane proteins identified by the pull-down experiment are cell wall proteins involved in membrane transport, it is possible that CD1687 directly affects transport of different nutrients and is consistent with the observed effect in our transcriptomes.

CD1687 is exposed at the cell surface

Since CD1687 was detected in the cell wall fraction[15], we wondered whether CD1687 is exposed at the cell surface. To verify this, we performed epifluorescence microscopy analysis of *C. difficile* 630*Δerm* strain and its derivatives using rabbit polyclonal antibodies raised against CD1687. When grown 48 h in BHISG with or without DCA, no signal was observed in the *Δ1687* mutant confirming the specificity of our antibody (Fig. 4 and Supplementary Figure 5). For the wild-type strain, we observed a weak signal when grown in absence of DCA, confirming that this protein is expressed at low levels under non-biofilm-inducing conditions. In the presence of DCA, the signal was stronger in the presence of DCA, although the expression of CD1687 was not homogeneous in the population. In contrast, the signal for CD1687 is homogeneous in the population of the complemented *Δ1687* strain (Fig. 4 and Supplementary Figure 5). Since the cells were not permeabilized during the experiment and PFA does not significantly affect membrane permability[31], we concluded that CD1687 is exported to the cell wall and exposed at the cell surface.

Based on the cellular localization of CD1687, we wondered if the addition of the anti-CD1687 antibodies during growth could prevent DCA-induced biofilm formation. As shown in Fig. 5a, the addition of the anti-CD1687 polyclonal antibodies to cells grown under biofilm inducing conditions (BHISG + 240 µM DCA) strongly inhibited biofilm formation in a dose-dependent manner. No inhibitory effect was observed when an unpublished non-specific antibody was used at the highest concentration of anti-CD1687 that inhibited biofilm formation (data not shown). In addition, bacterial growth was unaffected by the antibodies, regardless of the concentration used in the biofilm assays (Fig. 5b). Therefore, inhibiting extracellular function of CD1687 prevents biofilm formation, indicating both that CD1687 is exposed at the cell surface and that its presence at the surface of the cell wall is critical for DCA-induced biofilm formation.

To get some insights on the structure-function of CD1687, we used the software AlphaFold2[32] to predict the 3D protein structure of CD1687. As shown in Fig. 5c, CD1687 has an alpha helix N-terminal signal peptide and two putative beta domains. To search for possible functions of the beta domains, the putative structure of CD1687 was analyzed in the Ekhidna database through the Dali server[33], but no function was detected. Since the function of CD1687 could be assigned to one of the two beta domains, we complemented the *Δ1687* mutant by overexpressing CD1687 with either one of the two domains removed and growing these strains under biofilm-inducing conditions (BHISG + 240 µM DCA. Complementation of the mutant was not observed,

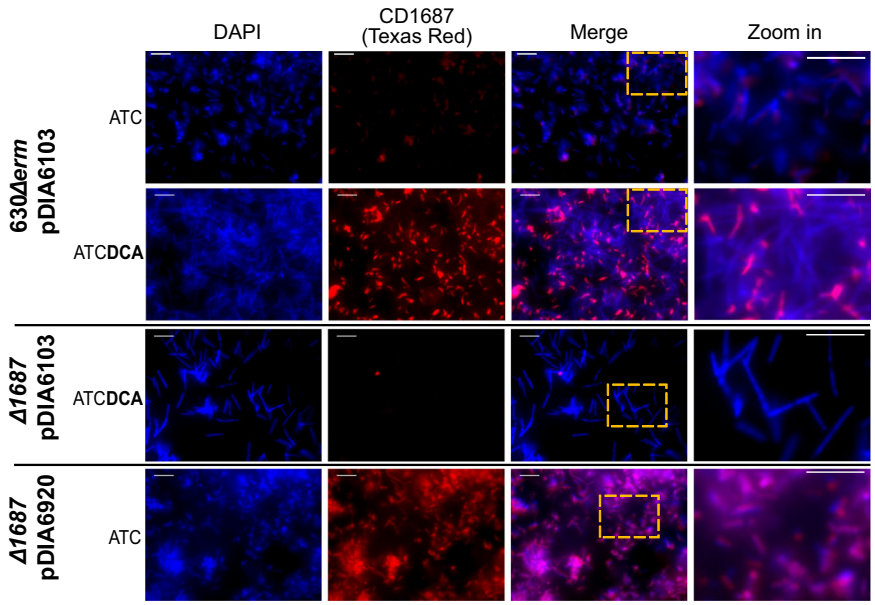

Fig. 4 CD1687 localizes at the cell surface of *C. difficile* and displays heterogenous distribution within the biofilm. In situ epifluorescence microscopy analysis was performed on 48 h biofilms grown in BHISG + ATC (100 ng/mL) either in the presence or absence of DCA (240 µM) as indicated. The strains tested were the wild-type strain (630Δ*erm*) carrying the control vector pDIA6103 and with the Δ*1687* strain carrying the plasmid with an inducible CD1687 (pDIA6920) or the control plasmid (pDIA6103). DNA is stained with DAPI (blue) and CD1687 is labeled with specific anti-CD1687 rabbit antibodies detected with a TexasRed-conjugated goat anti-rabbit antibody (red). Pictures are representative of three biological replicates and were taken with a Nikon Eclipse Ti inverted microscope (Nikon, Japan). Scale bar: 10 µm.

indicating that *C. difficile* needs both beta domains of the CD1687 to form DCA-induced biofilms (Fig. 5d).

CD1687 binds to DNA in a non-specific manner

Since we did not identify a potential function from the CD1687 structure, we sought to determine if CD1687 has a DNA-binding activity as observed for *Staphylococcus aureus* lipoproteins that promote eDNA-dependent biofilm formation[34]. Since the *C. difficile* biofilm matrix is mainly composed of eDNA[15], we tested the ability of CD1687 to bind to DNA by performing an electromobility shift assay (EMSA). When the purified CD1687 protein was incubated with the *E. coli* DNA plasmid pUC9 or a PCR-generated amplicon produced from *C. difficile* DNA (from a sequence in the region of *CD1438*), we observed that the migration of the DNA was shifted by the presence of the CD1687 and increasing CD1687 concentration correlates with more retention (Fig. 6a, b). However, we did not observe a shift when CD1687 was heat-inactivated or if BSA was used as control at the highest concentration of CD1687 that shift DNA fragments. To test whether CD1687 allows the anchoring of the bacteria to eDNA, we performed a DNA-binding experiment using whole *C. difficile* bacteria (Fig. 6d). We covalently linked the same amplicon used in EMSA (Fig. 6b) to a microarray plate before adding the *Δ1687 pDIA6920* strain (Supplementary Table 1) producing or not CD1687. We then counted the bacteria linked to DNA after adding DNAse I in the wells (Fig. 6d). We found that bacteria adhered more to DNA in the wells when CD1687 was produced than when DNA or CD1687 was absent (Fig. 6c). Therefore, with this experiment and the EMSA results, we conclude that CD1687 can bind to eDNA in a non-specific manner. This binding activity likely allows *C. difficile* to anchor itself to eDNA in the biofilm.

DISCUSSION

In this study, we confirmed that only *CD1687* in the *CD1685-CD1689* cluster was required for DCA-induced biofilm formation and this required the localization of CD1687 at the cell surface.

In fact, this protein is detected in the cell wall[15] as well as on the cell surface (Figs. 4 and 5a) yet it has been detected and described as a membrane-anchored lipoprotein[27]. The small size of the protein and its predicted structure imply that this protein should be closer to the membrane than to the surface of the cell wall. Since CD1687 can be easily recovered from the cell wall fraction, this suggests that there are possible as yet undescribed post-translational modifications on CD1687 that would cleave its myristoyl anchor, allowing the protein to bind to the cell wall. We noted that there is a significant heterogeneity in response to DCA for the expression and localization of CD1687 at cell surface in the population as observed by microscopy (Fig. 4 and Supplementary Figure 5). This would explain the relatively low transcriptional level of the *CD1685-CD1689* gene cluster at the population level[15]. Interestingly, the more CD1687 is homogeneously expressed in the cell population, the greater the biofilm formed (Fig. 4, Supplementary Figure 2c). To our knowledge, expression heterogeneity of critical biofilm components has not yet been reported in *C. difficile*. Phenotypic heterogeneity in biofilms is well characterized in several other bacterial species resulting in phenotypic diversification and division of labor in a clonal bacterial population[35]. For example, a subpopulation of cells synthesize the exopolysaccharides matrix during biofilm formation in *B. subtilis*[36]. Phenotypic heterogeneity has been described in planktonic cells of *C. difficile* and this affected the expression of the flagellum and toxins[37]. In this case, heterogeneity is controlled by a specific DNA recombination event mediated by RecV[38] and the Rho factor[39]. In addition, *C. difficile* colony morphology is also subjected to phenotypic heterogeneity resulting in changes in bacterial physiology and pathogenesis and this occurs through phase variation of the CmrRST signal transduction system expression[40,41].

Given that CD1687 forms an operon with a two-component regulatory system (CD1688-1689) and that CD1687 is a cell wall protein, we first hypothesized that CD1687 was involved in signal transduction leading to transcriptional modifications in response of DCA. However, CD1687 did not bind DCA, which eliminates the putative role of CD1687 as a DCA-sensing protein. Furthermore,

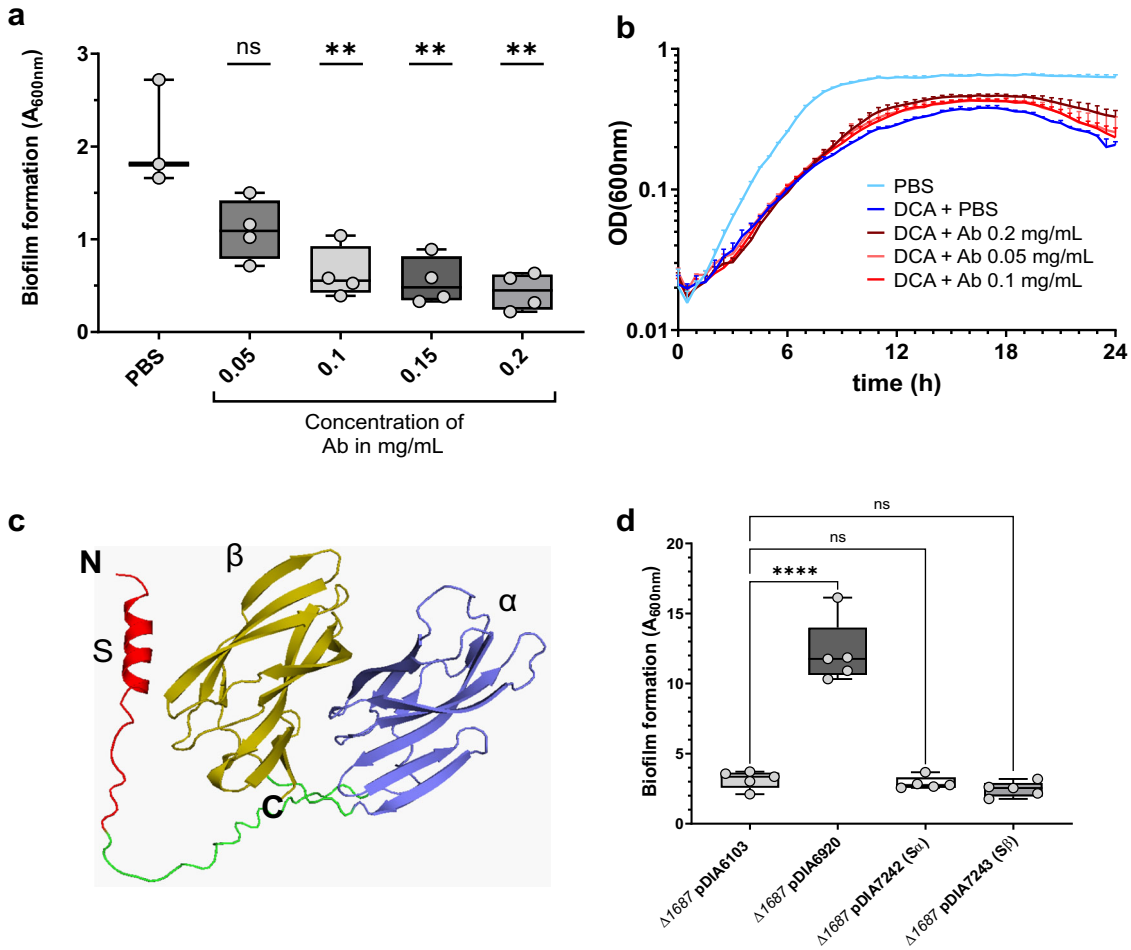

Fig. 5 DCA-induced biofilm formation is inhibited in the presence of anti-CD1687 antibodies. a Biofilm formation of the 630*Δerm* strain was assayed 48 h in BHISG with DCA (240 µM) cultures in presence of different concentration of anti-CD1687 rabbit antibodies (0.05 mg/mL to 0.2 mg/mL). **b** Growth kinetics (OD_{600nm}) of the WT (630*Δerm*) in BHISG medium with PBS or DCA supplemented with different concentrations of anti-CD1687 rabbit antibodies (0.05 mg/mL to 0.2 mg/mL). Ab: antibody; nsAb: non-specific antibody. **c** The alphafold2 predicted structure of CD1687 show a N-terminal signal peptide S (red) connected to the α beta domain (purple) by a linker peptide (green), with another similar β beta domain (yellow) in the C-terminal region. **d** 48 h biofilms form by various *Δ1687* strain complemented with an empty vector (pDIA6103) or plasmids overexpressing the full-length CD1687 (pDIA6920) or truncated CD1687 lacking either one of the two domains removed (pDIA7242 and pDIA7243, Supplementary Table 1) grown in BHISG with ATC (100 ng/mL) and DCA (240 µM). Each data point represents an independent biological replicate composed of 2 to 4 technical replicates. The boxplots used to represent quantitative data figure the median, minimum, maximum, and upper and lower quartiles. Asterisks indicate statistical significance with a one-way ANOVA test followed by Dunnett's multiple comparison test (**a**) (ns: not significant; $^{**}p < 0.01$) or a Tukey's multiple comparison test (**d**) (ns: not significant; $^{****}p < 0.001$).

with the exception of sporulation, genes regulated by CD1688[42] have limited overlap suggesting that CD1687 may not be part of the CD1688-CD1689 signaling cascade. This is consistent with the absence of CD1689 and CD1688 in our pull-down assay. However, several solute-binding proteins and transporter-associated proteins were isolated in a pull-down assay. This and the transcriptional analysis provide evidence that CD1687 influences the metabolism of *C. difficile*. In support of this, regulators (Spo0A, CodY, and SinRR') that manage metabolic priorities during growth phases, were differentially regulated when CD1687 was overexpressed[43–45]. Furthermore, the expression of the gene encoding toxin and those involved in sporulation were also affected and these processes are known to be dependent on the metabolic state of *C. difficile*. When we compared the genes differentially regulated in the absence of CD1687 under DCA-inducing conditions to those differentially regulated when CD1687 was overexpressed in the absence of DCA, there were only 69 common genes, which included genes involved in different metabolic pathways and transport. However, these changes in metabolism-associated genes did not overlap with our previous analyses on gene expression during DCA-induced biofilm formation[23], suggesting that CD1687 is not part of the immediate response to DCA and probably plays a role in the downstream response. Taken together, our data suggest that CD1687 helps reorganize metabolic priorities in response to DCA but this hypothesis alone does not explain the role of CD1687 in the biofilm formation without DCA. Therefore, CD1687 may have additional roles.

Interestingly, many proteins found at the bacterial cell surface interact with eDNA found in the biofilm matrix and this contributes to the organization and structural stability of the biofilm[46]. Membrane lipoproteins have already been shown to directly interact with eDNA and participate in biofilm architecture. In *S. aureus*, several membrane-attached lipoproteins interacting with the eDNA of the biofilm matrix have been identified as promoting *S. aureus* biofilm formation[34]. Here we confirmed that CD1687 interacts in vitro with DNA in a non-specific manner both with the purified protein and the bacteria producing CD1687, whose level of production is sufficient to increase bacterial

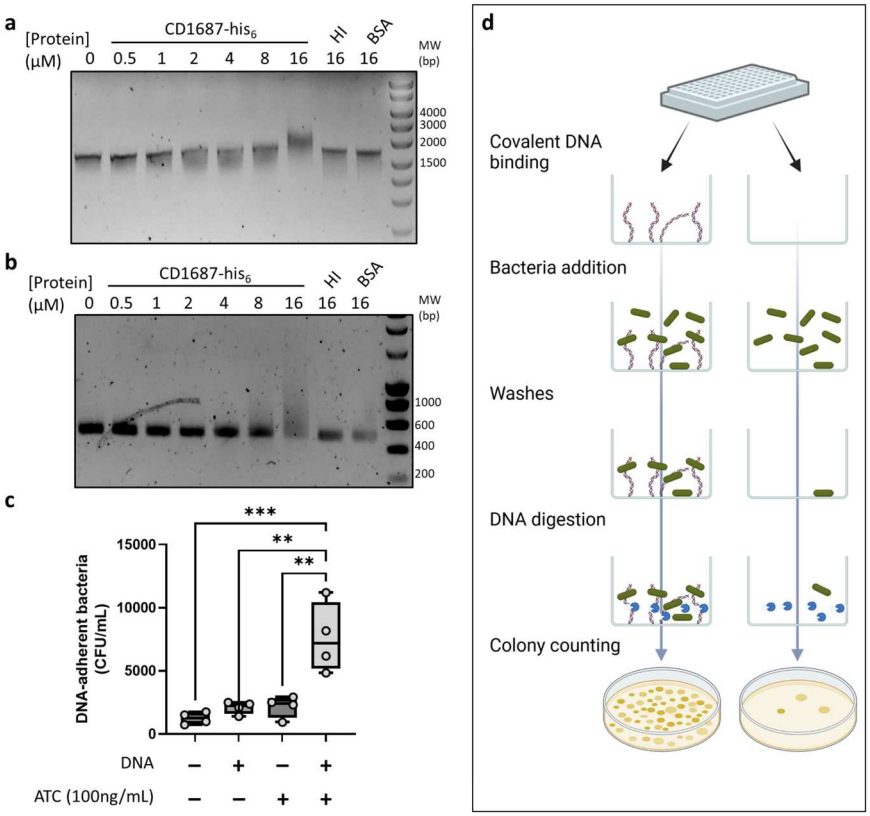

Fig. 6 CD1687 binds DNA and shifts DNA migration. Electrophoretic Mobility shift assay (EMSA) was performed with **a** *E. coli* plasmid pUC9 or **b** *C. difficile* DNA (450 bp PCR-amplicon) mixed with various concentrations of CD1687 (up to 16 μM), with 16 μM of heat-inactivated (HI) CD1687 or BSA used as controls. **c** *C. difficile* CFUs measured from the adhesion assay. The *Δ1687 pDIA6920* strain was used expressing or not *CD1687* in response to ATc as described in (**d**). Schema of the adhesion assay. We compared the adhesion of bacteria either expressing CD1687 or not in wells that contain or not covalently bound DNA. This schema was made with biorender.com. The boxplot used to represent quantitative data figure the median, minimum, maximum, and upper and lower quartiles. Each data point represents an independent biological replicate. Asterisks indicate statistical significance with a one-way ANOVA test followed by Dunnett's multiple comparison test (**$p < 0.01$; ***$p < 0.001$). Blots in **a** and **b** derive from the same experiments and were not processed.

adhesion to eDNA. These results support the hypothesis that CD1687 acts as an eDNA-binding protein during biofilm formation by creating anchor points for eDNA on the cell surface. Similar to our observation with CD1687, overexpressing eDNA-binding proteins in *S. aureus* resulted in an increased retention of surface eDNA and an enhanced biofilm biomass. However, deleting the *S. aureus* lipoproteins had minimal impact on biofilm formation but biofilm porosity increase indicating that interactions of the lipoprotein with eDNA contribute to overall biofilm structure. Unlike the lipoprotein found in *S. aureus*, a deletion or inactivation of *CD1687* abolished biofilm formation[34]. CD1687 interacting with eDNA seems to be an essential part of DCA-induced biofilm formation. Other structures may also interact with eDNA. Recently, two minor subunits (PilW and PilJ) of the *C. difficile* T4P were shown to directly interact with eDNA to promote biofilm formation[47]. Neither subunit have a predicted DNA-binding motif as observed with CD1687. The T4P is a structure that promotes biofilm formation in the absence[48,49] or presence of DCA[23]. In the presence of DCA, PilW is upregulated but is not required for biofilm formation[15,23]. Furthermore, the *pilW* gene was differently regulated in our transcriptome; upregulated in the WT vs *Δ1687* with DCA analysis (significantly but below the threshold) and downregulated in the overexpressed CD1687 vs WT without DCA analysis. Therefore, CD1687 and the T4P may have complementary role and the lack of eDNA-binding by one of these components may change the behavior of *C. difficile* during biofilm formation.

Despite the potential role of CD1687 as an eDNA-binding protein and in metabolism, we cannot exclude that the overexpression of CD1687 modifies the properties of the cell wall through the interactions of CD1687 with other membrane proteins and transporters (Supplementary Table 5). These interactions could be detected by different sensors, which would activate a feedback loop to modify the cell wall and the composition of the cell surface proteins. For example, the *dltABCD* operon was upregulated when CD1687 was overexpressed in the absence of DCA. The DltABCD proteins are responsible for the D-alanylation of teichoic acids, which changes the electrical charges of the cell wall and surface[50]. Overexpression of CD1687 also affected cell morphology; in response to DCA, cells expressing high levels of CD1687 show reduced size and shape distortion (Fig. 4 and Supplementary Figure 5). Overall, the overexpression of CD1687 may have downstream effects on the physiology of *C. difficile* and these changes may contribute to biofilm formation.

Finally, our hypothesis is that the mechanism for biofilm formation in the presence of DCA is different than the mechanism when DCA is absent and CD1687 is overexpressed. In the presence of DCA, we know that *C. difficile* goes through a metabolic reorganization[23] and, based on our data, CD1687 would help with metabolic priorities for long-term adaptation. Once there is enough eDNA, CD1687 would interact with eDNA binding and serve as an anchor point. When CD1687 is overexpressed independently of DCA, it increases homogeneity of CD1687 surface localization in the population and serves as multiple anchoring sites for eDNA resulting in a strongly adherent biofilm. As observed in *S. aureus*, other lipoproteins may bind eDNA in *C. difficile* and several are upregulated in response to

DCA[23]. Unlike the lipoproteins characterized in *S. aureus*, the lipoprotein CD1687 probably has a critical function in metabolism in response to DCA and other lipoproteins do not provide functional redundancy. This highlights the importance of CD1687 in promoting biofilm formation. More research will be needed to understand the role and the contribution of these other lipoproteins to biofilm.

METHODS

Bacterial strains and culture conditions

Bacterial strains and plasmids used in this study are listed in Supplementary Table 1 *C. difficile* strains were grown anaerobically (5% H2, 5% CO_2, 90% N_2) in TY medium (30 g/L tryptone, 20 g/L yeast extract) or in BHISG medium (BHI with 0.5% (w/v) yeast extract, 0.01 mg/mL cysteine and 100 mM glucose) and supplemented with cefoxitin (250 µg/ml), D-cycloserine (8 µg/ml) and thiamphenicol (15 µg/ml) when necessary. In addition, 100 ng/mL of anhydrotetracycline (ATC) was added to induce the P_{tet} promoter of pRPF185 vector derivatives in *C. difficile*. *E. coli* strains were grown in LB broth supplemented with chloramphenicol (15 µg/mL) and ampicillin (100 µg/mL).

Biofilm assays

Overnight cultures of *C. difficile* grown in TY medium with appropriate antibiotics were diluted to 1/100 into fresh BHISG containing the desired supplements (240 µM DOC, 100 ng/mL ATC or both). Depending on the assay, the diluted cultures were then aliquoted either with 1 mL per well in 24-well plates (polystyrene tissue culture-treated plates, Costar, USA) or with 200 µL in 96-well plates (polystyrene black tissue-culture-treated plates, Greiner Bio One, Austria). The plates were incubated at 37 °C in an anaerobic environment for 48 h. Biofilm biomass was measured in the 24-well plates using an established method[15]. For biofilm assays in 96-well plates used for microscopy, spent medium was carefully removed by pipetting and 200 µL PBS supplemented with 4% of paraformaldehyde (PFA) were added. Plates were incubated for an hour at room temperature and the media was then carefully removed by pipetting before adding PBS for 48 h at 4 °C. In all assays, sterile medium was used as a negative control and a blank for the assays.

Gene deletion in *C. difficile*

Gene deletion in *C. difficile* was performed as described in Peltier et al.[51]. Regions upstream and downstream of the genes of interest were PCR-amplified using primer pairs described in Supplementary Table 1. PCR fragments and linearized pDIA6754[51] were mixed and assembled using Gibson Assembly (NEB, France) and transformed by heat shock in *E. coli* NEB 10β strain. The plasmid constructions were verified by sequencing and plasmids with the right sequences were transformed in *E. coli* HB101 (RP4). The resulting strains were used as donors in a conjugation assay with the relevant *C. difficile* strains. Deletion mutants were then obtained using a counter-selection as described in Peltier et al.[51].

Protein extraction from *C. difficile* and pull-down assay

C. difficile strains were anaerobically grown for 48 h in 20 mL BHISG cultures with ATC in tubes. Cells and biofilms were harvested by centrifugation (10 min; 14,000 × *g*; 4 °C) and washed in a cold phosphate buffer (50 mM; pH = 7.0; 4 °C). Cells were then resuspended in 1 ml of the same phosphate buffer containing the purified catalytic domain of the endolysin CD27L (3 µg/mL) and suspension was incubated 1 h at 37 °C to lyse the bacterial cells. The total extracts were then vortexed for 1 min and used for pull-down assay with Ni-NTA beads as described below for CD1687 purification from *E. coli* expression. Five biological replicates of each condition were used in the pull-down assay (Supplementary Table 5).

Production and purification of CD1687 and anti-CD1687 antibodies

E. coli strain Bli5 containing a pET20-derived plasmid carrying the *CD1687* gene (Supplementary Table 1) was used to overexpress hexa-histidine-tagged CD1687 protein without its signal peptide. Cells were grown overnight at 37 °C in LB supplemented with glucose (1% w/v) and antibiotics (ampicillin 100 µg/mL and chloramphenicol 15 µg/mL). The overnight culture was transferred (1/100) in 1 L of the same medium and incubated at 37 °C. Once the culture reached an OD_{600nm} of 0.5, IPTG was added (final concentration 0.1 mM) and the culture was incubated for an additional 3 h. Cells were then harvested by centrifugation (5000 × *g*, 10 min, 4 °C) and the pellet was washed with cold PBS. After centrifugation, the supernatant was discarded and resulting pellet was frozen at −20 °C. The pellet was then resuspended in 15 mL of lysis buffer (50 mM sodium phosphate pH = 8.0; 300 mM NaCl) and sonicated. After centrifugation (5000 × *g*, 10 min, 4 °C), the supernatant was collected and mixed with Ni-NTA beads and incubated one hour at 4 °C. The beads were then transferred to an elution column and washed with washing buffer (50 mM sodium phosphate pH = 8.0; 300 mM NaCl; 10 mM imidazole). Proteins were eluted with 2 ml of sodium phosphate buffer (50 mM, pH = 8.0) supplemented with 300 mM NaCl and a gradient of imidazole ranging from 50 mM to 500 mM. Eluted proteins were analyzed by western immunoblotting and fractions containing CD1687 were dialyzed in TAE buffer (Tris-base (20 mM); acetic acid (10 mM); EDTA (0.5 mM); pH = 8.5) using Slide-A-Lyzer dialysis units (Thermo Fisher Scientific, USA). To raise polyclonal anti-CD1687 antibodies, two female rabbits (New Zealand White) were injected four times with 50 µg of purified CD1687(His_6) (0.5 mL of antigen with 0.5 mL of complete Freund's adjuvant at D0, D14, D28, and D42) with the Covalab company (France). Antibodies were purified at D53 of immunization.

Real-time surface plasmon resonance binding assay

All experiments were performed on a Biacore T200 instrument (Cytiva, USA) equilibrated at 25 °C in buffer TAE (20 mM Tris base, acetic acid 10 mM, EDTA 0.5 mM, pH = 8.5). CD1687(His_6) (100 µg/ml) was captured for 600 s at 2 µl/min on an $NiCl_2$-loaded NTA sensorchip, reaching a surface density of 1000–1200 RU (resonance units; 1RU ≈ 1 pg/mm^2). DCA (16–2000 µM) was then injected at 10 µl/min for 120 s, simultaneously on the CD1687 surface and on an empty reference chip from which non-specific signals were subtracted.

Protein sequencing assay via mass spectrometry

Protein digestion. Proteins were reduced using 5 mM TCEP for 30 min at room temperature. Alkylation of the reduced disulfide bridges was performed using 10 mM iodoacetamide for 30 min at room temperature in the dark. Proteins were then digested in two steps, first with 250 ng r-LysC Mass Spec Grade (Promega) for 4 h at 30 °C then samples were diluted below 2 M urea with 100 mM Tris HCl pH 8.5 and 500 ng Sequencing Grade Modified Trypsin was added for the second digestion overnight at 37 °C. Proteolysis was stopped by adding formic acid (FA) at a final concentration of 5%. The resulting peptides were cleaned using AssayMAP C18 cartridges on the AssayMAP Bravo platform (Agilent) according to the manufacturer's instructions. Peptides were concentrated to dryness and resuspended in 2% acetonitrile (ACN) and 0.1% FA just prior to LC-MS injection.

LC-MS/MS analysis. LC-MS/MS analysis was performed on a Q ExactiveTM Plus Mass Spectrometer (Thermo Fisher Scientific)

coupled with a Proxeon EASY-nLC 1200 (Thermo Fisher Scientific). 500 ng of peptides were injected onto a home-made 37 cm C18 column (1.9 µm particles, 100 Å pore size, ReproSil-Pur Basic C18, Dr. Maisch GmbH, Ammerbuch-Entringen, Germany). Column equilibration and peptide loading were done at 900 bars in buffer A (0.1% FA). Peptides were separated with a multi-step gradient from 3 to 6% buffer B (80% ACN, 0.1% FA) in 5 min, 6 to 31% buffer B in 80 min, 31 to 62% buffer B in 20 min at a flow rate of 250 nL/min. Column temperature was set to 60 °C. MS data were acquired using Xcalibur software using a data-dependent method. MS scans were acquired at a resolution of 70,000 and MS/MS scans (fixed first mass 100 *m/z*) at a resolution of 17,500. The AGC target and maximum injection time for the survey scans and the MS/MS scans were set to 3E6, 20 ms and 1E6, 60 ms, respectively. An automatic selection of the 10 most intense precursor ions was activated (Top 10) with a 30 s dynamic exclusion. The isolation window was set to 1.6 *m/z* and normalized collision energy fixed to 27 for HCD fragmentation. We used an underfill ratio of 1.0% corresponding to an intensity threshold of 1.7E5. Unassigned precursor ion charge states as well as 1, 7, 8, and >8 charged states were rejected and peptide match was disable.

Protein identification and quantification

Acquired Raw data were analyzed using MaxQuant software version 2.1.1.0[52] using the Andromeda search engine[53,54]. The MS/MS spectra were searched against the *C.difficile* 630 database (3957 entries).

All searches were performed with oxidation of methionine and protein N-terminal acetylation as variable modifications and cysteine carbamidomethylation as fixed modification. Trypsin was selected as protease allowing for up to two missed cleavages. The minimum peptide length was set to 7 amino acids and the peptide mass was limited to a maximum of 4600 Da. The false discovery rate (FDR) for peptide and protein identification was set to 0.01. The main search peptide tolerance was set to 4.5 ppm and to 20 ppm for the MS/MS match tolerance. Second peptides were enabled to identify co-fragmentation events. A false discovery rate cut-off of 1% was applied at the peptide and protein levels. The mass spectrometry proteomics data have been deposited to the ProteomeXchange Consortium via the PRIDE partner repository with the dataset identifier PXD038282. The statistical analysis of the proteomics data was performed as described previously[55]. Briefly, four biological replicates were acquired per condition. To highlight significantly differentially abundant proteins between two conditions, differential analyses were conducted through the following data analysis pipeline: (1) deleting the reverse and potential contaminant proteins; (2) keeping only proteins with at least two quantified values in one of the two compared conditions to limit misidentifications and ensure a minimum of replicability; (3) log2-transformation of the remaining intensities of proteins; (4) normalizing the intensities by median centering within conditions thanks to the normalizeD function of the R package DAPAR[56], (5) putting aside proteins without any value in one of both compared conditions: as they are quantitatively present in a condition and absent in another, they are considered as differentially abundant proteins and (6) performing statistical differential analysis on them by requiring a minimum fold-change of 2 between conditions and by using a LIMMA t test[57,58] combined with an adaptive Benjamini–Hochberg correction of the *p* values thanks to the adjust.p function of the R package cp4p[59]. The robust method of Pounds and Cheng was used to estimate the proportion of true null hypotheses among the set of statistical tests[60]. The proteins associated with an adjusted *p* value inferior to an FDR level of 1% have been considered as significantly differentially abundant proteins. Finally, the proteins of interest are therefore the proteins that emerge from this statistical analysis supplemented by those being quantitatively absent from one condition and present in another.

RNA isolation, qRT PCR

Cells were grown in 24-well plates and 10 wells per plate were used to produce one replicate for one condition. For biofilm conditions, the supernatant was removed by inverting the plate and the biofilms were carefully washed twice then resuspended in 3 mL of PBS. In other conditions, the whole bacterial population was collected and cells were harvested by centrifugation (10 min, 8000 × *g*, 4 °C) and resuspended in 1 ml of PBS. Cell suspensions in PBS were finally centrifuged (10 min, 8000 × *g*, 4 °C) and the pellets were frozen at −80 °C until further use. Extraction of total RNA from the bacteria and qRT PCR assay were performed as described in Saujet et al.[43].

Whole transcriptome sequencing and analysis

Transcriptome analysis for each condition was performed using 4 independent RNA preparations. Libraries were constructed using the Illumina Stranded Total RNA Prep Ligation with RiboZero Plus (Illumina, USA) kit. The ribodepletion step was carried using specific probes synthesized specifically to target *C. difficile* ribosomal sequences (Supplementary Table 1). After ribodepletion, libraries were prepared according to the supplier's recommendations. RNA sequencing was performed on the Illumina NextSeq 2000 platform using 67 bases for a target of 10 M reads per sample.

Electromobility shift assays (EMSA)

Only freshly purified CD1687 from *E. coli* were used in these assays. CD1687 (from 0.5 µM to 16 µM) was incubated with DNA (pUC9 or PCR product) in 10 µl of sodium phosphate buffer (50 mM; pH = 8.0) for 30 min at room temperature. Samples were loaded and migrated on TAE buffered agarose gels (1% w/v) for 90 min at 100 V. Controls were performed with CD1687 denatured at 100 °C for 15 min before the assay. Gels were stained with ethidium bromide and pictures were taken with an Amersham ImageQuant 800 (Cytiva). The pUC9 plasmid was prepared from *E. coli* stock using the Nucleospin plasmid kit (Macherey-Nagel, Germany) and the PCR amplicon used was generated using *C. difficile* 630*Δerm* as the DNA template and primers targeting the region of *CD1438* (Supplementary Table 1). gDNA was extracted from cell culture using the DNeasy Blood & Tissue Kit (QIAGEN, Netherlands).

5'RACE experiment

A 5'RACE was performed using the 5' RACE System for Rapid Amplification of cDNA Ends, version 2.0 kit (Invitrogen, USA). Briefly, cDNA was generated by reverse transcription from total RNA extract followed by degradation of the RNA. dC-tailing was then performed with the cDNA and the resulting dC-tailed DNA was used as the template in PCR as described in the kit instructions. The PCR products were analyzed by agarose gel electrophoresis (1% agarose in TAE buffer). To identify the transcription start sites, PCR products were inserted into the pGEM-T easy vector kit as described by the manufacturer (Promega, USA). Insert were then PCR-amplified and the resulting PCR products were sequenced.

Epifluorescence microscopy

For microscopy, 48 h biofilms were generated in 96-well plates (black, Greiner) as described above, washed and 50 µl of the polyclonal anti-CD1687 antibodies diluted in PBS (400 ng/mL) was then added to each well and incubated overnight at 4 °C. The wells were carefully washed twice with PBS followed by the

addition of a solution containing DAPI (1/1000 dilution) and secondary antibodies (goat anti-rabbit conjugated with Texas Red; 1/5000 dilution; Invitrogen, cat: T-2767) in PBS. The plates were incubated at room temperature for 2 h. Wells were then carefully washed with PBS and 200 µl of fresh PBS was added for data acquisition. Images were taken with the Nikon Eclipse Ti inverted microscope (Nikon, Japan).

Bacteria-DNA binding assay

A 433 bp amplicon modified at one end with a C6 amine and corresponding to the region of the *CD1438* gene was used to covalently coat a DNA-BIND Surface 96-well plate (Corning, USA) according to the manufacturer's guidelines. Briefly, 100 µL of a 250 nM solution of amplicon prepared in the binding buffer (50 mM sodium phosphate buffer pH = 8.5; 1 mM EDTA) were placed in the wells and the plate was incubated overnight at 4 °C. Control wells were made using only the binding buffer. Then, the wells were washed three times with 200 µL of PBS and the plate was introduced in the anaerobic chamber. Exponential phase cultures of the *Δ1687pDIA6920* strain (Supplementary Table 1) grown in BHISG and appropriate antibiotics with or without the ATc inducer, were diluted to an OD(600 nm) of 0.5 and 200 µL of these bacterial suspensions were placed in the wells of DNA-coated plate. The plate was incubated anaerobically at 37 °C for 20 min and then washed twice with BHISG before adding 200 µL of BHISG containing 25 µg of DNAse I in each well. The plate was incubated anaerobically for 20 min at 37 °C and bacteria were counted from suspension on BHI agar plates. The PCR amplification to obtain the modified amplicon was performed with chromosomal DNA of the *C. difficile* 630*Δerm* with primers targeting the region of *CD1438* (Supplementary Table 1).

Statistical analysis

The biofilm assays, bacteria-DNA binding assay, and RT-qPCR were analyzed using a one-way ANOVA test followed by either a Tukey's multiple comparison test or a Dunnett's multiple comparison test.

Reporting summary

Further information on research design is available in the Nature Research Reporting Summary linked to this article.

DATA AVAILABILITY

RNA-Seq data generated in this study are available in the NCBI-GEO with the accession number GSE218475. The mass spectrometry proteomics data have been deposited to the ProteomeXchange Consortium via the PRIDE partner repository with the dataset identifier PXD038282.

Received: 6 December 2022; Accepted: 27 April 2023;
Published online: 11 May 2023

REFERENCES

1. Rupnik, M., Wilcox, M. H. & Gerding, D. N. *Clostridium difficile* infection: new developments in epidemiology and pathogenesis. *Nat. Rev. Microbiol.* **7**, 526–536 (2009).
2. Giles, J. & Roberts, A. in *Advances in Protein Chemistry and Structural Biology* Vol. 129 (ed. Donev, R.) 215–245 (Academic Press, 2022).
3. Barbut, F. et al. Epidemiology of recurrences or reinfections of *Clostridium difficile*-associated diarrhea. *J. Clin. Microbiol* **38**, 2386–2388 (2000).
4. Guery, B., Galperine, T. & Barbut, F. *Clostridioides difficile*: diagnosis and treatments. *BMJ* **366**, l4609 (2019).
5. Sachsenheimer, F. E. et al. Genomic and phenotypic diversity of *Clostridium difficile* during long-term sequential recurrences of infection. *Int. J. Med. Microbiol.* **308**, 364–377 (2018).
6. Deakin, L. J. et al. The *Clostridium difficile* spo0A gene is a persistence and transmission factor. *Infect. Immun.* **80**, 2704–2711 (2012).
7. Castro-Córdova, P. et al. Entry of spores into intestinal epithelial cells contributes to recurrence of *Clostridioides difficile* infection. *Nat. Commun* **12**, 1140 (2021).
8. Tijerina-Rodríguez, L. et al. Virulence factors of *Clostridioides* (*Clostridium*) *difficile* linked to recurrent infections. *Can. J. Infect. Dis. Med. Microbiol.* **2019**, 7127850 (2019).
9. Normington, C. et al. Biofilms harbour *Clostridioides difficile*, serving as a reservoir for recurrent infection. *NPJ Biofilms Microbiomes* **7**, 1–10 (2021).
10. Hall-Stoodley, L. & Stoodley, P. Evolving concepts in biofilm infections. *Cell. Microbiol.* **11**, 1034–1043 (2009).
11. Jamal, M. et al. Bacterial biofilm and associated infections. *J. Chin. Med. Assoc* **81**, 7–11 (2018).
12. Vlamakis, H., Chai, Y., Beauregard, P., Losick, R. & Kolter, R. Sticking together: building a biofilm the *Bacillus subtilis* way. *Nat. Rev. Microbiol.* **11**, 157–168 (2013).
13. Vuotto, C., Donelli, G., Buckley, A. & Chilton, C. in *Updates on Clostridium difficile in Europe: Advances in Microbiology, Infectious Diseases and Public Health* Vol. 8 (eds. Mastrantonio, P. & Rupnik, M.) 97–115 (Springer International Publishing, 2018).
14. Poquet, I. et al. *Clostridium difficile* biofilm: remodeling metabolism and cell surface to build a sparse and heterogeneously aggregated architecture. *Front. Microbiol.* **9**, 2084 (2018).
15. Dubois, T. et al. A microbiota-generated bile salt induces biofilm formation in *Clostridium difficile*. *NPJ Biofilms Microbiomes* **5**, 14 (2019).
16. Semenyuk, E. G. et al. Analysis of bacterial communities during *Clostridium difficile* infection in the mouse. *Infect. Immun.* **83**, 4383–4391 (2015).
17. Soavelomandroso, A. P. et al. Biofilm structures in a mono-associated mouse model of *Clostridium difficile* infection. *Front Microbiol* **8**, 2086 (2017).
18. Ahmed, N. A., Petersen, F. C. & Scheie, A. A. AI-2/LuxS is involved in increased biofilm formation by *Streptococcus intermedius* in the presence of antibiotics. *Antimicrob. Agents Chemother.* **53**, 4258–4263 (2009).
19. Krzyściak, W., Jurczak, A., Kościelniak, D., Bystrowska, B. & Skalniak, A. The virulence of *Streptococcus mutans* and the ability to form biofilms. *Eur. J. Clin. Microbiol Infect. Dis.* **33**, 499–515 (2014).
20. Aguirre, A. M. & Sorg, J. A. Gut associated metabolites and their roles in *Clostridioides difficile* pathogenesis. *Gut Microbes* **14**, 2094672 (2022).
21. Đapa, T. & Unnikrishnan, M. Biofilm formation by *Clostridium difficile*. *Gut Microbes* **4**, 397–402 (2013).
22. Vuotto, C., Moura, I., Barbanti, F., Donelli, G. & Spigaglia, P. Subinhibitory concentrations of metronidazole increase biofilm formation in *Clostridium difficile* strains. *Pathog. Dis.* **74**, ftv114 (2016).
23. Tremblay Y. D. N. et al. Metabolic adaption to extracellular pyruvate triggers biofilm formation in *Clostridioides difficile*. *ISME J.* **21**, 3623–3635 (2021).
24. Meza-Torres, J., Auria, E., Dupuy, B. & Tremblay, Y. D. N. Wolf in sheep's clothing: *Clostridioides difficile* biofilm as a reservoir for recurrent infections. *Microorganisms* **9**, 1922 (2021).
25. Soutourina, O. et al. Genome-wide transcription start site mapping and promoter assignments to a sigma factor in the human enteropathogen *Clostridioides difficile*. *Front. Microbiol.* **11**, 1939 (2020).
26. Fuchs, M. et al. An RNA-centric global view of *Clostridioides difficile* reveals broad activity of Hfq in a clinically important gram-positive bacterium. *PNAS* **118**, e2103579118 (2021).
27. Charlton, T. M., Kovacs-Simon, A., Michell, S. L., Fairweather, N. F. & Tate, E. W. Quantitative lipoproteomics in *Clostridium difficile* reveals a role for lipoproteins in sporulation. *Chem. Biol.* **22**, 1562–1573 (2015).
28. Hosie, A. H. F. et al. Solute-binding protein-dependent ABC transporters are responsible for solute efflux in addition to solute uptake. *Mol. Microbiol.* **40**, 1449–1459 (2001).
29. Matilla, M. A., Ortega, Á. & Krell, T. The role of solute binding proteins in signal transduction. *Comput. Struct. Biotechnol. J.* **19**, 1786–1805 (2021).
30. Stefanović, C., Hager, F. F. & Schäffer, C. LytR-CpsA-Psr glycopolymer transferases: essential bricks in gram-positive bacterial cell wall assembly. *Int. J. Mol. Sci.* **22**, E908 (2021).
31. Zhu, L., Rajendram, M. & Huang, K. C. Effects of fixation on bacterial cellular dimensions and integrity. *iScience* **24**, 102348 (2021).
32. Jumper, J. et al. Highly accurate protein structure prediction with AlphaFold. *Nature* **596**, 583–589 (2021).
33. Holm, L. Dali server: structural unification of protein families. *Nucleic Acids Res.* **50**, W210–5 (2022).
34. Kavanaugh, J. S. et al. Identification of extracellular DNA-binding proteins in the biofilm matrix. *mBio* **10**, e01137–19 (2019).
35. Stewart, W. D., Haystead, A. & Pearson, H. W. Nitrogenase activity in heterocysts of blue-green algae. *Nature* **224**, 226–228 (1969).
36. Vlamakis, H., Aguilar, C., Losick, R. & Kolter, R. Control of cell fate by the formation of an architecturally complex bacterial community. *Genes Dev.* **22**, 945–953 (2008).
37. Anjuwon-Foster, B. R., Maldonado-Vazquez, N. & Tamayo, R. Characterization of Flagellum and Toxin Phase Variation in *Clostridioides difficile* Ribotype 012 Isolates. *J. Bacteriol.* **200**, e00056–18 (2018).

38. Anjuwon-Foster, B. R. & Tamayo, R. A genetic switch controls the production of flagella and toxins in *Clostridium difficile*. *PLoS Genet* **13**, e1006701 (2017).
39. Trzilova, D., Anjuwon-Foster, B. R., Torres Rivera, D. & Tamayo, R. Rho factor mediates flagellum and toxin phase variation and impacts virulence in *Clostridioides difficile*. *PLoS Pathog.* **16**, e1008708 (2020).
40. Garrett, E. M. et al. Phase variation of a signal transduction system controls *Clostridioides difficile* colony morphology, motility, and virulence. *PLoS Biol.* **17**, e3000379 (2019).
41. Garrett, E. M., Mehra, A., Sekulovic, O. & Tamayo, R. Multiple regulatory mechanisms control the production of CmrRST, an atypical signal transduction system in *Clostridioides difficile*. *mBio* **15**, e0296921 (2022).
42. Kempher, M. L. et al. Response regulator CD1688 is a negative modulator of sporulation in *Clostridioides difficile*. *J. Bacteriol.* **204**, e00130–22 (2022).
43. Saujet, L., Monot, M., Dupuy, B., Soutourina, O. & Martin-Verstraete, I. The key sigma factor of transition phase, SigH, controls sporulation, metabolism, and virulence factor expression in *Clostridium difficile*. *J. Bacteriol.* **193**, 3186–3196 (2011).
44. Purcell, E. B. et al. A nutrient-regulated cyclic diguanylate phosphodiesterase controls *Clostridium difficile* biofilm and toxin production during stationary phase. *Infect. Immun.* **85**, e00347–17 (2017).
45. Girinathan, B. P., Ou, J., Dupuy, B. & Govind, R. Pleiotropic roles of *Clostridium difficile sin* locus. *PLoS Pathog.* **14**, e1006940 (2018).
46. Campoccia, D., Montanaro, L. & Arciola, C. R. Extracellular DNA (eDNA). A major ubiquitous element of the bacterial biofilm architecture. *Int. J. Mol. Sci.* **22**, 9100 (2021).
47. Ronish, L. A., Sidner, B., Yu, Y. & Piepenbrink, K. H. Recognition of extracellular DNA by type IV pili promotes biofilm formation by *Clostridioides difficile*. *J. Biol. Chem.* **3**, 102449 (2022).
48. Maldarelli, G. A. et al. Type IV pili promote early biofilm formation by *Clostridium difficile*. *Pathog. Dis.* **74**, ftw061 (2016).
49. Allen, R., Rittmann, B. E. & Curtiss, R. Axenic biofilm formation and aggregation by *Synechocystis* sp. strain PCC 6803 are induced by changes in nutrient concentration and require cell surface structures. *Appl. Environ. Microbiol.* **85**, e02192–18 (2019).
50. Wood, B. M., Santa Maria, J. P., Matano, L. M., Vickery, C. R. & Walker, S. A partial reconstitution implicates DltD in catalyzing lipoteichoic acid d-alanylation. *J. Biol. Chem.* **293**, 17985–17996 (2018).
51. Peltier, J. et al. Type I toxin-antitoxin systems contribute to the maintenance of mobile genetic elements in *Clostridioides difficile*. Communications. *Biology* **3**, 1–13 (2020).
52. Cox, J. et al. A peptide search engine integrated into the MaxQuant environment. *J. Proteome Res.* **10**, 1794–1805 (2011).
53. Cox, J. & Mann, M. MaxQuant enables high peptide identification rates, individualized p.p.b.-range mass accuracies and proteome-wide protein quantification. *Nat. Biotechnol.* **26**, 1367–1372 (2008).
54. Tyanova, S., Temu, T. & Cox, J. The MaxQuant computational platform for mass spectrometry-based shotgun proteomics. *Nat. Protoc.* **11**, 2301–2319 (2016).
55. Chang, Y. Y. et al. Shigella hijacks the exocyst to cluster macropinosomes for efficient vacuolar escape. *PLOS Pathog.* **16**, e1008822 (2020).
56. Wieczorek, S. et al. DAPAR & ProStaR: software to perform statistical analyses in quantitative discovery proteomics. *Bioinformatics* **33**, 135–136 (2017).
57. Smyth, G. K. in *Bioinformatics and Computational Biology Solutions Using R and Bioconductor* Vol. 2 (eds. Gentleman, R., Carey, V. J., Huber, W., Irizarry, R. A. & Dudoit, S.) 397–420 (Springer, 2022).
58. Ritchie, M. E. et al. limma powers differential expression analyses for RNA-sequencing and microarray studies. *Nucleic Acids Res.* **43**, e47 (2015).
59. Giai Gianetto, Q. et al. Calibration plot for proteomics: a graphical tool to visually check the assumptions underlying FDR control in quantitative experiments. *Proteomics* **16**, 29–32 (2016).
60. Pounds, S. & Cheng, C. Robust estimation of the false discovery rate. *Bioinformatics* **22**, 1979–1987 (2006).

ACKNOWLEDGEMENTS

This work was funded by the Institut Pasteur, the "Integrative Biology of Emerging Infectious Diseases" (LabEx IBEID) funded in the framework of the French Government's "Programme Investissements d'Avenir" and The ANR DifBioRel AAPCE5. E.A. is a doctoral fellow of Université Paris-Cité. L.H. is a doctoral fellow of Sorbonne Université.

AUTHOR CONTRIBUTIONS

E.A. and B.D. designed the study and experiments; E.A., L.H., P.E., J.P.F., M.D., and B.D. performed experiments; M.Monot and M.Matondo provided assistance with the transcriptomic and proteomic analyses, respectively; E.A. and B.D. drafted and edited the manuscript; P.E., M.Monot, M.D., M.Matondo, and Y.D.T. helped with writing and editing; all authors read and approved the final manuscript.

COMPETING INTERESTS

The authors declare no competing interests.

ADDITIONAL INFORMATION

Supplementary information The online version contains supplementary material available at https://doi.org/10.1038/s41522-023-00393-5.

Correspondence and requests for materials should be addressed to Bruno Dupuy.

Reprints and permission information is available at http://www.nature.com/reprints

Publisher's note Springer Nature remains neutral with regard to jurisdictional claims in published maps and institutional affiliations.

Annex 2: Omicron BA.1 breakthrough infection drives long-term remodeling of the memory B cell repertoire in vaccinated individuals.

Aurélien Sokal*[1,2,7], Giovanna Barba-Spaeth*[3], Lise Hunault*[4], Matteo Broketa**[4], Annalisa Meola**[3], Ignacio Fernández**[3], Slim Fourati**[5,6], Imane Azzaoui**[7,8], Manon Broutin**[1,8], Alexis Vandenberghe**[1,7,8], Pauline Lagouge**[1,7,8], Anais Roeser[1,7], Magali Bouvier-Alias[5,6], Etienne Crickx[1,7,8], Laetitia Languille[7], Morgane Fournier[1,7], Marc Michel[7], Bertrand Godeau[7], Sébastien Gallien[9], Giovanna Melica[9], Yann Nguyen[10], Florence Canoui-Poitrine[11], France Noizat-Pirenne[8,12], Jérôme Megret[13], Jean-Michel Pawlotsky[5,6], Simon Fillatreau[14], , Claude-Agnès Reynaud[1], Jean-Claude Weill[1]†, Félix A. Rey†[3], Pierre Bruhns†[4] , Matthieu Mahévas†[1,7,8] & Pascal Chappert†[1,8].

* these authors contributed equally.

** these authors contributed equally.

†shared senior authorship

1. Institut Necker Enfants Malades, INSERM U1151/CNRS UMR 8253, Action thématique incitative sur programme-Avenir Team Auto-Immune and Immune B cells, Université Paris Cité, Université Paris-Est-Créteil, Créteil, France.

2 Service de Médecine interne, Hôpital Beaujon, Assistance Publique-Hôpitaux de Paris (AP-HP), Université de Paris Cité, Clichy, France.

3. Institut Pasteur, Université de Paris Cité, CNRS UMR 3569, Unité de Virologie Structurale, Paris, France.

4. Institut Pasteur, Université de Paris Cité, INSERM UMR1222, Unit of Antibodies in Therapy and Pathology, Paris, France.

5. Département de Virologie, Bactériologie, Hygiène et Mycologie-Parasitologie, Centre Hospitalier Universitaire Henri-Mondor, Assistance Publique-Hôpitaux de Paris (AP-HP), Créteil, France.

6. INSERM U955, équipe 18. Institut Mondor de Recherche Biomédicale (IMRB), Université Paris-Est Créteil (UPEC), Créteil, France.

7. Service de Médecine Interne, Centre Hospitalier Universitaire Henri-Mondor, Assistance Publique-Hôpitaux de Paris (AP-HP), Université Paris-Est Créteil (UPEC), Créteil, France.

8. INSERM U955, équipe 2. Institut Mondor de Recherche Biomédicale (IMRB), Université Paris-Est Créteil (UPEC), Créteil, France.

9. Service de Maladies Infectieuses, Centre Hospitalier Universitaire Henri-Mondor, Assistance Publique-Hôpitaux de Paris (AP-HP), Université Paris-Est Créteil (UPEC), Créteil, France.

10. Service de Médecine Interne, Centre Hospitalier Universitaire Cochin, Assistance Publique-Hôpitaux de Paris (AP-HP), Paris, France.

11. Département de Santé Publique, Unité de Recherche Clinique (URC), CEpiA (Clinical Epidemiology and Ageing), EA 7376- Institut Mondor de Recherche Biomédicale (IMRB), Centre Hospitalier Universitaire Henri-Mondor, Assistance Publique-Hôpitaux de Paris (AP-HP), Université Paris-Est Créteil (UPEC), Créteil, France.

12. Etablissement Français du Sang (EFS) Ile de France, Créteil, France.

13. Plateforme de Cytométrie en Flux, Structure Fédérative de Recherche Necker, INSERM US24-CNRS UMS3633, Paris, France.

14. Institut Necker Enfants Malades (INEM), INSERM U1151/CNRS UMR 8253, Université de Paris, Paris, France.

15. Institut Pasteur, Université de Paris, Evolutionary genomics of RNA viruses, Paris, France.

Immunity

SARS-CoV-2 Omicron BA.1 breakthrough infection drives late remodeling of the memory B cell repertoire in vaccinated individuals

Graphical abstract

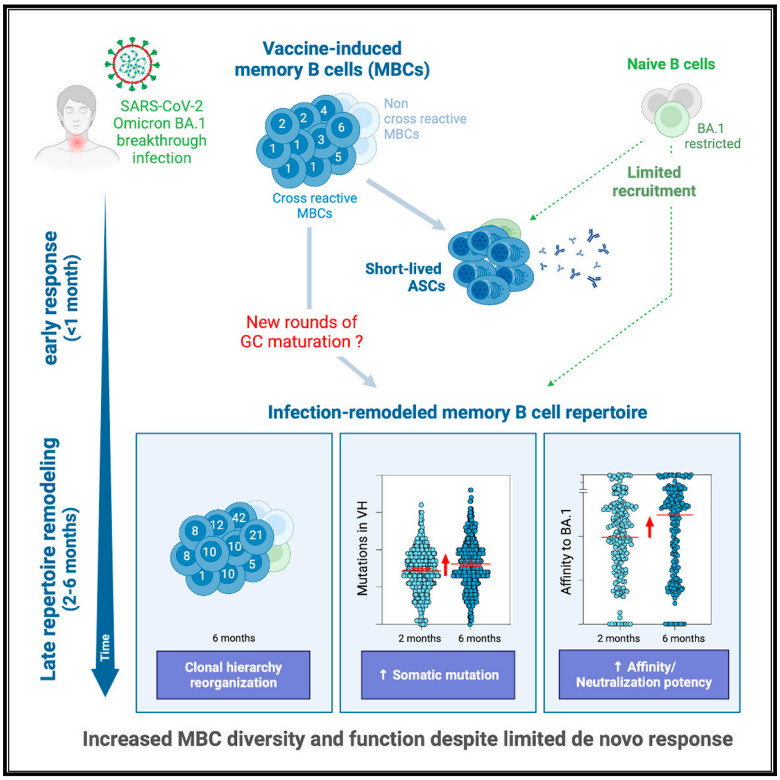

Highlights

- SARS-CoV-2 BA.1 breakthrough infection recalls cross-reactive RBD memory B cells (MBCs)
- Recruitment of BA.1-restricted naive B cells to ASC and MBC-repertoires is limited
- Longitudinal tracking reveals repertoire evolution up to 6 months post infection
- Late remodeling is associated with improved MBC affinity and neutralization breadth

Authors

Aurélien Sokal, Giovanna Barba-Spaeth, Lise Hunault, ..., Pierre Bruhns, Matthieu Mahévas, Pascal Chappert

Correspondence

matthieu.mahevas@aphp.fr (M.M.), pascal.chappert@inserm.fr (P.C.)

In brief

How infection by a viral variant showing antigenic drift impacts a preformed mature human memory B cell (MBC) repertoire remains unclear. Sokal et al. show that SARS-CoV-2 Omicron BA.1 breakthrough infections induce late remodeling and maturation of the pre-existing memory B cell pool, with progressively improved MBC affinity and neutralization breadth but limited recruitment of BA.1-restricted naive B cells.

Sokal et al., 2023, Immunity *56*, 1–15
October 10, 2023
https://doi.org/10.1016/j.immuni.2023.07.007

CellPress

Immunity

CellPress

Article

SARS-CoV-2 Omicron BA.1 breakthrough infection drives late remodeling of the memory B cell repertoire in vaccinated individuals

Aurélien Sokal,[1,2,3,17] Giovanna Barba-Spaeth,[4,17] Lise Hunault,[5,6,7,17] Ignacio Fernández,[4,17] Matteo Broketa,[5,6,18] Annalisa Meola,[4,18] Slim Fourati,[8,9,18] Imane Azzaoui,[3,10,18] Alexis Vandenberghe,[1,3,10,18] Pauline Lagouge-Roussey,[1,3,10,18] Manon Broutin,[1,10,18] Anais Roeser,[1,3] Magali Bouvier-Alias,[8,9] Etienne Crickx,[1,3,10] Laetitia Languille,[3] Morgane Fournier,[1,3] Marc Michel,[3] Bertrand Godeau,[3] Sébastien Gallien,[11] Giovanna Melica,[11] Yann Nguyen,[12] Florence Canoui-Poitrine,[13] France Pirenne,[9,14] Jérôme Megret,[15] Jean-Michel Pawlotsky,[8,9] Simon Fillatreau,[16] Claude-Agnès Reynaud,[1] Jean-Claude Weill,[1,19] Félix A. Rey,[4,19] Pierre Bruhns,[5,19] Matthieu Mahévas,[1,3,10,19,*] and Pascal Chappert[1,10,19,20,*]

[1]Institut Necker Enfants Malades, INSERM U1151/CNRS UMR 8253, Action thématique incitative sur programme-Avenir Team, Auto-Immune and Immune B cells, Université Paris Cité, Université Paris Est-Créteil, Créteil, France
[2]Service de Médecine interne, Hôpital Beaujon, Assistance Publique-Hôpitaux de Paris (AP-HP), Université de Paris Cité, Clichy, France
[3]Service de Médecine Interne, Centre Hospitalier Universitaire Henri-Mondor, Assistance Publique-Hôpitaux de Paris (AP-HP), Université Paris-Est Créteil (UPEC), Créteil, France
[4]Institut Pasteur, Université de Paris Cité, CNRS UMR 3569, Unité de Virologie Structurale, Paris, France
[5]Institut Pasteur, Université de Paris Cité, INSERM UMR1222, Unit of Antibodies in Therapy and Pathology, Paris, France
[6]Sorbonne University, ED394, Paris, France
[7]Sorbonne Université, INSERM, CNRS, Centre d'Immunologie et des Maladies Infectieuses (CIMI-Paris), 75013 Paris, France
[8]Département de Virologie, Bactériologie, Hygiène et Mycologie-Parasitologie, Centre Hospitalier Universitaire Henri Mondor, Assistance Publique-Hôpitaux de Paris (AP-HP), Créteil, France
[9]INSERM U955, équipe 18. Institut Mondor de Recherche Biomédicale (IMRB), Université Paris-Est Créteil (UPEC), Créteil, France
[10]INSERM U955, équipe 2. Institut Mondor de Recherche Biomédicale (IMRB), Université Paris-Est Créteil (UPEC), Créteil, France
[11]Service de Maladies Infectieuses, Centre Hospitalier Universitaire Henri Mondor, Assistance Publique-Hôpitaux de Paris (AP-HP), Université Paris-Est Créteil (UPEC), Créteil, France
[12]Service de Médecine Interne, Centre Hospitalier Universitaire Cochin, Assistance Publique-Hôpitaux de Paris (AP-HP), Paris, France
[13]Département de Santé Publique, Unité de Recherche Clinique (URC), CEpiA (Clinical Epidemiology and Ageing), EA 7376- Institut Mondor de Recherche Biomédicale (IMRB), Centre Hospitalier Universitaire Henri-Mondor, Assistance Publique-Hôpitaux de Paris (AP-HP), Université Paris-Est Créteil (UPEC), Créteil, France
[14]Etablissement Français du Sang (EFS) Ile de France, Créteil, France
[15]Plateforme de Cytométrie en Flux, Structure Fédérative de Recherche Necker, INSERM US24-CNRS UMS3633, Paris, France
[16]Institut Necker Enfants Malades (INEM), INSERM U1151/CNRS UMR 8253, Université de Paris, Paris, France
[17]These authors contributed equally
[18]These authors contributed equally
[19]Senior author
[20]Lead contact
*Correspondence: matthieu.mahevas@aphp.fr (M.M.), pascal.chappert@inserm.fr (P.C.)
https://doi.org/10.1016/j.immuni.2023.07.007

SUMMARY

How infection by a viral variant showing antigenic drift impacts a preformed mature human memory B cell (MBC) repertoire remains an open question. Here, we studied the MBC response up to 6 months after SARS-CoV-2 Omicron BA.1 breakthrough infection in individuals previously vaccinated with three doses of the COVID-19 mRNA vaccine. Longitudinal analysis, using single-cell multi-omics and functional analysis of monoclonal antibodies from RBD-specific MBCs, revealed that a BA.1 breakthrough infection mostly recruited pre-existing cross-reactive MBCs with limited *de novo* response against BA.1-restricted epitopes. Reorganization of clonal hierarchy and new rounds of germinal center reactions, however, combined to maintain diversity and induce progressive maturation of the MBC repertoire against common Hu-1 and BA.1, but not BA.5-restricted, SARS-CoV-2 Spike RBD epitopes. Such remodeling was further associated with a marked improvement in overall neutralizing breadth and potency. These findings have fundamental implications for the design of future vaccination booster strategies.

Please cite this article in press as: Sokal et al., SARS-CoV-2 Omicron BA.1 breakthrough infection drives late remodeling of the memory B cell repertoire in vaccinated individuals, Immunity (2023), https://doi.org/10.1016/j.immuni.2023.07.007

INTRODUCTION

Emergence of the severe acute respiratory syndrome coronavirus 2 (SARS-CoV-2) Omicron variant (BA.1) has marked a major antigenic shift in SARS-CoV-2 evolution.[1] The Spike (S) protein of SARS-CoV-2 Omicron BA.1 harbors 32 mutations as compared with the ancestral strain (Hu-1) originally identified in Wuhan. These mutations drastically impair neutralizing antibodies elicited by natural infection with the D614G SARS-CoV-2 and/or vaccination with mRNA vaccine encoding the ancestral Hu-1 S and have led to a massive wave of breakthrough infections in the early weeks of 2022 in vaccinated individuals, whether they had received 2 or 3 doses of mRNA vaccine.[2–7] Since, new sub-lineages, displaying additional mutations, continue to emerge, supplanting prior variants.[8]

Despite sizable immune escape by several SARS-CoV-2 variants, the diverse memory B cell (MBC) repertoire generated by two or three doses of mRNA vaccines has been shown to contain high-affinity neutralizing clones against all variants up to BA.1.[9–11] These MBCs, generated against the ancestral Hu-1 pre-fusion S encoded by the original mRNA vaccines, represent an underlying layer of immune protection associated with prevention of severe forms of COVID-19.[12–16] The impact of antigen imprinting in shaping the response and future B cell memory to breakthrough infection by drifted SARS-CoV-2 variants remains an open question of major importance in direct link with the current development of bivalent vaccines and rise in multiple antigenic exposures.

Upon re-infection, high-affinity cross-reactive MBCs are likely rapidly and selectively recruited from the repertoire, and MBC-derived antibodies provide a rapid protection against ongoing viral replication. When such antibodies merely mask their cognate immunodominant epitopes without effectively clearing the virus or when MBCs against specific epitopes carried by the variant strain are scarce or absent due to high antigenic distance between the original and latest strains encountered, a *de novo* naive B cell response can be initiated. These naive cells then undergo slow maturation within the germinal center (GC), resulting in the generation of new MBCs, further extending the diversity of the MBC repertoire. This point has been clearly documented in the context of influenza or SARS-CoV-2 infections[15,17,18] and in murine models.[19] Variant-specific MBCs, targeting mutated residues in the S receptor binding domain (RBD), have been detected in the context of Beta and Gamma SARS-CoV-2 primary infection,[20,21] suggesting that naive B cells solely specific for SARS-CoV-2 variants do exist in the repertoire. Recent reports, however, have suggested that the early response occurring in the context of Omicron BA.1 breakthrough infection or Hu-1 mRNA vaccination essentially mobilized cross-reactive clones against conserved S glycoprotein epitopes rather than recruiting novel naive B cells specific to mutated BA.1 residues.[22–25] This raises the question of the extent of repertoire remodeling and diversification that can occur in the context of such continued re-exposure to viral variants presenting low to moderate antigenic distance with the original strain, a key question in the design of future bivalent variant-based vaccines.

In this study, we combined single-cell multi-omics and functional analysis of several hundred naturally expressed antibodies from RBD-specific MBCs to provide an extensive characterization of the progressive repertoire remodeling of the MBC repertoire occurring up to 6 months after Omicron BA.1 breakthrough infection in a cohort of mRNA-vaccinated individuals. BA.1 breakthrough infection almost exclusively mobilized pre-existing cross-reactive MBC clones, with limited recruitment of *de novo* BA.1-restricted responses. Nonetheless, our results demonstrate a reorganization of clonal hierarchy and new rounds of GC reaction that combine to maintain diversity and induce progressive maturation of the MBC repertoire against both Hu-1 and BA.1 SARS-CoV-2 S RBD variants.

RESULTS

Omicron BA.1 breakthrough infection boosts humoral and memory B cell response in triple-vaccinated individuals

To understand how the MBC repertoire elicited by vaccination is reshaped by BA.1 breakthrough infection and whether a specific response against its new epitopes occurs, we longitudinally analyzed the SARS-CoV-2-specific B cell responses in 15 individuals with no previous history of COVID-19, which were infected between end of December 2021 and end of January 2022 with Omicron BA.1, shortly after receiving a third dose of BNT162b2 mRNA vaccine (median: 32 days [13–106]). These individuals were sampled at three time points (<1, 2, and 6 months) after BA.1 breakthrough infection to fully characterize the B cell response from the early extrafollicular reaction to the late settlement of long-term memory, combining multiparameter flow cytometry analysis, single-cell RNA sequencing (scRNA-seq) and single-cell culture of S and RBD-specific B cells (Figures 1A and S1). Four of these individuals had been previously sampled after their second and/or third dose of mRNA vaccine[9,26] (see also Table S1). This provided us with the opportunity to decipher the selection processes occurring at the level of the MBC repertoire upon BA.1 breakthrough infection on a per-individual basis. As control, a parallel cohort of fifteen vaccinated individuals with no history of SARS-CoV-2 infection (SARS-CoV-2-naive) were also sampled at similar time points (<1, 2, and 6 months) after their third dose of mRNA vaccine.

Anti-Hu-1 and BA.1 S, RBD, and Nucleocapsid (N) IgG titers were robustly induced in all individuals after breakthrough infection (Figure 1B), with a good correlation between final anti-Hu-1 and BA.1 RBD titers in both cohorts (Figure 1C). N-specific IgG antibodies elicited after BA.1 breakthrough infection waned over the 6 months period, confirming the absence of new SARS-CoV-2 breakthrough in this cohort. The decrease in anti-RBD IgG titers over time was slightly more pronounced in vaccinated SARS-CoV-2-naive individuals than after BA.1 breakthrough infection, probably reflecting the magnitude of the initial response. In line with two recent studies,[11,27] plasma from uninfected patients demonstrated poor neutralizing activity against the BA.1 SARS-CoV-2 strain and progressively waning titers against the authentic D614G strain (Figures 1D and 1E). In comparison, all infected individuals rapidly displayed equally high neutralizing potential against both D614G and BA.1 SARS-CoV-2 strains. And these titers remained stable up to 6 months post infection, in line with recent observations by others.[28] Finally, longitudinal analyses using a flow panel that included

Please cite this article in press as: Sokal et al., SARS-CoV-2 Omicron BA.1 breakthrough infection drives late remodeling of the memory B cell repertoire in vaccinated individuals, Immunity (2023), https://doi.org/10.1016/j.immuni.2023.07.007

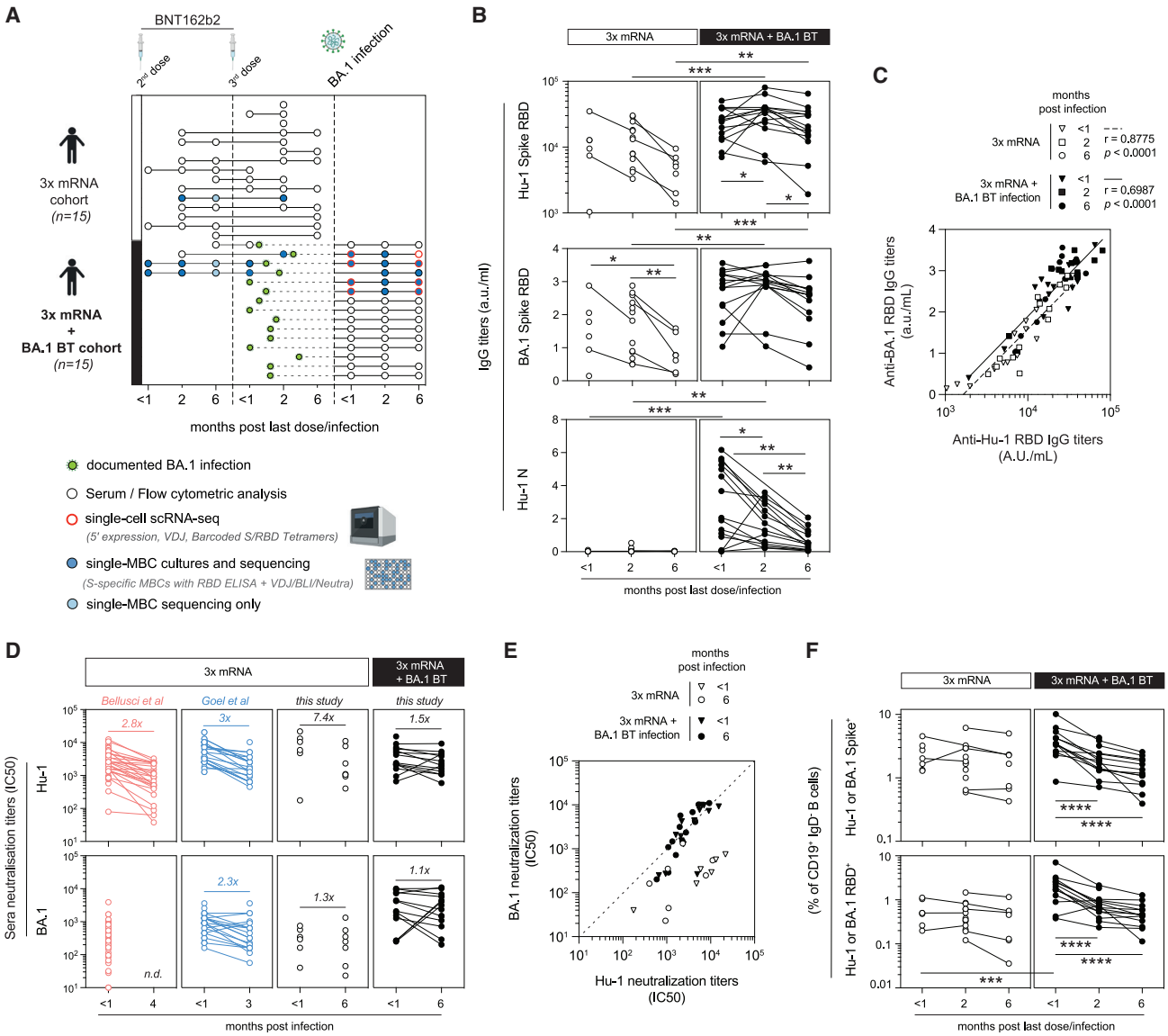

Figure 1. Omicron BA.1 breakthrough infection boosts humoral response in triple-vaccinated individuals

(A) Overview of cohort, sampling time points, and experimental procedures (see also Table S1 and Figure S1A for detailed sorting strategies). All donors received three doses of mRNA vaccine with or without a subsequent BA.1 breakthrough infection (3x mRNA + BA.1 BT [black dots] or 3x mRNA [white dots]).

(B and C) (B) Anti-SARS-CoV-2 Hu-1 (top) or BA.1 RBD IgG titers (middle) and anti-Hu-1 Nucleocapsid (N) serum IgG titers (bottom) (a.u./mL) and (C) correlation between the anti BA.1 and Hu-1 RBD serum IgG titers at indicated time points.

(D and E) (D) Half maximal inhibitory concentration (IC_{50}) for donors' sera *in vitro* neutralization assay against authentic D614G (left) or BA.1 (right) SARS-CoV-2 virus, and (E) correlation between the anti BA.1 and D614G neutralizing serum titers at indicated time points.

(F) Proportion of all Hu-1 or BA.1 Spike (top) or RBD (bottom) specific memory B cells among total $CD19^+$ IgD^- B cells using flow cytometry on donor's peripheral blood mononuclear cells (PBMCs) at indicated time points (see also Figure S2A for detailed gating strategies). In all panels, individual donors are represented as dots, and longitudinal samplings from individual donors are connected.

(B and F) Mixed model analysis with Tukey's correction for intra-group comparison and Sidak's correction for inter-group comparison. (C) Non-parametric Spearman correlation tests on pooled data from each cohort. ****p < 0.0001, ***p < 0.001, **p < 0.01, *p < 0.05.

See also Figures S1 and S2 and Table S1.

Hu-1 and BA.1 S and RBD tetramers, demonstrated a major expansion of RBD-specific $CD19^+IgD^-$ B cells shortly after BA.1 breakthrough infection, more pronounced than the S-specific response and with a higher magnitude than that observed after the third mRNA vaccine in SARS-CoV-2-naive individuals (Figure 1F). Both infected and triple-vaccinated individuals harbored a sizable and stable population of S and RBD-specific MBCs at the latest time point, after a contraction phase. These results show, as previously observed for SARS-CoV-2[29] or influenza,[30] that breakthrough infection in triple-vaccinated individuals induces a robust MBC and cross-neutralizing antibody response.

Please cite this article in press as: Sokal et al., SARS-CoV-2 Omicron BA.1 breakthrough infection drives late remodeling of the memory B cell repertoire in vaccinated individuals, Immunity (2023), https://doi.org/10.1016/j.immuni.2023.07.007

BA.1 breakthrough infection mobilizes cross-reactive Spike-specific pre-existing MBCs

To characterize the fine specificity and the dynamics of the B cell response after BA.1 breakthrough infection, we first performed multiparametric fluorescence-activated cell sorting (FACS) analysis on all individuals from both cohorts using major markers of circulating B cell subpopulations (CD19, IgD, CD27, CD38, CD21, CD71 and CD11c) along with Hu-1 and BA.1 S and RBD tetramers (Figures S2A and S2B). As previously reported,[23,31,32] BA.1 breakthrough infection mostly mobilized B cells that displayed cross-reactivity against shared epitopes between Hu-1 and BA.1 S proteins, representing 70%–80% of all RBD-positive cells at any given time point post infection (Figure 2A; Table S2). Almost no B cells uniquely specific for BA.1 epitopes could be observed both at early time points, as previously described,[23,31] and at later time points when one can expect to start detecting new GC output (Figure 2A). Phenotypic analysis of $CD19^+$ IgD^- switched B cell populations confirmed a massive expansion of S- and RBD-specific $CD19^+IgD^-CD38^-CD71^+$ activated B cells (ABCs) occurring in the first couple of weeks post-BA.1 infection (Figures 2B, 2C, S2C, and S2D), together with the mobilization of $CD27^{high}$ $CD38^{high}$ antibody-secreting cells (ASCs) (Figure S2E), as previously described upon vaccination or primary infection of SARS-CoV-2 naive individuals.[15,16] ABCs were enriched in Hu-1/BA.1 cross-reactive cells, confirming the preferential recruitment of these cells in the context of a BA.1 breakthrough infection (Figure 2D). S- and RBD-specific atypical $CD27^-$ IgD^- double-negative (DN) MBCs were also observed, but rarely in $CD21^-$ $CD11c^-$ DN2 cells (Figures 2C and S2C), a population that was previously described as a hallmark of the extrafollicular response in COVID-19.[33,34] After their initial expansion, the proportion of S- and RBD-specific ABCs decreased over time favoring, in a similar kinetic than observed in triple vaccinated individuals, the resting MBCs, which remain thereafter stable.

To further get access to the early ASC response, whose heterogeneous surface B cell receptor (BCR) expression prevents accurate specificity assessment, and to track potential recruitment of naive B cells to the extrafollicular response as well as repertoire and/or transcriptomic changes of the SARS-CoV-2 specific B cell response, we next performed scRNA-seq with parallel surface protein expression and immunoglobulin heavy chain (IgH) variable, diversity, and joining (VDJ) sequencing on sorted $CD19^+IgD^-$ B cells at both early (<1 month) and late time points (6 months) from 4 individuals infected with BA.1 (Figure S1A). To focus on cells involved in the ongoing response, $CD19^+IgD^-$ B cells were enriched in S- and/or RBD-specific B cells as well as in total ASCs (Figure S1A). Activated $CD19^{high}IgD^+$ B cells were also sorted to track the potential mobilization of naive B cells (Figure S1A). In parallel, we sorted and single-cell cultured Hu-1 and/or BA-1 S- and RBD-specific B cells at different time points, and IgV_H sequences obtained from these cells were further integrated to our scRNA-seq dataset to increase the number of identified S- and RBD-specific BCR sequences and add functional information regarding linked antibodies (Figures S1A, S1B, and S3A).

Unsupervised clustering analysis of scRNA-seq revealed 6 clusters according to their gene expression profile (Figure 2E). Among them, we distinguished $CD21^{low}CD38^+CD71^+$ ABCs, $CD21^-CD38^-CD27^-CD11c^+$ DN2, and 2 clusters of ASCs with both proliferative short-lived plasmablasts (PBs) and non-dividing plasma cells (PCs) based on surface protein and gene expression (Figures S2F and S2G). The remaining B cells were separated in two populations: a mixture of naive/transitional B cells and a resting MBC population (Figure 2E). At early time point after BA.1 breakthrough infection, S- and/or RBD-specific B cells mainly resided among the ABC and ASC clusters (Figures 2F and S2H), and they relocated to the resting MBC cluster at the 6 months' time point (Figure 2F). Concordant with our flow cytometry analysis, these cells were mostly cross-reactive against BA.1 and Hu-1 SARS-CoV-2 with only approximately 1.3% (14/1,075) of total specific cells analyzed only recognizing BA.1 S- or RBD-specific epitopes at any given time point.

Most of the RBD-specific B cells mobilized to the ASC and ABC responses upon BA.1 breakthrough infection harbored a high mutation load (median: 19 mutations), with less than 1% (4/546) unmutated sequences in ASCs and none in ABCs (Figure 2G; Table S3) and, overall, very limited frequencies of cells with intermediate number of mutational load (2–9 mutations). Similar results could be observed for S-specific B cells (Figures S2I–S2K). This is in stark contrast with our previous results showing that the RBD-specific ABC and ASC responses after primary infection[15] or 2 doses of mRNA vaccine mobilize cells with low IgV_H mutations[9] (Figure 2G). Non-cross-reactive BA.1 RBD-specific cells appeared to display lower mutational loads (Figure 2H), but the very low number of recovered sequences prevented us from drawing any definite conclusion on this point.

Altogether, our results are consistent with a preferential recall of highly mutated pre-existing cross-reactive MBCs, massively expanding as ABCs and fueling the ASC response, with limited recruitment of naive B cells against BA.1-specific epitopes.

BA.1 breakthrough infection remodels the MBC repertoire

One of the key questions in the context of immune imprinting relates to understanding how a secondary or tertiary antigen encounter reshapes the cognate MBC repertoire and impacts its diversity. First evidence of repertoire remodeling post-BA.1 breakthrough infection could be seen at the global S-specific repertoire level, with the proportion of RBD-specific MBCs among S-specific clones being significantly increased after BA.1 breakthrough infection (mean ± SEM of 51.8% ± 4.2% vs. 24.5% ± 3.4%; $p < 0.0001$) and remaining significantly higher at 6 months as compared with individuals having solely received 3 doses of mRNA vaccine (mean ± SEM of 38.8% ± 2.9% vs. 20.2% ± 2.4%; $p = 0.0007$) (Figure 3A). Further evidence of remodeling could be seen in the RBD-specific MBC repertoire at the clonal level. Longitudinal analysis of the overall RBD-specific MBC clonal diversity, reflected by Chao1 clonal richness index and Shannon entropy values showed no major loss of diversity, apart from the ASCs compartment post-BA.1 infection as expected (Figures 3B, S3A, and S3B). A sizable fraction of the RBD-specific clones was maintained over BA.1 infection ("sustained" clones) (Figure 3C), most of which being Hu-1/BA.1 cross-reactive (Figure 3D). However, in-depth analysis of the repertoire revealed marked remodeling at the clonal level, characterized by the loss of previously expanded clones, including Hu-1 RBD-specific only cells, and the emergence of new clones some of which eventually persisted over time (Figure 3C). In all longitudinally sampled individuals, sustained clones were still largely

Please cite this article in press as: Sokal et al., SARS-CoV-2 Omicron BA.1 breakthrough infection drives late remodeling of the memory B cell repertoire in vaccinated individuals, Immunity (2023), https://doi.org/10.1016/j.immuni.2023.07.007

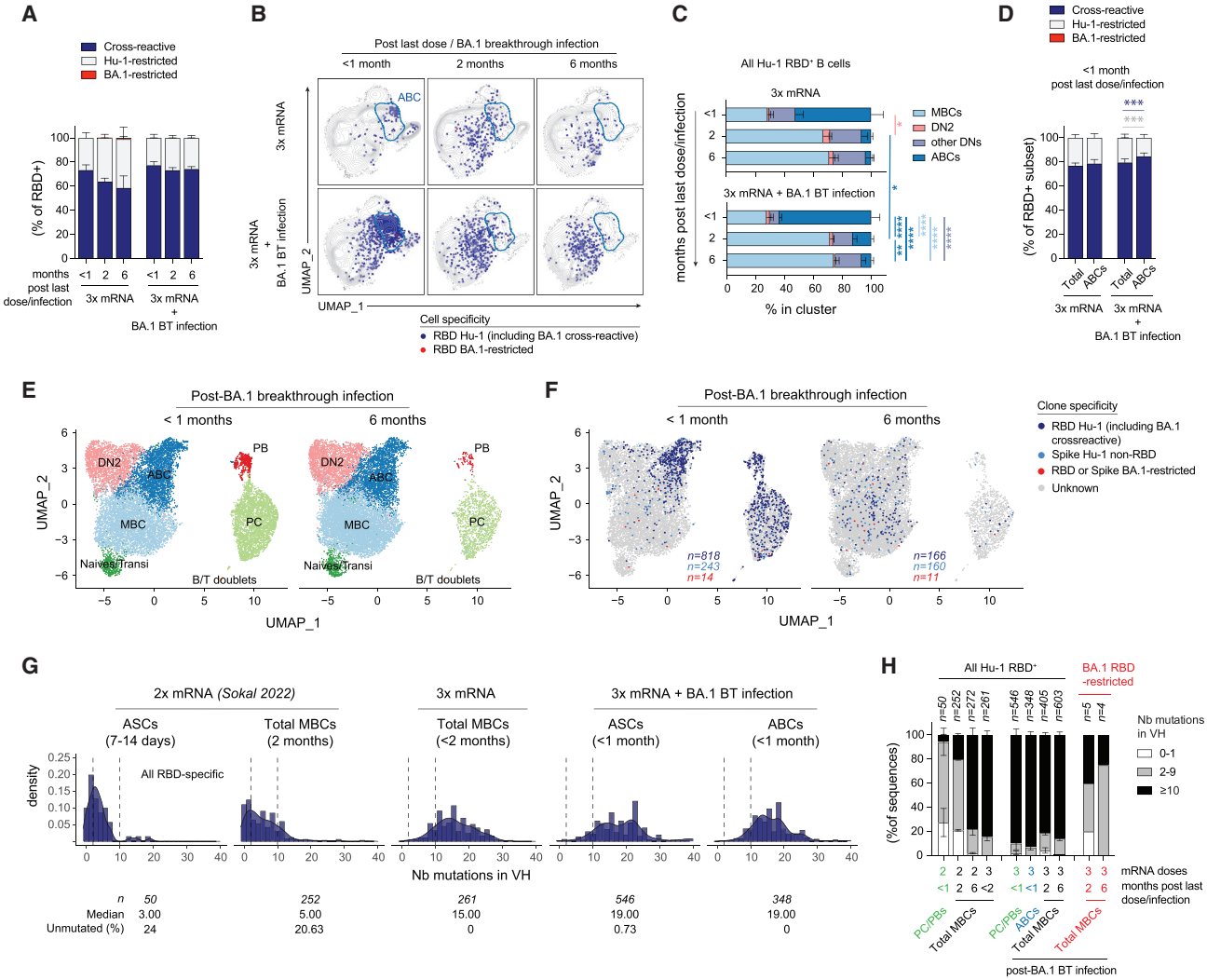

Figure 2. BA.1 breakthrough infection-induced early response recruits Hu-1/BA.1 cross-reactive RBD-specific memory B cells

(A–D) Flow cytometry analysis of PBMCs from donors at indicated time point after a third dose of mRNA vaccine with or without a subsequent BA.1 breakthrough infection (3x mRNA + BA.1 BT infection or 3x mRNA). (A) Frequency of SARS-CoV-2 Hu-1 and BA-1 cross-reactive (dark blue), Hu-1 (light gray), or BA.1-only (red) RBD-specific among all RBD-specific $CD19^+$ IgD^- cells. (B) Uniform Manifold Approximation and Projection (UMAP) for concatenated $CD19^+$ IgD^- cells from all donors analyzed by multiparametric fluorescence-activated cell sorting (FACS) analysis. RBD-specific B cells are overlaid in dark blue (Hu-1 ± BA.1 specific) or red (BA.1 only specific) dots on top of all cells. The CD71+ ABC cluster is delineated by a blue line. (C) Distribution of Hu-1 RBD-specific $CD19^+$ IgD^- B cells in cluster defined by manual gating strategies (see Figure S2A). (D) Mean percentage of Hu-1 and BA-1 cross-reactive (dark blue), Hu-1 (light gray), or BA.1-only (red) RBD-specific among total or CD71+ (ABCs) RBD-specific $CD19^+$ IgD^- B cells.

(E–H) scRNA-seq analysis of PMBCs from four donors within the 3x mRNA + BA.1 BT infection cohort. (E and F) UMAP for all VDJ-expressing cells at the <1 month (left, n = 13,644) and 6 months' time points post infection (right, n = 14,132), colored based on unsupervised clustering analysis (E) or indicated clone specificity (F). (G and H) Total number of IgV_H mutations (G) and distribution in IgV_H mutation groups (0–1, white; 2–9, gray; and ≥10 mutations, black) (H) for RBD-specific B cells at indicated time points post infection in indicated cell populations (2x mRNA data extracted from Sokal et al.,[16] antibody-secreting cells [ASCs] regroup both plasmablasts [PBs] and plasma cells [PCs]). In (G), dashed vertical lines indicate 1 and 10 mutations.

(A, C, and D) Mixed model analysis with Tukey's correction for intra-group comparison and Sidak's correction for inter-group comparison. ****p < 0.0001, ***p < 0.001, **p < 0.01, *p < 0.05.

See also Figure S2 and Tables S2 and S3.

represented in the MBC repertoire at 6 months (Figure 3C), with no clear reduction in the individual frequencies of these clones (Figure 3E). Germline V_H gene usage in RBD-specific sequences showed no major changes after BA.1 infection relative to those found after a third dose of mRNA vaccine in our longitudinally sampled donors (Figure 3F), albeit a progressive enrichment in IGHV1-69 gene usage, as previously described,[22] is to be noted.

These results suggest that the immune response against the Omicron BA.1 variant does not solely mobilize the top cross-reactive MBCs but also expands MBC clones previously found

Please cite this article in press as: Sokal et al., SARS-CoV-2 Omicron BA.1 breakthrough infection drives late remodeling of the memory B cell repertoire in vaccinated individuals, Immunity (2023), https://doi.org/10.1016/j.immuni.2023.07.007

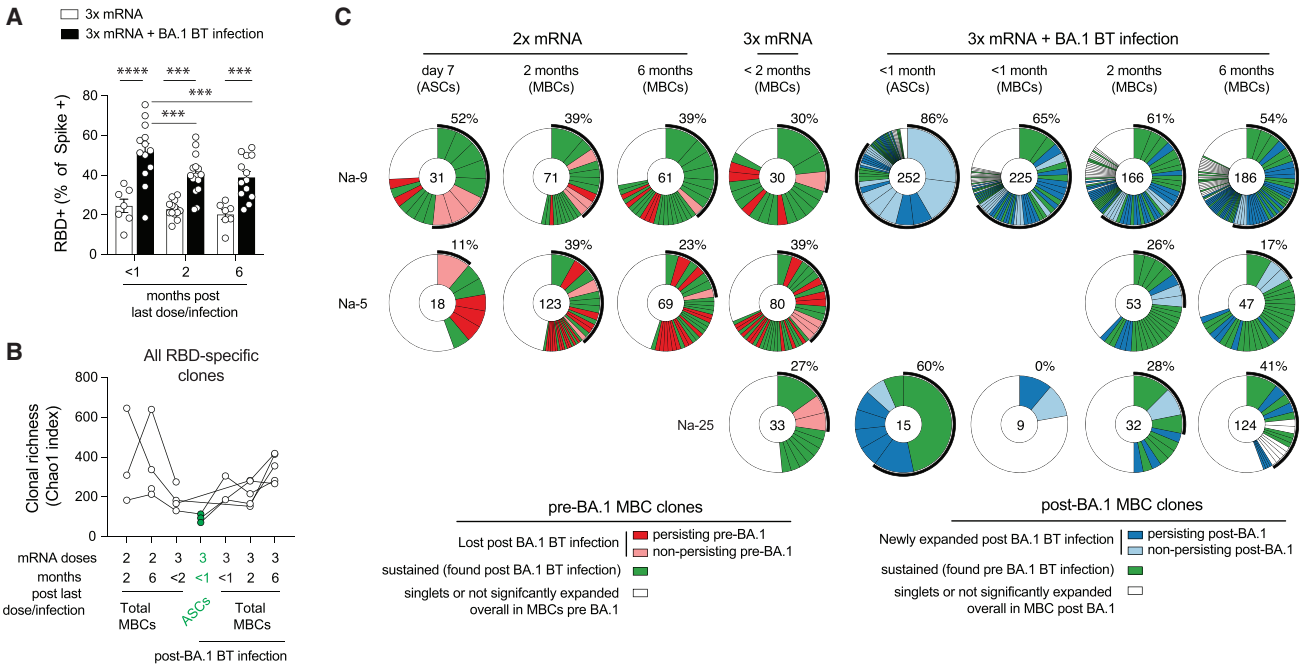

Figure 3. BA.1 breakthrough infection induces partial remodeling of the specific memory B cell repertoire

(A) Frequency of RDB (Hu-1 and/or BA.1) specific CD19$^+$ IgD$^-$ B cells among Spike (Hu-1 and/or BA.1) specific CD19$^+$ IgD$^-$ B cells in 3x mRNA (white) or 3x mRNA + BA.1 BT infection (black) cohorts at indicated time points.

(B–F) Repertoire analysis of RBD-specific MBCs and ASCs in individual donors from the second dose of mRNA vaccine up to 6 months after BA.1 breakthrough infection. (B) Evolution of clonal richness (Chao1 index) over time. Each line represents one individual donor. (C) Longitudinal clonal distribution in 3 donors. Slice sizes are proportional to the size of each clone. Clones found before and after BA.1 BT infection are depicted in green; expanded clones lost upon BA.1 BT infection are in light red if found at a single time point or in dark red if persisting at several time points pre-BA.1; and newly expanded clones found after BA.1 BT infection are in light blue if found at a single time point or in dark blue if found at several time points. Singletons or expanded clones whose overall frequency post-BA.1 did not reach the frequency of singletons pre-BA.1 are represented in white. Outer black semi-circular line indicates the proportion of sequences belonging to expanded clones at a given time point. The total number of sequences is indicated at the pie center. (D) Percentage of cells specific for Hu-1/BA.1, Hu-1, or BA.1 RBD among total RBD-specific cells sequenced, grouped according to their clone's evolution upon BA.1 BT infection, as defined in (C). (E) Frequency of sustained RBD-specific clones among total RBD-specific cells sequenced at any time point pre- or post-BA.1 BT infection. (F) IgV$_H$ gene usage distribution in CD19$^+$IgD$^-$ RDB (Hu-1 and/or BA.1) specific B cell at indicated time points.

(A and F) Mixed model analysis with Tukey's correction. (D) Two-tailed Wilcoxon test. ****$p < 0.0001$, ***$p < 0.001$, **$p < 0.01$, *$p < 0.05$.

See also Figure S3 and Table S3.

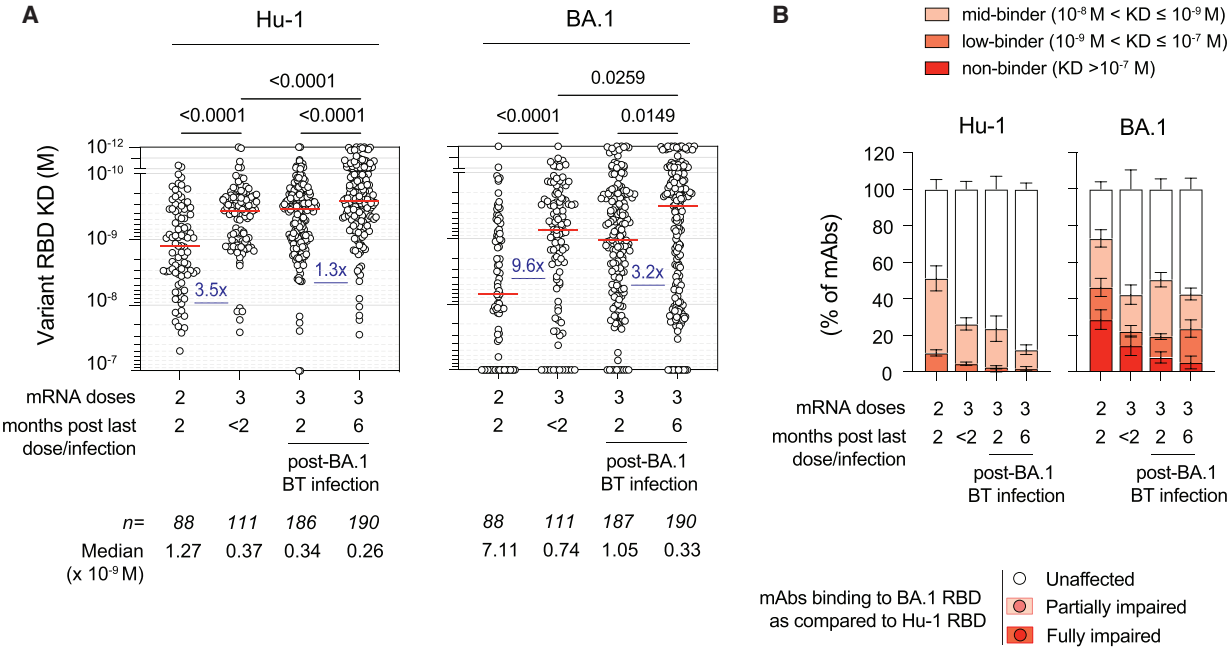

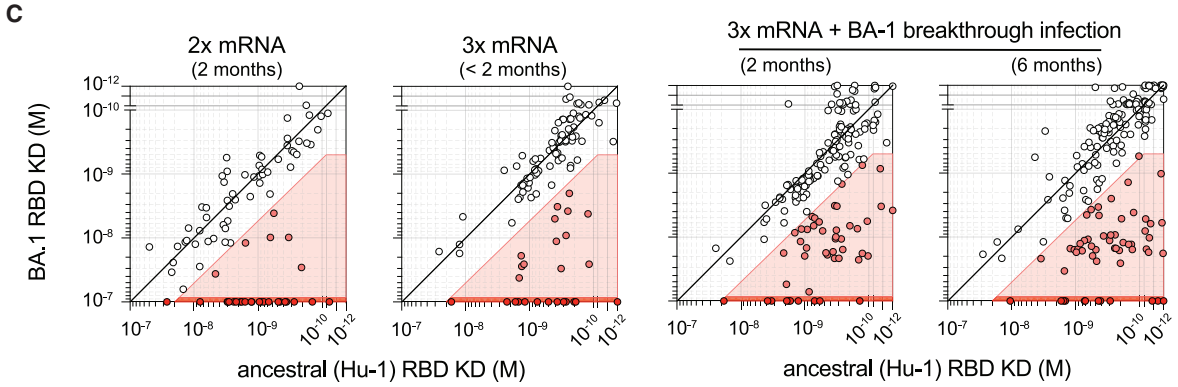

Partially impaired= 6/88 (6.8%) *13/112 (11.6%)* *37/185 (20%)* *45/192 (23.4%)*
Fully impaired = 24/88 (27.2%) *15/112 (13.4%)* *14/185 (7.5%)* *12/192 (6.3%)*

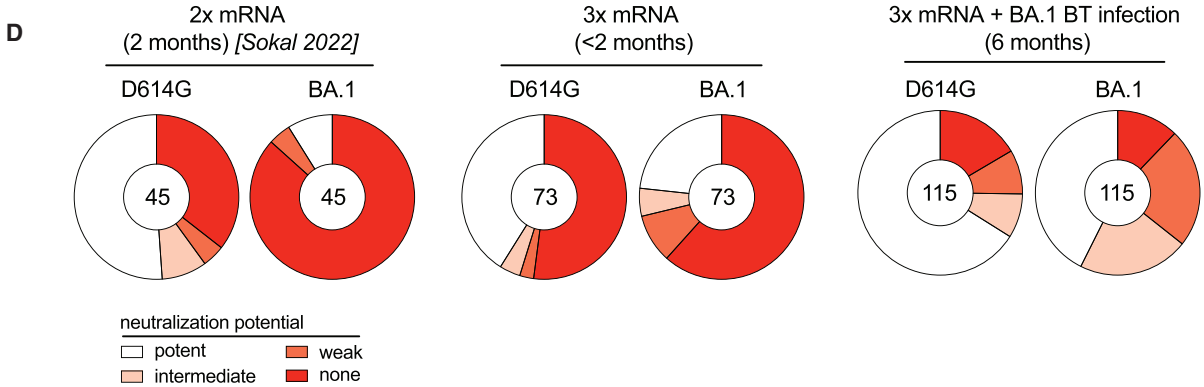

(legend on next page)

Please cite this article in press as: Sokal et al., SARS-CoV-2 Omicron BA.1 breakthrough infection drives late remodeling of the memory B cell repertoire in vaccinated individuals, Immunity (2023), https://doi.org/10.1016/j.immuni.2023.07.007

at low frequency in the repertoire or recruits cross-reactive naive B cells (Figure 3D), maintaining in the process the overall clonal diversity and thus likely mitigating the negative impact of immune imprinting.

BA.1 breakthrough infection drives additional affinity maturation and increased overall neutralization breadth of the MBC repertoire

To evaluate the functional consequences of the observed MBC repertoire evolution, we first assayed the affinity against Hu-1 and BA.1 RBD proteins of over 600 randomly selected monoclonal IgGs, isolated from the supernatants of single-cell cultured RBD-specific MBCs from longitudinally sampled donors pre- and post-BA.1 breakthrough infection. We detected a clear increase in affinity of the overall antibody pool against BA.1 RBD between 2 and 6 months after BA.1 infection (Figure 4A). Despite being already of high affinity against Hu-1 RBD proteins after 3 doses of mRNA vaccine—median dissociation constant (K_D) of 3.7 × 10^{-10} M (Figure 4A) and 73.7 ± 7.3% of tested monoclonal antibodies (mAbs) with measured affinity below 1 nM (Figure 4B)—further modest affinity increases against the Hu-1 RBD could also be observed, a trend seen in 4 out of 5 individuals (Figure S4A; Table S3). The increase in affinity against BA.1 RBD did not solely result from the selection of clones recognizing unmutated residues as the proportion of MBC-derived mAbs binding both ancestral Hu-1 and BA.1 RBD with similar affinities (labeled "unaffected," Figures 4C and S4B) remained stable over time, representing between 60% and 70% of the overall repertoire. Instead, the increase in affinity was seen in the "affected" clones pool, with a progressive loss of the non-binder/fully impaired clones against BA.1 RBD ($K_D > 10^{-7}$ M) up to the latest time point after BA.1 breakthrough infection (Figure 4C). This increased affinity was further paralleled by a progressive improvement in neutralization potential of the overall MBC repertoire against both D614G and BA.1 SARS-CoV-2 viruses (Figure 4D), with notably 40% of potent neutralizing antibodies (>75% at 16 nM) and a strong reduction in mAbs with no detectable neutralization potency against BA.1 SARS-CoV-2 (i.e., <25% neutralization at 16 nM) at the latest time point.

To analyze how this extended to later variants of the Omicron sublineages, we next tested affinity against BA.2 RBD, which shares most of BA.1 mutations, and BA.5 RBD, which notably contains two key additional mutations (L452R and F486V) inside immunodominant epitopes.[35] A similar, albeit non-significant, trend for an overall increase in affinity was observed for BA.2 RBD (Figures 5A and 5B). The median affinity of the MBC repertoire against BA.5 RBD, on the other hand, showed the opposite trend (Figures 5A and 5B), partly driven by an increase in the frequency of partially affected clones against BA.5 over time (Figure 5C). Two by two comparisons of binding affinities between Hu-1 and BA.1, BA.2, and BA.5 RBD variants further pinpointed toward a specific increase in mAbs solely affected in their binding to BA.5 (labeled "BA.5-affected") and thus likely targeting epitopes containing one of BA.5-specific mutations (L452R or F486V) (Figures 5D, S4C, and S4D). On the contrary, the frequency of mAbs showing weaker binding to all tested Omicron lineage RBDs (labeled "BA.1/2/5-affected") and likely targeting one of the core Omicron lineage mutations (G339D, S375F, K417N, N440K, G446S, S477N, T478K, E484K/Q/A) remained stable over time. And we only observed a few clones affected by BA.1-specific (G446S/G496S), BA.1/BA.2 (Q493R), and BA.2/BA.5-shared (T376A/D405N/R408S) mutations. Germline V_H gene usage according to RBD binding properties did not change over time (Figure S4E) and highlighted VH1-69 as a major component of mAbs specifically targeting RBD residues mutated in BA.5, as recently shown by others.[31]

Although the overall frequency of broadly binding antibodies did decrease over time, they still accounted for 44 ± 11% of all antibodies in all assayed donors 6 months after BA.1 breakthrough infection (Figures 5D and S4C). And, in line with the overall affinity maturation observed against Hu-1 and BA.1, and the fact that these antibodies likely recognize epitopes unmutated in BA.5, broadly binding antibodies also showed detectable affinity maturation against BA.5 (Figure 5E) and increased neutralization potency against all three tested SARS-CoV-2 variants (Figures 5F, S5A, and S5B). However, as previously described,[9] only a fraction of these broadly binding antibodies displayed intermediate or potent neutralization against all viruses, suggesting a lack of selective pressure. A similar increase in affinity and neutralization potency could be seen for BA.1/2/5-affected mAbs (Figures S5A and S5B). And this appeared to explain most of the overall increase in neutralization potency against BA.5 of the whole MBC repertoire (Figure 5F). This substantial gain of neutralization potency was equally observed for neutralizing antibodies using IGHV1-69, IGVH3-30, or IGHV3-53/66 genes, suggesting that these recurrent classes of anti-RBD antibodies can be recruited to participate in neutralization against mutated epitopes (Figures S5A and S5C).

Overall, these results demonstrate that the MBC repertoire remodeling observed following BA.1 breakthrough infection leads to an improved affinity and breadth of the MBC repertoire. Part of

Figure 4. BA.1 breakthrough infection drives additional maturation of Hu-1/BA.1 cross-reactive RBD-specific memory B cells

(A) Dissociation constants (K_D, expressed as moles/L) measured by biolayer interferometry against Hu-1 and BA.1 RBDs for naturally expressed monoclonal antibodies randomly selected from single-cell culture supernatants of RBD-specific MBCs isolated from 6 donors, including 3 longitudinally analyzed before and after BA.1 BT infection (see Figure S4A). Numbers of tested monoclonal and median affinity per time point are indicated at the bottom of each graph.

(B) Frequencies of Hu-1 and BA.1 RBD high-binders ($K_D < 10^{-9}$ M), mid-binders ($10^{-9} \leq K_D < 10^{-8}$ M), low-binders ($10^{-8} \leq K_D < 10^{-7}$ M), or non-binders ($K_D \geq 10^{-7}$ M) among tested monoclonals antibodies at indicated time points.

(C) Measured K_Ds against BA.1 versus Hu-1 RBDs for all tested monoclonal antibodies. Light and dark red shaded zones indicate partially and fully impaired BA.1-affected monoclonal antibodies, respectively (see STAR Methods). Respective frequencies are shown at the bottom of the graph (see also Figure S4B).

(D) Distribution in *in vitro* neutralization potency against authentic D614G and BA.1 SARS-CoV-2 virus for randomly selected RBD-specific monoclonal antibodies at indicated time points. Number at the center of the pie indicates the total number of tested monoclonal antibodies.

(A) Kruskal-Wallis tests with Benjamini, Krieger, and Yekutieli false discovery rate correction for multiple comparisons (q values are indicated in the figure). (B and E) Mixed model analysis with Tukey's correction. (D) Chi-squared test. ****$p < 0.0001$, *$p < 0.05$.

See also Figures S4 and S5 and Table S3.

Please cite this article in press as: Sokal et al., SARS-CoV-2 Omicron BA.1 breakthrough infection drives late remodeling of the memory B cell repertoire in vaccinated individuals, Immunity (2023), https://doi.org/10.1016/j.immuni.2023.07.007

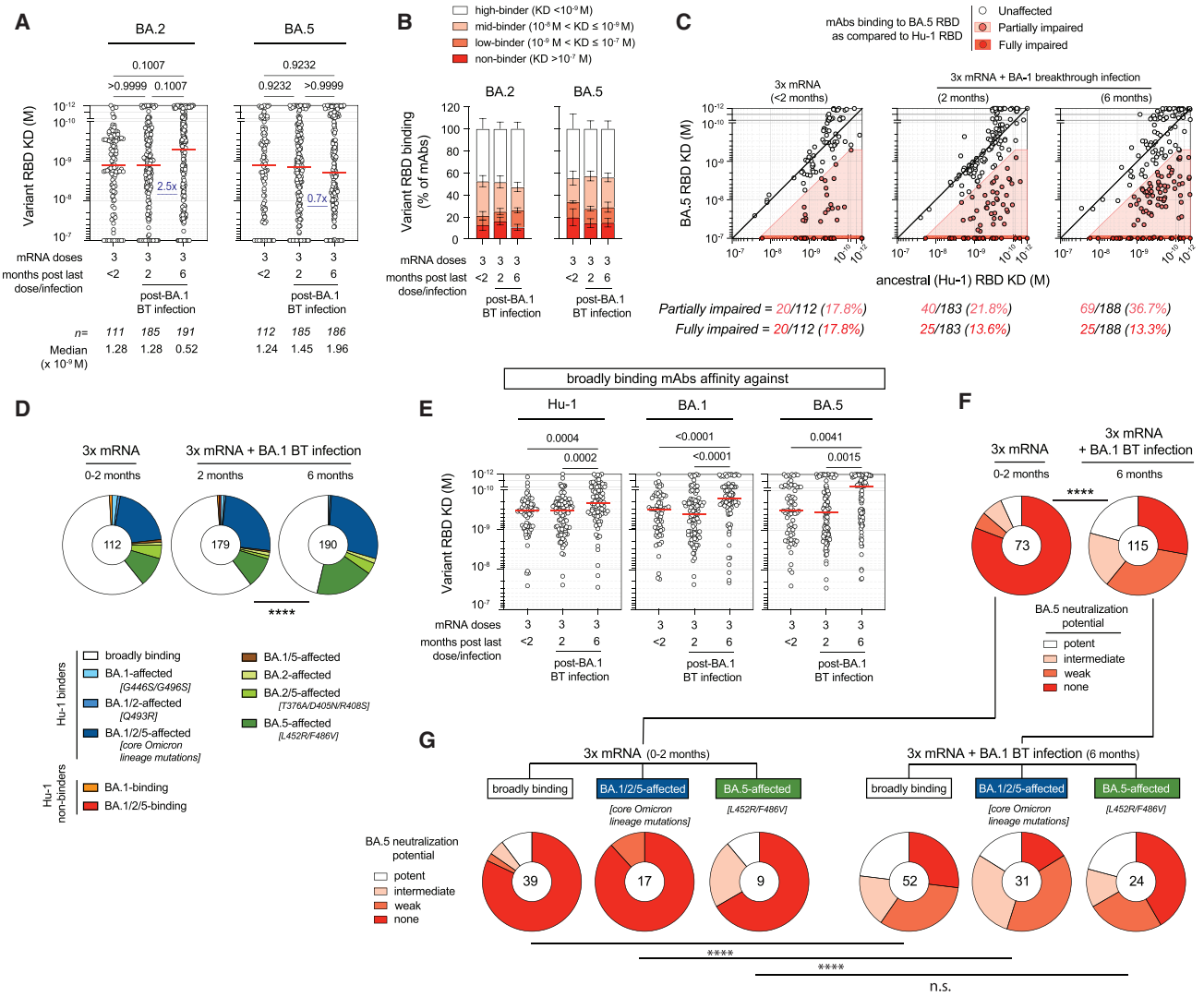

Figure 5. BA.1 breakthrough infection broadly increases neutralization breadth of MBC-derived mAbs

(A) Dissociation constants (K_D, expressed as moles/L) measured by biolayer interferometry against BA.2 and BA.5 RBDs for all tested monoclonal antibodies displayed in Figure 4A (see Figure S4A). Numbers of tested monoclonal and median affinity per time point are indicated at the bottom of each graph.

(B) Frequencies of BA.2 and BA.5 RBD high-binders ($K_D < 10^{-9}$ M), mid-binders ($10^{-9} \leq K_D < 10^{-8}$ M), low-binders ($10^{-8} \leq K_D < 10^{-7}$ M), or as non-binders ($K_D \geq 10^{-7}$ M) among tested monoclonal antibodies at indicated time point.

(C) Measured K_Ds against BA.5 versus Hu-1 RBDs for all tested monoclonal antibodies. Light and dark red shaded zones indicate partially and fully impaired BA.5-affected monoclonal antibodies, respectively (see STAR Methods). Respective frequencies are shown at the bottom of the graph (see also Figure S4B).

(D) Overall distribution of tested monoclonal according to their binding patterns against Hu-1, BA.1, BA.2, and BA.5 RBDs at indicated time points.

(E) Measured K_D against Hu-1, BA.1, and BA.5 RBDs for broadly binding monoclonal antibodies tested in (A) at indicated time point.

(F and G) Distribution in *in vitro* neutralization potency against authentic BA.5 SARS-CoV-2 virus at indicated time point for randomly selected naturally expressed monoclonal antibodies (F) or monoclonal antibodies falling in the broadly binding, BA.1/2/5-affected, and BA.5-affected groups as defined in (D) and (G). In (D), (F), and (G), numbers at the center of each pie chart indicate the total number of tested monoclonal antibodies.

(A and E) Kruskal-Wallis tests with Benjamini, Krieger, and Yekutieli false discovery rate correction for multiple comparisons (q values are indicated in the figure).

(D, F, and G) Chi-squared tests. ****$p < 0.0001$.

See also Figures S4 and S5 and Table S3.

this comes from redirecting the response toward conserved immunodominant epitopes in BA.1, with the inherent risk that these epitopes could be mutated in later variants, as seen with BA.5. Such risk, however, is counterbalanced by a global enhancement in affinity against all epitopes included in the BA.1 RBD. This mechanism provides substantial neutralization benefit against both past and future variants sharing similar epitopes.

Selective expansion of MBCs outside GC and additional cycles of GC maturation sequentially contribute to MBC repertoire remodeling

Such remodeling and maturation of the MBC repertoire post-BA.1 breakthrough infection could be simply explained by the expansion of high-affinity, pre-mutated MBCs independently of any GC reaction.[36] Alternatively, this could also reflect a

Please cite this article in press as: Sokal et al., SARS-CoV-2 Omicron BA.1 breakthrough infection drives late remodeling of the memory B cell repertoire in vaccinated individuals, Immunity (2023), https://doi.org/10.1016/j.immuni.2023.07.007

progressive output of clones having undergone new rounds of GC reaction, as recently shown in the context of a third mRNA vaccine dose.[25] The first hypothesis would be expected to lead to early changes post infection, also impacting the ASC response, whereas the second would be expected to have a more progressive impact associated with the progressive output of clones from GCs.

In line with the early recruitment and proliferation of MBC clones outside of a GC reaction, we could detect an increased frequency of cells within clones bearing identical sequences in multiple donors at the earlier time points post 2nd and 3rd vaccine doses and post-BA.1 infection (Figure S6A), resulting in an overall drop in sequence diversity (Figure S6B). The diversity, however, appeared mostly restored at the 6 months' time point. A preferential recruitment of a highly mutated subpopulation of pre-existing MBC clones to the ASC compartment could also be observed when analyzing total IgV_H mutations as well as replacing mutations in the heavy-chain complementarity-determining regions (CDRs) in Hu-1/BA.1 cross-reactive RBD-specific ASCs generated early after BA.1 infection (Figures 6A and S6C) and to a lesser extend in clonally related MBC clones at the same time point (Figure S6D). In parallel to the contraction of the early MBC/ASC response, longitudinal evolution in mutation profile in cross-reactive RBD-specific MBCs revealed an initial decrease in the average total number of V_H mutations, seen at 2 months post-BA.1 infection (Figures 6A, S6C, and S6D). This was notably associated with an increased presence of lowly mutated cells, including 2.77% of unmutated sequences (Figure 6B). Sequences with low numbers of mutations (<10 mutations) could mostly be seen in low-frequency clones early post-BA.1 infection, thereafter, slowly transiting to the newly expanded pool (Figures 6C and 6D). Subsequently, the average number of IgV_H mutations and replacing mutations in CDRs of cross-reactive MBCs significantly increased between 2 and 6 months after BA.1 infection (Figures 6A, S6B, and S6E, $p < 0.01$), reaching similar mutational loads as seen early post 3rd vaccine dose or BA.1 infection.

This parallel increase in mutational load and affinity maturation observed between 2 and 6 months after BA.1 infection in the MBC repertoire in our longitudinally sampled donors suggested that naive B cells or previously generated MBCs could be recruited to newly formed or vaccine-induced persisting GCs. To investigate this point at the clonal level, we next looked at IgV_H mutation number evolution in persisting clones pre- and post-BA.1 infection. Out of 22 total Hu-1/BA.1 cross-reactive RBD-specific clones with more than 7 sequences identified at least twice between the post-3rd mRNA vaccine dose time point and later time points after BA.1 breakthrough infection, 3 clones were detected to be significantly accumulating mutations over time (Figure 6E; $p = 0.00001$, $p = 0.0086$, and $p = 0.0203$, respectively). These numbers, although clearly reduced as compared with the frequency of clones in evolution seen between the 2nd and 3rd vaccine dose (3 out of 4 with more than 7 sequences, Figure 6F), are in line with a similar analysis recently performed in the context of influenza vaccine recall response in which such GC response could be validated by direct staining of draining lymph nodes.[18,37] These clones included both sustained (clone 5,584 from donor Na-25) and newly expanded clones, in line with the fact that cells from both sustained and newly expanded/low-frequency MBC clones showed a similar tendency to gain in affinity toward BA.1 RBD variant between 2 and 6 months after infection (Figure S6F). Nevertheless, we found no systematic correlation between the increase in total mutation load and affinity at the repertoire (Figure S6G) or clonal level, with notably only one out of the three clones identified as statistically increasing their overall mutational load over time after infection also increasing in affinity (Figure 6E). Differences between the two groups of clones were more marked for neutralization potency (Figure S6H). Although the majority of lost or low-frequency clones pre-BA.1 infection was non or poor-neutralizers of both the D614G and BA.1 SARS-CoV-2 viruses, newly expanded and low-frequency clones seen 6 months after BA.1 infection reached similar neutralization potency as their counterparts from sustained clones.

Overall, these analyses suggest that the MBC repertoire is dynamically reshaped by an early extra-GC expansion and subsequent contraction of a few selected highly mutated cross-reactive clones and the concomitant settlement of a more diverse pool of cells in the repertoire likely, but not necessarily exclusively, representing new GC outputs.

DISCUSSION

Little is known about the remodeling induced by an infection by a viral variant showing antigenic drift on a repertoire of preformed mature human MBCs. Selective boosting of cross-reactive antibody specificities by prior exposures was historically coined, in the context of influenza, "original antigenic sin."[38,39] Studies in mice have shown that upon reinfection or re-exposure to an antigen, the MBC pool can expand outside the GCs in an affinity-dependent selective process,[40] differentiate in PCs, or reenter GCs to undergo affinity maturation.[19,41] These secondary GCs, however, mostly engage naive clones, allowing diversification against new epitopes.[19,36,40,42,43] Understanding how these different paths shape the recall response in humans to an antigenic variant of respiratory viruses such as SARS-CoV-2 remains an open question with fundamental implications for the design of future vaccination booster strategies.

As previously reported for influenza[30] and more recently SARS-CoV-2 variant breakthrough infections[22,31] or variant-based vaccination,[25] the initial ABC response following BA.1 breakthrough infection is clearly dominated by highly mutated vaccine-induced cross-reactive MBC clones eliciting broadly cross-neutralizing antibodies, a point that we could further confirm at the level of ASCs. Here, we show that this imprinting was not limited to the early extrafollicular response but persisted over time, with very few BA.1-restricted naive B cell clones recruited in *de novo* GCs. High-affinity serum antibodies elicited during the primary response have recently been demonstrated to reduce the recruitment of naive B cells to GCs during secondary responses.[44] Such a process, however, is epitope-specific[44] and, in individuals infected during the first wave of COVID-19, MBCs specific for the S of seasonal coronaviruses elicited non-neutralizing antibodies against SARS-CoV-2 that did not impair the recruitment of near-germline B cell clones recognizing novel epitopes present in SARS-CoV-2 RBD.[13,16] Similarly, the massive antibody response against non-neutralizing immunodominant epitopes upon a second immunization with H5N1 vaccine or HIV

Please cite this article in press as: Sokal et al., SARS-CoV-2 Omicron BA.1 breakthrough infection drives late remodeling of the memory B cell repertoire in vaccinated individuals, Immunity (2023), https://doi.org/10.1016/j.immuni.2023.07.007

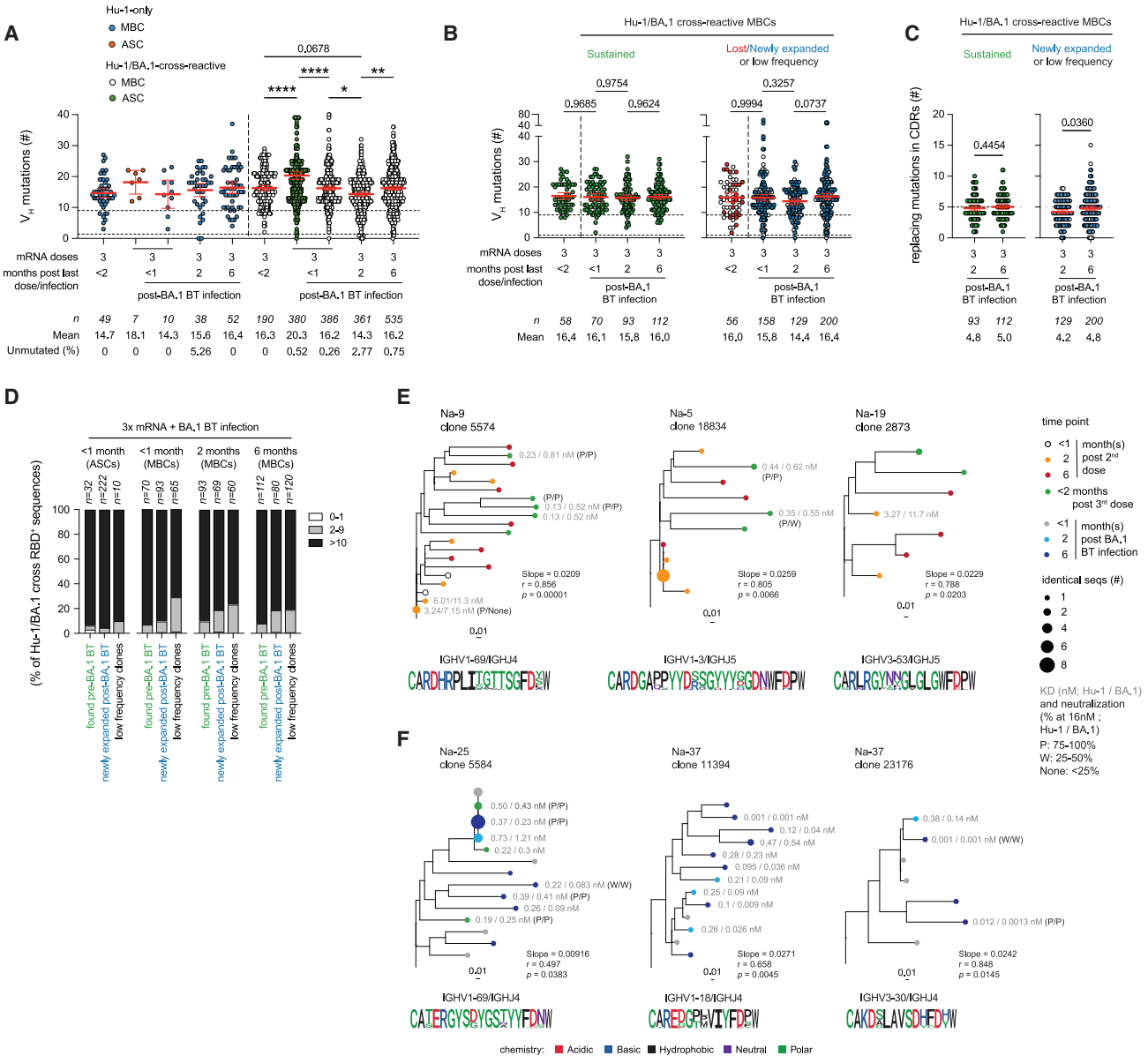

Figure 6. MBC repertoire remodeling and maturation post-BA.1 breakthrough infection reflects successive contributions from extra-GC and GC responses together with the recruitment of low-frequency lowly mutated MBC clones

(A) Total number of IgV_H mutations in RBD-specific MBCs or ASCs, sorted according to their specificity (Hu-1 RBD-only [left, blue and red dots] versus Hu-1/BA.1 RBD cross-reactive [right, white and green dot]) at indicated time points before and after BA.1 BT infection. Mean ± SEM are shown.

(B–D) Number of total (B) or CDR3 replacing IgV_H mutations (C), and (D) distribution in total number of IgV_H mutations (0–1, white; 2–9, gray; and ≥10, black) at indicated time points in Hu-1/BA.1 cross-reactive RBD-specific MBCs, grouped according to their clone's evolution upon BA.1 BT infection, as defined in Figure 3C.

(E and F) Phylogenetic trees for six RBD-specific clones identified as significantly evolving between 2 and 3 mRNA vaccinations (n = 3, E) and post-BA.1 BT infections (n = 3, F), scaled according to IgV_H mutation frequencies. Color code and dot size reflect, respectively, time of sampling and number of identical sequences found at each time point. CDR3 (amino acids) frequency plot logos, slope for the rate of somatic mutation accumulation over time (slope), and p value (p) of the date randomization test comparing the Pearson's correlation (r) between divergence and time in tree are shown at the bottom of each tree. Averaged (median) RBD affinity (gray) and neutralization potencies (black, : P: >75%, W: 25%–50%, and None: <25% neutralization at 16 nM) for Hu-1 (left) and BA.1 (right) are indicated on the right side of each tested monoclonal antibodies in the tree.

(A and B) ordinary one-way ANOVA with Sidak's correction for multiple comparisons.

(C) Unpaired t tests. ****p < 0.0001, **p < 0.01, *p < 0.05.

See also Figure S6 and Table S3.

Please cite this article in press as: Sokal et al., SARS-CoV-2 Omicron BA.1 breakthrough infection drives late remodeling of the memory B cell repertoire in vaccinated individuals, Immunity (2023), https://doi.org/10.1016/j.immuni.2023.07.007

Env proteins masked these epitopes, thereby promoting maturation of naive B cells in GCs against a different set of non-dominant epitopes.[45–47] In our study, all individuals had recently received a third dose of Hu-1-pre-fusion S protein-based mRNA vaccine, but this vaccine boost did not prevent subsequent BA.1 breakthrough infection and MBC recruitment to the extrafollicular response. Omicron's antigenic distance should thus have enabled exposure of mutated epitopes of the RBD, as previously described in the context of primary infection with SARS-CoV-2 variants.[21] One possible explanation for the limited strain-specific response against BA.1 could be the absence of a sufficient amount of viral antigen to activate naive B cells, as the virus is rapidly cleared by neutralizing antibodies produced by newly recruited cross-reactive MBCs. Alternatively, the high initial frequency of cross-reactive MBCs, even if displaying variable affinity to mutated BA.1 RBD epitopes, may also provide them with a competitive advantage that restricts antigen accessibility to naive B cells. It remains that we did observe a late recruitment of unmutated and lowly mutated cross-reactive cells in the MBC repertoire. These cells could represent naive B cells recruited to an ongoing GC reaction.[48,49] This would suggest the active selection of cross-reactive B cells in the GC. Alternatively, some of these cells could also be the result of the expansion of pre-existing lowly mutated MBCs outside any GC reaction.

The absence of *de novo* recruitment of BA.1-restricted naive B cells and the parallel focus on cross-reactive MBC clones could have induced progressive reduction in overall diversity, a point we only observed transiently upon infection and mostly in the ASCs. And, although non-cross-reactive Hu-1-specific MBCs tend to be excluded from the early ABC/extra-GC response, their frequency returned to pre-BA.1 infection baseline at later time points in the response. Changes in the repertoire up to 6 months after BA.1 infection, however, were not solely restricted to the expansion and later contraction of a cross-reactive MBC response through the extra-GC response. The longitudinal tracking of RBD-specific clones revealed a more complex picture with a progressive remodeling of the MBC repertoire, refining clonal hierarchy against BA.1 epitopes, and resulting in a clear improvement in both overall affinity and neutralization breadth. Although overall functional variations were clearly more subtle than what can be detected over time in newly vaccinated individuals[12–16] (and this study), our results suggest new cycles of GC maturation for naive B cells and vaccine-induced MBCs following BA.1 breakthrough infection. This is in line with the recent description of a sustained GC response following a vaccine boost in double-vaccinated individuals.[25] Additionally, the magnitude of the GC reaction was probably underestimated in our analysis as investigating such marks in the context of a recall response in the PBMCs, with an already fully mature MBC repertoire, is clearly challenging.[37] Limited longitudinal sampling and overrepresentation in the early repertoire post-antigenic exposure of sequences from cells having undergone recent expansion in the extra GC response likely add up to restrict our analysis to high-frequency persisting clones. The increase in mutational load observed in low-frequency and newly expanded clones later in the response clearly suggests a key contribution of these cells to the remodeling of the MBC repertoire. Whether such initially low-frequency clones reenter GCs remains to be demonstrated. This would require direct sampling of draining lymphoid organs. Altogether, the remodeling of the MBC repertoire upon BA.1 breakthrough infection is in line with a recent theoretical modeling study pointing toward the GC reaction during a secondary reaction as a key mechanism to reintroduce diversity in the MBC pool.[36] The contribution of the extra-GC expansion of MBC clones and the GCs output to remodel the MBC repertoire appears nevertheless variable from one individual to another.

Finally, our results also raise two clinically relevant points. First, breakthrough infection clearly switched the overall MBC response toward RBD epitopes. Second, post-breakthrough maturation of the MBC response could be considered to expand toward non-mutated immunodominant epitopes on the RBD. The modified pattern of immunodominance at the S level could be explained by the epitope masking of highly conserved region of the S2 domain by the pre-existing antibody response[31] or by differential conformational states of SARS-CoV-2 S protein between the vaccine and the virus. Whether this bears any functional relevance regarding overall protection against future infections, positive or negative, remains to be tested. The modified pattern of immunodominance at the RBD level suggests that repeated challenges with variant S proteins may simply increase the selective advantage of specific amino-acid substitutions, as exemplified here for the L452Q/R mutation responsible for part of the immune escape potential of the BA.5 strain from IGHV1-69 and IGHV3-9 class of antibodies.[31,50] In terms of vaccination, it suggests that further strategies to extend the immune response beyond the conserved RBD epitopes will be needed to favor diversity and cope with future antigenic drifts of the SARS-CoV-2.

Collectively, these data show that although BA.1 breakthrough infection induces a cross-reactive extra-GC expansion, the clonal diversity is maintained by the GCs' output to remodel and improve neutralization potency and breadth of the MBC repertoire.

Limitations of the study

Potential limitations of our work include the limited number of subjects that could be included in this study for in-depth MBC characterization as well as the sparse sampling that could be achieved for some of these donors at some time points. This may have introduced some bias in clonal representation. As such, the extent of observed clonal remodeling and affinity maturation should be interpreted with caution, notably in donors for which the number of analyzable sequences was low, potentially affecting the labeling of clones as "lost," "sustained," or "newly expanded" and limiting the contribution of individual donors to the overall pool of tested mAbs. To limit such biases, we have attempted to select similar number of clones per donor when testing affinities and neutralization and to display individual donor data in Figures S1–S6. All patients studied were infected with BA.1 early after their third vaccine boost (see Figure 1A; Table S1B), as has been the case for a sizable fraction of early Omicron breakthrough infections. In this setting, mRNA vaccine-induced residual GCs driven by the Hu-1 pre-fusion S were recently activated.[25] As we were not able to perform direct longitudinal comparisons with non-infected individuals having solely received 3 doses of mRNA vaccine, we cannot exclude that part of the observed clonal remodeling would have occurred in non-infected individuals. It also remains to be investigated whether such a situation, with two closely related antigens being presented

concomitantly as currently implemented in bivalent vaccines, might favor the selection of cross-reactive MBCs and affinity maturation against both antigens. Affinity maturation was only observed against the BA.1 RBD in a recent preprint analyzing MBCs following a similar BA.1 breakthrough infection in individuals mostly remote from their second mRNA vaccine dose.

STAR★METHODS

Detailed methods are provided in the online version of this paper and include the following:

- KEY RESOURCES TABLE
- RESOURCE AVAILABILITY
  - Lead Contact
  - Materials Availability
  - Data and Code Availability
- EXPERIMENTAL MODEL AND SUBJECT DETAILS
  - Study participants
  - Virus strains
- METHOD DETAILS
  - Anti- RBD (S) and -N SARS-CoV-2 antibodies assay
  - Recombinant protein purification
  - Flow cytometry and cell sorting
  - Single-cell culture
  - ELISA
  - Single-cell RNA-seq library preparation and sequencing
  - Single-cell IgH sequencing
  - Single-cell gene expression analysis
  - Computational analyses of VDJ sequences
  - Affinity measurement using biolayer interferometry (Octet)
  - Virus neutralization assay
- QUANTIFICATION AND STATISTICAL ANALYSIS
- ADDITIONAL RESOURCES

SUPPLEMENTAL INFORMATION

Supplemental information can be found online at https://doi.org/10.1016/j.immuni.2023.07.007.

ACKNOWLEDGMENTS

We thank Garnett Kelsoe (Duke University, Durham, NC, USA) for providing us with the human cell culture system, together with invaluable advice. We thank all the physicians, Constance Guillaud, Raphael Lepeule, Frédéric Schlemmer, Elena Fois, Henri Guillet, Nicolas De Prost, Sarah Feray, and Pascal Lim, whose patients were included in this study. Funding: this study has been labeled as a National Research Priority by the National Orientation Committee for Therapeutic Trials and other research on COVID-19 (CAPNET). The investigators would like to acknowledge ANRS|Emerging Infectious Diseases for their scientific support, the French Ministry of Health and Prevention, the French Ministry of Higher Education, Research, and Innovation, and the Fondation Princesse Grace for their funding and support. Assistance Publique – Hôpitaux de Paris (AP-HP, Département de la Recherche Clinique et du Développement) was the promotor and sponsor of MEMO-COV-2. Work in the Unit of Structural Virology was funded by the Institut Pasteur, Urgence COVID-19 Fundraising Campaign of Institut Pasteur. P.B. acknowledges funding from the Institut Pasteur and the Institut National de la Santé et de la Recherche Médicale (INSERM). A.S. was supported by a Poste d'accueil from INSERM.

AUTHOR CONTRIBUTIONS

Conceptualization, A.S., G.B.-S., J.-C.W., F.A.R., P.B., M. Mahévas, and P.C.; data curation, A.S., L.H., M. Broketa, G.B.-S., I.F., I.A, L.L., and P.C. ; formal analysis, A.S., P.C., L.H., M. Broutin, G.B.-S., I.A., A.R., M.B.-A., S. Fourati, A.V., and I.F.; funding acquisition, J.-C.W., C.-A.R., S. Fillatreau, P.B., P.C., and M. Mahévas; investigation, A.S., L.H., I.A., P.L.-R., M.F., J.M., and A.V.; methodology, A.S., J.-C.W., F.A.R., P.B., M. Mahévas, and P.C.; project administration, P.C. and M.Mahévas; resources, I.F., J.-M.P., F.P., S. Fourati, E.C., M. Michel, B.G., S.G., G.M., Y.N., P.B., F.A.R., and M. Mahévas; software, P.C.; supervision, J.-C.W., P.B., F.A.R., P.C., and M. Mahévas; validation, A.S., A.V., M. Broketa, P.C., and M. Mahévas; visualization, A.S., M. Broutin, I.A., M. Mahévas, and P.C.; writing – original draft, A.S., M. Mahévas, and P.C.; writing – review & editing, all authors.

DECLARATION OF INTERESTS

Outside of the submitted work, M. Mahévas received research funds from GSK and personal fees from LFB and Amgen. J.-C.W. received consulting fees from Institut Mérieux. P.B. received consulting fees from Regeneron Pharmaceuticals.

Received: January 27, 2023
Revised: May 12, 2023
Accepted: July 6, 2023
Published: August 4, 2023

REFERENCES

1. van der Straten, K., Guerra, D., van Gils, M.J., Bontjer, I., Caniels, T.G., van Willigen, H.D.G., Wynberg, E., Poniman, M., Burger, J.A., Bouhuijs, J.H., et al. (2022). Antigenic cartography using sera from sequence-confirmed SARS-CoV-2 variants of concern infections reveals antigenic divergence of Omicron. Immunity *55*, 1725–1731.e4. https://doi.org/10.1016/j.immuni.2022.07.018.
2. Dejnirattisai, W., Huo, J., Zhou, D., Zahradník, J., Supasa, P., Liu, C., Duyvesteyn, H.M.E., Ginn, H.M., Mentzer, A.J., Tuekprakhon, A., et al. (2022). SARS-CoV-2 Omicron-B.1.1.529 leads to widespread escape from neutralizing antibody responses. Cell *185*, 467–484.e15. https://doi.org/10.1016/j.cell.2021.12.046.
3. Garcia-Beltran, W.F., Lam, E.C., St. Denis, K., Nitido, A.D., Garcia, Z.H., Hauser, B.M., Feldman, J., Pavlovic, M.N., Gregory, D.J., Poznansky, M.C., et al. (2021). Multiple SARS-CoV-2 variants escape neutralization by vaccine-induced humoral immunity. Cell *184*, 2372–2383.e9. https://doi.org/10.1016/j.cell.2021.03.013.
4. Muik, A., Lui, B.G., Wallisch, A.-K., Bacher, M., Mühl, J., Reinholz, J., Ozhelvaci, O., Beckmann, N., de la Güimil Garcia, R., Poran, A., et al. (2022). Neutralization of SARS-CoV-2 Omicron by BNT162b2 mRNA vaccine-elicited human sera. Science *375*, 678–680. https://doi.org/10.1126/science.abn7591.
5. Cameroni, E., Bowen, J.E., Rosen, L.E., Saliba, C., Zepeda, S.K., Culap, K., Pinto, D., VanBlargan, L.A., De Marco, A., di Iulio, J., et al. (2022). Broadly neutralizing antibodies overcome SARS-CoV-2 Omicron antigenic shift. Nature *602*, 664–670. https://doi.org/10.1038/s41586-021-04386-2.
6. Planas, D., Saunders, N., Maes, P., Guivel-Benhassine, F., Planchais, C., Buchrieser, J., Bolland, W.H., Porrot, F., Staropoli, I., Lemoine, F., et al. (2022). Considerable escape of SARS-CoV-2 Omicron to antibody neutralization. Nature *602*, 671–675. https://doi.org/10.1038/s41586-021-04389-z.
7. Carreño, J.M., Alshammary, H., Tcheou, J., Singh, G., Raskin, A.J., Kawabata, H., Sominsky, L.A., Clark, J.J., Adelsberg, D.C., Bielak, D.A., et al. (2022). Activity of convalescent and vaccine serum against SARS-CoV-2 Omicron. Nature *602*, 682–688. https://doi.org/10.1038/s41586-022-04399-5.
8. Planas, D., Bruel, T., Staropoli, I., Guivel-Benhassine, F., Porrot, F., Maes, P., Grzelak, L., Prot, M., Mougari, S., Planchais, C., et al. (2023). Resistance of Omicron subvariants BA.2.75.2, BA.4.6, and BQ.1.1 to

neutralizing antibodies. Nat. Commun. *14*, 824. https://doi.org/10.1038/s41467-023-36561-6.

9. Sokal, A., Broketa, M., Barba-Spaeth, G., Meola, A., Fernández, I., Fourati, S., Azzaoui, I., de La Selle, A., Vandenberghe, A., Roeser, A., et al. (2022). Analysis of mRNA vaccination-elicited RBD-specific memory B cells reveals strong but incomplete immune escape of the SARS-CoV-2 Omicron variant. Immunity *55*, 1096–1104.e4. https://doi.org/10.1016/j.immuni.2022.04.002.
10. Wang, Z., Muecksch, F., Cho, A., Gaebler, C., Hoffmann, H.H., Ramos, V., Zong, S., Cipolla, M., Johnson, B., Schmidt, F., et al. (2022). Analysis of memory B cells identifies conserved neutralizing epitopes on the N-terminal domain of variant SARS-Cov-2 spike proteins. Immunity *55*, 998–1012.e8. https://doi.org/10.1016/j.immuni.2022.04.003.
11. Goel, R.R., Painter, M.M., Lundgreen, K.A., Apostolidis, S.A., Baxter, A.E., Giles, J.R., Mathew, D., Pattekar, A., Reynaldi, A., Khoury, D.S., et al. (2022). Efficient recall of Omicron-reactive B cell memory after a third dose of SARS-CoV-2 mRNA vaccine. Cell *185*, 1875–1887.e8. https://doi.org/10.1016/j.cell.2022.04.009.
12. Dugan, H.L., Stamper, C.T., Li, L., Changrob, S., Asby, N.W., Halfmann, P.J., Zheng, N.Y., Huang, M., Shaw, D.G., Cobb, M.S., et al. (2021). Profiling B cell immunodominance after SARS-CoV-2 infection reveals antibody evolution to non-neutralizing viral targets. Immunity *54*, 1290–1303.e7. https://doi.org/10.1016/j.immuni.2021.05.001.
13. Gaebler, C., Wang, Z., Lorenzi, J.C.C., Muecksch, F., Finkin, S., Tokuyama, M., Cho, A., Jankovic, M., Schaefer-Babajew, D., Oliveira, T.Y., et al. (2021). Evolution of antibody immunity to SARS-CoV-2. Nature *591*, 639–644. https://doi.org/10.1038/s41586-021-03207-w.
14. Rodda, L.B., Netland, J., Shehata, L., Pruner, K.B., Morawski, P.A., Thouvenel, C.D., Takehara, K.K., Eggenberger, J., Hemann, E.A., Waterman, H.R., et al. (2021). Functional SARS-CoV-2-specific immune memory persists after mild COVID-19. Cell *184*, 169–183.e17. https://doi.org/10.1016/j.cell.2020.11.029.
15. Sokal, A., Chappert, P., Barba-Spaeth, G., Roeser, A., Fourati, S., Azzaoui, I., Vandenberghe, A., Fernandez, I., Meola, A., Bouvier-Alias, M., et al. (2021). Maturation and persistence of the anti-SARS-CoV-2 memory B cell response. Cell *184*, 1201–1213.e14. https://doi.org/10.1016/j.cell.2021.01.050.
16. Sokal, A., Barba-Spaeth, G., Fernández, I., Broketa, M., Azzaoui, I., de La Selle, A., Vandenberghe, A., Fourati, S., Roeser, A., Meola, A., et al. (2021). mRNA vaccination of naive and COVID-19-recovered individuals elicits potent memory B cells that recognize SARS-CoV-2 variants. Immunity *54*, 2893–2907.e5. https://doi.org/10.1016/j.immuni.2021.09.011.
17. Koutsakos, M., and Ellebedy, A.H. (2023). Immunological imprinting: understanding COVID-19. Immunity *56*, 909–913. https://doi.org/10.1016/j.immuni.2023.04.012.
18. Turner, J.S., Zhou, J.Q., Han, J., Schmitz, A.J., Rizk, A.A., Alsoussi, W.B., Lei, T., Amor, M., McIntire, K.M., Meade, P., et al. (2020). Human germinal centres engage memory and naive B cells after influenza vaccination. Nature *586*, 127–132. https://doi.org/10.1038/s41586-020-2711-0.
19. Victora, G.D., and Nussenzweig, M.C. (2022). Germinal centers. Annu. Rev. Immunol. *40*, 413–442. https://doi.org/10.1146/annurev-immunol-120419-022408.
20. Evans, J.P., Zeng, C., Qu, P., Faraone, J., Zheng, Y.M., Carlin, C., Bednash, J.S., Zhou, T., Lozanski, G., Mallampalli, R., et al. (2022). Neutralization of SARS-CoV-2 Omicron sub-lineages BA.1, BA.1.1, and BA.2. Cell Host Microbe *30*, 1093–1102.e3. https://doi.org/10.1016/j.chom.2022.04.014.
21. Agudelo, M., Muecksch, F., Schaefer-Babajew, D., Cho, A., DaSilva, J., Bednarski, E., Ramos, V., Oliveira, T.Y., Cipolla, M., Gazumyan, A., et al. (2022). Plasma and memory antibody responses to Gamma SARS-CoV-2 provide limited cross-protection to other variants. J. Exp. Med. *219*, e20220367. https://doi.org/10.1084/jem.20220367.
22. Kaku, C.I., Starr, T.N., Zhou, P., Dugan, H.L., Khalifé, P., Song, G., Champney, E.R., Mielcarz, D.W., Geoghegan, J.C., Burton, D.R., et al. (2023). Evolution of antibody immunity following Omicron BA.1 breakthrough infection. Nat. Commun. *14*, 2751. https://doi.org/10.1038/s41467-023-38345-4.
23. Quandt, J., Muik, A., Salisch, N., Lui, B.G., Lutz, S., Krüger, K., Wallisch, A.K., Adams-Quack, P., Bacher, M., Finlayson, A., et al. (2022). Omicron BA.1 breakthrough infection drives cross-variant neutralization and memory B cell formation against conserved epitopes. Sci. Immunol. *7*, eabq2427. https://doi.org/10.1126/sciimmunol.abq2427.
24. Muik, A., Lui, B.G., Bacher, M., Wallisch, A.K., Toker, A., Finlayson, A., Krüger, K., Ozhelvaci, O., Grikscheit, K., Hoehl, S., et al. (2022). Omicron BA.2 breakthrough infection enhances cross-neutralization of BA.2.12.1 and BA.4/BA.5. Sci. Immunol. *7*, eade2283. https://doi.org/10.1126/sciimmunol.ade2283.
25. Alsoussi, W.B., Malladi, S.K., Zhou, J.Q., Liu, Z., Ying, B., Kim, W., Schmitz, A.J., Lei, T., Horvath, S.C., Sturtz, A.J., et al. (2023). SARS-CoV-2 Omicron boosting induces de novo B cell response in humans. Nature *617*, 592–598. https://doi.org/10.1038/s41586-023-06025-4.
26. Sokal, A., Bastard, P., Chappert, P., Barba-Spaeth, G., Fourati, S., Vanderberghe, A., Lagouge-Roussey, P., Meyts, I., Gervais, A., Bouvier-Alias, M., et al. (2023). Human type I IFN deficiency does not impair B cell response to SARS-CoV-2 mRNA vaccination. J. Exp. Med. *220*, e20220258. https://doi.org/10.1084/jem.20220258.
27. Bellusci, L., Golding, H., and Khurana, S. (2023). Therapeutic potential of convalescent plasma and hyperimmune immunoglobulins against SARS-CoV-2 BQ.1, BQ.1.1, and XBB variants. J. Clin. Invest. *133*, e168583. https://doi.org/10.1172/JCI168583.
28. Lee, W.S., Tan, H.-X., Reynaldi, A., Esterbauer, R., Koutsakos, M., Nguyen, J., Amarasena, T., Kent, H.E., Aggarwal, A., Turville, S.G., et al. (2023). Durable reprogramming of neutralising antibody responses following breakthrough Omicron infection. Preprint at medRxiv. https://doi.org/10.1101/2023.02.19.23286159.
29. Park, Y.J., Pinto, D., Walls, A.C., Liu, Z., De Marco, A., Benigni, F., Zatta, F., Silacci-Fregni, C., Bassi, J., Sprouse, K.R., et al. (2022). Imprinted antibody responses against SARS-CoV-2 Omicron sublineages. Science *378*, 619–627. https://doi.org/10.1126/science.adc9127.
30. Dugan, H.L., Guthmiller, J.J., Arevalo, P., Huang, M., Chen, Y.Q., Neu, K.E., Henry, C., Zheng, N.Y., Lan, L.Y.-L., Tepora, M.E., et al. (2020). Preexisting immunity shapes distinct antibody landscapes after influenza virus infection and vaccination in humans. Sci. Transl. Med. *12*, eabd3601. https://doi.org/10.1126/scitranslmed.abd3601.
31. Kaku, C.I., Bergeron, A.J., Ahlm, C., Normark, J., Sakharkar, M., Forsell, M.N.E., and Walker, L.M. (2022). Recall of preexisting cross-reactive B cell memory after Omicron BA.1 breakthrough infection. Sci. Immunol. *7*, eabq3511. https://doi.org/10.1126/sciimmunol.abq3511.
32. Wang, Z., Zhou, P., Muecksch, F., Cho, A., Ben Tanfous, T., Canis, M., Witte, L., Johnson, B., Raspe, R., Schmidt, F., et al. (2022). Memory B cell responses to Omicron subvariants after SARS-CoV-2 mRNA breakthrough infection in humans. J. Exp. Med. *219*, e20221006. https://doi.org/10.1084/jem.20221006.
33. Woodruff, M.C., Ramonell, R.P., Haddad, N.S., Anam, F.A., Rudolph, M.E., Walker, T.A., Truong, A.D., Dixit, A.N., Han, J.E., Cabrera-Mora, M., et al. (2022). Dysregulated naive B cells and de novo autoreactivity in severe COVID-19. Nature *611*, 139–147. https://doi.org/10.1038/s41586-022-05273-0.
34. Woodruff, M.C., Ramonell, R.P., Nguyen, D.C., Cashman, K.S., Saini, A.S., Haddad, N.S., Ley, A.M., Kyu, S., Howell, J.C., Ozturk, T., et al. (2020). Extrafollicular B cell responses correlate with neutralizing antibodies and morbidity in COVID-19. Nat. Immunol. *21*, 1506–1516. https://doi.org/10.1038/s41590-020-00814-z.
35. Tuekprakhon, A., Nutalai, R., Dijokaite-Guraliuc, A., Zhou, D., Ginn, H.M., Selvaraj, M., Liu, C., Mentzer, A.J., Supasa, P., Duyvesteyn, H.M.E., et al. (2022). Antibody escape of SARS-CoV-2 Omicron BA.4 and BA.5 from vaccine and BA.1 serum. Cell *185*, 2422–2433.e13. https://doi.org/10.1016/j.cell.2022.06.005.
36. Van Beek, M., Nussenzweig, M.C., and Chakraborty, A.K. (2022). Two complementary features of humoral immune memory confer protection

against the same or variant antigens. Proc. Natl. Acad. Sci. USA *119*. e2205598119. https://doi.org/10.1073/pnas.2205598119.

37. Hoehn, K.B., Turner, J.S., Miller, F.I., Jiang, R., Pybus, O.G., Ellebedy, A.H., and Kleinstein, S.H. (2021). Human B cell lineages associated with germinal centers following influenza vaccination are measurably evolving. eLife *10*, e70873. https://doi.org/10.7554/eLife.70873.
38. Monto, A.S., Malosh, R.E., Petrie, J.G., and Martin, E.T. (2017). The doctrine of original antigenic sin: separating good from evil. J. Infect. Dis. *215*, 1782–1788. https://doi.org/10.1093/infdis/jix173.
39. Francis, T. (1953). On the doctrine of original antigenic sin. Proc. Am. Philos. Soc. 572–578.
40. Shlomchik, M.J. (2018). Do memory B cells form secondary germinal centers? Yes and no. Cold Spring Harb. Perspect. Biol. *10*, a029405. https://doi.org/10.1101/cshperspect.a029405.
41. Shlomchik, M.J., and Weisel, F. (2012). Germinal center selection and the development of memory B and plasma cells. Immunol. Rev. *247*, 52–63. https://doi.org/10.1111/j.1600-065X.2012.01124.x.
42. Mesin, L., Schiepers, A., Ersching, J., Barbulescu, A., Cavazzoni, C.B., Angelini, A., Okada, T., Kurosaki, T., and Victora, G.D. (2020). Restricted clonality and limited germinal center reentry characterize memory B cell reactivation by boosting. Cell *180*, 92–106.e11. https://doi.org/10.1016/j.cell.2019.11.032.
43. Pape, K.A., Taylor, J.J., Maul, R.W., Gearhart, P.J., and Jenkins, M.K. (2011). Different B cell populations mediate early and late memory during an endogenous immune response. Science *331*, 1203–1207. https://doi.org/10.1126/science.1201730.
44. Tas, J.M.J., Koo, J.H., Lin, Y.C., Xie, Z., Steichen, J.M., Jackson, A.M., Hauser, B.M., Wang, X., Cottrell, C.A., Torres, J.L., et al. (2022). Antibodies from primary humoral responses modulate the recruitment of naive B cells during secondary responses. Immunity *55*, 1856–1871.e6. https://doi.org/10.1016/j.immuni.2022.07.020.
45. Cirelli, K.M., Carnathan, D.G., Nogal, B., Martin, J.T., Rodriguez, O.L., Upadhyay, A.A., Enemuo, C.A., Gebru, E.H., Choe, Y., Viviano, F., et al. (2019). Slow delivery immunization enhances HIV neutralizing antibody and germinal center responses via modulation of immunodominance. Cell *177*, 1153–1171.e28. https://doi.org/10.1016/j.cell.2019.04.012.
46. Ellebedy, A.H., Nachbagauer, R., Jackson, K.J.L., Dai, Y.N., Han, J., Alsoussi, W.B., Davis, C.W., Stadlbauer, D., Rouphael, N., Chromikova, V., et al. (2020). Adjuvanted H5N1 influenza vaccine enhances both cross-reactive memory B cell and strain-specific naive B cell responses in humans. Proc. Natl. Acad. Sci. USA *117*, 17957–17964. https://doi.org/10.1073/pnas.1906613117.
47. Lee, J.H., Sutton, H.J., Cottrell, C.A., Phung, I., Ozorowski, G., Sewall, L.M., Nedellec, R., Nakao, C., Silva, M., Richey, S.T., et al. (2022). Long-primed germinal centres with enduring affinity maturation and clonal migration. Nature *609*, 998–1004. https://doi.org/10.1038/s41586-022-05216-9.
48. de Carvalho, R.V.H., Ersching, J., Barbulescu, A., Hobbs, A., Castro, T.B.R., Mesin, L., Jacobsen, J.T., Phillips, B.K., Hoffmann, H.H., Parsa, R., et al. (2023). Clonal replacement sustains long-lived germinal centers primed by respiratory viruses. Cell *186*, 131–146.e13. https://doi.org/10.1016/j.cell.2022.11.031.
49. Hägglöf, T., Cipolla, M., Loewe, M., Chen, S.T., Mesin, L., Hartweger, H., ElTanbouly, M.A., Cho, A., Gazumyan, A., Ramos, V., et al. (2023). Continuous germinal center invasion contributes to the diversity of the immune response. Cell *186*, 147–161.e15. https://doi.org/10.1016/j.cell.2022.11.032.
50. Pushparaj, P., Nicoletto, A., Sheward, D.J., Das, H., Castro Dopico, X., Perez Vidakovics, L., Hanke, L., Chernyshev, M., Narang, S., Kim, S., et al. (2023). Immunoglobulin germline gene polymorphisms influence the function of SARS-CoV-2 neutralizing antibodies. Immunity *56*, 193–206.e7. https://doi.org/10.1016/j.immuni.2022.12.005.
51. Bruel, T., Stéfic, K., Nguyen, Y., Toniutti, D., Staropoli, I., Porrot, F., Guivel-Benhassine, F., Bolland, W.H., Planas, D., Hadjadj, J., et al. (2022). Longitudinal analysis of serum neutralization of SARS-CoV-2 Omicron BA.2, BA.4, and BA.5 in patients receiving monoclonal antibodies. Cell Rep. Med. *3*, 100850. https://doi.org/10.1016/j.xcrm.2022.100850.
52. Hsieh, C.L., Goldsmith, J.A., Schaub, J.M., DiVenere, A.M., Kuo, H.C., Javanmardi, K., Le, K.C., Wrapp, D., Lee, A.G., Liu, Y., et al. (2020). Structure-based design of prefusion-stabilized SARS-CoV-2 spikes. Science *369*, 1501–1505. https://doi.org/10.1126/science.abd0826.
53. Crickx, E., Chappert, P., Sokal, A., Weller, S., Azzaoui, I., Vandenberghe, A., Bonnard, G., Rossi, G., Fadeev, T., Storck, S., et al. (2021). Rituximab-resistant splenic memory B cells and newly engaged naive B cells fuel relapses in patients with immune thrombocytopenia. Sci. Transl. Med. *13*. https://doi.org/10.1126/scitranslmed.abc3961.
54. Luo, X.M., Maarschalk, E., O'Connell, R.M., Wang, P., Yang, L., and Baltimore, D. (2009). Engineering human hematopoietic stem/progenitor cells to produce a broadly neutralizing anti-HIV antibody after in vitro maturation to human B lymphocytes. Blood *113*, 1422–1431. https://doi.org/10.1182/blood-2008-09-177139.
55. Tiller, T., Meffre, E., Yurasov, S., Tsuiji, M., Nussenzweig, M.C., and Wardemann, H. (2008). Efficient generation of monoclonal antibodies from single human B cells by single cell RT-PCR and expression vector cloning. J. Immunol. Methods *329*, 112–124. https://doi.org/10.1016/j.jim.2007.09.017.
56. Hao, Y., Hao, S., Andersen-Nissen, E., Mauck, W.M., Zheng, S., Butler, A., Lee, M.J., Wilk, A.J., Darby, C., Zager, M., et al. (2021). Integrated analysis of multimodal single-cell data. Cell *184*, 3573–3587.e29. https://doi.org/10.1016/j.cell.2021.04.048.
57. Hafemeister, C., and Satija, R. (2019). Normalization and variance stabilization of single-cell RNA-seq data using regularized negative binomial regression. Genome Biol. *20*, 296. https://doi.org/10.1186/s13059-019-1874-1.
58. Korsunsky, I., Millard, N., Fan, J., Slowikowski, K., Zhang, F., Wei, K., Baglaenko, Y., Brenner, M., Loh, P.R., and Raychaudhuri, S. (2019). Fast, sensitive and accurate integration of single-cell data with Harmony. Nat. Methods *16*, 1289–1296. https://doi.org/10.1038/s41592-019-0619-0.
59. Gupta, N.T., Vander Heiden, J.A., Uduman, M., Gadala-Maria, D., Yaari, G., and Kleinstein, S.H. (2015). Change-O: a toolkit for analyzing large-scale B cell immunoglobulin repertoire sequencing data. Bioinformatics *31*, 3356–3358. https://doi.org/10.1093/bioinformatics/btv359.
60. Hoehn, K.B., Pybus, O.G., and Kleinstein, S.H. (2022). Phylogenetic analysis of migration, differentiation, and class switching in B cells. PLoS Comput. Biol. *18*, e1009885. https://doi.org/10.1371/journal.pcbi.1009885.
61. Lad, L., Clancy, S., Kovalenko, M., Liu, C., Hui, T., Smith, V., and Pagratis, N. (2015). High-throughput kinetic screening of hybridomas to identify high-affinity antibodies using bio-layer interferometry. J Biomol Screen *20*, 498–507. https://doi.org/10.1177/1087057114560123.

Please cite this article in press as: Sokal et al., SARS-CoV-2 Omicron BA.1 breakthrough infection drives late remodeling of the memory B cell repertoire in vaccinated individuals, Immunity (2023), https://doi.org/10.1016/j.immuni.2023.07.007

STAR★METHODS

KEY RESOURCES TABLE

REAGENT or RESOURCE	SOURCE	IDENTIFIER
Antibodies		
CD3	Biolegend	Clone ID: UCHT1; Cat#300425; RRID: AB_830754
CD14	BD Bioscience	Clone ID: M φP9; Cat#561709; RRID: AB_1645464
CD19	BD Bioscience	Clone ID: HIB19; Cat# 562321; RRID: AB_11154408
CD38	BD Bioscience	Clone ID: HIT2; Cat# 551400; RRID AB_394184
CD27	Biolegend	Clone ID: M-T271; Cat# 356417; RRID: AB_2562598
CD11c	BD Bioscience	Clone ID: S-HCL-3; Cat#744436; RRID: AB_2742232
IgD	Life technologies	Clone ID: Polyclonal; Cat# H15501; RRID: AB_2536563
CD71	Biolegend	Clone ID: CY1G4; Cat# 334111; RRID: AB_2563118
CD21	BD Bioscience	Clone ID: B-ly4; Cat#563163; RRID: AB_2741028
CD38 (TotalSeq-C)	Biolegend	Clone ID: HB-7; Cat#356637; RRID: AB_2820007
CD27 (TotalSeq-C)	Biolegend	Clone ID: O323; Cat#302853; RRID: AB_2800747
CD71 (TotalSeq-C)	Biolegend	Clone ID: CY1G4; Cat#334125; RRID: AB_2800885
CD21 (TotalSeq-C)	Biolegend	Clone ID: Bu32; Cat#354923; RRID: AB_2800953
CD11c (TotalSeq-C)	Biolegend	Clone ID: S-HCL-3; Cat#371521; RRID: AB_2801018
CD39 (TotalSeq-C)	Biolegend	Clone ID: A1; Cat#328237; RRID: AB_2800853
CD307e (FCRL5; TotalSeq-C)	Biolegend	Clone ID: 509f6; Cat#340309; RRID: AB_2819969
CD95 (TotalSeq-C)	Biolegend	Clone ID: DX2; Cat#305651; RRID: AB_2800787
N SARS-CoV-2	Institut Pasteur	Rabbit polyclonal (N.Escriou)
Anti-Human Fc Capture Biosensors	Sartorius	Cat#18-5060
Biological samples		
Cryopreserved PBMCs from triple vaccinated subjects	Henri Mondor Hospital, Assistance Publique des Hôpitaux de Paris	N/A
D614G SARS-CoV-2 virus (hCoV-19/France/GE1973/2020)	Institut Pasteur, CNR Respiratory Viruses (S.Van der Werf)	N/A
Omicron BA.1 SARS-CoV-2 virus (B.1.1.529 GISAID ID: EPI_ISL_6794907)	Institut Pasteur, Olivier Schwartz	N/A
Omicron BA.5 (BA.5:EPI_ISL_13660702)	Institut Pasteur, Olivier Schwartz	N/A
Chemicals, peptides, and recombinant proteins		
Hu-1 SARS-CoV-2 Spike	Institut Pasteur, Virologie Structurale (F. Rey)	N/A

(*Continued on next page*)

Continued

REAGENT or RESOURCE	SOURCE	IDENTIFIER
BA.1 SARS-CoV-2 Spike	Institut Pasteur, Virologie Structurale (F. Rey)	N/A
Hu-1 SARS-CoV-2 RBD	Institut Pasteur, Virologie Structurale (F. Rey)	N/A
BA.1 SARS-CoV-2 RBD	Institut Pasteur, Virologie Structurale (F. Rey)	N/A
BA.2 SARS-CoV-2 RBD	Institut Pasteur, Virologie Structurale (F. Rey)	N/A
BA.5 SARS-CoV-2 RBD	Institut Pasteur, Virologie Structurale (F. Rey)	N/A
BirA biotin ligase	Avidity	Cat#BirA500
PE streptavidin	Biolegend	Cat#405203
APC streptavidin	Biolegend	Cat#405207
BUV395 streptavidin	Biolegend	Cat#564176
BV785 streptavidin	BD Bioscience	Cat#405249
BUV737 streptavidin	BD Bioscience	Cat#612775
PE streptavidin (TotalSeq-C)	Biolegend	Cat#405261; 405263; 405265; 405267
Live dead aqua	Life technologies,	Cat#L34957
Recombinant human IL-2	PeproTech	Cat#200-02
Recombinant human IL-4	PeproTech	Cat#200-04
Recombinant human IL-21	PeproTech	Cat#210-21
Recombinant human BAFF	PeproTech	Cat#310-13
Deposited data		
Raw and analyzed scRNA-seq dataset	This paper	ArrayExpress: E-MTAB-12651
Single cell culture VDJ sequences	Sokal et al.[9]	DDBJ/EMBL/GenBank: KFPV00000000-KFQZ00000000 (BioProject: PRJNA819082)
Single cell culture VDJ sequences	Sokal et al.[26]	DDBJ/EMBL/GenBank: KFVZ00000000–KFWQ00000000 (BioProject: PRJNA819082)
Single cell culture VDJ sequences	This paper	DDBJ/EMBL/GenBank: KFXD00000000-KFXQ00000000 (BioProject: PRJNA819082)
Experimental models: Cell lines		
MS40lo cell line	G. Kelsoe's lab (Duke University)	Planas et al.[6]
Software and algorithms		
Kaluza v2.1	Beckman Coulter	https://www.beckman.fr
Flowjo v10.7.1	FlowJo, LLC	https://www.flowjo.com; RRID: SCR_008520
GraphPad Prism v9	GraphPad	https://www.graphpad.com; RRID: SCR_002798
Codon Code Aligner v9	Codon Code Corporation	https://www.codoncode.com/
R v4.0.2	R Foundation	https://www.r-project.org; RRID: SCR_001905
RStudio v1.3.1056	RStudio	https://rstudio.com; RRID: SCR_000432
IgBLASTn v1.19.0	NCBI	https://www.ncbi.nlm.nih.gov/igblast/; RRID: SCR_002873
HT Data analysis software 12.2.2.26	Sartorius/ForteBio	https://www.sartorius.com; RRID: SCR_003935
Adobe Illustrator (CS6)	Adobe	https://www.adobe.com/products/illustrator.html; RRID: SCR_010279
Biorender	Biorender	https://biorender.com

Please cite this article in press as: Sokal et al., SARS-CoV-2 Omicron BA.1 breakthrough infection drives late remodeling of the memory B cell repertoire in vaccinated individuals, Immunity (2023), https://doi.org/10.1016/j.immuni.2023.07.007

RESOURCE AVAILABILITY

Lead Contact

Further information and requests for resources and reagents should be directed to and will be fulfilled by the Lead Contact, Pascal Chappert (pascal.chappert@inserm.fr).

Materials Availability

No unique materials were generated for this study.

Data and Code Availability

- All scRNA-seq data have been deposited in the ArrayExpress database at EMBL-EBI (www.ebi.ac.uk/arrayexpress) and will be made available as of the date of publication. Accession numbers are listed in the key resources table. Single cell culture VDJ sequencing data reported in Figures 3 and S3 are included in Table S3 and have been deposited as Targeted Locus Study projects at DDBJ/EMBL/GenBank are available as of the date of publication. Accession numbers are listed in the key resources table. The version described in this paper is the first version, KFXD01000000- KFXQ01000000.
- Any additional information required to reanalyze the data reported in this paper is available from the lead contact upon request.

EXPERIMENTAL MODEL AND SUBJECT DETAILS

Study participants

In total, 30 patients who received a booster (3rd dose) of BNT162b2 mRNA vaccine with no history of COVID-19 were enrolled. Among them, 15 developed Omicron BA.1 breakthrough infection, including 4 (Na-5, Na-9, Na-25 and Na-31) who were sampled after the third dose and before the BA.1 breakthrough infection, providing the opportunity for a longitudinal assessment of the remodeling at the scale of one individual, especially in 2 of them whose memory B cell repertoire had been extensively characterized after 2 doses of mRNA vaccine. All the breakthrough infection occurred between 12/24/2021 and 01/30/2022 when BA.1 was responsible for > 85% of SARS-CoV-2 infections in France. They received their third dose 240 ± 40.4 (mean ± SD) days after second dose and 39 days before BA.1 breakthrough infection (range: 31 to 106 days). The remaining 15 patients were sampled at least once after their third dose of BNT162b2 mRNA vaccine, including 11 previously sampled in the MEMOCoV2 cohort (IRB 2018-A01610-55). Negative nucleocapsid IgG were assessed at each sampling during all the follow-up for these patients.

Detailed information on the individuals, including gender and health status, can be found in Table S1.

Samples were collected shortly after the boost and/or breakthrough infection (mean: 9; range: 5-12 days for 3x mRNA; mean: 14.1; range: 7-22 days for BT), 2.5 months after the boost and/or breakthrough infection (mean: 62; range: 45-79 days for 3x mRNA; mean: 75; range: 57-101 days for BT) and 5.5 months after the booster or and/or breakthrough infection (mean: 193; range: 129-227 days for 3x mRNA; mean: 164; range: 145-191 days for BT). Clinical and biological characteristics of these patients are summarized in Table S1. In depth longitudinal analysis, including scRNA-seq around day 10 and at 6 months post infection as well as single-cell MBC culture at day 10, 3 months and 6 months post infection (see Figure 1A), was performed on four patients (Na-9, Na-25, Na-37 and Na-38) for which we had been able to collect enough PBMCs (at least two vials of 10-15*10e6 mononuclear cells) early after infection and had assurance that these donors would come back for the 3 and 6 months' time points. Two of these donors were further chosen because we had already collected and analyzed samples from them at various time point after their second and third vaccine dose[9] and this study). A fifth donor, for which we had samples prior to infection but missed sampling early after infection, was further added for the single-cell MBC cultures and analysis reported as part of Figures 3, 4, 5, and 6, but no scRNA-seq analysis was performed on this donor (Figure 1A).

Patients were recruited at the Henri Mondor University Hospital (AP-HP), between March 2020 and July 2022. MEMO-COV-2 study (NCT04402892) was approved by the ethical committee Ile-de-France VI (Number: 40-20 HPS) and performed in accordance with the French law. Written informed consent was obtained from all participants.

Virus strains

The reference D614G strain (hCoV-19/France/GE1973/2020) was supplied by the National Reference Centre for Respiratory Viruses hosted by Institut Pasteur and headed by Sylvie van der Werf as described in Sokal et al.[15,16] The Omicron strains (B.1.1.529 GISAID ID: EPI_ISL_6794907) and BA.5 (BA.5:EPI_ISL_13660702) were a generous gift from Olivier Schwartz, Institut Pasteur, and were generated as described in Planas et al.[6] and Bruel et al.[51] respectively.

METHOD DETAILS

Anti- RBD (S) and -N SARS-CoV-2 antibodies assay

Serum samples were analyzed for anti-S-RBD Hu-1 IgG titers with the SARS-CoV-2 IgG Quant II assay (ARCHITECT®, Abbott Laboratories). The latter assay is an automated chemiluminescence microparticle immunoassay (CMIA) that quantifies anti-RBD IgG, with 50 a.u./mL as a positive cut-off and a maximal threshold of quantification of 40,000 a.u./mL. Dilutions were performed for samples over the maximal threshold.

Serum samples were analysed for anti-S-RBD BA.1 using the Anti-SARS-CoV-2 (B.1.1.529) Antibody IgG Titer Serologic Assay Kit (Spike RBD) kit from Acrobiosystem (RAS-T057). Sampled were diluted at 1/1000 after calibration and validation of the assay using control sera. Assay was performed according to the manufacturer instructions.

Serum samples were also processed for anti-Nucleoprotein (N) detection on Abbott SARS-CoV-2 IgG chemiluminescent microparticle immunoassay following the manufacturer's instructions.

All assays were performed by trained laboratory technicians according to the manufacturer's standard procedures.

Recombinant protein purification

Construct design

Genes coding for SARS-CoV-2 Spike (S) ectodomains (Hu-1 and BA.1) with Hisx8 and Strep tags were synthesized by Genscript and cloned into the pcDNA3.1(+) vector. Both ectodomains (residues 1-1208) were stabilized to preserve their trimeric prefusion conformation by introducing six proline substitutions (F817P, A892P, A899P, A942P, K986P, V987P, Hu-1 numbering), a GSAS substitution at the furin cleavage site (residues 682–685) and a C-terminal Foldon trimerization motif.[52]

The SARS-CoV-2 Hu-1 and BA.1 Receptor Binding Domains (RBDs) were cloned in pcDNA3.1(+) encompassing residues 331-528 (Hu-1 numbering) from the Spike ectodomains, and they were flanked by an N-terminal IgK signal peptide and a C-terminal Thrombin cleavage site followed by Hisx8-Strep-Avi tags in tandem. The BA.2 and BA.5 RBDs were obtained using the BA.1 RBD plasmid as a template, on which the remaining mutations were introduced by PCR mutagenesis following standard techniques.

Protein expression and purification

The plasmids coding for the recombinant proteins were transiently transfected in Expi293F™ cells (Thermo Fischer) using FectroPRO® DNA transfection reagent (Polyplus), according to the manufacturer's instructions. The cells were incubated at 37°C (Hu-1 S, BA.1 S, Hu-1 RBD) or 32°C (BA.1 RBD, BA.2 RBD, BA.5 RBD) for 5 days and then the culture was centrifuged, and the supernatant was concentrated. The proteins were purified from the supernatant by affinity chromatography on a StrepTactin column (IBA). The Spike proteins were further purified by size-exclusion chromatography (SEC) on a Superose6 10/300 colum (Cytiva) equilibrated in PBS, while the RBDs were loaded onto a Superdex200 10/300 column (Cytiva).

Protein biotinylation

Hu-1, BA.1 RBD and Spike Avi-tagged proteins were biotinylated using the Avidity BirA biotin-protein ligase kit according to the manufacturer instruction. Bovine serum albumin was biotinylated using EZ link NHS biotin (Thermofischer) according to the manufacturer instruction.

Flow cytometry and cell sorting

PBMCs were isolated from venous blood samples via standard density gradient centrifugation and used after cryopreservation at -150°C. Cells were thawed in RPMI-1640 (Gibco)-10% FBS (Gibco), washed twice and incubated with a mixture of Hu-1 and BA.1 Spike +/- Hu-1 and BA.1 RBD tetramers in 100 μL of PBS (Gibco)-2% FBS during 40 min on ice. For cell sorting, cells were stained with 500 ng of Hu-1Spike APC-streptavidin and 500 ng of BA.1 Spike PE-streptavidin; for flow cytometry analysis cell were stained with 500 ng of Hu-1Spike BUV395-streptavidin and 500 ng BA.1 Spike PE-streptavidin 50ng of Hu-1 RBD APC-streptavidin and 50 ng of BA.1 RBD BV785 Streptavidin. To exclude cells with nonspecific binding, a non-relevant tetramer was constructed using biotinylated bovine serum albumin coupled to BV785-streptavidin (for cell sorting) or BU737-streptavidin for flow cytometry. Tetramer were made by incubating biotinylated proteins with fluorochrome-conjugated streptavidin at 4:1 molar ratio for 1 hour at 4°C. 2.4 ng of free biotin was then added for 10 additional minutes before mixing of the tetramer. Cells were then washed and resuspended in the same conditions, then the fluorochrome-conjugated antibody cocktail at pre-titrated concentrations (1:100 for CD19, CD21, CD11c, CD71, CD38, CD3, CD14 and IgD, 1:50 for CD27) for 20 min at 4°C and viable cells were identified using a LIVE/DEAD Fixable Aqua Dead Cell Stain Kit (Thermo Fisher Scientific, 1:200) incubated with conjugated antibodies. Samples were acquired using a LSR Fortessa SORP (BD Biosciences). For cell sorting, cells were stained using the same protocol and then sorted in 96 plates using the ultra-purity mode on a MA900 (SONY) or an Aria II cell sorter (BD Biosciences) and Data were analyzed using FlowJo or Kaluza softwares. Detailed gating strategies for cell sorting and analysis are depicted in Figures S1 and S2 respectively and in Table S3B.

For UMAP generation and visualization (Figures 2 and S2), viable dump$^-$ CD19$^+$ IgD$^-$ cells from each sample included in the final analysis (Table S1) were first downsampled to 4000. The UMAP (v3.1) plugin in FlowJO was then used on a concatenated FCS file containing all donors and time points to calculate the UMAP coordinates for the resulting 264.000 cells (with 30 neighbors, metric = euclidian and minimum distance = 0.5 as default parameters), considering fluorescent intensities from the following parameters: FSC-A, SSC-A, CD19, CD21, CD11c, CD71, CD38, CD27 and IgD, while excluding the dump (CD3 and CD14), viability and Tetramers channels. Contour plots (equal probability contouring, with intervals set to 5% of gated populations) for each manually gated population (Figure S2A) were further overlaid on UMAP projection in FlowJO (Figure S2B). For visualization purposes, only the outermost density representing 95% of the total gated cells was kept for the final figure, all other contour lines were removed in Adobe Illustrator.

Single-cell culture

Single cell culture was performed as previously described.[53] Single B cells were sorted in 96-well plates containing MS40L^{lo} cells expressing CD40L (kind gift from G. Kelsoe, Luo et al.[54]). Cells were co-cultured at 37°C with 5% CO2 during 21 or 25 days in RPMI-1640 (Invitrogen) supplemented with 10% HyClone FBS (Thermo Scientific), 55 μM 2-mercaptoethanol, 10 mM HEPES,

1 mM sodium pyruvate, 100 units/mL penicillin, 100 μg/mL streptomycin, and MEM non-essential amino acids (all Invitrogen), with the addition of recombinant human BAFF (10 ng/ml), IL2 (50 ng/ml), IL4 (10 ng/ml), and IL21 (10 ng/ml; all Peprotech). Part of the supernatant was carefully removed at days 4, 8, 12, 15 and 18 and the same amount of fresh medium with cytokines was added to the cultures. After 25 days of single cell culture, supernatants were harvested and stored at -20°C. Cell pellets were placed on ice and gently washed with PBS (Gibco) before being resuspended in 50 μL of RLT buffer (Qiagen) supplemented with 1% β-mercaptoethanol and subsequently stored at -80°C until further processing.

ELISA

Total IgG and SARS-CoV-2 Hu-1 RBD, Hu-1 S, BA.1 RBD and BA.1 S-specific IgG from culture supernatants were measured using homemade ELISA. 96 well ELISA plates (Thermo Fisher) were coated with either goat anti-human Ig (10 μg/ml, Invitrogen) or recombinant SARS-CoV-2 Hu-1 -RBD or -S or BA.1-RBD or -S protein (2.5 μg/ml each) in sodium carbonate during 1h at 37°C. After plate blocking, cell culture supernatants were added for 1hr, then ELISA were developed using HRP-goat anti-human IgG (1 μg/ml, Immunotech) and TMB substrate (Eurobio). OD450 and OD620 were measured, and Ab-reactivity was calculated after subtraction of blank wells. Supernatants whose ratio of OD450-OD620 over control wells (consisting of supernatant from wells that contained spike-negative MBCs from the same single cell culture assay) was over 10 were considered as positive for Hu-1 RBD or BA.1 RBD. PBS was used to define background OD450-OD620.

Single-cell RNA-seq library preparation and sequencing

Frozen PBMC from 4 donors (Na-9, Na-25, Na-37 and Na-38) were thawed and washed 2 times as described above. 10-15x10^6 PMBCs were then resuspended in 100μL PBS 2%FBS and incubated for 40 minutes at 4°C with a decoy tetramer (biotinylated Bovine Serum albumin coupled with BV785 streptavidin) and Hu-1 Spike, BA.1 Spike, Hu-1 RBD and BA.1 RBD tetramers (constructed as described above using PE-labelled Total-seqC streptavidin with different barcodes for each individual antigens). Cell were washed, resuspended in 100μL PBS 2%FBS and stained with a cocktail of fluorochrome conjugated (CD3, CD14 both APC-H7 at 1:100 each; CD15 and CD56 BV785 at 1:100 each, CD19 PECF594 at 1:100, IgD FITC at 1:100, CD38 PercP-Cy5.5 at 1:100) and CITE-seq (CD38, CD27, CD71, CD21, CD11c, CD39, FCRL5, CD95 all at 1:40) antibodies for 40 minutes on ice. Viable cells were identified using a LIVE/DEAD Fixable Aqua Dead Cell Stain Kit (Thermo Fisher Scientific, 1:200) incubated with conjugated antibodies. B cells were FACS-sorted (MA900, Sony) in PBS/0.08% FCS from 4 patients at baseline (M0) and 6 months (M6). An initial pool of 50.000 total $CD19^+IgD^-$ cells were always sorted and afterward, to enrich for cells of interest, only $CD19^+CD38^{low}$ antibody secreting cells (ASCs), PE/tetramer positive and $CD19^{hi}$ cells, leading to approximately 55000-60000 total sorted cells per sample. Sorted cells were then counted and up to 20 000 cells were loaded in the 10x Chromium Controller to generate single-cell gel-beads in emulsion. The scRNA-seq libraries for gene expression (mRNA), surface protein expression (TotalSeq-C antibody-derived tags (ADT)) and VDJ BCR libraries were generated using Chromium Next GEM Single Cell V(D)J Reagent Kit v.1.1 with Feature Barcoding (10x Genomics) according to the manufacturer's protocol. Briefly, after reverse transcription, gel-beads in emulsion were disrupted. Barcoded complementarity DNA was isolated and amplified by PCR. Following fragmentation, end repair and A-tailing, sample indexes were added during index PCR. The purified libraries were sequenced on a Novaseq S2 flowcell (Illumina) with 26 cycles of read 1, 8 cycles of i7 index and 91 cycles of read 2, targeting a median depth of 50000 reads per cell for gene expression and 5000 reads per cell for each other two libraries (BCR VDJ and ADT Feature barcoding).

Single-cell IgH sequencing

Clones whose culture had proven successful (IgG concentration $\geq$ 1 μg/mL at day 21-25) were selected and extracted using the NucleoSpin96 RNA extraction kit (Macherey-Nagel) according to the manufacturer's instructions. A reverse transcription step was then performed using the SuperScript IV enzyme (ThermoFisher) in a 14 μl final volume (42°C 10 min, 25°C 10 min, 50°C 60 min, 94°C 5 min) with 4 μl of RNA and random hexamers (Thermofisher scientific). A PCR was further performed based on the protocol established by Tiller et al.[55] Briefly, 3.5 μl of cDNA was used as template and amplified in a total volume of 40 μl with a mix of forward L-VH primers (Table S3) and reverse Cγ primer and using the HotStar® Taq DNA polymerase (Qiagen) and 50 cycles of PCR (94°C 30 s, 58°C 30 s, 72°C 60 s). PCR products were sequenced with the reverse primer CHG-D1 and read on ABI PRISM 3130XL genetic analyzer (Applied Biosystems). Sequence quality was verified using CodonCode Aligner software (CodonCode Corporation).

For specific patients and time points (see Table S1), some IgH sequences were obtained directly from single cell sorting in 4μL lysis buffer containing PBS (Gibco), DTT (ThermoFisher) and RNAsin (Promega). Reverse transcription and a first PCR was performed as described above (50 cycles) before a second 50-cycles PCR using 5'AgeI VH primer mix and Cγ-CH1 3' primer, before sequencing.

Single-cell gene expression analysis

Paired end FASTQ reads for all three libraries were demultiplexed and aligned against the GRCh38 human reference genome (GENCODE v32/Ensembl 98; July 2020) using 10x Genomics' Cell Ranger v6.0.0 pipeline. Outputs of Cell Ranger were directly loaded into Seurat v4.1.1[56] for further QC steps and analysis. Following manual inspection of cell quality, only genes detected in at least 10 cells and cells with more than 750 unique genes detected and less than 5% of UMI counts mapped to mitochondrial genes were kept (Figure S1B). Upon analysis of parallel VDJ library (see computational analyses of VDJ sequences section below), only cells with exactly one resolved heavy chain sequence were retained for final analysis. Transcript counts were first normalized using the scTransform algorithm v0.3.4,[57] using the vst.flavor "v2" parameter and additionally correcting for potential bias related to the

detected percentage of mitochondrial genes and selecting for the top 3000 variable features for downstream visualization and clustering analysis. After principal component analysis, performed excluding all remaining Ig genes to avoid unwanted clustering based solely on differential isotype expression (https://www.genenames.org/data/genegroup/#!/group/348 and AC233755.1 gene), potential donor and sort-specific batch effects were removed using the Harmony algorithm.[58] The first 15 corrected PCA dimensions were then used to construct a knn graph (k=20 neighbors) and perform graph-based clustering (Louvain) with a resolution parameter of 0.2 as well as compute the UMAP coordinates for each cell. G2M and S cell cycle signatures were calculated using the CellCycleScoring() function and the associated gene lists in Seurat (G2M scoring: HMGB2, CDK1, NUSAP1, UBE2C, BIRC5, TPX2, TOP2A, NDC80, CKS2, NUF2, CKS1B, MKI67, TMPO, CENPF, TACC3, FAM64A, SMC4, CCNB2, CKAP2L, CKAP2, AURKB, BUB1, KIF11, ANP32E, TUBB4B, GTSE1, KIF20B, HJURP, CDCA3, HN1, CDC20, TTK, CDC25C, KIF2C, RANGAP1, NCAPD2, DLGAP5, CDCA2, CDCA8, ECT2, KIF23, HMMR, AURKA, PSRC1, ANLN, LBR, CKAP5, CENPE, CTCF, NEK2, G2E3, GAS2L3, CBX5, CENPA; S scoring: MCM5, PCNA, TYMS, FEN1, MCM2, MCM4, RRM1, UNG, GINS2, MCM6, CDCA7, DTL, PRIM1, UHRF1, MLF1IP, HELLS, RFC2, RPA2, NASP, RAD51AP1, GMNN, WDR76, SLBP, CCNE2, UBR7, POLD3, MSH2, ATAD2, RAD51, RRM2, CDC45, CDC6, EXO1, TIPIN, DSCC1, BLM, CASP8AP2, USP1, CLSPN, POLA1, CHAF1B, BRIP1, E2F8).

Computational analyses of VDJ sequences

Processed FASTA sequences from cultured single-cell heavy chain sequencing and 10x single-cell RNA sequencing were annotated using Igblast v1.19.0 against the human IMGT reference database (Figure S1B). Sequences from cells that did not pass the initial QC cut-offs from our scRNA-seq analysis were removed at that step. Cases of 10x barcodes with two or more consensus heavy chain sequences for which more than ten UMI were detected were generally flagged as potential doublets for removal from our scRNA-seq analysis. Similarly, cases where no clear heavy chains could be attributed (none above 10 UMIs) were also flagged for removal. Two exceptions were made: 1/ in cases of identical CDR3s but differing isotypes (c_call), in which case the isotype switched sequence was kept and UMI counts from both contigs were aggregated; and 2/ in cases when one the heavy chains was clearly overrepresented (at least three time the number of UMI counts as compared to the next most represented heavy chain detected) and the second most represented sequences did not exceed ten UMIs, in which case the most represented sequence was kept.

Clonal cluster assignment (DefineClones.py) and germline reconstruction (CreateGermlines.py) was performed using the Immcantation/Change-O toolkit[59] on all heavy chain V sequences. Sequences that had the same V-gene, same J-gene, including ambiguous assignments, and same CDR3 length with maximal length normalized nucleotide hamming distance of 0.15 were considered as potentially belonging to the same clonal group. Mutation frequencies in V genes were then calculated using the calcObservedMutations() function from Immcantation/SHazaM v1.1.1 R package. For the analysis of the initial ASC response in our 10x dataset (Figures 2E and 2F), clonal assignments were further corrected using available light chain information (light_cluster.py script from Immcantation). Further clonal analyses on all productively rearranged sequences were implemented in R.

Based on heavy-chain only clonal affectation, clones were defined as Hu-1 or BA.1 SARS-Cov-2 S or RBD-specific if they contained 1 or more validated single-cell culture sequence or cells positively stained by our barcoded His-tagged S or RBD protein in our scRNAseq dataset. Staining with barcoded S or RBD tetramer in our scRNAseq dataset were analyzed in FlowJO using log-normalized sequencing data (see Figure S1B). Clones containing RBD-specific cells were labelled as RBD-specific. Clones containing Hu-1/BA.1 cross-reactive cells were labelled as cross-reactive. All specific clones were manually curated based on available light chain information and CDR3 sequences and clones containing less than ten percent of barcoded S or RBD tetramer-stained cells and no in vitro validated cells were manually labeled as unknown specificity.

Clones from which members were found before and after BA.1 BT infection were labelled as ‘‘sustained’’. Clones seen at least twice before BA.1 BT infection, never after BA.1 BT infection and whose overall frequency pre-BA.1 BT infection was superior to the frequency of singletons post-BA.1 BT infection in that donor, to account for differences in sampling pre- and post- BA.1 BT infection, were labelled as ‘‘lost’’. Clones never seen before BA.1 BT infection, seen at least twice after BA.1 BT infection and whose overall frequency post-BA.1 BT infection was superior to the frequency of singletons pre-BA.1 BT infection in that donor were labelled as ‘‘newly expanded’’. Both ‘‘lost’’ and ‘‘newly expanded’’ clones were further labelled as ‘‘persisting’’ if found at multiple time points.

VH repartitions and Shannon entropies were calculated using the countGenes() and alphaDiversity() functions from the Immcantation/alakazam v1.2.0 R package. Chao1 richness indexes were calculated using the iNEXT v3.0.0 package (https://doi.org/10.1111/2041-210X.12613). Identical sequences were identified using the collapseDuplicates() function from the Immcantation/alakazam v1.2.0 R package. To account for differences in sampling, we computed the average frequency of duplicates found upon 1000 bootstrapping, downsampling to 65 sequences per time point for each donor. Phylogenetic trees and date randomization test to detect evolution over time were generated and performed using the Dowser v1.0.0 package[60] and the Immcantation/IgPhyML toolkit (Immcantation/suite v4.3.2) and further visualized in R using the Alakazam v1.2.0 and ggtree v3.4.2 packages.

Graphics were obtained using the ggplot2 v3.3.6, pheatmap v1.0.12 and circlize v0.4.15 packages.

Affinity measurement using biolayer interferometry (Octet)

This high-throughput kinetic screening of supernatants using single antigen concentration has recently been extensively tested and demonstrated excellent correlation with multiple antigen concentration measurements.[61] Biolayer interferometry assays were performed using the Octet HTX instrument (ForteBio). Anti-Human Fc Capture (AHC) biosensors (18-5060) were immersed in supernatants from single-cell MBC cultures (or control monoclonal antibody) at 25°C for 1800 seconds. Biosensors were equilibrated for 10 minutes in 10x PBS buffer with surfactant Tween 20 (Xantec B PBST10-500) diluted 1x in sterile water with 0.1% BSA added

Please cite this article in press as: Sokal et al., SARS-CoV-2 Omicron BA.1 breakthrough infection drives late remodeling of the memory B cell repertoire in vaccinated individuals, Immunity (2023), https://doi.org/10.1016/j.immuni.2023.07.007

(PBS-BT) prior to measurement. Association was performed for 600s in PBS-BT with Hu-1 or variant RBD (BA.1, BA.2 and BA.5) at 100nM followed by dissociation for 600s in PBS-BT. Biosensor regeneration was performed by alternating 30s cycles of regeneration buffer (glycine HCl, 10 mM, pH 2.0) and 30s of PBS-BT for 3 cycles. Traces were reference sensor subtracted and curve fitting was performed using a local 1:1 binding model in the HT Data analysis software 11.1 (ForteBio). Sensors with response values (maximum RBD association) below 0.1nm were considered non-binding. Hu-1 RBD non-binding monoclonal antibodies (n=14/414) were excluded from further analysis. For variant RBD non-binding mAbs, sensor-associated data (mAb loading and response) were manually checked to ensure that this was not the result of poor mAb loading. For binding clones, only those with full R^2>0.8 were retained for KD reporting and Omicron lineage binding. mAbs were defined as affected against a given variant RBD if the ratio of calculated KD value against that RBD variant and the Hu-1 RBD was superior to five and final KD > $5x10^{-10}$ M. Omicron lineage binding residues prediction was simply made based on mutations repartition in the different variants.

Virus neutralization assay

Virus neutralization was evaluated by a focus reduction neutralization test (FRNT). Vero E6 cells were seeded at $2x10^4$ cells/well in a 96-well plate 24h before the assay. Two-hundred focus-forming units (ffu) of virus were pre-incubated with serial dilutions of heat-inactivated sera for 1hr at 37°C before infection of cells for 2hrs or with supernatants from single-cell cultured memory B cells at 16nM. The virus/antibody mix was then removed, and foci were left to develop in presence of 1.5% methylcellulose for 2 days (D614G) or 3 days (Omicron BA.1 and BA.5). Cells were fixed with 4% formaldehyde and foci were revealed using a rabbit anti-SARS-CoV-2 N antibody (gift of Nicolas Escriou) and anti-rabbit secondary HRP-conjugated secondary antibody. Foci were visualized by diaminobenzidine (DAB) staining and counted using an Immunospot S6 Analyser (Cellular Technology Limited CTL). Pre-pandemic serum (March 2012) was used as negative control for sera titration and was obtained from an anonymous donor through the ICAReB platform (BRIF code n°BB-0033-00062) of Institut Pasteur that collects and manages bioresources following ISO (International Organization for Standardization) 9001 and NF S 96-900 quality standards.

Percentage of virus neutralization was calculated as (100 - ((#foci sample / #foci control)*100)). Sera IC50 were calculated over 8 four-fold serial dilutions from 1/10 to 1/164000 using the equation log (inhibitor) vs. normalized response – Variable slope in Prism 9 (GraphPad software LLC). Tested supernatants were defined as ''potent'' when displaying over 75% neutralization potential when tested at 16nM, ''intermediate'' when displaying 50 to 75% neutralization potential, ''weak'' when displaying 25 to 50% neutralization potential and weak if below 25%.

QUANTIFICATION AND STATISTICAL ANALYSIS

Ordinary One-way ANOVA, Two-way ANOVA, Repeated measures mixed effects model analysis, Kruskal-Wallis test and Mann-Whitney test were used to compare continuous variables as appropriate (indicated in Figures). Benjamini, Krieger and Yekutieli FDR correction was used for all multiple comparisons. A P-value ≤ 0.05 was considered statistically significant. Statistical analyses were all performed using GraphPad Prism 9.0 (La Jolla, CA, USA).

ADDITIONAL RESOURCES

ClinicalTrials.gov Identifier: MEMO-CoV2, NCT04402892.

Résumé :
Clostridioides difficile, bactérie Gram-positive, anaérobie et sporulée est le principal agent responsable des diarrhées et colites nosocomiales chez l'adulte à la suite d'un traitement antibiotique. Suite à la constante augmentation de l'incidence depuis le début du nouveau millénaire, et les évolutions rapides des souches impliquées dans l'infection à *C. difficile* (ICD), le Center for Disease Control a catégorisé l'ICD comme une menace urgente à combattre dans les prochaines décennies. De nouvelles stratégies sont donc nécessaires pour (i) réduire la consommation d'antibiotiques dans le traitement de l'ICD et (ii) prévenir la propagation du *C. difficile* dans les établissements de santé.
Si les toxines de *C. difficile* ont été largement étudiées, d'autres facteurs de virulence, tels que les adhésines et les protéines de surface, suscitent un intérêt croissant. Ces protéines sont impliquées dans l'échappement à la surveillance du système immunitaire et jouent donc un rôle majeur dans l'initiation de la pathogenèse. Parmi ces protéines, l'une d'entre elles a suscité un intérêt croissant : la protéine A de la couche superficielle (couche S) (SlpA). La SlpA est composée de deux sous-unités : la SlpA de haut poids moléculaire (HMW) et la SlpA de bas poids moléculaire (LMW), la dernière étant la plus externe. SlpA joue un rôle central dans le maintien de l'intégrité de la membrane bactérienne et la physiologie de *C. difficile*. En outre, la SlpA a également été impliquée dans l'adhésion bactérienne aux entérocytes et est nécessaire à la réussite de la colonisation de l'hôte. Par ailleurs, les protéines de la couche S sont immunogènes, des anticorps anti-SlpA ayant été détectés dans le sérum de patients convalescents. Cependant, les interactions entre *C. difficile* et les anticorps de l'hôte restent largement inexplorées. Un autre point d'intérêt de la LMW SlpA est le haut degré de variabilité des différents ribotypes de *C. difficile*, ce qui suggère un mécanisme permettant d'échapper à la surveillance immunitaire de l'hôte. Néanmoins, la recherche fondamentale s'est concentrée sur une souche de C. difficile.
Dans ce travail, nous avons produit la première collection d'anticorps monoclonaux anti-LMW SlpA (AcM) reconnaissant divers ribotypes cliniques de *C. difficile*. Ces AcM ont été entièrement caractérisés en termes d'affinité, de réactivité et de liaison aux bactéries entières. Ces AcM sont intéressants en tant qu'outils de recherche pour détecter différentes souches de *C. difficile*, et peuvent être utilisés en ELISA, en cytométrie de flux, en microscopie et en histologie. Nous avons ensuite tiré parti de cette collection pour mettre au point un test d'identification rapide "Quick-Ribodif" à des fins de diagnostic et de surveillance épidémiologique. Nous avons détecté spécifiquement *C. difficile* à partir des ribotypes cliniques les plus fréquents dans un microbiote humain complexe.
Dans une autre partie de ce travail, nous nous sommes concentrés sur les AcM dirigés vers la souche de référence *C. difficile* 630 et avons évalué les effets des AcM sur différents paramètres physiologiques de *C. difficile*. Nous avons observé des effets distincts sur la physiologie de *C. difficile* en fonction de l'épitope reconnu par l'AcM. De manière frappante, un AcM a entravé la croissance bactérienne et a augmenté la sensibilité de *C. difficile* aux agents de stress. En outre, deux AcM ont aboli la production de toxines, ce qui suggère que la flexibilité de la couche S est entravée lorsque le *C. difficile* est recouvert de ces AcM. Enfin, deux AcM ont augmenté la formation de biofilms, soulignant le rôle de la couche S dans la formation et la structure des biofilms. Cette partie du travail fournit des informations importantes sur le rôle de la couche S dans la physiologie de *C. difficile*. Ces résultats révèlent également les effets ambivalents des anticorps anti-couche S, remettant en question les approches thérapeutiques axées sur cette protéine.

Mots clés : [*C. difficile*, monoclonal antibodies, S-layer, ribotype]

[Identification and evaluation of monoclonal antibodies against surface-layer proteins of *Clostridioides difficile*]

Abstract :
Clostridioides. difficile is an anaerobic bacterium, Gram-positive and spore-forming rod, that is the main agent responsible for nosocomial diarrhea and colitis in adults following an antibiotic treatment[311]. With an incidence that is constantly increasing since the turn of the new millennium, the emergence of hypervirulent strains such as RT027, and rapid changes in strains involved in *C. difficile* infection (CDI), Center for Disease Control categorized CDI as an urgent threat to tackle[4]. New strategies are therefore needed to (i) reduce the consumption of antibiotics in the treatment of CDI and (ii) prevent *C. difficile* spread in health care institutions.
While *C. difficile* toxins have been largely studied, other virulence factors such as adhesins and surface proteins have focused a growing interest. These proteins are involved in colon localization, evasion of the immune system surveillance and are therefore playing a major role in the initiation of bacterial pathogenesis[307,308]. Among these proteins, one gained substantial interest: the Surface-Layer (S-layer) Protein A (SlpA). SlpA is composed of two subunits *i.e.* the High Molceular Weight (HMW SlpA) and the Low Molecular Weight (LMW SlpA), the latest being the most external one. SlpA is central for maintaining bacterial membrane integrity and bacterial fitness. Moreover, SlpA has been also involved in bacterial adhesion to enterocytes and is needed for successful colonization of the host[28,297]. While these data suggest that SlpA is crucial in the early stages of CDI, detailed analysis are still needed. Besides, S-layer proteins are immunogenic as anti-S-layer antibodies have been detected in sera from convalescents patients[43]. However, *C. difficile*-host antibodies interactions remain largely unexplored. Another point of interest of the LMW SlpA is the high degree of variability of the different ribotypes of *C. difficile*, suggesting a mechanism to escape host immune surveillance[35]. Nevertheless, fundamental research focused on one strain of *C. difficile,* missing other members of *C. difficile* family.
In this work, we produced the first collection of anti-LMW SlpA monoclonal antibodies (mAbs) recognizing various clinical ribotypes of *C. difficile*. These mAbs were fully characterized in terms of affinity, reactivity/cross-reactivity and binding to whole bacteria. These mAbs are of interest as research tools to detect different strains of *C. difficile*, and can be used in ELISA, flow cytometry, microscopy and histology assay. We then took advantage of this collection to develop a rapid identification test "Quick-Ribodif" for diagnostic and epidemiological monitoring purposes. We specifically detected *C. difficile* from the most frequent clinical ribotypes among a complex human microbiota.

In another part of this work, we focused on mAbs directed towards the reference strain *C. difficile* 630 and evaluated mAbs effects on *C. difficile* fitness. We observed distinct effects on *C. difficile* physiology depending on mAbs epitope. Strikinlgy, one mAb impaired bacterial growth and increase *C. difficile* sensitivity to stress agents. Furthermore, two mAbs abolished toxin production suggesting that S-layer flexibility is hampered when *C. difficile* is coated with these mAbs. Finally, two mAbs increased biofilm formation, pointing out the role of S-layer in biofilm formation and structure. Altogether, this part of work provides important insights on the role of S-layer in *C. difficile* fitness. These results also reveal the ambivalent effects of anti-S-layer antibodies, questioning the S-layer directed therapeutic approaches. Precise determination of the epitopes that are recognized by these anti-LMW mAbs could deepen this work and lead to the generation of antibodies targeting a precise peptide of the S-layer crucial for the bacteria and beneficial to treat CDI.